UNIVERSITY OF SOUTHAMPTON

FACULTY OF ENGINEERING AND THE ENVIRONMENT

Use of voyage simulation to investigate hybrid fuel cell systems for marine propulsion

by

Ameen Bassam

Thesis for the degree of Doctor of Philosophy

June 2017

UNIVERSITY OF SOUTHAMPTON

ABSTRACT

FACULTY OF ENGINEERING AND THE ENVIRONMENT

Doctor of Philosophy

USE OF VOYAGE SIMULATION TO INVESTIGATE HYBRID FUEL CELL SYSTEMS FOR MARINE PROPULSION

by Ameen Bassam

The design of green ships has received significant attention with the goal of reducing the negative environmental impacts of shipping and to comply with the more stringent environmental regulations. Therefore, in 2009 the International Maritime Organisation (IMO) published the Energy Efficiency Design Index (EEDI) measures to be adopted by new ships to reduce the Greenhouse Gases (GHG). Hybrid electric power and propulsion is one of the EEDI measures and fuel cell technologies are considered as a candidate to be used due to their high efficiency, lower emissions, lower maintenance, and quiet operation. This project aims to investigate the use of hybrid propulsion systems for marine propulsion which utilise fuel cells as a main source of power and the effect of energy management on the performance of these systems through voyage simulation.

In order to assess the effectiveness of fuel cells as a source of power for ship propulsion systems, the development of a time-domain three degree of freedom total ship system simulator using MATLAB/Simulink is completed. Different components of the ship, including its propulsion system, and the ship's interaction with the surrounding environment are mathematically modelled. Considered power sources in the thesis include conventional two and four-stroke diesel engines, fuel cells and batteries to enable the comparison between conventional and hybrid fuel cell power trains. The verification and validation of the developed ship system simulator are also conducted using numerical, experimental and real ship operational data. The thesis demonstrates the use of the developed total ship system simulator in proposing a hybrid fuel cell/battery propulsion system for a domestic ferry. The results indicate that the hybrid fuel cell system has less weight and requires less space than the conventional diesel system. However, the hybrid fuel cell system's associated costs are still higher than diesel propulsion system.

For hybrid fuel cell systems, the design of a suitable energy management strategy is essential in order to handle properly the required power split between the fuel cell and the battery systems. Therefore, the developed ship system simulator is also used to study and compare the most common energy management strategies. An improvement to the classical proportional-integral controller based strategy is presented in this thesis. This improvement results in minimizing the fuel cell operational stress and hydrogen consumption. Alongside this work, a novel multi-scheme energy management strategy with a main objective of reducing the total consumed energy is also developed for the world's first fuel cell passenger ship *FCS Alsterwasser*.

Contents

List of Figures

List of Tables

Declaration of Authorship

I, Ameen Bassam, declare that the thesis entitled *Use of voyage simulation to investigate hybrid fuel cell systems for marine propulsion* and the work presented in the thesis are both my own, and have been generated by me as the result of my own original research. I confirm that:

- this work was done wholly or mainly while in candidature for a research degree at this University;
- where any part of this thesis has previously been submitted for a degree or any other qualification at this University or any other institution, this has been clearly stated;
- where I have consulted the published work of others, this is always clearly attributed;
- where I have quoted from the work of others, the source is always given. With the exception of such quotations, this thesis is entirely my own work;
- I have acknowledged all main sources of help;
- where the thesis is based on work done by myself jointly with others, I have made clear exactly what was done by others and what I have contributed myself;
- parts of this work have been published as:
  - Bassam, Ameen, Phillips, Alexander, Turnock, Stephen and Wilson, Philip. An Improved Energy Management Strategy For A Hybrid Fuel Cell/Battery Passenger Vessel, *International Journal of Hydrogen Energy* (2016). `http://dx.doi.org/10.1016/j.ijhydene.2016.08.049`.
  - Bassam, Ameen, Phillips, Alexander, Turnock, Stephen and Wilson, Philip. Development of A Multi-Scheme Energy Management Strategy For A Hybrid Fuel Cell Driven Passenger Ship, *International Journal of Hydrogen Energy* (2016). `http://dx.doi.org/10.1016/j.ijhydene.2016.08.209`.

– Bassam, Ameen, Phillips, Alexander, Turnock, Stephen and Wilson, Philip (2014) Assessment of The Effectiveness of Fuel Cells as an Alternative Technology for Marine Propulsion Systems. In, *The 5th Marine Technology Postgraduate Conference*, Newcastle upon Tyne, UK, 9 - 10 Jun 2014.

– Bassam, Ameen M., Phillips, Alexander B., Turnock, Stephen R. and Wilson, Philip A. (2015) Ship voyage energy efficiency assessment using ship simulators. In, *VI International Conference on Computational Methods in Marine Engineering (MARINE 2015)*, Rome, IT, 15 - 17 Jun 2015.

– Ameen M. Bassam, Alexander B. Phillips, Philip A. Wilson, Stephen R. Turnock. Hybrid Fuel Cell Electric Propulsion for Marine Transport Applications : A Case Study of A Domestic Ferry, *Next Generation Marine Power & Propulsion Conference*, Southampton, UK, 26 - 27 Apr 2016.

– Bassam, Ameen, Phillips, Alexander, Turnock, Stephen and Wilson, Philip. Design, Modelling and Simulation of a Hybrid Fuel Cell Propulsion system for a Domestic Ferry. In, *The 13th International Symposium on Practical Design of Ships and Other Floating Structures (PRADS 2016)*, Copenhagen, Denmark, 4 - 8 Sep 2016.

– Bassam, Ameen, Phillips, Alexander, Turnock, Stephen and Wilson, Philip. Sizing optimization of a fuel cell/battery hybrid system for a domestic ferry using a whole ship system simulator. In, *2016 International Conference on Electrical Systems for Aircraft, Railway, Ship Propulsion and Road Vehicles & International Transportation Electrification Conference (ESARS-ITEC)*, Toulouse, France, 2 - 4 Nov 2016.

Signed:
Date:

Acknowledgements

Firstly, I would like to praise and thank ALLAH, the Almighty, for giving me the strength and for blessing me with many great people who have supported the development of this work and I want to thank them all. I would like to express my deepest thanks and appreciation to my supervisors, Professor Philip Wilson for his thoughtful guidance and help even before the start of my PhD, Professor Stephen Turnock who guided me with his expertise and critical comments, and Dr Alexander Phillips for his warm encouragement, enthusiasm and supervision even after leaving the university.

Secondly, I want to thank my family, especially my parents, for their encouragement, prayers and sacrifice throughout my life. My lovely wife, I am so blessed of having you and I would like to thank you for your care, support, and being there during all the ups and downs I have been through. Furthermore, thanks to all my Egyptian friends here in UK, my second family, who make me feel at home. Finally, I wish to thank the Egyptian Government for the financial support of my study and all the members of the Naval Architecture and Marine Engineering department at my home university, Port Said University, for allowing me to grow as an academic researcher

Abbreviations

AC: Alternating Current

AFC: Alkaline Fuel Cell

AHTS: Anchor Handling Tug Supply

AIS: Automatic Identification System

APU: Auxiliary Power Unit

AUV: Autonomous Underwater Vehicle

BEMT: Blade Element Momentum Theory

BN: Beaufort Number

BOP: Balance of Plant

BSRA: British Ship Research Association

BTF: Blade Thickness Fraction

BV: Bureau Veritas

CCDoTT: Centre for the Commercial Deployment of Transportation Technologies

CCHP: Combined Cooling, Heating and Power Systems

CCS: Carbon Capture and Storage

CDCS: Charge-Depleting Charge-Sustaining

CHP: Combined Heat and Power

CO: Carbon Monoxide

CODLAD: Combined Diesel Electric and Diesel

CODLAG: Combined Diesel Electric and Gas Turbine

CODLOD: Combined Diesel Electric or Diesel

COGLOG: Combined Gas Electric or Gas Turbine

CO_2: Carbon Dioxide

CP: Controllable Pitch

DC: Direct Current

DE: Diesel Engine

DMFC: Direct Methanol Fuel Cell

DND: Department of National Defence

DOE: Department of Energy

DOF: Degree of Freedom

DOH: Degree Of Hybridization

ECAs: Emission Control Areas

ECMS: Equivalent Consumption Minimization Strategy

EEDI: Energy Efficiency Design Index

EEOI: Energy Efficiency Operational Indicator

EMS: Energy Management Strategy

EMSA: European Maritime Safety Agency

EU: European Union

FCSHIP: Fuel Cell Technology in Ships

FCV: Fuel Cell Vehicles

FFT: Fast Fourier Transform

FOB: Free On Board

FP: Fixed Pitch

GDP: Group Design Project

GFS: Global Forecast System

GHG: Greenhouse Gases

GL: Germanischer Lloyd

GPS: Global Positioning System

GRIB: General Regularly-distributed Information in Binary form

GT: Gas Turbine

HDW: Howaldtswerke-Deutsche Werft shipyards

HTPEM: High Temperature Proton Exchange Membrane

HVAC: Heating, Ventilation and Air Conditioning

ICE: Internal Combustion Engines

IEA: International Energy Agency

IMO: International Maritime Organisation

ISO: International Organization for Standardization

ITTC: International Towing Tank Conference

Jp-5, 8: Jet Fuel

LNG: Liquefied Natural Gas

LPG: Liquefied Petroleum Gas

MARAD: Maritime Administration

MARPOL: Marine Pollution

MCFC: Molten Carbonate Fuel Cell

MDO: Marine Diesel Oil

MEPC: Marine Environmental Protection Committee

MMG: Manoeuvring Modelling Group

Mtoe: Million Tons of Oil Equivalent

MVM: Mean Value Model

MW_e: Mega Watt (electrical power)

MWR: Mean Width Ratio of propeller

NAM: North American Model

NASA: National Aeronautics and Space Administration

NATO F-76: primary naval fuel

NCDC: National Climatic Data Centre

NEXT: North European Storm Study Extension

N_2O: Nitrous Oxide

NOAA: National Oceanic and Atmospheric Administration

NOMADS: NOAA's Operational Model Archive Distribution System

NO_x: Nitrogen Oxides

O&M: Operation and Maintenance

ONR: Office of Naval Research

OSV: Offshore Supply Vessel

PAFC: Phosphoric Acid Fuel Cell

PEMFC: Proton Exchange Membrane Fuel Cell

PI: Proportional-Integral

PM: Particular Matter

QM2: Queen Mary 2

R&D: Research and Development

RPM: Revolutions per Minute

SECA: Sulphur Emission Control Area

SEEMP: Ship Energy Efficiency Management Plan

SFC: Specific Fuel Consumption

SO_2: Sulphur Dioxide

SOC: State of Charge

SOFC: Solid Oxide Fuel Cell

SOLAS: Safety of Life At Sea

SPS: SimPowerSystem MATLAB toolbox

SSFC: Ship Service Fuel Cell

SSPA: Statens Skeppsprovingansalt, Götaborg, Sweden

TEU: Twenty-foot Equivalent Unit

UK: United Kingdom

UNCTAD: The United Nations Conference on Trade and Development

UNFCCC: United Nations Framework Convention on Climate Change

US: United States

USA: United States of America

UTC: Coordinated Universal Time

UUV: Unmanned Undersea Vehicle

ZEMShip: Zero Emission Ship

Nomenclature

A: Tafel slope (V)

A: Battery exponential voltage (V)

A_F: Ship frontal projected area (m^2)

A_L: Ship lateral-plane area (m^2)

a, b, c, and d: Constants of the propeller thrust and torque coefficients

$a_{0..6}$, $b_{0..9}$: Constants of wake fraction and thrust deduction's equations

B: Breadth (m)

B: Exponential capacity $(Ah)^{-1}$

BAR: Blade area ratio

C_B: Block coefficient

C_F: CO_2 mass to fuel mass conversion factor (tonne CO_2/tonne fuel)

CN: Non-dimensional wind force yawing-moment coefficient

C_p: Environmental damage cost factor $(\$/GJ)$

C_{ph}: Horizontal prismatic coefficient

C_{pv}: Vertical prismatic coefficient

C_R: Residual resistance coefficient

C_V: Viscous resistance coefficient

CX: Non-dimensional longitudinal wind force coefficient

CY: Non-dimensional lateral wind force coefficient

D_{env}: Environmental damage cost ($)

D_P: Propeller diameter (m)

D_t: Thrust deduction parameter

D_w: Wake fraction parameter

D_{wt}: Deadweight tonnage ($tonne$)

E: Open circuit voltage (V)

E_{charge}: Battery open circuit charging voltage (V)

$E_{discharge}$: Battery open circuit discharging voltage (V)

EAR: Expanded area ratio

$\text{Energy}_{\text{Batt}}$: Battery consumed energy (kWh)

E_{batt}: Battery open circuit voltage (V)

$\text{Energy}_{\text{Batt}_{\text{Ch}}}$: Required energy to recharge the battery (kWh)

$\text{Energy}_{\text{FC}}$: Consumed fuel cell energy (kWh)

E_{fc}: Fuel cell required energy (kWh)

E_n: Energy consumption (kWh)

F: Faraday constant (C/mol)

H_{2Cons}: Fuel cell hydrogen consumption (kg)

HHV_{H_2}: Hydrogen higher heating value (MJ/kg)

H_w: Wave height (m)

h_p: Engine fuel flow rate (kg/s)

h_{pmcr}:Engine fuel flow rate at maximum continuous rating (kg/s)

i: Battery current (A)

i^*: Low frequency current dynamics (A)

i_0: Exchange current (A)

i_a: Motor armature current (A)

I_{ew}: Entrained water moment of inertia (kgm^2)

i_{fc}: Fuel cell current (A)

I_m: Inertia of rotating parts (kgm^2)

I_p: Propeller moment of inertia (kgm^2)

I_{zz}: Moment of inertia of yawing (kgm^2)

J: Advance Ratio

J_m: Motor moment of inertia (kgm^2)

K: 4-stroke engine gain constant

k: Stern coefficient

K_y: Engine gain constant

K_T, K_Q: Non-dimensional thrust and torque coefficients

K_{T0}, K_{Q0}: Non-dimensional thrust and torque coefficients at J=0.

K_t: Motor torque constant (Nm/A)

K_e: Motor electromotive force constant ($V/rad/sec$)

K_y: 2-stroke engine gain constant

L: Motor inductance (H)

$LatA$ and $LatB$: Latitudes of point A and B

L_{OA}: Length over all (m)

L_{OS}: Length over surface (m)

$LongA$ and $LongB$: Longitudes of point A and B

L_{PP}: Length between perpendiculars (m)

L_{WL}: Length over waterline (m)

M: Ship displacement ($tonne$)

m_x: Added mass on x direction (kg)

m_y: Added mass on y direction (kg)

m and n: Constants of speed loss equation

N: Number of cells in fuel cell stack

N: Hydrodynamic moment acting on midship (Nm)

N_0: Steady state propeller speed (rpm)

N_{Brac}: Number of brackets

N_{Boss}: Number of bossing

N_{cyc}: Number of battery cycles

N_{eng}: Engine rotational speed (rpm)

N_{Thr}: Number of thrusters

N_W: Wind yawing-moment (Nm)

n_{eng}: Engine rotational speed (rps)

n_{H_2}: Number of Hydrogen molecules (mole)

n_{mcr}: Engine rotational speed at maximum continuous rating (rps)

n_p: Propeller rotational speed (rps)

n_{sh}: Shaft rotational speed (rps)

P/D: pitch to diameter ratio

P_B: Brake power (kW)

$\text{power}_{\text{Batt}}$: Consumed battery power (kW)

P_{BATopt}: Battery optimum power (kW)

P_D: Developed power (kW)

P_E: Effective power (kW)

P_f: Friction loss pressure (N/m^2)

P_{FCmax}: Fuel cell maximum power (kW)

P_{FCmin}: Fuel cell minimum power (kW)

P_{FCopt}: Fuel cell optimum power (kW)

P_T: Thrust power (kW)

P_{load}: Hybrid system required load power (kW)

P_m: Motor mechanical power (kW)

P_{optchar}: Battery optimum charge power (kW)

P_{optdis}: Battery optimum discharge power (kW)

Q: Maximum battery capacity (Ah)

Q_P: Propeller torque (Nm)

Q_{eng}: Engine torque (Nm)

Q_f: Frictional torque (Nm)

Q_{mcr}: Engine torque at maximum continuous rating (Nm)

R: Total resistance (N)

R: Electrical resistance (Ohm)

R_A: Model-ship correlation resistance (N)

R_{APP}: Appendage resistance (N)

R_B: Pressure resistance due to bulbous bow (N)

R_F: Frictional resistance (N)

R_{max}: Maximum total resistance (N)

R_{mean}: Mean total resistance (N)

R_{ohm}: Fuel cell internal resistance (Ω)

R_R: Residual resistance (N)

R_{TR}: Pressure resistance due to transom immersion (N)

R_W: Wave resistance (N)

r: Rate of turn (deg/sec)

S: Wetted surface area (m^2)

S_L: Distance between the the lateral-plane area centre and the midship section (m)

SOC_{ini}: Initial battery SOC (%)

SOC_{fin}: Final battery SOC (%)

SOC_H: Upper limit of battery SOC (%)

SOC_L: Lower limit of battery SOC (%)

T: Time constant (sec)

T: Ship draft (m)

t: Thrust deduction

T_a: Draft aft (m)

T_d: Fuel cell response time (sec)

T_f: Draft fore (m)

T_P: Propeller thrust (N)

u: Wind speed (m/s)

V: Speed (kn)

V: Voltage (V)

V_A: Speed of advance (kn)

V_{batt}: Battery voltage (V)

V_d: Engine cylinder empty volume (m^3)

V_{fc}: Fuel cell voltage (V)

W_p: Propeller weight (lb)

w: Wake fraction

w: Motor rotational speed (rad/sec)

X: Hydrodynamic forces in X-direction (N)

x_G: Location of the ship centre of gravity from the midship in x-axis (m)

$X_{\dot{u}}$: Added mass in surge direction (kg)

X_W: Longitudinal wind force (N)

Y: Fuel index

Y: Hydrodynamic forces in Y-direction (N)

Y_W: Side wind force (N)

Z: Propeller number of blades

Z_{eng}: Number of engine cylinders

α: Ship course angle (deg)

δLCB: Longitudinal centre of buoyancy deviation percentage (%)

ΔR: Wind and wave external forces (N)

ϵ: Wind apparent angle (deg)

η: Propeller angle of rake (deg)

η_{Conv}: DC-DC converter efficiency (%)

η_D : Quasi propulsive efficiency (%)

η_H : Hull efficiency (%)

η_O : Open water efficiency (%)

η_R : Relative rotative efficiency (%)

η_S : Shaft efficiency (%)

γ: Water specific weight (N/m^3)

γ: Wind direction (deg)

γ_R: Wind angle off bow (deg)

μ: SOC constant

∇: Ship volume of displacement (m^3)

ρ: Water density (kg/m^3)

ρ_a: Air density (kg/m^3)

ρ_{mH_2}: Hydrogen gravimetric density (ρ_{mH_2})

ρ_{vH_2}: Hydrogen volumetric density (ρ_{vH_2})

τ: Engine time delay (sec)

τ: Propeller dynamic inflow time constant (sec)

τ_c: Engine torque build-up time constant (sec)

τ_{prop}: Propeller load fluctuation time constant

Chapter 1

Introduction

1.1 Motivation

1.1.1 Importance of Shipping

According to the United Nations Conference on Trade and Development (UNCTAD), shipping handles over 80% of the world trade by volume [1] due to comparatively low cost, more safe and greater capacity than other means of transport [51]. The global demand for energy, raw material, food, and finished products are serviced by seaborne transport which has grown with the world's population and associated economy. Development of international seaborne trade has increased from 2605 millions of tons in 1970 to 9842 millions of tons in 2014 as shown in Figure 1.1 [1].

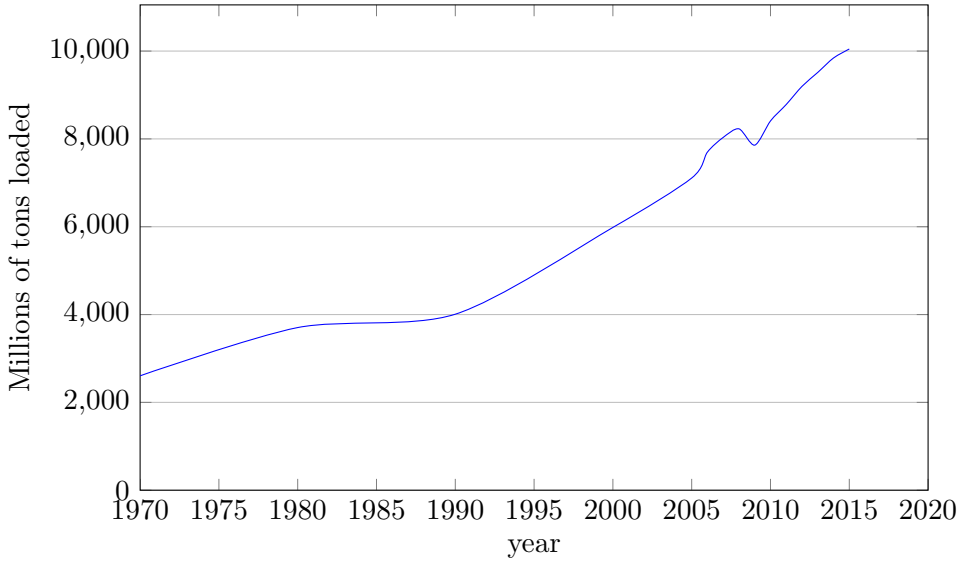

Figure 1.1: Development of international seaborne trade [1]

The increase in the volume of cargoes to be transported by sea has contributed in the development of both ship size and number as shown in Figure 1.2. For example, the average size of a container ship has doubled in 20 years from 1250 TEU in 1990 to 3064 TEU at the beginning of 2012 [52].

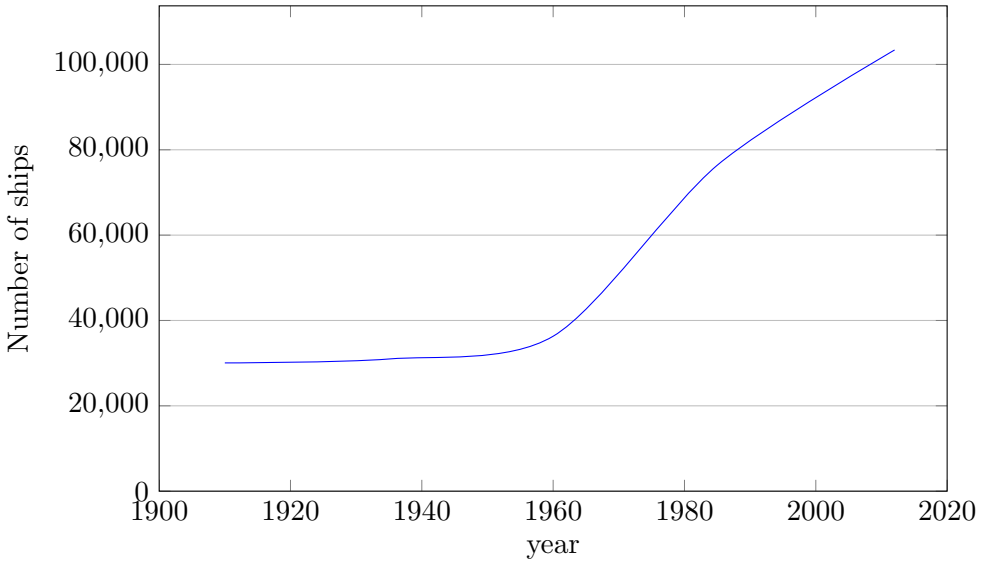

Figure 1.2: World fleet size by number of ships: 1900-2010 [2]

The increase in maritime activities, the number of ships and their size have some negative economical and environmental impacts which makes ship emissions and energy efficiency of ship propulsion systems areas of growing interest.

1.1.2 Economical Impacts of Shipping

Maritime industries and shipping are of significant economic importance. Due to the growth in ships size and number, global energy use is expected to increase as shown in Figure 1.3 and unfortunately most of it will come from fossil fuels as shown in Figure 1.4. The total shipping fuel consumption increased by 68% between 1990 to 2012 where international shipping was responsible for consuming 257 million tonnes of fuel in 2012 according to the latest IMO study [3].

The growing demand for energy causes a rise in its price. As shown in Figure 1.5 the prices of Europe Brent crude oil as for example is increasing with time. Although oil prices are decreasing now, there is still a desire to reduce ship operational cost. Moreover, the drop in oil prices may be temporary. So, the marine industry is facing pressure to reduce ships operational costs and GHG emissions; both may be addressed by reducing fuel consumption and increasing energy efficiency.

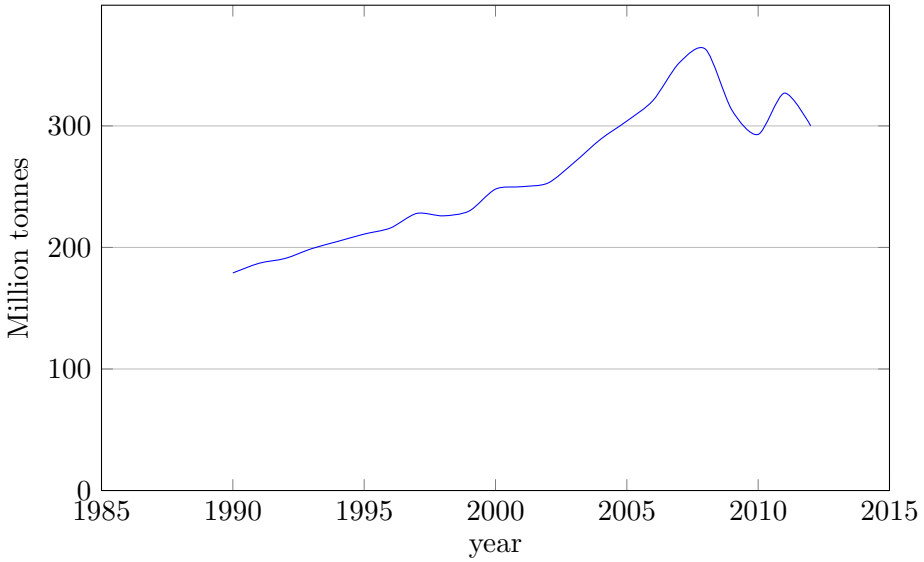

Figure 1.3: Total shipping fuel consumption [3]

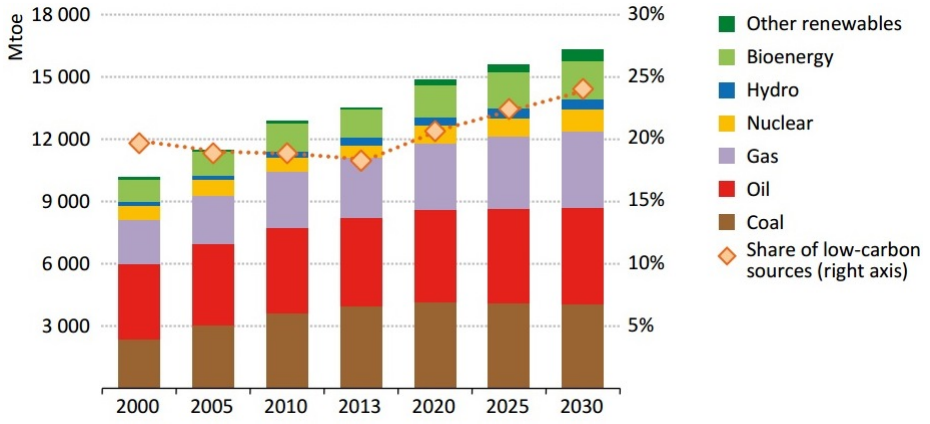

Figure 1.4: World energy demand by fuel (Million Tonnes of Oil Equivalent)[4]

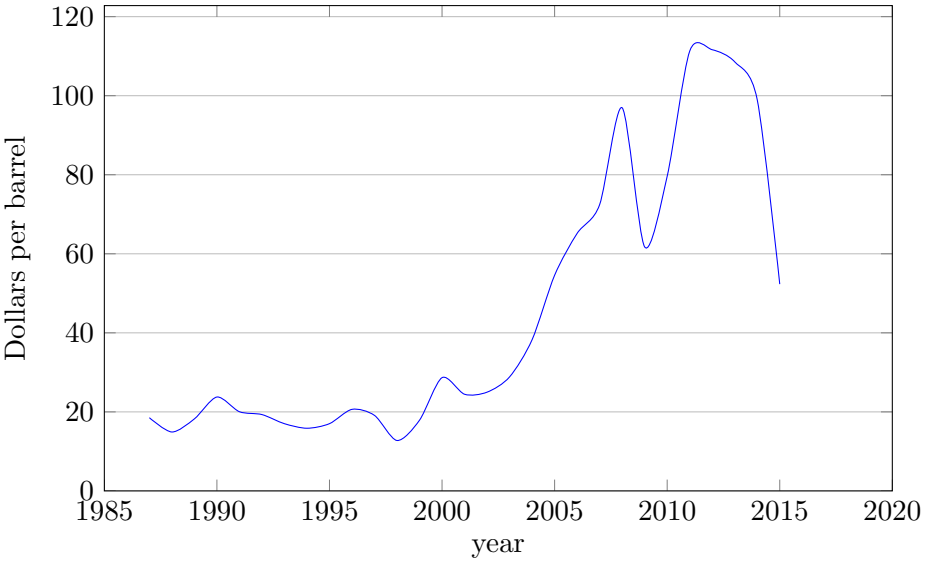

Figure 1.5: Europe Brent spot price FOB [5]

1.1.3 Environmental Impacts of Shipping

Alongside its economical impacts, shipping has negative environmental impacts as well. Ship operation impacts on the marine environment in a number of ways such as [53]:

- Air pollution through emissions of exhaust gases, cargo emissions, and emissions of refrigerants.
- Oil pollution and toxic substances from operation and illegal discharge.
- Pollution and physical impact through loss of ships and cargo.
- Release of toxic chemicals used in anti-fouling paints.
- Discharge of operational waste from ships, including discharge of raw sewage and garbage.
- Noise and collision with marine mammals.

A recent IMO study estimates that shipping in 2012 emitted 949 million tonnes of CO_2, which is about 2.7% of the global emissions during 2012. 796 million tonnes of CO_2 was due to international shipping. In the absence of new emission reduction policies, mid-range emissions scenarios show that by 2050 CO_2 emissions from international shipping may have an increase of between 50% to 250% with reference to emissions in 2012 [3]. Figure 1.6 shows another study of CO_2 from international marine bunker done by the International Energy Agency (IEA).

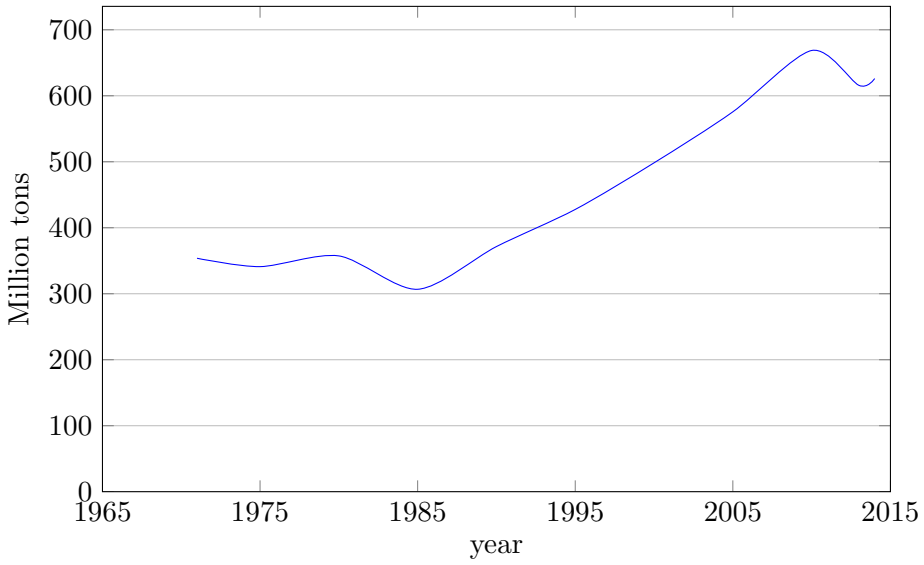

Figure 1.6: CO_2 emissions from international marine bunker (IEA) [6]

Moreover, shipping is also responsible for a greater percentage of NO_x emissions which is about 20 % of the global NO_x emissions from all sources [54] because of high engine temperature and combustion [55; 56]. Also, compared to other transport

modes, shipping has the highest SO_2 emissions because of the fuel sulphur content [57]. European Maritime Safety Agency (EMSA) studies estimate that European Union (EU) flagged ships are responsible for about 45% of all emissions and about 20% of emissions are emitted within the 12 mile limit of the territorial seas [58].

1.1.4 Regulations

In order to reduce ships greenhouse gases (GHG) emissions, there is a significant interest in improving the energy efficiency of ship propulsion systems which is important for both new and existing ships. Therefore, emissions reduction policies, regulations, and measures have been proposed and applied to increase the energy efficiency of ships and control its environmental impacts such as the Energy Efficiency Operational Indicator (EEOI), the Energy Efficiency Design Index (EEDI), the Ship Energy Efficiency Management Plan (SEEMP), the introduction of Emission Control Areas (ECAs), Polar Code, and Noise Code as presented hereafter.

1.1.4.1 EEOI

Regarding CO_2 emissions, IMO developed the EEOI to be voluntarily used to monitor the ship performance and efficiency as a function of the emitted mass of CO_2 [25] as shown in Equation 1.1.

$$EEOI = \frac{\text{actual } CO_2 \text{ emissions}}{\text{performed transport work}} \tag{1.1}$$

where the actual CO_2 emissions equals to mass of the consumed fuel multiplied by the a CO_2 mass conversion factor C_F which depends on the fuel type as shown in Table 1.1. The performed transport work equals to the distance multiplied by cargo carried, number of containers or passengers. This indicator can be used by ship's owner and operator to evaluate the performance of their ship or fleet with regard to CO_2 emissions in which a smaller EEOI means a more efficient ship.

Table 1.1: Carbon mass content factor [24]

Type of fuel	C_F (tonne CO_2/tonne fuel)
Diesel/Gas oil	3.206
Light fuel oil	3.15104
Heavy fuel oil	3.1144
Liquefied petroleum gas	3
Liquefied natural gas	2.75

1.1.4.2 ECAs

Designated sea areas have been introduced as Emission Control Areas (ECAs) with stringent international emission standards to control NO_x, SO_x, and particulate matter (PM) such as Baltic Sea in 2005, North Sea in 2006, North American ECA in 2011, and United States Caribbean Sea ECA in 2013 as shown in Figure 1.7. More areas are also under consideration to be designated as an ECA in the future. Therefore, ships have more stringent standards regarding engine emissions and fuel sulphur content should be 0.1% in January 2015 [59]. Ships which operate outside and inside ECAs will have to carry different fuels to comply with the limits of ECAs. However, it is predicted that fuel cost will increase by up to 87% for ships work within ECAs because of using very low-sulphur fuel [60].

Figure 1.7: ECAs as defined by the IMO

1.1.4.3 Noise code

High noise levels from ships are recognised by IMO as a threat to seafarers' health and marine species as well. Noise affects people living near ports and channels beside, noise can travel long distances [61]. Also, noise has harmful effects on sea animals because they rely on sound for communication, attracting mates, feeding, sensing obstacles. Therefore, IMO developed a noise code to provide international standards to protect seafarers and passengers from high noise levels under the provisions of regulation of the SOLAS Convention and it entered into force on the 1^{st} of July 2014 [62]. Also, identifying and minimizing incidental noise introduction into the marine environment from commercial shipping was added to the Marine Environment Protection Committee (MEPC) agenda in 2008 which resulted in inviting the committee to develop non-mandatory technical guidelines as well as introducing noise control areas [63].

1.1.4.4 EEDI/SEEMP measures

The MEPC published a package of technical and operational measures to be used by new and existing ships to reduce the amount of CO_2 emission which are EEDI and SEEMP measures. EEDI considers as another measure of ships CO_2 efficiency in terms of ship's power, specific fuel consumption (SFC), fuel C_F, ship's capacity and speed as shown in Equation 1.2 [25].

$$EEDI = \frac{\text{power} \times SFC \times C_F}{\text{capacity} \times \text{speed}} \tag{1.2}$$

In addition to EEDI, SEEMP aims to improve the operational energy efficiency of ships through four key processes [64] which are:

- Planning
- Implementation
- Monitoring
- Self-evaluation and improvement

This work was completed in 2011 resulting in amendments to MARPOL Annex VI by making mandatory the Energy Efficiency Design Index for new ships and the Ship Energy Efficiency Management Plan for all ships which entered into force on January 2013 and are applied to all ships of 400 gross tonnage and above [25]. Table 1.2 shows these technologies and measures suggested by IMO to be adopted to reduce ship's fuel consumption and increase its efficiency.

Deltamarin [65] conducted a study requested by EMSA in order to provide EMSA with trails and tests on the EEDI for different ship types to assess this index's applicability. This study concluded that current EEDI philosophy and methodology are not suitable for short sea shipping and small ships in general. Also, some of the existing technologies approach its physical limits. This is why engineers need to investigate alternative power sources, propulsion systems, and fuels for ships in order to reduce its negative environmental impact and improve its energy efficiency.

Decarbonizing ships by using hydrogen in combination with fuel cells has generated considerable research interest. Hydrogen offers great potential as a marine fuel due to its high gravimetric energy density and its potential for zero emissions by using renewable energy sources in the hydrogen production. Although cheaper hydrogen production methods exist, real environmental benefits of using hydrogen can be seen by generating it from clean renewable energy sources. Moreover, fuel cells can convert the chemical energy of hydrogen to electrical energy directly without combustion and it is being

Table 1.2: Technologies for EEDI reductions and SEEMP related measures [25]

EEDI reduction measure	**SEEMP related measure**
Optimised hull dimensions and form	Engine tuning and monitoring
Lightweight construction	Hull condition
Hull coating	Propeller condition
Hull air lubrication system	Reduced auxiliary power
Optimisation of propeller-hull interface and flow devices	Speed reduction (operation)
Contra-rotating propeller	Trim/draft
Engine efficiency improvement	Voyage execution
Waste heat recovery	Weather routing
Gas fuelled (LNG)	Advanced hull coating
Hybrid electric power and propulsion concepts	Propeller upgrade and aft body flow devices
Reducing on-board power demand (auxiliary system and hotel loads)	
Variable speed drive for pumps, fans, etc.	
Wind and solar power	
Design speed reduction (new builds)	

considered for marine applications due to its advantages such as the high efficiency even at part load, quiet operation, fuel flexibility, suitability for air independent propulsion, and low or zero emissions when hydrogen is used as a fuel [28; 66; 67].

The performance of fuel cell based power systems can be improved through hybridization by adding an energy storage system to supplement the fuel cell system. Moreover, hybrid electric power and propulsion concepts is one of the EEDI measures as shown in Table 1.2. So, using hydrogen fuelled fuel cells in a hybrid electric propulsion system will combine the advantages of hydrogen, fuel cells and hybrid electric propulsion systems. The presence of multiple power sources in hybrid fuel cell propulsion systems requires an energy management strategy (EMS) in order to realise the benefits of hybrid fuel cell power systems and improve its electrical integration. However, most of the work reported in the literature on EMS tends to focus on the automotive industry applications. Also, fuel cell marine applications is limited to low propulsion power requirements, electricity generation, or emergency power supply [68; 69]. Besides, hydrogen and fuel cell associated technologies are continuously developing. Therefore, more comprehensive work in this field is required to assess the effectiveness of fuel cells as a main source of power for ships with several megawatts of power. Also, the selection and development of a suitable EMS for marine application is a basic issue for hybrid fuel cell propulsion systems and it is an area of focus in this research to discuss its effect on the performance of fuel cell based power systems.

The results of this study can be used to answer questions regarding the viability of hydrogen fuel cells ships economically and environmentally. Moreover, questions regarding the relation between the nature of the ship operational profile and the used

EMS can be answered. Also, studying how fuel consumption and energy efficiency of hybrid fuel cell propulsion systems can be improved through the design of efficient EMS. Then, by increasing the energy efficiency of hybrid fuel cell systems, the hydrogen consumption and the required weight and size of its storage system can be reduced. Furthermore, the endurance between refuelling can be increased which will help in speeding the process of depending on fuel cell as a marine power source and aid in fuel cell commercialization.

Two ships are considered in this study which are the passenger ferry *M/S Smyril* and the first fuel cell passenger ship *FCS Alsterwasser*. Both ships are good candidates for using fuel cells to make use of its advantages of lower emissions and noise which are required for these ships. Moreover, both ships work in emission control areas in Faroe Islands and Germany hence, fuel cells are a suitable solution to help ships complying with the environmental regulations. Also, because of the limited availability and confidentiality of real ship operational data, these ships are considered due to the availability of their real operational data.

1.2 Aims and Objectives

Having identified the economical and environmental impacts of shipping, the project aims to investigate the use of fuel cells as a main source of power for marine hybrid propulsion systems making use of the advantages of fuel cells and hybrid electric propulsion concepts in order to reduce air emissions and noise from global shipping. The effect of energy management on the dynamic behaviour of these hybrid systems should also be investigated through voyage simulation. To help achieve this, the following objectives have been outlined:

1. Investigate different fuel cell types and their applications to identify the most suitable type for marine applications.
2. Model main components of the ship and its propulsion system, including fuel cell and battery, and the ship interaction with the surrounding environment mathematically in order to use numerical simulation to represent an overall ship system.
3. Incorporate the above mathematical modelling in MATLAB/Simulink environment to develop a time-domain quasi-steady three degree of freedom total ship simulator to predict ship performance and power requirements during realistic voyages.
4. Validate the developed total ship simulator using real operational data of the domestic ferry *M/S Smyril* to establish its accuracy. Then, the developed total ship system simulator is used to assess the effectiveness of fuel cells as a main source of power for the targeted ship.

5. Find the optimum sizes of the fuel cell stack and the energy storage system for the proposed hybrid fuel cell propulsion system of the targeted ship using the developed ship simulator. The considered sizing objective in this study is to minimize the total first and operational costs taking into consideration maintenance and replacement costs of the fuel cell and the energy storage system. Four different EMS are used in this study to show the effect of using different EMS on the resulting optimal sizes of the fuel cell and the energy storage systems.

6. Perform a comprehensive assessment of the environmental and economical impacts of using fuel cell in a hybrid electric propulsion system for *M/S Smyril* against its conventional diesel propulsion system in terms of emissions, operational costs, required size and weight of the machinery.

7. Present a comparative analysis of different energy management strategies for the hybrid fuel cell propulsion system of the first fuel cell passenger ship *FCS Alsterwasser* which are: state-based strategy, proportional-integral (PI) based strategy, charge-depleting charge-sustaining (CDCS) strategy, and equivalent consumption minimization strategy (ECMS). The addressed strategies are the most commonly used and the comparison is made in terms of hydrogen consumption, operational stresses, total consumed energy and cost.

8. Develop a multi-scheme energy management strategy using the examined four strategies with an objective of minimizing the total energy consumption of *FCS Alsterwasser* in order to increase its energy efficiency.

1.3 Report Structure

Having outlined the research problem, aims and objectives in this chapter, Chapter 2 shows a review of hybrid systems, fuel cell types, advantages, disadvantages and different fuel cell applications to identify the most suitable type of fuel cell technology for marine applications. After selecting the suitable fuel cell technology in Chapter 2, Chapter 3 is about the mathematical modelling of the developed ship simulator which will be used to study hybrid fuel cell propulsion systems. Chapter 3 presents a literature review about previous ship simulators and the mathematical modelling used for every block of the developed ship simulator.

Chapter 4 shows the implementation of the mathematical equations presented in Chapter 3 into MATLAB/Simulink to develop the ship simulator and it includes a validation of calm water resistance block as well as verification and validation of added resistance block, propeller block, manoeuvrability block and power block. Moreover, an overall validation of the developed ship simulator is also included. Chapter 5 and 6 comprise the simulation results of the test cases that are performed using the developed ship simulator discussed in Chapter 3 and 4. Chapter 7 introduces the conclusions which includes a likely plan of the future work to be done as well as the novelty and contributions. Appendix 1 shows the existing marine fuel cell projects and demonstrations from year 2000 and Appendix 2 contains miscellaneous calculations.

Chapter 2

Hybrid Fuel Cell Propulsion

2.1 Introduction

A marine hybrid propulsion system can be defined as a system that has more than one type of power source for propulsion or the system that can run the propeller mechanically or electrically depending on the required power and speed. Hybrid propulsion systems aim to make the best use of its power sources by optimising the propulsion efficiency and the operating points of its power sources in their regions of highest efficiency. Power sources can be diesel engines, steam turbines, gas turbines, fuel cells, batteries, capacitors, etc. Moreover, hybrid propulsion systems are more flexible than conventional systems because multiple power sources can be used; e.g. propeller can be driven mechanically or electrically depending on the operational load which results in more economical and reliable systems. Hybrid systems have also more redundancy and less noise. However, for the same reasons of multiple power sources, hybrid propulsion systems can be more complex and it requires developing of an energy management plan to optimally control the hybrid propulsion system and in some cases it requires more space or weight as will be discussed. As diesel engines dominate the marine propulsion systems, an overview of hybrid diesel engine propulsion systems is first presented.

2.1.1 Hybrid Diesel Propulsion Systems

Diesel engines (DE) can be used in hybrid propulsion systems in different architectures and different modes. For example, a propeller can be driven by mechanical or electrical power delivered by DE using Combined Diesel eLectric Or Diesel (CODLOD) or using both of them in a Combined Diesel eLectric And Diesel (CODLAD) as shown in Figure 2.1. These systems have been developed for an Anchor Handling Tug Supply (AHTS) vessels in order to minimize the fuel consumption and emissions [70].

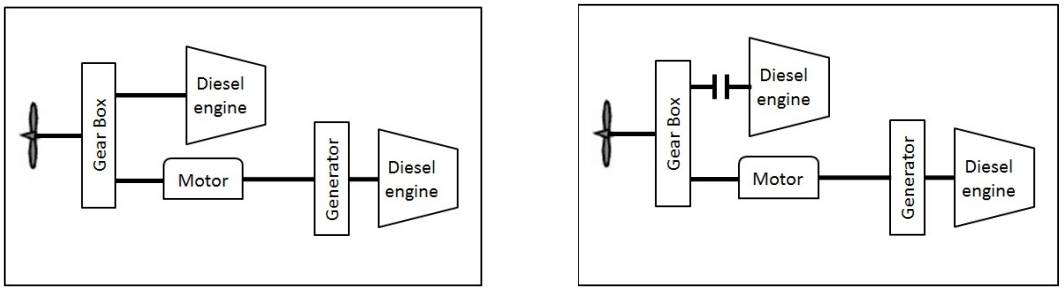

(a) CODLAD configuration (b) CODLOD configuration

Figure 2.1: Different hybrid diesel propulsion systems

DE can be combined with batteries as investigated for bulk carriers showing flexibility, fuel saving and emission reduction [71]. DE has also been studied to be combined with wind sail-assisted technology in a hybrid propulsion system for the sake of reducing fuel consumption and emissions [72]. Moreover, a conceptual design of a hybrid diesel generator and a fuel cell has been developed for an Offshore Supply Vessel (OSV) to fulfil the new IMO environmental regulations [73].

For fast vessels propulsion including military ships, Combined Diesel eLectric And Gas turbine (CODLAG) and Combined Gas eLectric Or Gas turbine (COGLOG) have been studied by the Royal Navy proving reliability and flexibility. However, hybrid COGLOG system required 40% more space and weight and 30% more annual fuel consumption than the mechanical system for their conventional combatant [74]. A Korean Navy study showed that CODLAG would result in better fuel efficiency by 11 % for a typical operating profile of a destroyer class naval ship but with higher maintenance cost [75]. For a Dutch Navy's destroyer, CODLAG combined with batteries resulted in achieving top speed with less prime movers in an investigation to replace its current propulsion system [76].

As can be noticed, diesel engines play a key role in hybrid propulsion systems as well as conventional propulsion systems and that is due to its advantages such as using inexpensive heavy fuel oil, higher efficiency, lower fuel consumption and higher reliability, system power density and lifetime as shown in Table 2.1 compared to other types of power sources such as gas turbine, steam turbines, petrol and Stirling engines [77–79]. Therefore, the propulsion system for more than 99 % of large commercial vessels use diesel engines [80].

However, diesel engines operation results in harmful emissions such as CO, CO_2, PM, NO_x, SO_x and unburned hydrocarbons. Also below 50% of the engine maximum continuous rating, the efficiency of diesel engines drops fast which results in higher fuel consumption and higher emissions because of the inefficient combustion [86]. As a result, advanced combustion technologies, emissions control and reduction systems gain attention to improve diesel engine efficiency and reduce its emissions. However, the

Table 2.1: Comparison of different power sources [26]

	diesel engine	Turbine generator	Photo voltaic	Wind turbines	Fuel cells
Efficiency (%)	35 48-51 [77]	29-42	6-19	25	40-60 25-70 [27]
Capital cost ($\$/kW$)	200-350 500 [67]	450-870	6600	1000	50-10000
Operation& ($\$/kW$) Maintenance cost	0.005-0.015	0.005-0.0065	0.001-0.004	0.01	0.0019-0.0153
Lifetime (years)	30 [81]	20-35 [82]	20-30 [83]	20 [84]	0.5-5 [28] 5-10 [85]

addition of these systems increases the first and operational costs of diesel propulsion systems. Also, diesel engine technology is mature and it reaches its physical limits so, improving its efficiency becomes harder and harder and environmental regulations become more stringent so using different technologies or fuels must be considered.

Hybrid propulsion systems has been studied for different ship types such as tankers, bulk carriers [71], tugs [87], military vessels [74–76], OSV [73], AHTS [70], ferries [76], Liquefied Natural Gas (LNG) carriers [88], etc. resulting in more economical, flexible and reliable systems with lower emissions and noise. However, in some cases, hybrid propulsion systems required more space, weight, it was more complex or it had higher first cost compared to the conventional propulsion system. For example, less than 2% weight addition was required to add batteries to the propulsion system of a tanker however, battery power would be sufficient to enter and leave harbours which would eliminate emissions problem in port areas [76]. For a bulk carrier, using hybrid propulsion systems would result in an increase of the overall efficiency by a value between 2% and 10% which would result in a fuel saving up to $ 1.27 million per year [71].

Since ships have different routes, functions, operating profiles and captains, and because there are different power sources, many hybrid propulsion system configurations can be designed to suit each case. Hybrid propulsion systems design depends on ship's type, operational profile, its class, route, and function. So, there is no certain type of hybrid propulsion system that is perfect for a certain type of ships. However, some studies showed that hybrid propulsion systems is more efficient for ships with larger variation in speed profile such as OSV or for ships having relatively short voyages such as ferries and passenger boats. Also, using conventional power sources in hybrid propulsion system is insufficient to solve the emission problem especially for ships working in ECAs or ports which requires using a more clean power source such as fuel cells [76; 87; 70].

2.1.2 Hybrid Fuel Cell systems

Hybrid fuel cell propulsion systems which combine a fuel cell and an energy storage system have been used successfully in different applications such as automotive industry which contributes to higher efficiency and reduced CO_2 emissions [89]. These systems combine the high energy density of fuel cells and the high power density of storage systems which leads to higher efficiency, lower fuel consumption and emissions [90; 73].

In these systems fuel cells are used to generate electricity from fuel such as hydrogen or methanol depending on fuel cell type and the generated electricity is used in propulsion using electric motors or used to charge the energy storage system which can be a battery or a capacitor. The efficiency and behaviour of these systems depend on the degree of hybridization and the control methodology used [91] which is considered a main focus of this research. There are two basic categories of hybrid fuel cell propulsion system; series hybrid and parallel hybrid as shown in Figure 2.2.

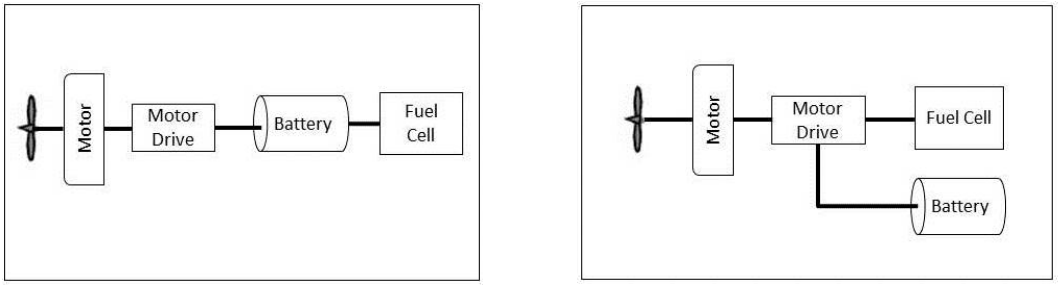

(a) Series hybrid fuel cell electric propulsion

(b) Parallel hybrid fuel cell electric propulsion

Figure 2.2: Hybrid fuel cell propulsion systems architecture

In this chapter different fuel cell types and applications are presented focusing on the fuel cell marine applications in order to identify the most suitable fuel cell type for marine applications. Also, different energy storage devices are discussed.

2.2 Fuel Cells

Fuel cells are electrochemical devices that convert the chemical energy of fuel directly to electricity via electrochemical reactions without any conventional combustion. In 1839, William Grove developed the first fuel cell; he demonstrated that using two platinum electrodes fed with hydrogen and oxygen, an electric current was generated [28; 7]. However, in 1838 Christian Friedrich Schönbein discovered the principle of fuel cell by observing its effect shortly before William Grove. Electrochemistry itself was discovered in 1791 by Luigi Galvani when one of his co-workers was dissecting a frog.

Fuel cells consist of two electrodes, an anode and cathode, separated by an electrolyte. An example of fuel cell construction is shown in Figure 2.3. Hydrogen is supplied at the

anode where it is oxidised releasing electrons and oxygen is supplied at the cathode where it is reduced reacting with electrons taken from hydrogen according to Equation 2.1. The ions travel through the electrolyte and electrons flow in the external circuit producing electric current.

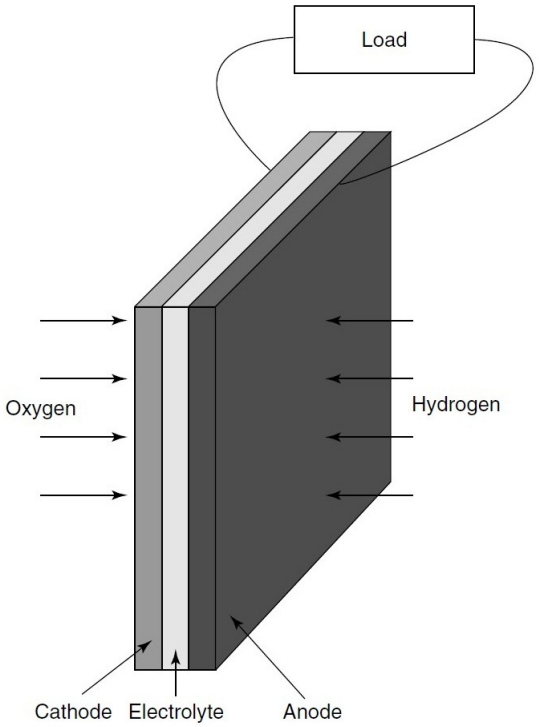

Figure 2.3: Basic cathode-electrolyte-anode construction of a fuel cell [7]

$$\begin{aligned} O_2 + 4e^- + 4H^+ &\rightarrow 2H_2O && Cathode \\ 2H_2 &\rightarrow 4e^- + 4H^+ && Anode \end{aligned} \tag{2.1}$$

Fuel cells may be classified according to their temperature; low (10 to 80 °C), intermediate (120 to 200 °C) and high temperature fuel cell (650 to 1000 °C) but normally fuel cells are classified according to their electrolyte type [28]. Different types of fuel cell includes:

- Proton exchange membrane fuel cell (PEMFC) which works at low temperature and has a solid polymer electrolyte.
- Solid oxide fuel cell (SOFC) operates at high temperature which means there is no need to use expensive catalysts.
- Alkaline fuel cell (AFC) was used in the Apollo Orbiter craft but it is very sensitive to CO_2.
- Phosphoric acid fuel cell (PAFC) whose electrodes are porous was the first to be commercially produced.

- Molten carbonate fuel cell (MCFC) which has liquid electrolyte and works at high temperature.
- Direct methanol fuel cell (DMFC) that uses methanol as a fuel.

These types of fuel cell have different efficiencies and operate at wide range of temperature as shown in Table 2.2.

Table 2.2: Types of fuel cells [27]

Type	**Temperature °C**	**Efficiency %**
AFC	50 - 90	50 -70
PAFC	175 - 220	40 - 45
MCFC	600 - 650	50 - 60
SOFC	800 - 1000	50 -60
PEMFC	60 - 100	40 - 50
DMFC	50 - 120	25 - 40

A fuel cell system consists of a fuel cell stack which contain hundreds of combined fuel cells to increase the amount of electricity generated and an auxiliary components or Balance of Plant (BOP). BOP systems include fuel supply, oxidant supply, water management, heat management, power conditioning, instrumentation and controls such as sensors, controllers, etc. Fuel cell technology can be used in different applications such as portable, stationary and transportation applications as will be discussed later which makes it a promising substitute for conventional power sources. Fuel cells can also be used in harsh operating environment for military applications as well as civilian applications. Table 2.1 shows a general comparison between fuel cells and other power sources.

2.2.1 Advantages of fuel cells

- Fuel cells offer better fuel efficiency as shown in Table 2.2 which is higher than conventional thermal power plants, which are limited by Carnot efficiency, by a factor of 2 [28]. This is because fuel cells convert the chemical energy to electrical energy directly without converting it to mechanical energy first.
- Part load applications will also make use of fuel cells because fuel cells maintain high efficiency across most of their power range unlike turbines and internal combustion engines (ICE) [92].
- Fuel cells have lower air emissions than marine diesel engines or gas turbines as fuel is reformed first in fuel supply system of the fuel cell. Moreover, in case of using pure hydrogen, only water and heat are the emissions of fuel cell [67]. Also, using

hydrogen or natural gas as a fuel will reduce the oil pollution caused by leakage during fuelling or illegal discharge of oily wastes produced during the operation.

- Fuel cells can be used in air independent propulsion systems for submarines and underwater vehicles applications.
- Quiet operation since fuel cell has no moving parts except for noise produced by auxiliary equipment which means less need for noise insulation and will reduce the harmful impacts of noise on marine life. This impact made MEPC in its 58th session agreed to the development of a new work program agenda to reduce the incidental noise from commercial shipping operation [53].
- Waste heat of fuel cell generated by the electrochemical reactions can be used in cogeneration and trigeneration systems using organic Rankine cycles, chillers, etc. which can increase the overall efficiency of some systems to close to 90% [93].
- Fuel flexibility because hydrogen, which is the main fuel of fuel cells, can be produced from many sources including renewable energy which can be used to generate hydrogen, beside some fuel cells can use methanol or ethanol as a fuel.
- Lower maintenance and operation cost as there are no moving parts which makes fuel cells simple to operate. For example, for periods of one year or more, several PAFC systems have run continuously with little maintenance requiring human intervention [7].

2.2.2 Disadvantages of fuel cells

- Capital cost of fuel cell is higher than other options as it is a new and commercially limited technology but the mass production of fuel cell and the grow of hydrogen infrastructure will solve this problem. The capital cost of fuel cells lies between $ 50 to 10,000 /kW depending on its technology [28]; for MCFC, the capital cost was about $ 1500/kW versus $ 500/kW for medium speed diesel engines [67]. For PEMFC, the fuel cell stack cost is $ 180/kW [94].
- Periodic replacement is required for fuel cell stack after about 5 years of use [28]; so, life time of fuel cell may be a negative factor but R&D areas are to be focused on increasing the life of some fuel cell stack life to 10 years [95].
- Fuel cells have a time-delayed response because of its electrochemical reaction slow dynamics which is why most fuel cell systems need energy storage devices to provide additional power during peak demands and absorb excess energy during low power demand [96].
- Hydrogen is not a readily available fuel and its generation from renewable energy sources is still lower than its generation from non-renewable sources because of

the higher cost and the lower efficiency of renewable energy power plants. Also, its infrastructure is not ready yet but the number of hydrogen fuelling stations is increasing [9].

2.3 Applications of Fuel Cells

Due to the advantages of fuel cells, this technology has been used since the Fifties in the space industry after the demonstration of the first 5 kW AFC by Francis Bacon at Cambridge University [26]. Fuel cell power systems have attracted attention and become important for a wide variety of applications with a wide range of power including portable power, transportation power, stationary power such as distributed power generation (grid and non-grid concept applications), and power for buildings [97].

2.3.1 Portable Applications of Fuel Cells

When we say portable power, we mean systems that generate a power range from few Watts to a few hundreds and can be transported by a person such as power for electronic devices like laptops and mobile phones instead of batteries, power for camping, lighting instead of electrical generators, and power for military applications for field operations. For many of these applications, PEMFC and DMFC are well suited [98–100] because of their simple construction and low operating temperature. Compared with generators, fuel cells work quietly and emit lower emissions. Compared with batteries which are approaching practical energy density limits, fuel cell can offer higher energy density [28], the recharging is eliminated, and fuel cell portable systems can be smaller in weight and volume for an equivalent amount of energy because of the hydrogen higher energy density by weight and volume compared to batteries as shown in Figure 2.4 [8].

2.3.2 Stationary Application of Fuel Cells

Unlike transportation and portable applications, most stationary applications operate continuously at their high efficiency region. Stationary applications include commercial, industrial, residential applications and electricity generation as supplement or replace power. The power ranges from 1 kW for backup power to multi-megawatts for large power generation systems.

There are four fuel cell types that are making commercial progress more than other technologies which are PEMFC, PAFC, SOFC and MCFC [101]. PEMFC are used for backup power due to its rapid start-up or for residential applications to provide electricity, heat and hot water in a combined heat and power (CHP) or cogeneration system. In Germany, *Viessmann* developed a PEMFC system for residential applications

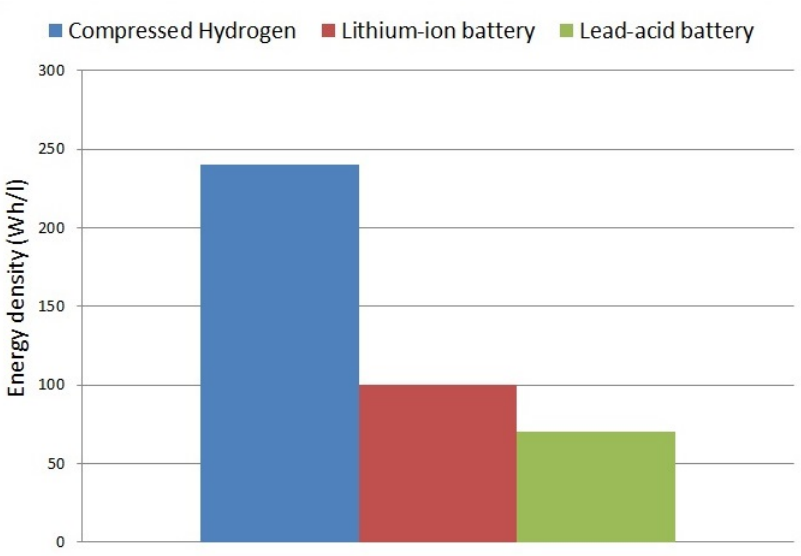

(a) Storage energy by volume

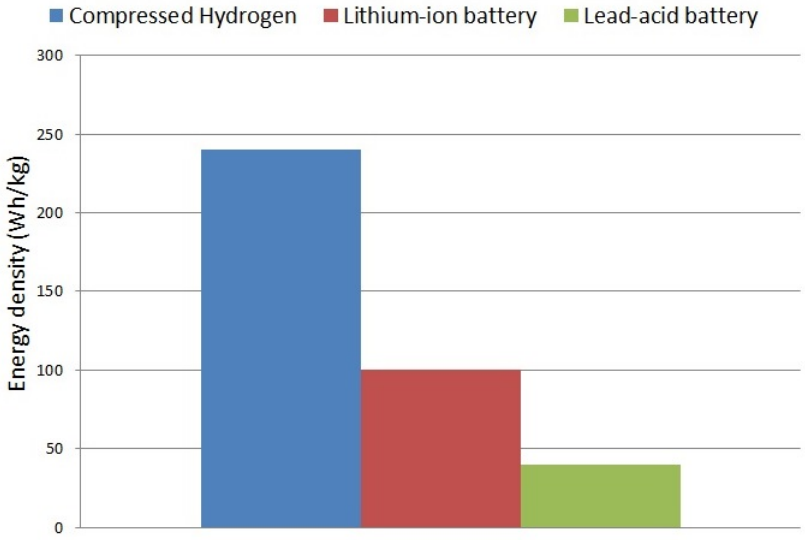

(b) Storage energy by weight

Figure 2.4: Compressed hydrogen energy density compared to lithium-ion and lead-acid batteries [8]

with overall efficiency of 76% [102]. In Japan, *Ballard Power Systems* has developed a 1 kW system to supply electricity and heating with electrical efficiency of 42% and overall efficiency of 85% using cogeneration [8]. For a residential application in Malaysia, using PEMFC cogeneration systems can result in 30 to 40% saving in its primary energy use [103].

The high temperature fuel cell systems such as SOFC and MCFC can be used in a combined cycle to generate electricity using their high temperature exhaust gases in distributed power plants; plants are located near the consumer, as primary power. SOFC and MCFC are more suitable for large-scale power plants than low temperature fuel cells,

but the starting time of these systems are higher. Moreover, high temperature fuel cell systems have the ability to work without external reforming of fuel which is normally natural gas [98]. High temperature fuel cells can be used in trigeneration systems or combined cooling, heating and power systems (CCHP) producing electricity, heating and cooling for houses, hospitals, etc. which increase the overall efficiency of the system. These systems can be in a small scale (below 1 MW_e) or large scale.

Using SOFC and absorption chiller in a trigeneration system can achieve a power and heating efficiency of 84% and power and cooling of 89% [104]. Another study proposed SOFC combined with gas turbine (GT) in a trigeneration power plant that based on ammonia-water mixture showing an efficiency of more than 80% [105]. The Swiss company *Hexis Ltd.* tested 17 SOFC micro-CHP systems in field with a continuous operation of more than 13500 h showing a power degradation rate of 1.6%/1000 h. Some tests showed 36% net alternating current (AC) efficiency while another test showed a total efficiency of more than 90% [106]. *Ceramic Fuel Cells Ltd.* demonstrated a world record of 60% net AC efficiency in 2009 using SOFC system fuelled with natural gas and a total efficiency up to 85% [107]. MCFC hybrid system with gas turbine can reach an electrical efficiency of 58.5% for a 148 kW power generation [108].

PAFC is more attractive for small-power generation because its start-up time is lower than that of high temperature fuel cells. Also, PAFC operating temperature is high enough to generate steam which can be used in steam reforming [109]. In Germany, PAFC power plants were used for producing electricity and air conditioning in summer for the St. Anges Hospital in Bocholt with working rate of 8000 h/year and another PAFC power plant used in residential area in Germany surpassing 40,000 h of operation in 2004 [110]. As shown in Figures 2.5 and 2.6, there is a continuous growth in number of fuel cell shipments exceeding 70,000 units in 2015 especially in stationary applications and a growth in shipped megawatts exceeding 350 megawatts in 2015 [9].

2.3.3 Transportation Applications of Fuel Cells

Many countries have invested billions of dollars in developing fuel cell systems for use in transportation applications. Their motivation is to make use of fuel cells' low emission operation, high efficiency, low noise and vibration operation. Transportation applications include light duty vehicles, vans, trucks, trains, trams, marine transportation and even in air crafts. Automakers in many countries have supported the research work into the development of fuel cell to use it in fuel cell vehicles (FCV) because fuel cells are considered as the best replacement for ICE [98; 111]. Fuel cells can be used as prime powers or as auxiliary power units (APU) with focus on two types of fuel cells which are PEMFC and SOFC due to their solid electrolyte [112–114].

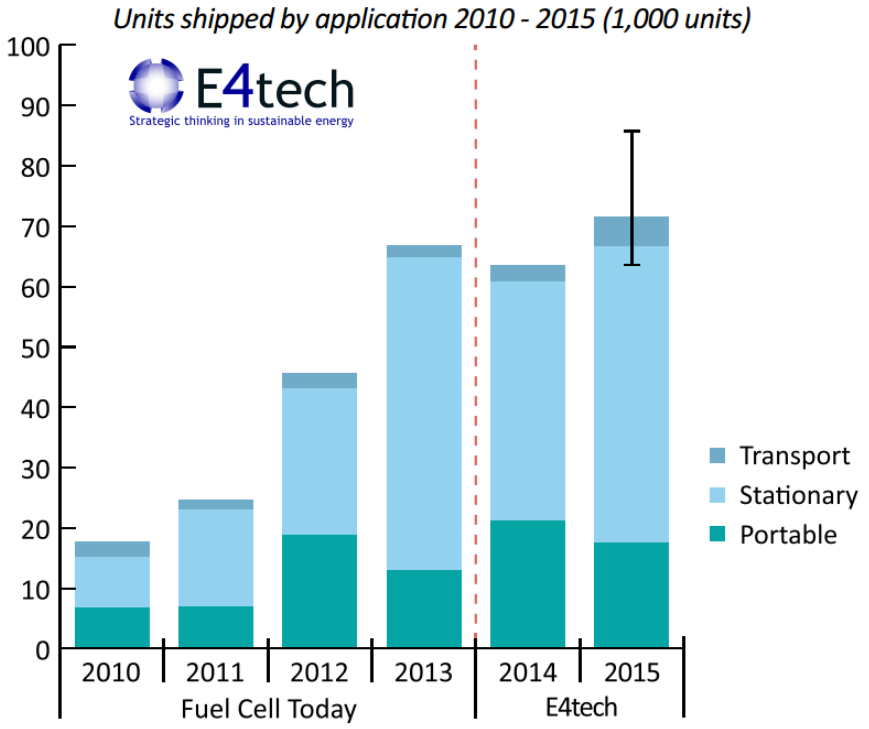

Figure 2.5: Fuel Cell Shipments by Applications [9]

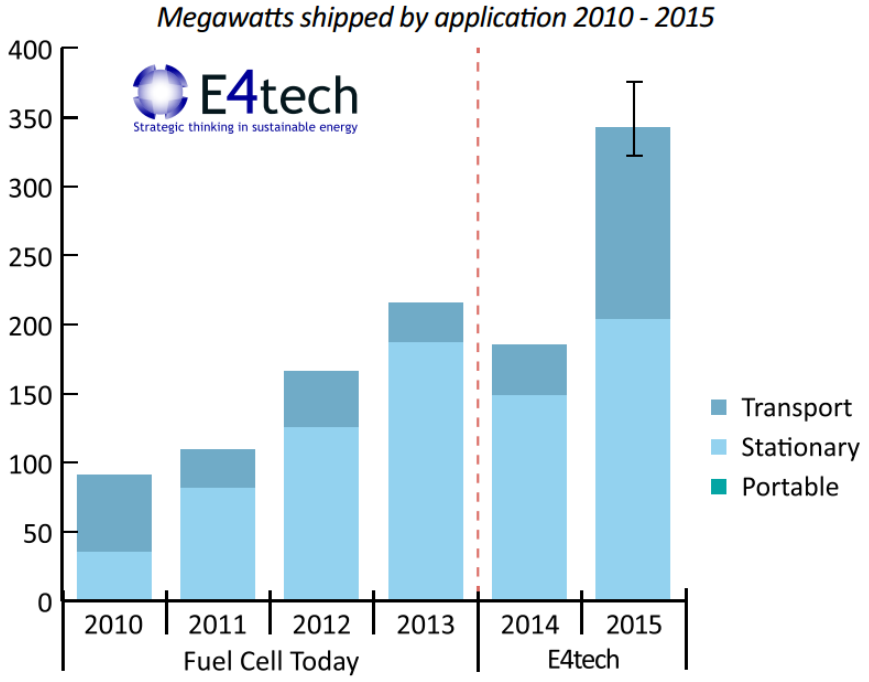

Figure 2.6: Fuel Cell Megawatts by Applications [9]

PEMFC is considered as the most promising type because of its low operating temperature which means quick start-up, its high efficiency, high power density, low corrosion and its solid electrolyte which make it a suitable replacement for ICE in cars, trucks, etc. [115; 116]. Many barriers to the commercialization of PEMFC are close to be solved as a density of 1.35 kW/litre has been demonstrated [98] and the cost of automotive fuel cells can be reduced as shown in Figure 2.7 from \$275/kW in 2002 to \$47/kW in 2012 which is more than 80% reduction with a target of \$30/kW in 2017 [10].

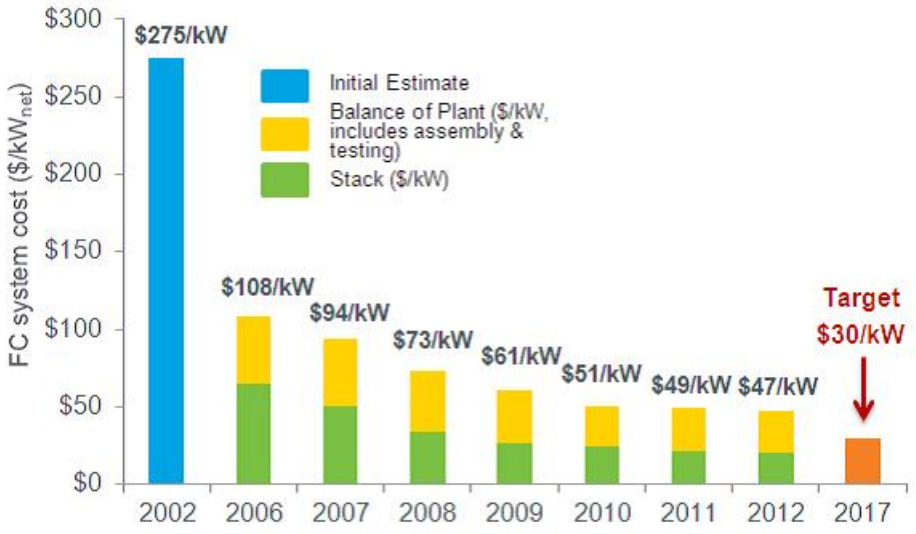

Figure 2.7: Modelled cost of an 80-kW_{net} PEM fuel cell system based on projection to high volume manufacturing (500,000 units/year) [10]

SOFC with its high temperature is also suitable for automotive applications as APU because SOFC high temperature gives the potential for internal reforming of hydrocarbons fuels to generate hydrogen-rich gas for fuel cell [111; 117]. Besides high temperature of operation, there are other advantages of SOFC such as high efficiency, no expensive catalysts are required, high power density and fuel flexibility [118].

Buses, tramways and locomotives have been studied as users of fuel cells combined with batteries in some cases to recover the energy during braking and to supply additional energy during acceleration. This hybrid fuel cell/battery system was proposed for a tramway showing its capability of achieving the real driving cycle [96]. For locomotives, the hybrid fuel cell system couldn't fully reach their potential because of the lack of available energy during braking which will require either a reduction in operating time, or an increase in the fuel capacity [119]. Another study on hybrid fuel cell locomotives found out that scaling up the vehicles would result in more challenges regarding hydrogen storage, heat transfer and shock loads [120].

Buses on the other hand are considered as a good strategy to commercialise fuel cells because of their well-defined duty cycles, visible in the community and have room to accommodate the fuel cell power system. The number of fuel cell buses has increased

from around 65 in 2003 worldwide [121] to over 110 hybridised fuel cell buses in 2011 [122] which raises the number of hydrogen refuelling stations to 215 by the end of 2011, 85 of them in Europe and 80 in North America [123].

PEMFC and SOFC have also been studied to be used in aircraft to make use of their advantages which are very important for the comfort of passengers such as the quiet operation, high efficiency and reduction in emissions. Commercial aircraft such as Boeing and Airbus examined the use of fuel cell for on-board electrical power generation. NASA also has studied fuel cell use for aircraft. Results from Boeing showed a 20% reduction in fuel consumption and 60% reduction in noise using fuel cells [124; 125].

Using fuel cells in marine transportation applications has been also done and demonstrated showing promising performance since the Sixties. From yachts to ferries, submarines, tugs, offshore and merchant vessels utilize fuel cell technology successfully which will be discussed in detail in the following section.

2.4 Marine Applications of Fuel Cells

Efforts have been made to design the so called Green Ships in order to protect the environment and earth's climate and try to alleviate the energy crisis. Using hydrogen as a fuel for fuel cells could achieve the goal of a zero-emission ship. Cruise ships, ferry boats, tugs, offshore supply vessels, submersibles, powered barges and submarines are all candidates to use fuel cells, even offshore oil platforms and isolated systems such as refrigerated containers on container ships are suggested to use fuel cell [126–128].

Fuel cell systems can be used for main propulsion power, electric power generation for the ship as APU, or for emergency power supply. It has been used in marine applications since the 1960s and many programs were carried for the design, development and production of fuel cells to be used in marine applications. Marine applications of fuel cell in the literature includes submarines, AUV, passenger ships, ferries, sail boats, yachts, whale watching boats, research vessels, OSV, car carriers, and merchant vessels. Many overviews concerning fuel cells marine applications were made due to their advantages discussing different types of fuel cell and the possibilities of using it onboard ships which would help in speeding the commercialization of fuel cells [126; 129–132].

R&D efforts concentrate mostly on three types of fuel cell to be used in marine applications which are PEMFC, MCFC and SOFC. A life cycle and cost analysis of using these three types of fuel cells was performed in the framework of FCSHIP project for two case ships, a 140 m Ro-Ro fast ferry and a 30 m ferry using natural gas as fuel. This study showed an environmental improvement by 20-40% but, economically, cost needs to be reduced to make fuel cells more competitive with conventional power sources [133]. Another life cycle assessment of MCFC plant for marine application was

made with an environmental comparison to diesel engines onboard a passenger ferry for auxiliary power generation where the MCFC used diesel oils with a reformer as a fuel. This study showed that the emitted pollutants' amount from the MCFC plant were very small compared with the diesel engines [134].

The first marine MCFC was installed onboard '*Viking Lady*' the offshore supply vessel. It has been modelled thermodynamically to show the electrochemical reactions and heat transfer phenomena within layers and the model was calibrated and validated using measured data collected onboard from the MCFC unit which resulted in a low prediction error of 4% [135]. Another thermodynamic and economic model was made for a PEMFC onboard merchant ship using hydrogen as fuel to study the performance of the system [136]. For small ship applications, PEMFC combined with supercapacitor hybrid system was modelled dynamically where an emulator was used successfully to imitate the PEMFC behaviour during simulations [137].

PEMFC has been studied for APU operation onboard sailing yacht using LPG as a fuel achieving a total system efficiency of 25% [138]. Also, PEMFC was suggested as a candidate to replace batteries in a US destroyer which resulted in higher efficiency, fuel saving and a reduction in emissions [139]. An exergy analysis of PEMFC and DMFC systems was made for marine applications on surface ships and submarines using hydrogen generated from methanol to show the exergy losses in each unit of the fuel cell system [140].

CHP systems for shipboard applications were studied using PEMFC and SOFC which increase the overall efficiency [141–143]. SOFC was dynamically modelled in some studies to be used on marine applications combined with batteries [144], and combined with Rankine cycle for underwater propulsion [145]. Heat recovery options for SOFC onboard ships as APU were studied using WTEMP software; the study showed 5% increase in efficiency and 12% reduction in energy cost but more studies are needed to focus on the safety of fuel cell operation which needs more demonstration projects [146].

SOFC combined with GT in a trigeneration system for marine applications was examined with a thermodynamic model to analyse four proposed configurations to drive the heating, ventilation and air conditioning (HVAC) systems using single and double effect absorption chiller which raise the efficiency from 12.1% for the conventional system to 34.9% for the system with single effect absorption chiller and 43.2% for the system with double effect absorption chiller which make the overall efficiency of the trigeneration system higher than systems with waste heat recovery [93]. Also, a conceptual design of a SOFC and diesel generator system has been proposed in [73] for a platform supply vessel to fulfil the new IMO environmental and SECA regulations.

2.4.1 Fuel Cell Programs and Projects

2.4.1.1 USA

Quiet operation and high efficiency attracted attention to fuel cell power especially in submerged vessels such as submarines and submersibles. In the 1960s, the US navy has supported fuel cell development to use it in small submersibles and submarines as fuel cells enable greater endurance of submerged vessels. The world's first fuel cell powered submersible was in 1964 named STAR I tested in the marine research laboratory of Connecticut's University and the fuel cells produced 750 Watt [147]. In 1978, *Lockhead Missiles & Space Systems* tested an AFC of 30 kW on board a deep submergence search vessel called *Deep Quest* which made about 50 successful dives with its fuel cell power system [128]. The Office of Naval Research (ONR) has a fuel cell program to focus on solving research gaps to meet the requirements of naval platforms and systems using Jp-5 and Jp-8 logistics fuels to reduce fuel cost. The ONR program has expanded to cover power applications of portable, unmanned vehicles and mobile power fuel cell applications [148].

In 1994, the feasibility of fuel cells for use in propulsion application was investigated by the US Coast Guard because of the Clean Air Act Amendments of 1990 law to reduce the emissions by non-road vehicles including marine vessels. US Coast Guard plan selected *CGC VINDIATOR* as a fuel cell demonstration platform to replace its diesel electric generators. MCFC was selected to be used with NATO F-76 diesel fuel. Fuel cell power was slightly higher than diesel electric configuration and the results were higher efficiency of the system, which meant greater vessel range, and 14.7 LT less weight because of the removal of exhaust stack and sound insulation which resulted in small increase in speed [130]. A container vessel with 434 TEU was selected to use fuel cell in an investigation by the US Maritime Administration (MARAD) in 1998 with a total power of 5440 kW but this project used natural gas as a fuel instead of diesel oil which is cheaper [130]. A marine fuel cell market analysis was done by US Coast Guard R&D centre to assess the potential of PEMFC and MCFC in the market showing that fuel cell can capture a significant marine market if the life cycle cost of fuel cells is economically competitive with conventional sources of power which can be made by mass production and advances in materials [149].

In 1997, ONR initiated a program to demonstrate a fuel cell power generation module called Ship Service Fuel Cell (SSFC) with 3 phases; phase I finished in 2000 generating two conceptual design of 2.5 MW_e SSFC using MCFC from *FuelCell Energy* and PEMFC from *McDermott Technology* and *Ballard Power Systems* fuelled by NATO F-76 diesel fuel by reforming it and removing sulphur. The conclusion of phase 1 was that both systems were suitable for shipboard applications[114; 150; 151]. In phase II, a detailed design and fabrication of SSFC module of 625 kW using MCFC and 500 kW using

PEMFC were done. A dynamic simulation model and factory testing were made for this module and phase II ended by 2004. Phase III was in 2005 and it was a demonstration of MCFC power system at sea using diesel fuel in the marine environment and the requirements of ship service power was successfully met [152; 153].

FuelCell Energy engaged with US Department of Energy (DOE)/ONR in a shipboard fuel cell workshop to develop high temperature PEMFC stacks for shipboard applications as APU and it was concluded that HTPEM stack experience can be advanced to demonstration. Also, in this workshop SOFC was studied to be used in torpedo systems because of its high efficiency. The proposed power will depend on the torpedo's length that 5kW for 13", 8 kW for 18", 10.7 kW for 22" and 16 kW for 33" length [154]. SOFC technology is also being adapted for use in advanced unmanned undersea vehicles (UUVs) by the US ONR because of its fuel flexibility and high efficiency. Size limits, rapid start-up and shut down, air-independent operation and refuelability are challenges facing SOFC to be used in UUV that's why in 2012 ONR gave a contract to *NexTech Materials Ltd.*, and other companies to develop SOFC technology. Also in 2012, ONR gave *FuelCell Energy* a contract under the Large Displacement Unmanned Underwater Vehicle Innovative Naval Prototype program to develop SOFC-based systems [155].

Millennium Cell Inc., *Anuvu* and *Duffy Electric Boat Company* teamed up in 2003 in a demonstration project for California's Centre for the Commercial Deployment of Transportation Technologies (CCDoTT) to use PEMFC in a water taxi for 18 passengers called *Duffy-Herreshoff 30* using hydrogen as a fuel and the water taxi served successfully in public 10 to 12 hours daily [148; 156]. Another PEMFC marine application is a student project at Rensselaer Polytechnic Institute in 2009 used two PEMFC 2.2 kW units in a 22' boat called *New Clermont* running on hydrogen with zero-emissions sailed successfully from New York City to Albany [157].

2.4.1.2 Canada

Since the 1980s, the Canadian Department of National Defence (DND) has engaged in a program to develop PEMFC technology to be used in submarines. *Ballard* built and tested a 40 kW PEMFC power plant to be used in Canadian submarines using a fuel processor to utilize diesel fuel. *Ballard* also awarded a contract to build an air-independent fuel cell propulsion system with a power of 3 kW to power the Perry PC-14 submersible in 1989 [148; 158].

2.4.1.3 Europe

The United Kingdom has generated considerable recent research interest on fuel cell and hydrogen applications. In 2007, the hydrogen-powered fuel cell boat *Ross Barlow* was

constructed at the University of Birmingham as a part of the Protium Project. *Ross Barlow* is a waterway maintenance boat that uses PEMFC technology hybridized with lead-acid battery and the ship is used as a testing facility for fuel cell and new hydrogen storage materials [148]. The UK first fuel cell passenger ship named *Hydrogenesis* also uses PEMFC technology to have a zero emission marine transportation system. A hydrogen fuelling station was built for this ship which works around Bristol Harbour with a capacity of 12 passengers [159]. More than 10 hydrogen fuelling stations are available now around the UK and the number is expected to be 65 stations by 2020. Also, there are several UK fuel cell applications of yachts, sail boats and rowing boats which use methanol as a fuel using DMFC technology as APU for navigation and communication units [160–162].

Due to its silent operation, PEMFC, developed by *Siemens*, was used in non-nuclear submarines built by *Thyssen-Krupp* Marine Systems *Howaldtswerke-Deutsche Werft* (HDW) shipyards. HDW's first submarine class 212A entered the service with the German Navy in 2005 with a 1450 tonne surface displacement and 56 m long. There is another German submarine class which is 212B with a power of 240 kW uses PEMFC technology [148; 150; 163]. These vessels have been used by Italy, Greece, Sweden, Norway, Portugal and Turkey Navy forces beside Germany. HDW's submarine class 214 was launched in 2005 with the Greek Navy's *Papanikolis* with a length of 65 m and a displacement of 1700 tonnes. Class 212A provides power up to 300 kW and class 214 provides power up to 240 kW. Both classes use liquid oxygen and hydrogen stored using metal hydride giving submerged endurance of two to three weeks [148].

The Spanish Navy has its own submarine program; S-80 built by *Navantia SA* in its *Cartagena* shipyard using PEMFC technology with a power of 300 kW but to be operated on reformed ethanol and oxygen. S-80 was designed for coastal protection with 2400 metric tonne displacement. PEMFC technology was used by Germany in Autonomous Underwater Vehicle (AUV) project called *DeepC* in 2004 with a fund of US$3.7M provided by the German federal research ministry. The applications of *DeepC* were underwater inspection of cables, oil and energy lines, sea bed examination and oceanographic research [164].

Another PEMFC system developed by *Ballard* was used by *MTU Friedrichshafen* in 2003 to power a 12 meter yacht with a power of 20 kW fuel cell/battery system. The system is fuelled by compressed hydrogen and works at a speed of 6 km/h with a range of 225 km while at a speed of 12 km/h, the range is only 25 km. The yacht was tested on Lake Constance in Germany and this yacht is the first fuel cell powered craft to be certified by a Germanischer Lloyd (GL) the German classification society [163]. *Hydra* is another successful German application of fuel cell which is a boat designed for 20 passengers, 12 m long and 3 m wide developed by the *etaing GmbH Company* using AFC technology with output of 5 kW using hydrogen as fuel and atmospheric oxygen as oxidant [148]. In 1998, a 40 kW PEMFC/battery system was used in Italy to power a

90 passengers boat using hydrogen as a fuel with a range of 300 km but the boat wasn't certified because of safety concerns associated with hydrogen usage [148].

EU-Life program founded a project called *Zemship* (Zero Emission Ship) from 2007 to 2010 with an aim of testing the operation of emission-free ships on the size of commercial passenger vessels which was '*FCS Alsterwasser*'. *FCS Alsterwasser* is the first inland passenger ship with a capacity of 100 passengers, 25.46 m long and 5.36 m wide using two PEMFC modules and lead-gel batteries with an efficiency of more than 50% working in Hamburg, Germany [165]. In Amsterdam another successful fuel cell passenger ship, *Nemo H2* , was developed with a capacity of 86 passenger, 22 m long and 4.25 m wide using 30 kW PEMFC and 70 kWh battery. The ship also uses hydrogen as a fuel and it was classified by GL [166].

EU founded another project called MethAPU from 2006 to 2009 to develop and validate the use of SOFC running on methanol as APU for marine applications. The test platform in this project was a car carrier called '*M/S Undine*' which used WFC20 system developed by *Wartsila* in 2010 with an output of 20 kW [167]. FellowSHIP is another program funded by the research Council of Norway, Innovation Norway and the German Federal Ministry of Economics and Technology with an aim of developing and demonstrating the use of MCFC in marine applications. As part of this project, the 320 kW MCFC was installed and tested onboard the offshore supply vessel '*Viking Lady*' serving as APU [135].

e4ships is another project in Germany to develop fuel cell systems for seagoing vessels using HTPEM and SOFC technologies to have more climate-friendly energy supply systems [168]. e4ships project consists of two demonstration projects which are Project SchIBZ and Project Pa-X-ell. SchiBZ uses SOFC technology and diesel engines to have a diesel-operated hybrid fuel cell system using low-sulphur diesel as a fuel with an objective of reducing fuel consumption and emissions. A 50 kW SOFC system is supplied for this project to be installed onboard the merchant vessel *MS Forester* for sea trails in 2016. Using the high temperature operational gases of SOFC, it is possible to have an overall efficiency of 90% [169]. Meanwhile, Pa-X-ell project tests HTPEM fuel cell technology onborad seagoing passenger vessels using methanol as a fuel. A 90 kW HTPEM fuel cell system was installed on the Viking Line ferry *MS Mariella* to be tested under everyday condition. The results of the successful demonstration of the two e4ships projects on *MS Forester* and *MS Mariella* was presented recently in September 2016 showing the suitability and reliability of fuel cell systems for marine transportation applications [168].

Iceland has a program to become a hydrogen economy by 2030 that includes the conversion of its fishing vessels which are about 2500 vessels to use hydrogen in a fuel cell propulsion system [170]. *SMART-H2* (Sustainable Marine & Road Transport on Hydrogen in Iceland) was another demonstration project in Iceland with a goal of testing hydrogen on vehicles and vessels. The *Elding* is a 125 tonne whale watching boat which

uses 10 kW fuel cell/battery as APU for 150 passengers. The operation start date was April 2008 and compressed hydrogen was the fuel for the fuel cell system [171]. In Finland, a 300 W AFC stack was used in a boat as a demonstration presented at the Kuopio Boat Fair 2001 and the fuel cell manufacturer was *Hydrocell* [172]. Switzerland also has its own program of hydrogen and fuel cell which includes research, development and demonstration of hydrogen and fuel cell projects. One of the visible projects is a boat for 7 passengers using PEMFC technology called *Hydroxy 3000* with a power of 3 kW and a speed between 11-15 km/h. The boat is based on catamaran design and it is good for a family leisure on lakes and channels with zero noise and zero emission [148].

2.4.1.4 Rest of the World

South Korean and Brazilian Navies use fuel cell HDW's submarines Class 214 using PEMFC [150]. In Japan, Mitsubishi Heavy industries developed an AUV using PEMFC technology called *Urashima* with a length of 11 m and a continuous cruising range of 220 km in 2004 using Hydrogen from metal hydride and pure oxygen giving a power of 4 kW at 120 V [173]. Another Japanese successful application of fuel cell was *MALT'S Mermaid III* which is a 5.8 m long sail boat using DMFC for Auxiliary power using methanol as a fuel to charge lead-acid battery crossing the Pacific Ocean successfully in 2002 [148]. A partnership between the Singaporean company (*HorizonFC*) and (*Minn Kota*) from USA represented a 300 W PEMFC system into a trolling boat propelled by 1500 W electric motor in 2007 reaching 45% efficiency of the fuel cell system and a speed of 8 km/h [174]. Also, a hybrid PEMFC/battery system with an electric power of 90 *kW* was developed for a 20 m long tourist boat in Korea where the PEMFC system supplies 50 kW of the total power exhibiting its reliable operation and it is ready for future deployment [175].

Overall, there are many successful demonstration projects of fuel cell marine application and a summary table of the application is attached in Appendix 1. Beside these existing projects, there are several future design concepts of future ship using fuel cell to be more environmental friendly such as *NYK Super Eco Ship 2030* which will focus on fuel cell as a promising clean energy option with a target of zero emission by 2050 [176]. *E/S Orcelle* is the future car carrier by *Wallenius Wilhelmsen* Logistics which will combine fuel cells, solar, wind and wave power to propel the ship with zero emissions [177]. Moreover, a zero-emission fuel cell ferry has been developed by the GL subsidiary FutureShip for shipping company Scandlines to work on Fehmarn link [178]. In Scotland, the main ferry operator is planning to develop a zero-emissions car and vehicles ferry which will run on hydrogen using fuel cell. The hydrogen will be produced by wind farms near to the port where the vessel will serve. This vessel will be built within a few years with an investment of £15 million [179]. A Norwegian engineering specialist is also planning to use a 200 kW PEMFC combined with a 100 kWh batteries to replace one of the two

diesel engines of the car ferry *MF Ole Bull* to be the first hydrogen car ferry in Norway [180].

Finally, there are more than 60 identified fuel cell demonstration projects on surface ships from open literature which have been developed since 2000 and of course it is possible that there are other unlisted projects. As shown in Figure 2.8, the average of fuel cell projects is 4 each year with a significant number of projects in 2009 and the reason probably is the increasing environment awareness such as the United Nations Framework Convention on Climate Change (UNFCCC) in 2007 when representatives from more than 180 countries started on a plan to face climate change to be agreed by 2009 in next UNFCCC in Copenhagen [181].

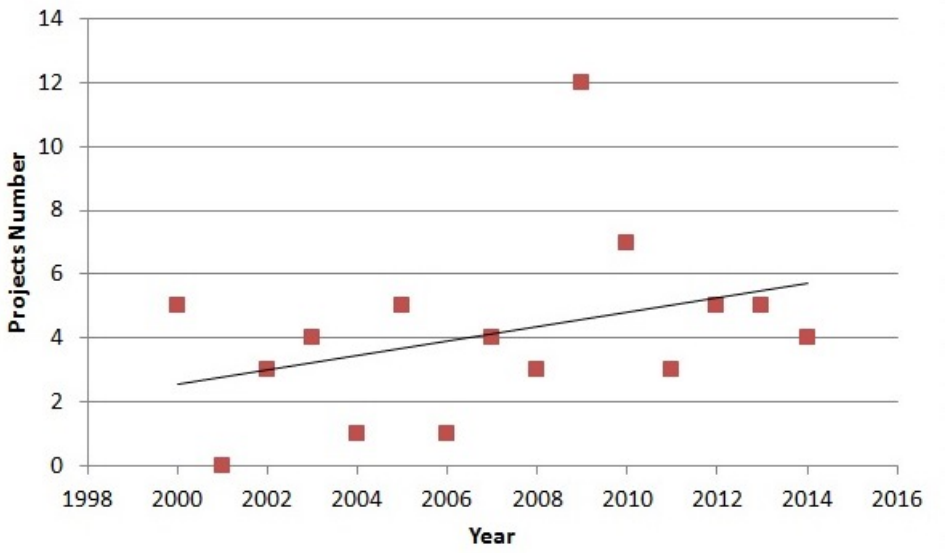

Figure 2.8: Yearly number of fuel cell projects and demonstrations

2.4.2 Guidelines for Fuel Cell Systems

Marine applications of fuel cells have developed positively and many types of ships using fuel cell such as yachts, sail boat, water taxi, car carrier, ferries, offshore supply vessels, whale watching boats, submarines, research ships and passenger ships as shown in appendix 2. That's why guidance on safety and regulations regarding using fuel cells are being demanded by clients from classification societies. As for example, Bureau Veritas (BV) and Germanischer Lloyd (GL) have made guidelines to provide safe design, operations and maintenance of fuel cell power systems onboard ships. BV guidelines apply to fuel cell which use gas as a fuel such as natural gas and hydrogen which can be stored in a gaseous state or liquid state. There are references that were used for fuel cell technology and hydrogen incorporating into BV guidelines such as ISO 23273 parts 1 and 2 in 2006 which is about fuel cell road vehicles. The BV guideline is also based on the IMO's "Interim Guidelines for Natural Gas-Fuelled Engine Installations in Ships" [182].

While BV guideline was released in April 2009, GL guideline for the use of fuel cell systems onboard ships and boats was come into force on March 2003. The first application of GL guidelines was '*No-1*' a 12 m yacht in 2003 in Germany. In 2008 '*Elding*' the whale watching ship was certified by GL in Iceland and '*FCS Alsterwasser*' in Germany. In 2009 '*Nemo H2*' in Netherlands was certified by GL [163; 166]. GL guidelines cover the full scope of a fuel cell systems. These guidelines will be refined through feedback resulting from testing these guidelines on number of projects to gain experience which will help in developing it [183].

2.5 Energy Storage Devices

Since fuel cells have a time-delayed response due to their slow dynamics, energy storage devices are usually combined with fuel cells to meet the dynamic and rapid changes in power requirement [96; 126]. Energy storage include many energies, technologies and scales and can be stored in different forms such as chemical, electrical, thermal or kinetic media [184]. For transport applications, batteries, super-capacitors, hydrogen and flywheels are being considered [185].

Batteries and electrochemical capacitors, often referred as super-capacitors or ultra-capacitor, are used for energy storage in fuel cell power plants since electricity is the fuel cell output. Both batteries and capacitors are higher dynamically than fuel cells as shown in Figure 2.9. Comparing batteries to electrochemical capacitors, batteries have slower response times and charging rates, lower power density and slower discharge cycles. However, batteries have more energy density and higher power range which is important in transportation applications that is why batteries are considered to be the main energy storage device for fuel cell applications [126; 186].

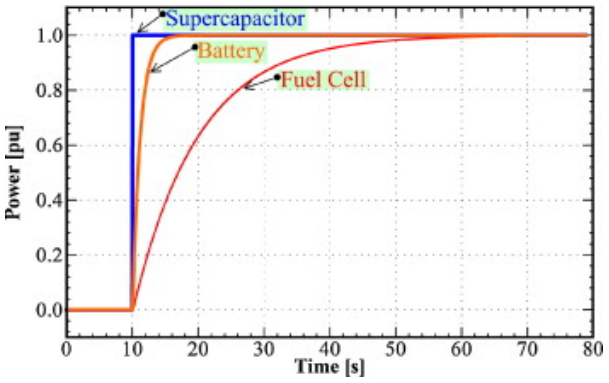

Figure 2.9: Dynamic classication of fuel cells, batteries, and capacitors [11]

Fuel cells and batteries have some 'electrochemical similarities' such as ions and electrons are transported separately and chemical processes happen at the electrode/electrolyte interface's boundaries, also both consist of two electrodes in contact with electrolyte. However, there are differences between batteries and fuel cells such as batteries are

closed systems where energy storage and conversion take place in the same cell. Fuel cells are open systems where fuel and oxidant come from outside the cell which is an advantage for fuel cells as it does not need to be recharged. As long as fuel and oxidant are supplied, it will produce electricity and a comparison between fuel cells and batteries is shown in Table 2.3.

Table 2.3: Fuel cells and batteries comparison [27–29]

	Fuel cells	Batteries
Efficiency (%)	25-70	70-90
System specific power (W/kg)	100-500	1-1000
System power density (W/l)	10-600	200-300
Lifetime of electrochemical stack (year)	0.5-5	0.1-10
Capital cost ($)	50-10000/kW	10-1000/kWh
Operating and maintenance cost ($/$kWh$)	0.1-1	≈ 0

Many studies have been conducted to investigate the use of batteries in transportation applications combined with fuel cells showing increase in fuel efficiency and consequently reduction in emissions such as trams [96], locomotives [119], vehicles [187], trucks [188] and buses [122]. The feasibility of using batteries in hybrid applications and the GHG reduction percentage will depend on the cycle efficiency of the batteries as discussed for vehicles in [189; 89]. There are different types of batteries but because of weight and space limitation of naval applications, higher energy density and lighter types have to be identified. Table 2.4 shows a comparison between different battery types.

Table 2.4: Comparison of battery types [29–35]

Type	Wh/kg	Wh/l	Durability (years)	Cost ($/$kWh$)
Lead-acid	30-50	50-80	5-15	200-400
Nickel-cadmium	50-75	60-150	5-20	800-1500
Nickel-metal hydride	30-110	140-435	3-15	350-500
Lithium ion	75-250	200-600	5-20	600-2500
Sodium-sulphur	150-240	150-240	15	300-500
ZEBRA (Sodium-nickel chloride)	100-140	150-280	8-14	100-200
Zinc-bromine	60-85	30-60	5-20	150-1000

2.6 Summary

Hybrid electric propulsion systems are now gaining popularity because it combines the advantages of different power sources which raise the overall efficiency, flexibility, redundancy and reduce fuel consumption, noise and emissions. However, it adds complexity and requires more weight and volume in some cases but with better space utilization. Therefore, hybrid electric power and propulsion concepts is one of the EEDI measures suggested by IMO to increase ships energy efficiency. Using conventional

power sources in hybrid propulsion systems could solve the emissions problem in the short term but for the medium and long terms with the more stringent regulations, it won't be enough [190]. So, more clean power sources such as fuel cell should be studied and used. Using fuel cell as a source of power with a battery as a storage system has been used successfully in transportation applications especially automotive industry.

Fuel cells have been deployed in marine applications since 1960s successfully not only for small applications but also for commercial shipping and in many types such as submarines, AUVs, passenger boats, water taxi, yachts, OSV, car carriers, ferries, research vessels, and merchant vessels. PEMFC is considered as the optimal type to be used in marine applications. PEMFC offers the advantages of low operating temperature which means quick start-up, quiet operation, high efficiency, high power density, low corrosion, low emissions and its solid electrolyte which make it a suitable replacement for ICE in cars, trucks, etc. Also, PEMFC has wide range of power starting from 12 W and it has proven suitability in the hostile marine environment through the successful testing of it under shock, vibration, and salt-air conditions therefore, it is selected to be used in this study. Also, different types of energy storage devises were discussed for fuel cell operation and batteries are selected for fuel cell applications because of its higher power range and energy density. Different types of batteries have been presented and a comparison has been made in terms of durability, cost, energy and power density.

However, why do fuel cells not have a good market share compared to conventional power sources? And the answer is, there are some barriers of its adoption such as higher first cost, shorter lifetime, hydrogen infrastructure is not ready yet to facilitate the wide adoption of fuel cell, and most of fuel cell models were not validated. As a result, many countries have spent millions on developing fuel cell in order to overcome these barriers especially the durability and first cost of fuel cells by mass production and reducing the use of expensive materials such as platinum which will reduce the cost of a PEMFC system to 30 $\$/kW$ in 2017 while it was 275 $\$/kW$ in 2002 and increase its life to 10 years. The number of hydrogen fuelling stations is also increasing and it will increase more and more with wider use of fuel cells.

Moreover, one of the problems facing the spread of fuel cells in marine application is the lack of validated total ship system models that uses fuel cell as a source of power to assess the effectiveness of using fuel cell onboard ships which is an objective of this thesis. A suitable simulation tool is developed to represent the ship behaviour and predict propulsion power requirements for real journeys which will be supplied by fuel cells and batteries through an Energy Management Strategy (EMS) in a hybrid propulsion system. In the next chapter the mathematical modelling of the simulation tool or 'ship simulator' is presented with a literature review about previous ship simulators.

Chapter 3

Mathematical Modelling

3.1 Introduction

In order to assess the effectiveness of fuel cells for marine applications and how it will affect the ship performance, numerical simulation can be very effective especially when actual testing is limited because of its large cost or lack of a proper testing facility. As discussed in the previous chapter, a hybrid fuel cell propulsion system, which is one of the EEDI measures, can be used to solve the emissions problem and can help ships to meet environmental regulations in the short, medium and long terms. Therefore, a total ship system model is developed to analyse and foresee the behaviour of ships using fuel cells as a main source of power. The developed simulator can be used to study the effect of different hybrid structure, different degree of hybridization, and different control methodologies on the overall efficiency of the system.

This chapter presents the governing equations used in the developed ship simulator to describe the dynamics of the ship including its propulsion system and the interaction between the ship and the surrounding environment with an overview about previous ship simulators. These equations will be implemented in the Simulink environment in order to develop the ship simulator which is presented in chapter 4 while chapters 5 and 6 include simulation results of cases analysed by the developed ship simulator.

3.2 Ship simulators

Various examples of ship propulsion system modelling and simulation have been presented however most of them are focusing on a specific ship type, a ship component or on a specific system configuration. A conventional ship propulsion model consists of a diesel engine and a propeller has been presented and it has a focus on both propeller types, controllable pitch (CP) and fixed pitch (FP) propellers with one degree of

freedom (DOF). A constant ship added mass of 20% was assumed in this model and no calculation of added resistance due to wind and waves was made [191].

A model of the ship and its propulsion system are required to study fault-tolerant control new ideas and compare its methods. Faults related to diesel engine and its generated torque, propeller pitch, or shaft speed measurement are important to be detected which received attention in modelling and simulation. A one DOF model of ship hull, CP propeller, shaft and two-stroke diesel engine was developed to study fault-tolerant control in [192]. However, diesel engine dynamics and ship added mass were not taken into consideration and added resistance was not calculated. This model was improved later by adding diesel engine dynamics and taking added mass effect into consideration but still with one DOF and no calculation of added resistance [193; 194].

Also, simulation is used to study the performance of the ship and its propulsion system in transient conditions such as manoeuvring to optimise the dynamic behaviour of ships during manoeuvring and make sure that the ship complies with the international standards of navigation. A three DOF (surge, sway, yaw) ship simulator with a rudder block developed for single screw and twin screw ships was developed using a comprehensive approach to analyse ship's different manoeuvres in [195]. Another three DOF simulation model was built in [196] using Simulink for merchant vessels to investigate the overall energy efficiency of the ship propulsion system consisting of diesel engine, gearbox, and propeller excluding the added resistance effect on the ship performance. A four DOF model was developed in [197] in order to study the interaction between diesel engines, ship and propellers during manoeuvring. Another four DOF time-domain simulator was developed in [198] to investigate the performance of high speed planning crafts using diesel engines during turning circle and zig-zag manoeuvres.

For extreme manoeuvring such as crash stop, full ahead or full astern, a modular model has been developed consisted of a 4-stroke diesel engine, a CP propeller and a ship hull module with a simple structure to reduce the computational time [199]. Another one DOF modular model has been developed for twin-screw ship propulsion system to study ship response in transient conditions and it was validated using full-scale data [200].

Modelling and simulation have been also used in the prediction and control of marine diesel engines performance in different conditions [201; 202; 12]. As shown in Figure 3.1, a conventional two-stroke diesel propulsion plant model used to study the engine speed control taking waves effect into consideration. Also, simulation has been used for evaluating the economical and technical feasibility of the propulsion system including hull dynamics in a four DOF model (surge, sway, yaw and roll) [203]. Moreover, simulation can be used in mapping the performance and emissions of a diesel engine propulsion systems using a mean value model (MVM) of the engine in a one DOF model [204]. Ship simulators can also be used to estimate exhaust gas emissions of ship engines

in transient and partial loading conditions which can help with voyage optimization to reduce ship emissions [205].

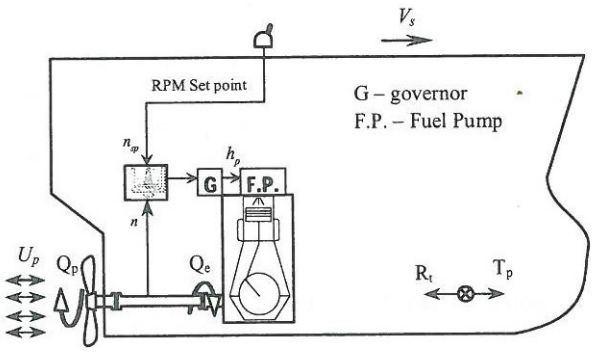

Figure 3.1: A two-stroke ship propulsion plant [12]

Although there has been relatively large volumes of research on ships driven by diesel engines and propellers, combined cycle power plants were also modelled and simulated for system design and performance prediction such as combined gas turbine and steam turbine (COGAS) where steam turbine is used to recover some of the heat from the gas turbine exhaust as shown in Figure 3.2. In this work attention was paid only for the COGAS cycle and no hull or propeller dynamics was presented [13].

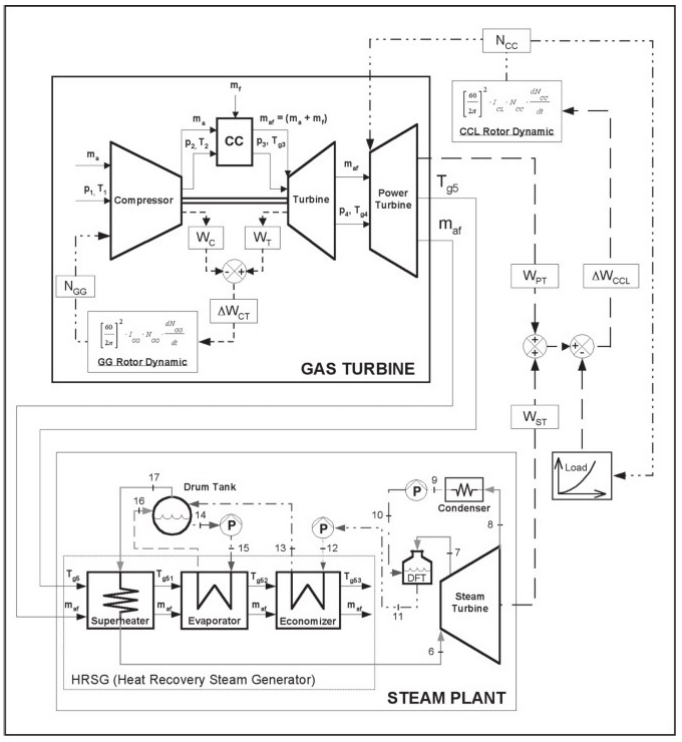

Figure 3.2: COGAS propulsion system dynamic modelling [13]

Modelling and simulation have been used as well to study the performance of electric and hybrid propulsion systems. A combined diesel electric and gas turbine cycle (CODLAG) was simulated for a fast military vessel to study the design of propulsion control systems

taking into account the ship manoeuvrability represented by a three DOF (surge, sway and yaw) equations of motions [206]. For preliminary design stage studies of all-electric ships, a gas turbine was the main source of power for a ship power system modelled and simulated in [207] to compare between different architectures and topologies of electric propulsion systems in terms of size, cost, and efficiency. A ship model for a diesel-electric propulsion system was constructed for control design and studying the performance of the electrical components focusing on the power generation system consisted of diesel generators using a variable speed thruster [208]. For training purposes, a one DOF ship electric propulsion system simulation was developed in [209] where it can be used to study man-machine interface, power management, and fault diagnosis. Another model was developed in [210] in order to investigate hybrid diesel propulsion system for bulk carriers and analysis ship's emission profile during voyages. This model was built in a modular manner and used regression analysis to predict calm water resistance which is similar to the model developed in this project. However, no manoeuvrability model was used in this model.

Ship power system simulation has also been used to study the performance of energy storage systems such as flywheel in [211]. This study showed that using flywheels could result in increasing the reliability and improving the quality of the ship electric propulsion system consisted of gas turbines and diesel generators but the developed mathematical model didn't take the hull or propeller dynamics into consideration. Another simulation of a ship power system was developed to study how energy storage system would improve the ship performance where the storage system consisted of flywheel combined with batteries and capacitors in [212].

According to the literature reviewed, most research in recent years using total ship system is limited to one DOF and diesel engine modelling. In this project, a three DOF (surge, sway, and yaw) total ship system is developed to have more realistic representation of ship performance, its propulsion power requirements, and fuel consumption. Different power sources can be used in the developed total ship system which include conventional diesel engines as well as fuel cell and battery models to assess the effectiveness of hybrid fuel cell propulsion system and compare it with conventional diesel propulsion systems.

3.3 Modelling approach

The developed time-domain ship simulator is based on building block modular approach where ship hull, propeller and different parts of the propulsion system are represented by separate submodels which facilitate the modelling process. The ship manoeuvrability is represented by a three DOF (surge, sway, and yaw) model developed for single screw and twin screw ships. Ship hull parameters and speed dynamics are taken into consideration

including the added mass effect and added resistance due to wind and waves are also estimated. Different power sources which are four-stroke, two-stroke diesel engines, fuel cell, and battery are included in the ship model to power the ship using single or twin-screw propulsion systems. To have more powerful ship simulator, the control of the ship propulsion system is modelled using two different modelling approaches which are the forward facing and the backward facing models which can be used to study different voyage execution methods. The developed ship model is intended to be generic, can be used for several purposes and not complicated to avoid the problem of excessive computational time.

Prediction of ship's propulsion power during real voyages is the main output of the developed simulator in addition to the ship speed and fuel consumption. The calculated propulsion power is then used to determine ship's fuel consumption and emission of the used power source which includes two and four-stroke diesel engines, fuel cells and batteries. Therefore, the developed simulator contains models of four-stroke, two-stroke diesel engines, fuel cell, and battery to compare between conventional diesel engine propulsion system and hybrid fuel cell propulsion system.

If the ship installed power is not yet known, the components of the ship propulsion power estimation starts with estimating the ship total calm water resistance (R) which is used to calculate the effective power (P_E) using Equation 3.1 as a function of ship speed (V).

$$P_E = R \times V \tag{3.1}$$

Then, the delivered power (P_D) is calculated as a function of (P_E) according to the Equation 3.2 as follows

$$P_D = \frac{P_E}{\eta_D} \tag{3.2}$$

where η_D is the quasi propulsive efficiency and it is calculated as a function of open water efficiency (η_O), hull efficiency (η_H), and relative rotative efficiency (η_R) as follows

$$\eta_D = \eta_O \times \eta_H \times \eta_R \tag{3.3}$$

The brake power of the main engines (P_B) is then calculated as a function of (P_D) and shaft efficiency (η_S) as follows taking into consideration sea margin power which depends on ship service and route.

$$P_B = \frac{P_D}{\eta_S} + \text{sea margin} \tag{3.4}$$

The consumed brake power can be used to calculate the total fuel consumption using specific fuel consumption (SFC) of the used engines as shown in Equation 3.5 and the emissions is then calculated as a function of the total fuel consumption using fuel-based emissions factor as suggested by the IMO.

$$\text{Fuel consumption} = P_B \times SFC \tag{3.5}$$

The previous approach can be used in the early design stage of conventional ship propulsion systems. However, in order to assess the effectiveness of fuel cells as a main source of propulsion power during real voyages, more detailed representation of the ship power requirements is required. Hybrid fuel cell propulsion system should meet the required power demand for the examined voyages including ship acceleration and manoeuvring. The components of the hybrid fuel cell system should be sized properly. Moreover, different energy management strategies used to split the required power between different components of the hybrid fuel cell system should also be studied to select the suitable strategy for marine applications. Therefore, a total ship system simulator is developed and its mathematical modelling is presented in the following sections.

3.3.1 Calm water resistance

The total resistance of a ship is the force required to propel this ship at a given speed. This force can be classified into two principal components according to the theory developed by William Froude [213]; tangential shear forces caused by the flow of water along the hull surface which is the frictional resistance and residual resistance resulted due to the pressure developed by the hull to push the water. The basic approaches to predict ship resistance can be resolved into empirical/statistical, experimental, and numerical approaches [214].

In order to calculate the ship calm water resistance, there are many prediction methods which can be used however, each method has applicability restrictions. These methods are expressed by tabular, graphical, mathematical models or combination of them. Mathematical models which contains regression analysis equations can be implemented directly in simulation environment. However graphical models and tabular models can be indirectly used in simulation after deriving representing equations or by using interpolation which may affect the accuracy of calculations.

Data from model testing can be statistically processed using regression analysis to estimate the relation between different variables which can be used to predict the calm water resistance of ships. Sufficient data is required to provide an adequate regression analysis. Also, publication data is important to decide whether this analysis still valid or

not for modern ship forms. Examples of resistance prediction methods using regression analysis equations includes Sabit regression of BSRA series [215], Series 60 [216], and SSPA series [217]. Holtrop-Mennen regression analysis [218], Hollenbach [14], Radojcic's analysis of Series 62 [219] , Oortmerssen's regression equations to estimate the resistance of small ships [220] and Robinson's analysis on chine and round bilge hull forms [221]. On the basis of range of application, publication date, and ease of programming, methods of Hollenbach and Holtrop-Mennen consider as best choices.

Holtrop-Mennen's statistical method, based on regression analysis, was based on the results of testing 191 models of various ship types at the Dutch Model Basin MARIN in addition to full-scale test data [218]. Then, some of its regression's coefficients were updated later by Holtrop after increasing the number of the tested models to 334 to increase the accuracy of resistance prediction [222]. In this method, the total ship resistance R is calculated according to:

$$R = R_F.(1 + K_1) + R_{APP} + R_W + R_B + R_{TR} + R_A \tag{3.6}$$

where R_F: frictional resistance according to ITTC-1957 formula,

$1 + K_1$: form factor of the hull,

R_{APP}: appendage resistance,

R_W: wave resistance,

R_B: additional pressure resistance due to bulbous bow near the water surface,

R_{TR}: additional pressure resistance due to transom immersion,

R_A: model-ship correlation resistance.

The regression analysis of Hollenbach is based on the results of testing 433 models from 1980 to 1995 at the Vienna Ship Model Basin with the aim of evaluating the accuracy of traditional methods of estimating ship resistance and improving its reliability at the design stage. The total ship resistance in Hollenbach's methods is given by:

$$R = R_F + R_R \tag{3.7}$$

where R_R is the residual resistance and it is given by:

$$R_R = \frac{1}{2}.C_R.\rho.V^2.\frac{B.T}{10} \tag{3.8}$$

The residual coefficient C_R is calculated according to:

$$C_R = C_{R,Standard}.C_{R,FnKrit}.K_L.(T/B)^{a1}.(B/L_{PP})^{a2}.(L_{os}/L_{wl})^{a3}.(L_{wl}/L_{PP})^{a4}.(D_P/T_A)^{a6} .(1+(T_A-T_F)/L_{PP})^{a5}.(1+N_{Rud})^{a7}.(1+N_{Brac})^{a8}.(1+N_{Boss})^{a9}.(1+N_{Thr})^{a10} \tag{3.9}$$

where T_A and T_F are the drafts at aft and fore perpendiculars, D_P is the propeller diameter, N_{Rud} is the number of rudders, N_{Brac} is the number of brackets, N_{Boss} is the number of bossing, N_{Thr} is the number of thrusters, K_L is calculated as a function of L_{PP} and L_{os} is the length over surface defined by Hollenbach as shown in Figure 3.3.

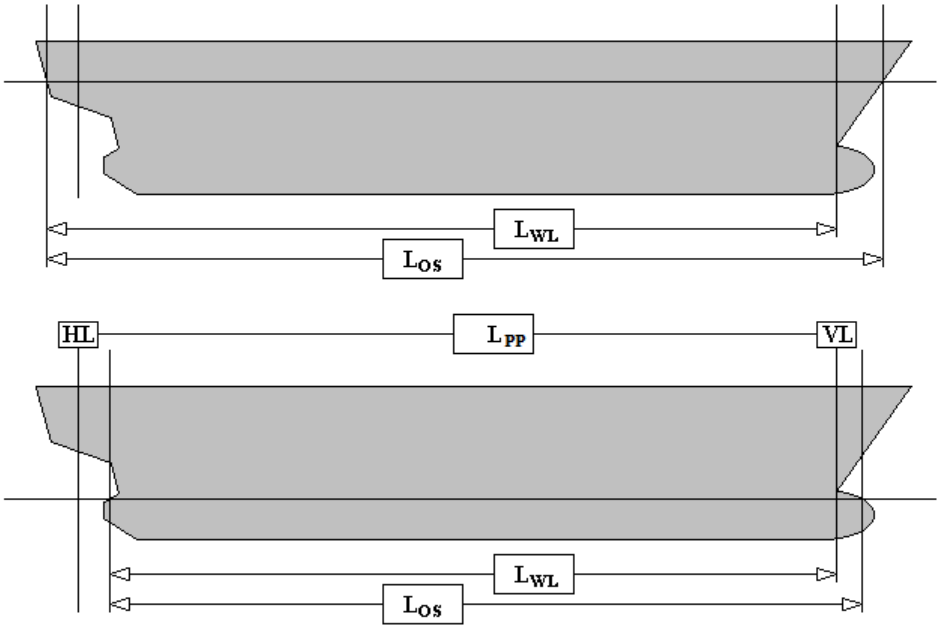

Figure 3.3: Ship lengths definitions [14]

The frictional resistance R_F is approximated using the ITTC-1957 formula as follows

$$R_F = \frac{0.075}{(log_{10}Rn-2)^2}.\frac{\rho}{2}.S.V^2 \tag{3.10}$$

where wetted surface area (S) according to Hollenbach's empirical formula [223] including appendages is calculated as follows

$$S = k.L_{PP}.(B+2T) \tag{3.11}$$

$$k = a_0 + a_1.L_{os}/L_{wl} + a_2.L_{wl}/L_{PP} + a_3.C_B + a_4.B/T + a_6.L_{PP}/T + a_7.(T_A - T_F)/L_{PP} + a_8.D_P/T + K_{Rudd}.N_{Rudd} + K_{Brac}.N_{Brac} + K_{Boss}.N_{Boss} \tag{3.12}$$

where $a_{1..10}$, K_{Rudd}, K_{Brac}, K_{Boss} are coefficients presented by Hollenbach depends on the draft, single or twin-screw ship and it has two values for a 'mean' and 'minimum' value of the resistance. Hollenbach also gave the following equation to calculate the 'maximum' total resistance R_{max} as a function of mean resistance R_{mean}

$$R_{max} = h_1.R_{mean} \tag{3.13}$$

Hollenbach's and Holtrop-Mennen's regression analysis are both modelled and used in this project to calculate calm water resistance. However, Hollenbach's method is selected to be the default method used to calculate the calm water resistance because of its relatively modern database and it requires less inputs parameters which is favourable in early design stage. The limits of Hollenbach method are given in Table 3.1.

Table 3.1: Hollenbach method limits [36]

	single screw ships		twin screw ships
	design draft	ballast draft	
L_{PP}	42 ... 205.3	50.2 ... 224.8	30.5 ... 206.8
C_B	0.601 ... 0.83	0.559 ... 0.79	0.512 ... 0.775
L_{PP}/B	4.71 ... 7.106	4.949 ... 6.623	3.96 ... 7.13
B/T	1.989 ... 4.002	2.967 ... 6.12	2.308 ... 6.11
L_{OS}/L_{WL}	1 ... 1.05	1 ... 1.05	1 ... 1.05
L_{WL}/L_{PP}	1 ... 1.055	0.945 ... 1	1 ... 1.07
$L_{PP}/\nabla^{(1/3)}$	4.49 ... 6.008	5.45 ... 7.047	4.405 ... 7.265
D/T_A	0.43 ... 0.84	0.655 ... 1.05	0.495 ... 0.86

3.3.2 Added resistance due to wind and waves

Ships rarely operate in a calm environment, therefore estimating the added resistance due to wind and waves is crucial in predicting speed loss which can affect the voyage duration or increase the consumed power. Added resistance due to wind may be estimated using coefficients derived from wind tunnel tests for a particular ship type [224], meanwhile, estimating added resistance due to waves is more complicated. Factors that attribute to the added resistance of ships are waves generated due to the forward speed and motion of the ship, incident waves and its interference with the ship called drifting forces and damping force generated because of the vertical motion of the ship [225].

The approaches used to solve the problem of added resistance due to waves can be classified into two main groups; far-field and near-field methods. Maruo in [226] introduced the first far-field approach based on energy and momentum conservation elaborated further by him in [227]. Many researchers followed Marou's far-field approach and analysed the added resistance problem using radiated energy approach [228]. Sea keeping strip theory was used with radiated energy approach to provide more accurate results of added resistance [229] and an overview of the methods to calculate the added resistance for ships in seaways has been presented in [230]. Similarly to added resistance due to wind, added resistance due to waves can be estimated from self propulsion model testing in regular waves with a given spectrum however the chance to perform model tests in wind tunnels and propulsion model testing is not always available. Therefore, in early design stage it is useful to calculate the effect of weather on ship performance using approximate methods.

Many studies on ship performance were performed by Aertssen [231; 232] who propose a simple formula to estimate the speed loss due to wind and waves derived from his analysis of full scale ship performance as a function of ship length, weather direction and Beaufort number (BN) [37]. The speed loss percentage is determined according to Equation 3.14 where m and n vary with weather direction and Beaufort number as shown in Table 3.2. For Beaufort number less than 5, speed loss is assumed to be 1% in all directions.

$$\frac{\Delta V}{V} = \frac{m}{L_{PP}} + n \tag{3.14}$$

Table 3.2: Aertssen values for m and n [37]

	Head Sea		Bow Sea		Beam Sea		Following Sea	
BN	m	n	m	n	m	n	m	n
5	900	2	700	2	350	1	100	0
6	1300	6	1000	5	500	3	200	1
7	2100	11	1400	8	700	5	400	2
8	3600	18	2300	12	1000	7	700	3

Another attempt to provide a simple method to estimate speed loss percentage due to bad weather has been made by Townsin and Kwon who updated Aertssen formula by taking into consideration the ship volume of displacement ∇, BN, and weather direction [233] and three approximate formulas have been offered. The three formulas consist of two terms where the first term represents the wind effect alone on the speed loss. These formulas were updated to extend the range of C_B from 0.55 to 0.85 and and F_n from 0.05 to 0.3 [38]. For all ships in laden condition except container ships, C_B = 0.75, 0.8, and 0.85, the speed loss percentage is:

$$\alpha.\mu.\frac{\Delta V}{V} = 0.5BN + \frac{BN^{6.5}}{2.7\nabla^{2/3}} \tag{3.15}$$

For all ships in ballast condition except container ships, $C_B = 0.75$, 0.8, and 0.85, the speed loss percentage is:

$$\alpha.\mu.\frac{\Delta V}{V} = 0.7BN + \frac{BN^{6.5}}{2.7\nabla^{2/3}} \tag{3.16}$$

For container ships in normal condition, $C_B = 0.55$, 0.6, 0.65 and 0.7, the speed loss percentage is:

$$\alpha.\mu.\frac{\Delta V}{V} = 0.7BN + \frac{BN^{6.5}}{22\nabla^{2/3}} \tag{3.17}$$

where α is the correction factor for C_B and F_n as given in Table 3.3 and μ is the reduction factor for weather direction calculated according to Equations 3.18.

Table 3.3: Correction factor values [38]

C_B	Condition	Correction factor (α)
0.55	normal	1.7 - 1.4 F_n - 7.4 $(F_n)^2$
0.6	normal	2.2 - 2.5 F_n - 9.7 $(F_n)^2$
0.65	normal	2.6 - 3.7 F_n - 11.6 $(F_n)^2$
0.7	normal	3.1 - 5.3 F_n - 12.4 $(F_n)^2$
0.75	laden or normal	2.4 - 10.6 F_n - 9.5 $(F_n)^2$
0.8	laden or normal	2.6 - 13.1 F_n - 15.1 $(F_n)^2$
0.85	laden or normal	3.1 - 18.7 F_n - 28 $(F_n)^2$
0.75	ballast	2.6 - 12.5 F_n - 13.5 $(F_n)^2$
0.8	normal	3 - 16.3 F_n - 21.6 $(F_n)^2$
0.85	normal	3.4 - 20.9 F_n - 31.8 $(F_n)^2$

$$\begin{aligned} 2\mu_{\text{bow}} &= 1.7 - 0.03(BN-4)^2 && 30^\circ - 60^\circ \\ 2\mu_{\text{beam}} &= 0.9 - 0.06(BN-6)^2 && 60^\circ - 150^\circ \\ 2\mu_{\text{following}} &= 0.4 - 0.03(BN-8)^2 && 150^\circ - 180^\circ \end{aligned} \tag{3.18}$$

The speed loss can be used to estimate the resistance increase according to Equation 3.19 assuming that the resistance is proportional to the speed squared ($R \propto V^2$) over small changes and constant thrust.

$$\frac{\Delta V}{V} = \left[1 + \frac{\Delta R}{R}\right]^{1/2} - 1 \tag{3.19}$$

For added resistance due to wind calculations, Blendermann has derived mathematical expressions for the prediction of wind loads on different type of ships including ferries from the statistical analysis of wind tunnels experimental results obtained at the Institute of Naval Architecture, University of Hamburg [234]. The longitudinal wind force X_W, the side wind force Y_W, and the yawing-moment N_W are calculated as follows

$$\begin{aligned} X_W &= \frac{1}{2}\rho_a u^2 A_F CX \\ Y_W &= \frac{1}{2}\rho_a u^2 A_L CY \\ N_W &= \frac{1}{2}\rho_a u^2 A_L L_{OA} CN \end{aligned} \tag{3.20}$$

where ρ_a is the air density, u is wind speed, A_F and A_L are the ship frontal projected area and lateral-plane area respectively. CX and CY are the coefficients of longitudinal and lateral wind forces, and CN is the yawing-moment coefficients calculated as follows

$$\begin{aligned} CX &= -CD_1 \frac{A_L}{A_F} \frac{cos\epsilon}{1 - \frac{\delta}{2}(1 - \frac{CD1}{CDt})sin^2 2\epsilon} \\ CY &= CDt \frac{sin\epsilon}{1 - \frac{\delta}{2}(1 - \frac{CD1}{CDt})sin^2 2\epsilon} \\ CN &= CY \left[\frac{S_L}{L_{OA}} - 0.18(\epsilon - \frac{\pi}{2}) \right] \end{aligned} \tag{3.21}$$

where ϵ is the wind apparent angle, S_L is the distance between the the lateral-plane area center and the midship section. Values of CD_1, CDt, and δ are different for each ship type as illustrated in [234]. Compared to Isherwood, Gould, and OCIMF, Blendermann experimental work is reported to be more reliable and comprehensive [235], therefore it is used in this work.

Regarding added resistance due to wave, it has been continually reported that it is difficult to determine acceptable values of it due to its complexity. However, ITTC [236] recommends the use of Kreitner formula to estimate the increase in resistance due to the effect of waves with heights up to 2 m as follows

$$\triangle R_W = 0.64 H_w^2 B^2 C_B \gamma / L_{PP} \tag{3.22}$$

where H_w is the wave height, γ is water specific weight.

3.3.2.1 Weather conditions

To calculate the added resistance during the simulation of a certain voyage, wind speed and direction which are changing over time should be provided. Many methods are there to forecast the weather such as climatology method, analogue method, persistence method, trends method, and numerical weather prediction. However, not all these methods can be implemented mathematically [237].

The National Oceanic and Atmospheric Administration (NOAA) has developed several validated numerical methods for meteorological predictions. Some for regional applications such as the North American Model (NAM) and other for the entire globe such as the Global Forecast System (GFS). Meteorological data of these models are stored in the National Climatic Data Center (NCDC) where a part of this data are free and can be downloaded from the NOAA's Operational Model Archive Distribution System (NOMADS) [238].

GFS model covers the entire globe and it runs four times a day at 0, 6, 12 and 18 UTC. Also, it provides a forecast for the upcoming 16 days in three hour intervals [239]. GFS model data are provided in General Regularly-distributed Information in Binary form (GRIB) and (GRIB2) [240]. Required data for this study to be extracted are wind speed and direction which can be done using software to view these files format such as zyGrib [241] as shown in Figure 3.4 which shows wind speed at 10 m on the 23^{th} of July 2014 at 6 UTC.

In order to use Aertssen or Kwon's formula, wind speed in (m/s) should be converted to Beaufort number scale according to Table 3.4 and the wind angle off bow γ_R is calculated as a function of wind direction γ and ship course angle α as follows

$$\gamma_R = \cos^{-1}(\cos(\alpha) * \cos(\gamma) + \sin(\gamma) * \sin(\alpha)) \tag{3.23}$$

Ship course angle α can be calculated as a function of ship's latitudes and longitudes as follows

$$\alpha = MOD(ATAN2(\cos(LatA) * \sin(LatB) - \sin(LatA) * \cos(LatB) * \cos(LongB - LongA), \sin(LongB - LongA) * \cos(LatB)), 2\pi) \tag{3.24}$$

where MOD is a function that returns the remainder after the results is divided by 2π, $ATAN2$ evaluates the arctangent or inverse tangent of specified x and y, $LatA$ and $LatB$ are the latitudes of point A and B and $LongA$ and $LongB$ are the longitudes of point A and B. Latitudes and longitudes are converted from decimal degrees to radians

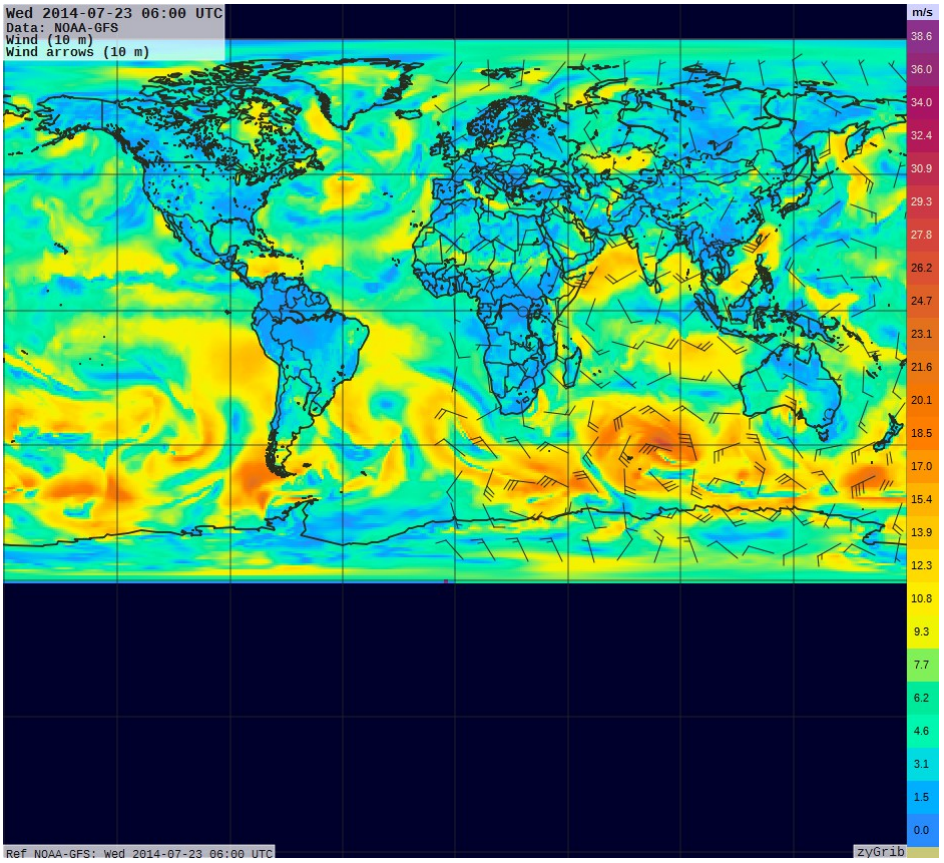

Figure 3.4: Wind analysis of GFS model on 23-07-2014 at 6 UTC

Table 3.4: The Beaufort wind scale [39]

Number	Wind speed (Kn)	Wind description
0	Less than 1	Calm
1	1 - 3	Light air
2	4 - 6	Light breeze
3	7 - 10	Gentle breeze
4	11 - 16	Moderate breeze
5	17 - 21	Fresh breeze
6	22 - 27	Strong breeze
7	28 - 33	Near gale
8	34 - 40	Gale
9	41 - 47	Severe gale
10	48 - 55	Storm

first using Equation 3.25 then α will be in radians as well. To calculate added resistance, α, γ_R, and γ will be in degrees.

$$LatA_{radians} = LatA_{degrees}\frac{\pi}{180} \tag{3.25}$$

Another method to provide wind speed and direction for the simulation is by using probability theory which can be used in weather prediction [242] where the required environmental parameters are randomly generated based on its probability of occurrence. The source of weather observation can be a weather ship, measurement buoys, coastal weather stations, or climatic data center, UK Met Office, etc. Table 3.5 shows an example of wind speed and direction database of the North European Storm Study extension (NEXT) model's of a station in the Northern North Sea [40]. However, using random weather profile increases the uncertainty of results. Therefore, multiple runs should be made using different weather profiles in a Monte Carlo simulation mode to calculate the mean and sample standard deviation of outcomes to capture the uncertainty.

Table 3.5: Mean wind speed and direction [40]

Direction / Speed (m/s)	N	NE	E	SE	S	SW	W	NW	Total
0.3 to 1.6	9	3	1	1	2		4	8	28
1.6 to 3.4	452	524	459	421	512	495	489	449	3801
3.4 to 5.5	1248	1288	1037	965	1453	1316	1368	1347	10022
5.5 to 8	2240	1751	1311	1539	2837	2774	2292	2381	17125
8 to 10.8	2622	1837	800	1840	3922	3432	2598	2382	19433
10.8 to 13.9	1732	1106	284	1495	3650	3509	1967	1727	15470
13.9 to 17.2	656	387	42	1066	2525	2138	1155	805	8774
17.2 to 20.8	219	119		429	1114	712	494	301	3388
20.8 to 24.5	55			123	222	102	99	51	652
24.5 to 28.5	20			15	58	8	23	4	128
18.5 to 32.7	3				1	1	9	2	16
32.7 to 51.5						2	4		6
Total	9256	7015	3934	7894	16296	14489	10502	9458	78843

3.3.3 Ship hydrodynamics coefficients

In order to predict the performance of ship hydrodynamics, interaction of the surrounding environment with the ship and interaction of the ship with the propeller

must be analysed. Because of the interaction between the hull and the propeller, the propulsive efficiency is affected. This interaction can be presented by three values; wake fraction, thrust deduction, and relative rotative efficiency. The wake fraction results from the difference between the speed of the hull (V) and the speed of flow into the propeller (V_A). This difference is caused due to the presence of the hull and the wake (w) is defined as follows

$$w = \frac{(V - V_A)}{V} \tag{3.26}$$

The action of the propeller increases the velocity of the flow over the hull surface which reduce the local pressure field over the after part of the hull which affects the resistance. This effect is expressed as the thrust deduction which can be defined with the following equation.

$$t = \frac{T - R}{T} \tag{3.27}$$

Estimation of mean wake and thrust deduction is of fundamental importance as it affects the propeller thrust and it should be determined along with the propeller rpm, diameter, and power. The flow speed in the wake field can be measured experimentally or predicted using CFD or from model self-propulsion experiments. For preliminary design, empirical equations which can be in the form of regression equations are suitable. Wake fraction can be calculated using simple Taylor formula [243] as a function of C_B as follows:

For single screw:

$$w = 0.5C_B - 0.05 \tag{3.28}$$

For twin screw:

$$w = 0.55C_B - 0.2 \tag{3.29}$$

Methods based on model experiments in the period from 1896 to 1940 were analysed by Harvald [244] and he concluded that Schoenherr formula is the most reliable for single screw ships which is the following:

$$w = 0.1 + 4.5\frac{C_{pv}C_{ph}(B/L)}{(7 - C_{pv})(2.8 - 1.8C_{ph})} + 0.5(E/T - D/B - K\eta) \tag{3.30}$$

where E is the hight of the propeller shaft above the keel, C_{pv} is the vertical prismatic coefficient, C_{ph} is the horizontal prismatic coefficient, η is the propeller angle of rake, and k is the stern coefficient.

For single screw ships, Holtrop developed the following formulas for the calculation of wake fraction and thrust deduction:

$$w = c_9 c_{20} C_V \frac{L}{T_A}(0.050776 + 0.93405 c_{11} \frac{C_V}{(1 - C_{p1})}) + 0.27915 c_{20} \sqrt{\frac{B}{L(1 - C_{p1})}} + c_{19} c_{20} \tag{3.31}$$

$$t = \frac{0.25014(B/L)^{0.28956}(\sqrt{BT}/D)^{0.2624}}{(1 - C_P + 0.0225 lcb)^{0.01762}} + 0.0015 C_{stern} \tag{3.32}$$

where C_V is the viscous resistance coefficient and c_9, c_{11}, c_{19}, and c_{20} are coefficient depends on the ship wetted surface area, length, breadth, draft, form factor, and form coefficients as detailed in [222]. In preliminary design, detailed information about the ship is not available therefore, the wake formula developed by the British Ship Research Association (BSRA) is used to calculate the wake fraction and thrust deduction of single screw ships which is suitable for C_B range of 0.65-0.80 [245]:

$$w = a_0 + a_1 C_B + a_2 C_B^2 + a_3 \frac{V}{\sqrt{L_{PP}}} C_B + a_4 (\frac{V}{\sqrt{L_{PP}}} C_B)^2 + a_5 D_w C_B + a_6 \delta LCB \tag{3.33}$$

$$t = b_0 + b_1 C_B + b_2 C_B^2 + b_3 \frac{V}{C_B \sqrt{L_{PP}}} + b_4 (\frac{V}{C_B \sqrt{L_{PP}}})^2 + b_5 (\frac{V}{C_B \sqrt{L_{PP}}})^3 + b_6 \frac{V}{\sqrt{L_{PP}}} + b_7 D_t + b_8 \delta LCB + b_9 C_B \delta LCB \tag{3.34}$$

where D_w is wake fraction parameter, D_t is thrust deduction parameter, and δLCB is the percentage of LCB deviation from the basis position forward of midship as follows:

$$\begin{aligned} D_w &= B/\sqrt{D\nabla^{1/3}} \\ D_t &= BD/\nabla^{2/3} \\ LCB &= 20(C_B - 0.675) \end{aligned} \tag{3.35}$$

For twin screw ships, wake fraction is calculated using Taylor's equation and the following formula developed by Holtrop and Mennen [218] is used to calculate the thrust deduction:

$$t = 0.325 C_B - 0.1885 D_P/\sqrt{BT} \tag{3.36}$$

3.3.4 Propeller modelling

The Propeller's function is to produce sufficient thrust to achieve the required speed. Propeller block of the developed ship simulator uses wake fraction, thrust deduction, ship speed, propeller rotational speed, and other geometrical data about the propeller as inputs to estimate the produced thrust and torque which is calculated according to the following equations as a function of non-dimensional thrust and torque coefficients, water density, propeller rotational speed, and propeller diameter.

$$T_P = K_T.\rho.n_p^2.D_p^4 \tag{3.37}$$

$$Q_P = K_Q.\rho.n_p^2.D_p^5 \tag{3.38}$$

where non-dimensional thrust and torque coefficients are calculated as a function of propeller advance coefficient using the following approximate equations for Wageningen B-screw series [246]

$$\frac{K_T}{K_{T0}} = \left[1 - \left(\frac{J}{a}\right)^n\right] \tag{3.39}$$

$$\frac{K_Q}{K_{Q0}} = \left[1 - \left(\frac{J}{b}\right)^m\right] \tag{3.40}$$

The non-dimensional thrust and torque coefficients can be also calculated using the following polynomials fitted to Wageningen data.

$$\begin{aligned} K_T &= \sum_{n=1}^{39} c_n (J)^{S_n} (P/D)^{t_n} (A_E/A_0)^{u_n} (Z)^{v_n} \\ K_Q &= \sum_{n=1}^{47} c_n (J)^{S_n} (P/D)^{t_n} (A_E/A_0)^{u_n} (Z)^{v_n} \end{aligned} \tag{3.41}$$

Values of the polynomials required parameters can be found in [246]. The advance coefficient J is given by:

$$J = \frac{V_A}{n_p D_p} \tag{3.42}$$

where n_p is the propeller rotational speed and V_A is the speed of advance and it is calculated as follows

$$V_A = V \times (1 - w) \tag{3.43}$$

The thrust power delivered by the propeller to the water P_T is calculated as a function of the produced thrust as shown in Equation 3.44. The propeller torque also is used to calculate the delivered power P_D according to Equation 3.45.

$$P_T = T_P V_A \tag{3.44}$$

$$P_D = 2\pi n_p Q_P \tag{3.45}$$

Propeller efficiency is then determined as a function of the propeller thrust and delivered powers according to the following formula

$$\eta = \text{power output/power input} = \frac{P_T}{P_D} \tag{3.46}$$

3.3.5 Manoeuvrability

In order to improve maritime safety, IMO has developed standards for ship manoeuvrability to be used to evaluate the manoeuvring performance of ships. A manoeuvrability mathematical model is added to the developed ship simulator to have more real representation of ship performance during voyages. Since manoeuvring motions of the ship affects its speed and power requirements, the behaviour of hybrid fuel cell propulsion systems during ship manoeuvring needs to be investigated which is why a manoeuvrability model is included.

According to IMO, at the design stage, mathematical models can be used to assess the manoeuvrability of ships. Most of models that deal with the total ship system simulation in the literature is limited to one DOF manoeuvring model where ship acceleration $\frac{dV}{dt}$ is calculated as shown in Equation 3.47.

$$(m - X_{\dot{u}})\frac{dV}{dt} = \sum F_x \tag{3.47}$$

where $(-X_{\dot{u}})$ is the added mass in surge direction and it is a function of ship mass (m), and $\sum F_x$ is the resultant of forces in surge direction on the ship hull which are calm water resistance, added resistance, and propeller thrust. In this study, a three DOF (surge, sway, and yaw) mathematical model is used to take into account manoeuvrability effect on both ship speed and power requirements as recommended by the IMO. Ship

manoeuvrability has been usually studied using three DOF manoeuvring models showing good agreement with real and experimental results as reported in [197; 247].

Generally, manoeuvring behaviour is considered as a quasi-steady problem. Therefore, a well known mathematical model for ship manoeuvrability developed by a research group called Manoeuvring Modelling Group (MMG) [248] in Japan which follows the semi-empirical methodology is used in this project. It was originally developed for single-propeller single-rudder ships. However, it has been successfully expanded to include other types of ships. The basic equations of motion of this model [249] are shown below.

$$\begin{aligned} m\dot{u} - mvr &= X \\ m\dot{v} + mur &= Y \\ I_{zz}\dot{r} &= N - x_G Y \end{aligned} \tag{3.48}$$

where, X, Y, and N are hydrodynamic forces and moment acting on midship, x_G: location of the ship centre of gravity from the midship in x-axis, u and v are the component of ship speed in x and y direction, r: rate of turn, and I_{zz}: moment of inertia of yawing where the ship centre of gravity is the origin of manoeuvring. These equations describe ship motion in the horizontal plane which is suitable for ship manoeuvring prediction. The hydrodynamic forces and moments are expressed as follows:

$$\begin{aligned} X &= X_H + X_P + X_R \\ Y &= Y_H + Y_P + Y_R \\ N &= N_H + N_P + N_R \end{aligned} \tag{3.49}$$

where subscripts H, P, R refer to hull, propeller, and rudder respectively. In this study, approximate formulae are used to predict hydrodynamics forces and moments obtained from the analysis of model testing results involving 15 kinds of ship and their 48 loading conditions [250]. The mathematical expressions of the hydrodynamic derivatives are given in Appendix 2.

3.3.6 Diesel engine

Modelling of diesel engines has attracted much attention in recent years because it is used by the majority of ships. Diesel engine models can be used in studying the combustion process inside the cylinders, control studies, faults diagnostics, etc. Therefore, there are different types of diesel engine models in the literature with different level of complexity such as CFD models, phenomenological multi-zone models, filling and emptying models, mean value models and transfer function models.

A suitable diesel engine model should be selected based on the requirements of the simulation. In the context of conceptual design stage, a transfer function model of diesel engine can be used to provide the relation between shaft speed and the generated torque through the fuel pump index. Diesel engine transfer function models introduce the basic dynamical aspects of time delay between the the fuel injection and torque build-up.

3.3.6.1 Two-stroke diesel engine

Slow speed two-stroke diesel engine combined with fixed pitch propeller is considered as the most favourable combination for large seagoing ships' propulsion systems. It is simple and efficient because no gearbox is used and it operates most of the time at its optimum operating range because large seagoing ships don't have a large variation in power demand [251]. In a transfer function model of diesel engine, the dynamics of diesel engines are divided into two parts. The first part describes the produced torque developed by the engine (Q_{eng}) which is calculated as a function of fuel index (Y). An early example of transfer function diesel engine model was developed by Blanke [252] as follows which is valid for steady-state operation:

$$Q_{eng}(s) = \frac{K_y e^{-\tau s}}{1 + \tau_c s} Y(s) \tag{3.50}$$

where τ is the time delay or dead time , τ_c is the torque build-up time constant, and K_y is the gain constant. Dead time of the engine torque equation has been found to lie within the following range [253]:

$$15/N_{eng} < \tau < 15/N_{eng} + 60/(N_{eng} Z_{eng}) \tag{3.51}$$

where N_{eng} is the engine rotational speed in rpm and Z_{eng} is number of engine cylinders. Another effective diesel engines mathematical model has been presented to describe the generated torque as a function of fuel flow and rotational speed as follows [12]:

$$\begin{aligned} \bar{Q} &= 0.5\bar{h_p}^{\frac{2}{3}} + 1.5\bar{h_p}^{\frac{1}{3}}\bar{n} - \bar{n}^2 \\ \bar{Q} &= \frac{Q_{eng}}{Q_{mcr}}; \bar{h_p} = \frac{h_p}{h_{pmcr}}; \bar{n} = \frac{n_{eng}}{n_{mcr}} \end{aligned} \tag{3.52}$$

where Q_{mcr}, h_{pmcr}, and n_{mcr} are the values of the engine torque, fuel flow rate, and rotational speed at the maximum continuous rating.

3.3.6.2 Four-stroke diesel engine:

Due to its efficiency, compact size, and wide speed range, four-stroke diesel engines are also used for propulsion of small ships as well as large ferries, RO-RO, and cruise ships. A four-stroke marine diesel engine can be modelled using a simple first order transfer function as follows [254]

$$\frac{Q}{Y} = \frac{K}{1+Ts} \tag{3.53}$$

where Y is the fuel index, K is the gain constant and T is time constant. Another diesel engine transfer function model which is used in this study because it contains the dynamics of the engine speed governor and actuator where the following second order transfer function is used to represent the dynamics of the speed governor [255]

$$\frac{\tau s+1}{\tau_1 s^2+\tau_2 s+1} \tag{3.54}$$

The actuator response is modelled by the following transfer function

$$\frac{\tau_3 s+1}{(\tau_4 s+1)(\tau_5 s+1)} \tag{3.55}$$

and the engine is represented by a time delay model as follows

$$e^{-\tau_6 s} \tag{3.56}$$

where $\tau_{1..6}$ are time constants for the speed governor, actuator and diesel engine. The calculated engine torque is then used to calculate the engine brake power as follows

$$P_B = 2\pi n Q_{eng} \tag{3.57}$$

The consumed energy can be calculated as a function of the engine brake power using an energy approach as suggested in [210] as follows

$$\text{Consumed energy} = \int P_B.dt \tag{3.58}$$

The second part of diesel engine dynamics describes the rotational motion and torque balance of the shaft as shown in Equation 3.59

$$2\pi I_m \dot{n} = Q_{eng} - Q_p - Q_f \tag{3.59}$$

where I_m: inertia of the rotating parts including the propeller and added inertia of the water (Kgm^2), n: shaft speed (rps), Q_p: propeller torque (N m), Q_f: friction torque (N m).

Friction torque has two components, static friction component and shaft speed dependent component. This friction affects the mechanical efficiency of the engine and it can be calculated as a function of the friction mean effective pressure. The friction mean effective pressure is the difference between the engine's indicated and brake mean effective pressure [256] which can be studied using physical models or experimental models [257]. An average friction torque value can be estimated by:

$$Q_f = \frac{10^3 V_d P_f}{2\pi N_{st}} \tag{3.60}$$

where friction torque is a function of the empty volume in cycle (V_d), friction loss pressure (P_f) and (N_{st})=1 for two-stroke and =2 for four-stroke diesel engine [258]. However, friction torque doesn't affect the engine's developed torque and speed greatly when the engine is giving more than 30 % of its torque [259]. Therefore, friction torque can be assumed to be from 5% to 8% of maximum torque of the engine [193].

Total inertia of the rotating parts is also required because it affects the acceleration of the rotational motion. It includes inertia of the engine, shaft, propeller, and propeller's entrained water inertia. Because of the interaction between propeller and water during operation, water causes added mass to the propeller mass which increase the propeller inertia. The propeller moment of inertia can be calculated as a function of its weight (W_p) and diameter as follows:

$$I_p = \frac{W_p D_p^2}{z} \tag{3.61}$$

where z = 19 to 28 [260]. Propeller's weight estimation should be done based on its detailed drawings. However, approximate approaches can be used to calculate propeller's weight such as the analytical expression presented by Schoenherr in [261]. For manganese bronze propellers, the following equation can be used [262]

$$W_p = ED^3(MWR)(BTF) \tag{3.62}$$

where W_p is the propeller weight in lb, E is constant, approximately = 0.26, and MWR is the mean width ratio =

$$\frac{\text{developed area per blade}}{D(\text{blade radius - hub radius})} \tag{3.63}$$

BTF is the blade thickness fraction =

$$\frac{\text{maximum blade thickness extrapolated to shaft axis}}{D_p} \tag{3.64}$$

Propeller's entrained water moment of inertia can be expressed as a percentage of propeller inertia which varies between 5 to 30 % [253] or it is 25% of the propeller inertia [263]. For merchant ship propeller, Schwaneeke suggested the following formula to estimate the entrained water moment of inertia [260; 263]

$$I_{ew} = \frac{0.0703(P/D)^2(EAR)^2\rho_w D_p^5}{\pi Z} \tag{3.65}$$

The engine turning wheel's moment of inertia also should be taken into consideration and its values recommended to be ranged from 5000 to 22000 $kg.m^2$ [264].

3.3.6.3 Emissions calculations

Diesel engines convert the chemical energy of fuels into mechanical energy through the combustion of fuels. Emissions are formed as a result of this process which includes hydrocarbons, oxides of nitrogen, sulphur, and carbon and particulate matter. There are two approaches used in order to determine greenhouse gases resulted from shipping, top-down and bottom-up approaches [265]. The main difference between them is; in top-down approaches emissions are calculated without respect to a specific location while bottom-up approaches emissions are calculated within a spatial context [266; 267]. However, both of them estimate emissions as a function of consumed energy and emissions factors. There are two types of emissions factors, factors related to main engine power 'power-based emission factors' and factors related to total fuel consumption 'fuel-based emission factors'. In IMO's second GHG study, fuel-based emission factors were used to calculate the emissions except for NO_x emissions to take MARPOL Annex VI into consideration which is done in this study and these factors are shown in Table 3.6. Also, engines' pollution maps are not always available therefore using fuel-based emission factors is suitable.

These emissions cause damages to the environment and quality of life which is associated with the global warming, acidic rain, photochemical smog, etc. The cost of

Table 3.6: Fuel-based emissions factors [41]

	(kg/tonne of fuel)	
CO	7.4	
CO_2	3130	*Residual fuel oil*
	3190	*Marine diesel oil*
NO_X	85	*Slow-speed diesel engine*
	56	*Medium-speed diesel engine*
N_2O	0.08	
PM	6.7	*Residual fuel oil*
	1.1	*Marine diesel oil*
SO_2	54	*Residual fuel oil (2.7 % S)*
	10	*Marine diesel oil (0.5 % S)*

this environmental damage caused by the use of petroleum fuels can be calculated as follows:

$$D_{env} = E_n C_p \tag{3.66}$$

where D_{env} is the cost of environmental damage, E_n is the energy consumption, and C_p is the environmental damage cost. For petroleum fuels, the environmental damage cost is 12.52 $\$/GJ$ [268]. This cost includes the negative impacts of using fossil fuels on the human, animals, plants, aquatic ecosystems, structures, and climatic changes. This cost should be added to the fuel price and taken into consideration while calculating the total operational cost of ships to reflect the various side effects of using petroleum fuels. Ships environmental damage can be reduced by using hybrid fuel cell propulsion systems and its mathematical modelling is described in the following section.

3.3.7 Hybrid fuel cell propulsion

In order to face the ever increasing pressure on the maritime industry to reduce its environmental impacts, a hybrid fuel cell electric propulsion system is proposed as a solution as discussed in the previous chapter. Fuel cell and battery are the main components of the hybrid fuel cell system in addition to an EMS which splits the propulsion power requirements between the fuel cell and the battery systems. To assess the effectiveness of fuel cell hybrid propulsion systems, fuel cell and battery mathematical models are included in the developed total ship system simulator. In this work, the generic models included in the SimPowerSystems (SPS) toolbox of Simulink of fuel cell [15] and battery [16] are used to simulate the performance of the fuel cell and battery.

3.3.7.1 Fuel cell

Modelling of fuel cells has received much attention in order to study and investigate their behaviour. Fuel cell models can be used in optimizing and controlling its performance, increasing its efficiency, reducing its associated costs and in the analysis of its reliability, feasibility, safety, and profitability. Due to its advantages, PEMFC has been used and studied for different applications including portable, transportation and stationery applications. Modelling of PEMFC has attracted attention and many performance models of PEMFC have been developed. There are three classes of PEMFC modelling; empirical, semi-empirical, or theoretical models [269]. It can also be classified into chemical, experimental and electrical models [270]. Empirical models are built based on experimental data to develop a relation between fuel cell inputs and outputs. Therefore, it is simple and does not require long computational time but it cannot represent well the fuel cell performance and phenomena. On the other hand, theoretical or mechanistic models are developed based on the fuel cell electrochemistry and physics that's why it provides detailed understanding of fuel cells but it requires excessive computational time. Fuel cell semi-empirical models combine fuel cells empirical relationships with its theoretically derived algebraic and differential equations. Therefore, it contains more details than the empirical models but requires less computational time than the mechanistic models [269; 271].

A generic fuel cell model is proposed and validated in [270] to represent both the dynamic and steady state performances of fuel cells fuelled with hydrogen and air. This model combines the electrical and chemical features of fuel cell models which makes it suitable for fuel cell systems simulations. Moreover, this model is integrated in SimPowerSystems library of electrical power systems as a generic hydrogen fuel cell stack model. The user of the fuel cell block can define the parameters of the fuel cell block from fuel cell data sheets provided by the manufacturer or choose between 4 pre-set fuel cell models, 3 PEMFC stacks varying from 1.26 kW to 50 kW or an AFC stack of 2.4 kW is also available. The fuel cell block has been validated against data sheet for a *NetStack PS6* fuel cell [15]. An equivalent circuit of fuel cell stack model is shown in Figure 3.5.

where fuel cell voltage (V_{fc}) is calculated as a function of open circuit voltage (E), internal resistance (R_{ohm}) and fuel cell current (i_{fc}) using Equation 3.67 and (E) is calculated using Equation 3.68

$$V_{fc} = E - R_{ohm}.i_{fc} \tag{3.67}$$

$$E = E_{OC} - N.A.ln\left(\frac{i_{fc}}{i_0}\right).\frac{1}{(s.T_d/3)+1} \tag{3.68}$$

where E_{OC}: open circuit voltage (V),

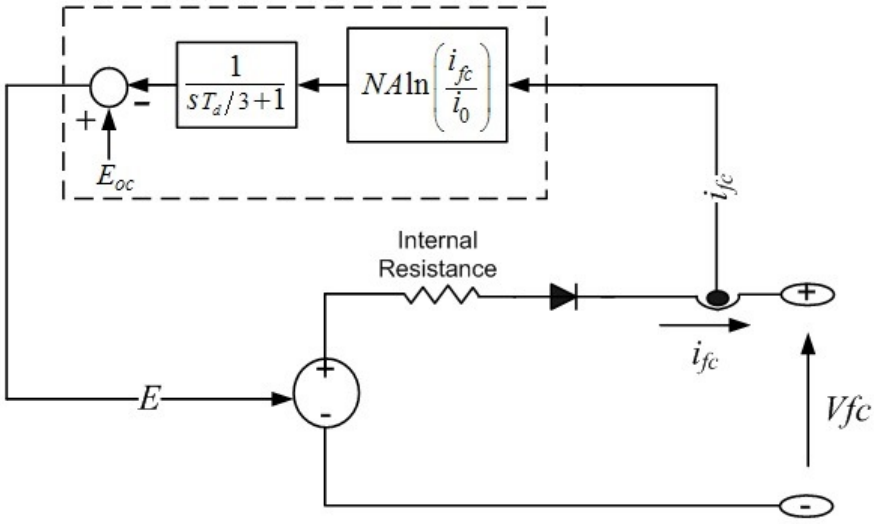

Figure 3.5: Simplified fuel cell stack model [15]

N: Number of cells,

A: Tafel slope (V),

i_0: Exchange current (A),

T_d: Fuel cell response time (sec).

This model capable of predicting fuel cell performance for both steady state and transient operation with an error of ± 1% taking into account fuel cell response time (T_d) or fuel cell stack settling time which represents time delay of fuel cell during sudden changes in fuel cell stack current as shown in Figure 3.6. The fuel cell response time is usually provided by the manufacturer and it depends on the fuel cell type.

Hydrogen consumption of PEMFC in grams can be calculated using Equation 3.69 as a function of fuel cell stack's number of cells (N), fuel cell current (i_{fc}) and Faraday constant (F).

$$H_{2cons} = \frac{N}{F} \int i_{fc} dt \tag{3.69}$$

Then, the hydrogen consumption is used to calculate the hydrogen cost and energy input to the PEMFC as a function of hydrogen higher heating value (HHV_{H_2}) as follows:

$$\text{Energy}_{\text{FC}} = \text{H}_{\text{2Cons}} \times \text{HHV}_{\text{H}_2} \tag{3.70}$$

Finally the required weight and volume of hydrogen storage system can be calculated as a function of the hydrogen gravimetric (ρ_{mH_2}) and volumetric density (ρ_{vH_2}) which depends on the storage method as shown in Table 3.7. In this study, hydrogen weight,

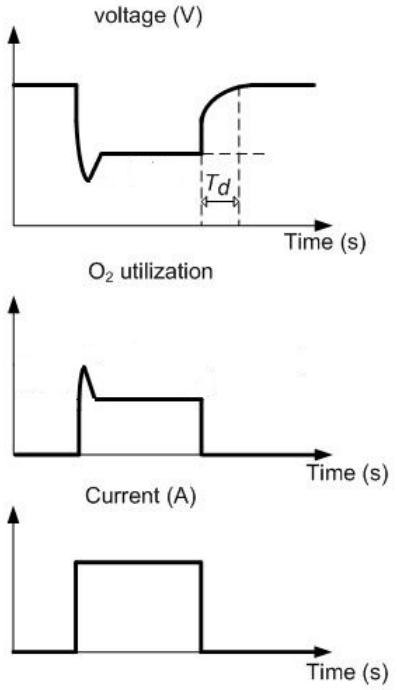

Figure 3.6: Fuel cell dynamics [15]

size, and cost are only taken into consideration and hydrogen is assumed to be stored as a cryogenic liquid in tanks as suggested in [272] for marine transportation applications. The shore hydrogen production facility, fuelling equipments, fuel venting arrangement, etc. are not within the scope of this study. However, the concept of hydrogen-powered ships is already developed by classification societies based on the safety standards. The used hydrogen in this study is proposed to be produced from wind energy through electrolysis. Although cheaper hydrogen production methods exist, wind energy is used to have a real zero emission fuel and eliminate the dependency on petroleum fuels. However, in case of using fossil fuels in producing hydrogen, a technology such as Carbon Capture and Storage (CCS) should be used. By using hydrogen based on petroleum fuels without technologies such as CCS, no advantages of reducing CO_2 emissions can be seen.

Table 3.7: Different methods of hydrogen storage [42–44]

	ρ_{mH_2} kgH_2/kg	ρ_{vH_2} kgH_2/m^3	Temperature °C	Pressure bar
High pressure gas cylinders	0.012	16	RT	200
	0.032	21	RT	350
	0.06	35	RT	700
Liquid hydrogen in cryogenic tanks	0.142	70.8	-253	1
Adsorbed hydrogen	0.02	20	-80	100
	0.071	29.6	-80	100
Absorbed on interstitial sites in host metals	0.02	115	RT	1

RT refers to room temperature

3.3.7.2 DC-DC converter

The voltage of the hybrid system components varies according to the demanded current from each power source. Therefore, an electronic circuit is needed to stabilise the power source voltage while providing the required power to the load. In order to regulate the output power of the PEMFC, an unidirectional DC-DC converter is used. Different types of converters include: boost converters which are used to step up the voltage, buck converters which are used to reduce the voltage, and buck-boost converters which are able to both boosting or bucking the voltage. The input current to the DC-DC converter (I_{in}) is readjusted according to the operating voltage ratio (k) [273] as follows:

$$\begin{aligned} \mathrm{k} &= \mathrm{V_{out}}/\mathrm{V_{in}} \\ \mathrm{I_{in}} &= \mathrm{I_{out}} \times \mathrm{k}/\eta_{Conv} \end{aligned} \tag{3.71}$$

where ($\mathrm{V_{out}}$) is the output voltage, ($\mathrm{V_{in}}$) is the input voltage and ($\mathrm{I_{out}}$) is the required current from the DC-DC converter subsystem as shown in Figure 3.7. A constant efficiency of the converter (η_{Conv}) of 95% can be assumed [114].

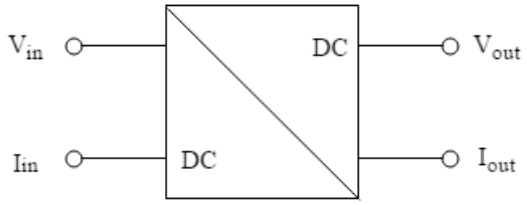

Figure 3.7: DC-DC converter block diagram

3.3.7.3 Battery

Because batteries are considered the main energy storage device for transportation applications, modelling of batteries receives much attention. Batteries modelling can be classified into two main approaches; electrochemical models and equivalent-circuit models. Electrochemical or mathematical battery models are developed based on Shepherd equation which describes the electrochemical behaviour of batteries. Meanwhile, equivalent-circuit or circuit-oriented battery models use a combination of voltage sources, capacitors and resistors to represent the battery electrical characteristics. Electrochemical battery models are more accurate than circuit-oriented models which includes battery lifetime modelling. However, equivalent-circuit models are easy to use and simpler [274; 275].

SimPowerSystems library includes an improved easy-to-use mathematical dynamic battery model that can represent both steady state and dynamic behaviour of the battery taking into account the response time of the battery. The generic battery block

can simulate four types of battery which are: lead acid, lithium-ion, nickel-cadmium or nickel-metal-hydride and it has been validated as well against experimental results with a maximum error of 5% however error increase to ± 10% when battery state of charge (SOC) decreases below 20% [275] but it is not recommended to fully discharge a battery. Figure 3.8 shows the equivalent circuit of the battery model [16].

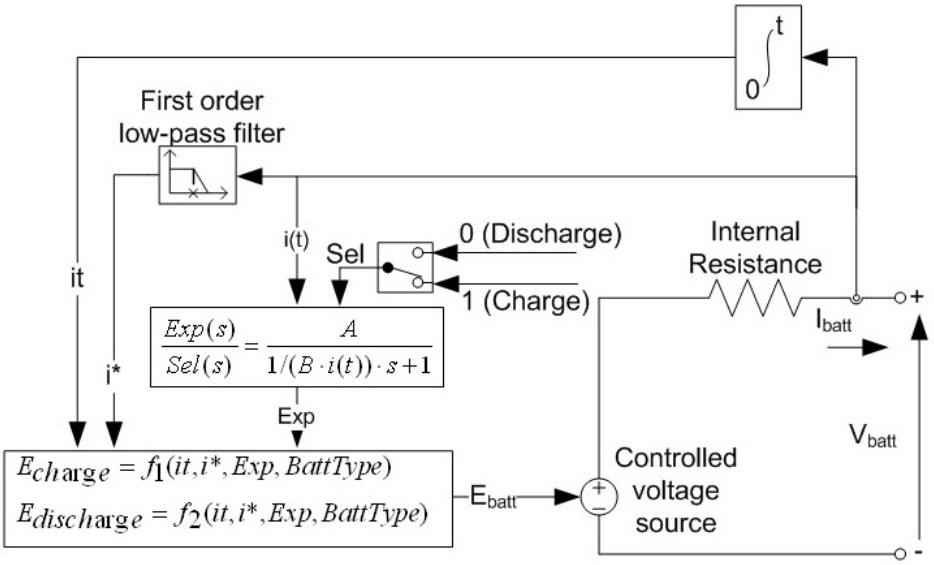

Figure 3.8: Simplified battery model [16]

Battery voltage (V_{batt}) is calculated as a function of open circuit voltage (E_{batt}), internal resistance (R_{ohm}) and battery current (i) as follows

$$V_{batt} = E_{batt} - R_{ohm}.i \tag{3.72}$$

where (E_{batt}) depends on battery type and whether the battery is charging or discharging and it is calculated as follows

$$\begin{aligned} E_{discharge} &= E_0 - K.\frac{Q}{Q-it}.i^* - K.\frac{Q}{Q-it}.it + A.exp(-B.it) \\ E_{charge} &= E_0 - K.\frac{Q}{it+0.1Q}.i^* - K.\frac{Q}{Q-it}.it + A.exp(-B.it) \end{aligned} \tag{3.73}$$

where E_0: Constant voltage (V), K: Polarization constant (A/h) or polarization resistance (ohm), Q: Maximum battery capacity (Ah), i^*: Low frequency current dynamics (A), A: Exponential voltage (V), and B: Exponential capacity $(Ah)^{-1}$.

The drained power and energy from the battery can be calculated as follows:

$$\begin{aligned} \text{power}_{\text{Batt}} &= \text{V}_{\text{batt}} \times \text{I}_{\text{Batt}} \\ \text{Energy}_{\text{Batt}} &= \int \text{power}_{\text{Batt}}.dt \end{aligned} \tag{3.74}$$

Number of consumed battery cycles (N_{cyc}) over time can be calculated as a function of its capacity (Q) and consumed current as follows:

$$\int abs(\mathrm{I_{Batt}}(t))dt/Q/2 \tag{3.75}$$

The required energy to recharge the battery ($\mathrm{Energy_{Batt_{Ch}}}$) back to its initial battery SOC (SOC_{ini}) can be calculated as a function of the final battery SOC (SOC_{fin}), the battery capacity and voltage as follows:

$$\mathrm{Energy_{Batt_{Ch}}} = \frac{(SOC_{ini} - SOC_{fin}) \times Q \times V_{batt}}{\text{Charging efficiency}} \tag{3.76}$$

3.3.7.4 Motor

In order to convert the electrical power into mechanical power, electrical motor is the most commonly used device. Electrical motors are widely used onboard ships for propulsion, thrusters, pumps, fans, winches, etc. Different types of electrical motors include direct current (DC) motors, synchronous motors, induction motors, permanent magnet motors, high temperature superconducting motors. In this project, DC motor is selected because of its wide range of speed and torque, smooth running capability, low cost and less complex control system [276].

DC motors must be fed with DC current which makes fuel cell a suitable source of current. Based on Kirchhoff's voltage law and Newton's 2nd law, the governing equations of the DC motor are:

$$\begin{aligned} J_m\dot{w} + bw &= K_t i_a \\ L\tfrac{di_a}{dt} + Ri_a &= V - K_e w \end{aligned} \tag{3.77}$$

where J_m is the motor moment of inertia, w is the rotational speed, K_t is the motor torque constant, i_a is the motor armature current, L is the motor inductance, R is the motor electrical resistance, V is the applied voltage and K_e is the motor electromotive force constant. The generated torque by a DC motor (T_m) is proportional to the armature current as follows assuming constant magnetic field.

$$T_m = K_t i_a \tag{3.78}$$

The mechanical power of the motor is then calculated as a function of the generated torque and rotational speed as follows

$$P_m = T_m w \tag{3.79}$$

3.3.7.5 Energy management strategy

For hybrid fuel cell propulsion systems, the proper split of the required power between the fuel cell and the battery is a challenging problem which requires the design of an energy management strategy. The EMS controls the dynamic behaviour of hybrid systems, which affects the system performance, size, weight, lifetime of its components, efficiency and fuel consumption. Therefore, developing a suitable EMS for hybrid propulsion systems has been a very important research topic.

Based on the the function and requirements of the hybrid propulsion system, a suitable EMS should be selected. The objectives of an EMS include reducing hydrogen consumption [277], increasing the fuel cell efficiency, reducing the size and weight of the power system, reducing the operation cost, reducing the stress on the power system components to prolong its working lifetime [17; 42; 278; 279]. EMS objectives also include reducing emissions, maintaining the battery SOC or the bus voltage at a certain level [11; 280].

Most of the work reported in the literature on EMS tends to focus on the automotive industry applications; however, several studies have been made on developing EMS for marine applications. A state-based EMS has been developed in [20] for a passenger vessel equipped with a fuel cell/battery hybrid power system with the main objective of maximizing the system efficiency. For the same vessel, a fuel cell/battery/ultra-capacitor hybrid power system with a fuzzy logic EMS has been proposed in [281] to further enhance the performance of the hybrid system. A hybrid fuel cell/battery system was developed for a 20 m long tourist boat in Korea with a total power of about 90 kW. The developed EMS for this boat aims to provide the required power using mainly the fuel cell system in a load-following mode and discharge the battery power whenever the required power is higher than the fuel cell system available power [175]. For underwater vehicles and small ships, an EMS has been developed which requires the fuel cell to provide an average power demand in a load-levelling mode, while the energy storage system is discharged or recharged when the required power is higher or lower the average power demand supplied by the fuel cell [42; 282].

There are several types of EMS exist such as the state-based EMS [20], equivalent consumption minimization strategy (ECMS) [283], rule-based fuzzy logic strategy [17], charge depleting and charge sustaining (CDCS) strategy [284], wavelet transform based strategy [285], variable frequency control techniques [286], classical PI and PID strategies [17], stochastic dynamic programming [287], and adaptive optimal control [288]. Computational time and complexity of each EMS are different, therefore only

four EMS are selected to be modelled and compared which are state-based EMS, PI EMS, CDCS EMS, and ECMS. The selected strategies are the most commonly used with less computational complexity and they are chosen for their simplicity and ease of realizability using standard microprocessor based solution [17].

- **State-based EMS:**

  State-based control is one of the deterministic rule-based methods used to control each component of the hybrid system for different transportation applications. This kind of strategy can have many operating states to decide the operating points of the fuel cell and battery systems according to the required power and the battery SOC taking into consideration the operational limits of the hybrid system components [289; 290].

  In order to maximize the propulsion system efficiency, a state-based EMS was developed in [20] to determine the proper split of the required power between the components of the hybrid fuel cell/battery system of the 'FCS Alsterwasser'. This EMS consists of 11 states for 11 possible cases of combination between battery SOC, required load power (P_{load}), fuel cell minimum power (P_{FCmin}), optimum fuel cell power (P_{FCopt}), maximum fuel cell power (P_{FCmax}), battery optimum discharge power (P_{optdis}), battery optimum charge power (P_{optchar}) and battery optimum power (P_{BATopt}) as shown in Table 3.8.

Table 3.8: Summary of a state-based EMS [20]

Battery SOC	State	Load Power	Fuel cell reference power
SOC > 80%	1	$P_{\text{load}} \leq P_{\text{FCmin}}$	P_{FCmin}
	2	$P_{\text{load}} \leq P_{\text{FCmin}} + P_{\text{optdis}}$	P_{FCmin}
	3	$P_{\text{load}} \leq P_{\text{FCmax}} + P_{\text{optdis}}$	$P_{\text{FC}} = P_{\text{load}} - P_{\text{optdis}}$
	4	$P_{\text{FCmax}} + P_{\text{optdis}} < P_{\text{load}}$	P_{FCmax}
50% ≤ SOC ≤ 80%	5	$P_{\text{load}} \leq P_{\text{FCmin}}$	P_{FCmin}
	6	$P_{\text{load}} \leq P_{\text{FCopt}} - P_{\text{BATopt}}$	P_{load}
	7	$P_{\text{load}} \leq P_{\text{FCopt}} + P_{\text{BATopt}}$	P_{FCopt}
	8	$P_{\text{load}} \leq P_{\text{FCmax}}$	P_{load}
	9	$P_{\text{load}} > P_{\text{FCmax}}$	P_{FCmax}
SOC < 50%	10	$P_{\text{load}} \leq P_{\text{FCmax}} - P_{\text{optchar}}$	$P_{\text{load}} + P_{\text{optchar}}$
	11	$P_{\text{load}} > P_{\text{FCmax}} - P_{\text{optchar}}$	P_{FCmax}

  Values of battery optimum charge, discharge and optimum power and fuel cell minimum and maximum power should be selected based on the current and voltage limits of the battery and fuel cell systems in order to maximize the system efficiency which is the main objective of this EMS [20]. The main inputs of this EMS are the required load power and the battery SOC which are used to decide the fuel cell power. Then, the difference between the required load power and the fuel cell power is used to charge or discharge the battery.

As can be seen in Table 3.8, based on the battery SOC and load power, the fuel cell power is chosen. The difference between fuel cell power and load power is drained from the battery if its SOC is higher than 50% as in states 2 and 4 or the power difference will be used to charge the battery if its SOC is less than 50% as in states 5 and 10. In states 3, 6, 8 and 10, fuel cell is regulated to follow the load power meanwhile in other states the fuel cell power is constant and the battery will compensate the transient power or the battery will be charged if the fuel cell power is higher than the required load power. The fuel cell works at its optimum power value in state 7 only.

- **Classical PI EMS:**

  Recently, EMS based on PI and PID controllers have been proposed due to their simplicity and it can be easily tuned for the examined mission profile [17]. The main goal of classical PI EMS is to maintain the battery SOC at its nominal value in order to reduce the battery stress and extend its lifetime [280]. In classical PI EMS, the current battery SOC is compared to a reference value of battery SOC (SOC_Ref) to control the battery power or current using PI controller as shown in Figure 3.9. This battery power is subtracted from the load power to calculate the fuel cell power. Then, the battery and fuel cell power are divided by the voltage to calculate the current drained from the fuel cell and battery. By discharging/charging the battery, battery SOC will change and will be fed back to the EMS block to close the loop of the PI controller.

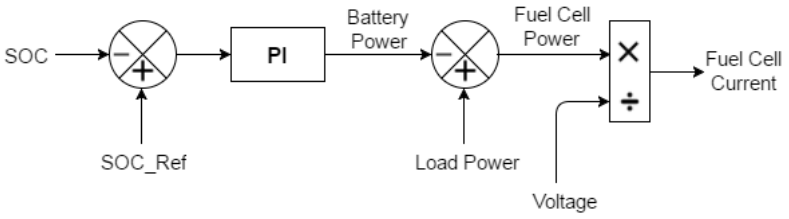

Figure 3.9: Classical PI control energy management strategy [17]

This strategy tends to use more power from the battery system when the battery SOC is above its reference value meanwhile the fuel cell provides low power. When the battery SOC drops below its reference value, the fuel cell system is used to provide the load power and charge the battery to its reference value. The inputs of this EMS are the battery SOC and the required load power with an ultimate goal of maintaining the battery SOC around its reference value which regulates the fuel cell to follow the required load power or operate at its maximum power when the current battery SOC drops below its reference value. This can affects the fuel cell efficiency, hydrogen consumption and lifetime. Therefore, an improvement to the classical PI EMS is proposed in this study that takes fuel cell efficiency into account as an input to the strategy to avoid the operation of fuel cells in a poor efficiency region which can reduce its fuel consumption. Furthermore, its operational stresses

can be lowered that allows the reduction of fuel cell maintenance cost and extending its lifetime.

- **Improved PI EMS:**

  In the proposed PI EMS, fuel cell efficiency (FC_Eff) is taken into consideration as an input by comparing it to a reference value (FC_Eff_Ref) in order to control the fuel cell current which is removed from the required load current to obtain the battery current. Then, the battery current is updated according to the difference between the current battery SOC and its reference value as shown in Figure 3.10 ensuring that the power requirement is completely satisfied. By consuming power from the battery and fuel cell, battery SOC and fuel cell efficiency will change and fed back to the EMS to close the loops of the PI controllers.

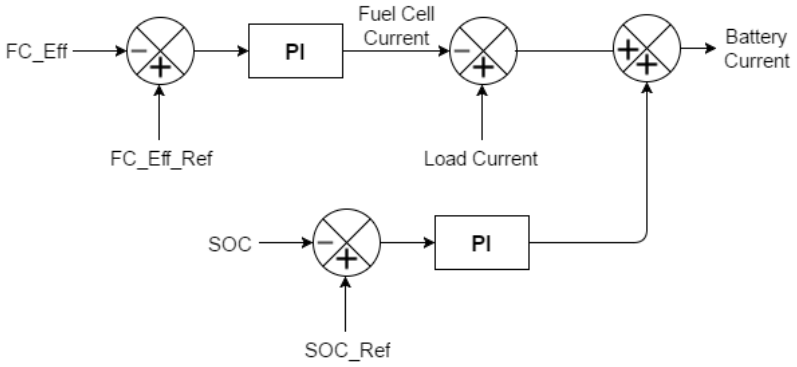

Figure 3.10: Proposed PI control energy management strategy

PI controllers can be reliably used for the proposed PI EMS, since fuel cell efficiency is linear with the fuel cell current for approximately 80% of load currents after an initial non-linearity region at low loads as shown in Figure 3.11 which can be neglected [291]. Moreover, using fuel cell efficiency as an input allows the fuel cell to operate more at higher efficiency which means less hydrogen consumption, less stress and longer lifetime. Moreover, the proposed PI EMS maintains the required battery SOC which is the main objective of the classical PI EMS. The gains of the PI controllers of the original and the proposed PI strategies can be manually tuned for the examined driving cycle with the help of the MATLAB control system toolbox in order to have balance between the controller performance and robustness [292].

- **Equivalent fuel consumption minimization strategy (ECMS):**

  ECMS is one of the most common real-time optimization approach control methods based on cost functions which generates a near-optimal solution of the required power split problem. ECMS doesn't require a priori knowledge of the future power requirement and its concept is to minimize the instantaneous fuel consumption of the hybrid system [17; 293]. This concept was proposed in [294] to develop an instantaneous optimization EMS for hybrid vehicles. The equivalent fuel

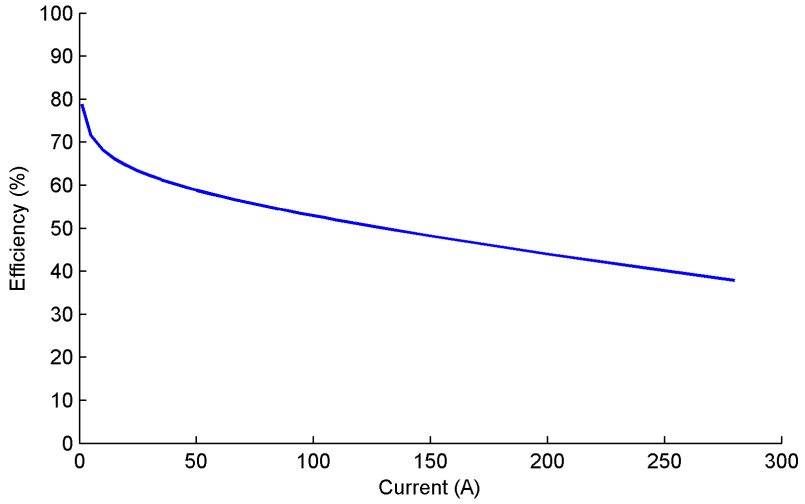

Figure 3.11: Fuel cell stack efficiency versus current

consumption (C) includes the actual fuel cell hydrogen consumption (C_{FC}) as well as the equivalent consumption of the battery (C_{Batt}). The optimization problem to minimize the hydrogen consumption can be defined as follows:

$$P_{\mathrm{FCopt}} = \overset{\mathrm{argmin}C}{P_{\mathrm{FCopt}}} = \overset{\mathrm{argmin}(C_{\mathrm{FC}}+\alpha.C_{\mathrm{Batt}})}{P_{\mathrm{FCopt}}} \tag{3.80}$$

where (α) is a penalty coefficient which is used to accomplish the charge-sustaining operation of the battery. It is calculated as a function of battery SOC limits as follows:

$$\alpha = 1 - 2\mu \frac{(\mathrm{SOC} - 0.5(\mathrm{SOC_H} + \mathrm{SOC_L}))}{\mathrm{SOC_H} - \mathrm{SOC_L}} \tag{3.81}$$

where ($\mathrm{SOC_H}$) and ($\mathrm{SOC_L}$) are the upper and lower limit of the battery SOC respectively. Meanwhile, μ is the SOC constant which is used to reflect the characteristics of the battery charge/discharge process [295]. As shown in Figure 3.12, based on the load power and the battery SOC, fuel cell power is decided. The fuel cell power is limited between a minimum and maximum fuel cell powers to avoid the operation in a poor efficiency region. This fuel cell power is then removed from the load power to calculate the battery power. Then, fuel cell and battery powers are divided by voltage to calculate the value of current.

- **Charge depleting and charge sustaining**

  In order to minimize the fuel cost, CDCS strategy has been proposed. This strategy prioritizes the usage of the battery energy until the battery SOC decreases to a certain value. Then, this EMS sustains the battery SOC and the fuel cell system starts to supply the required power [284]. At the start of the journey, a charge depleting (CD) mode is applied where the fuel cell system is turned off or works

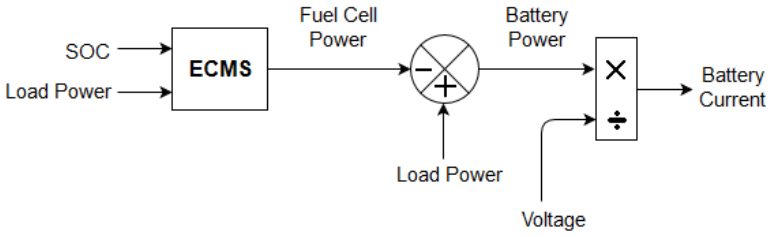

Figure 3.12: Equivalent fuel consumption minimization strategy scheme

at its minimum power and the battery system provides the required power. When the battery SOC is low, the hybrid fuel cell system shifts to a charge sustaining (CS) mode for the rest of the journey as shown in Figure 3.13.

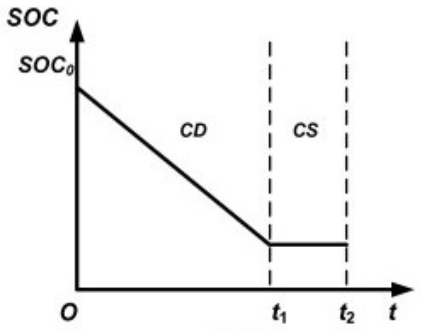

Figure 3.13: Charge depleting charge sustaining strategy scheme [18]

Due to the fact that the electric power is less expensive than hydrogen and normally the trip length is not known a priori, CDCS EMS is used to save the fuel cost. As shown in Figure 3.14 the main inputs to CDCS EMS are the required load power and the current battery SOC which are used to decide the battery power. After that, fuel cell power is calculated according to the applied depleting or sustaining mode.

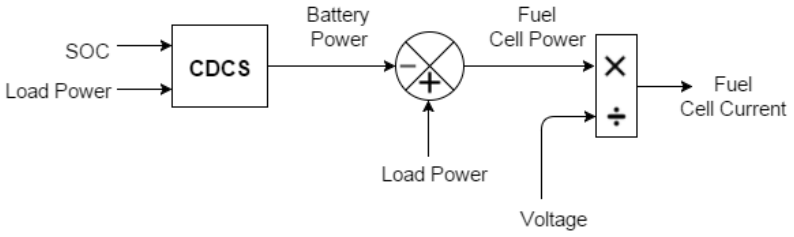

Figure 3.14: Charge depleting and charge sustaining strategy scheme

- **Multi-scheme EMS**

  Due to the fact that each EMS has its main objective and has different impact on the overall efficiency, hydrogen and total energy consumption and total cost of the hybrid system, a multi-scheme EMS should be used [17]. A multi-scheme EMS is developed in this project which contains different strategies. The developed

multi-scheme EMS switches between different strategies during ship operation and chooses the suitable strategy instantaneously based on the required load power and current battery SOC to achieve the required objective. Whilst most of the studies about EMS give their attention to the hydrogen consumption, which is certainly important, more focus should be on the total consumed energy taking into consideration the battery depleted energy and the required energy to recharge the battery back to its initial SOC. The objective of the developed multi-scheme EMS is to minimize the total consumed energy by the hybrid system which includes the used fuel cell energy, depleted energy from the battery system during the voyage, and the required energy to charge the battery system back to its initial SOC. This objective has been selected for the sake of increasing the energy efficiency of ships which is a major current focus of the IMO and for fairly comparing different strategies. The developed multi-scheme EMS consists of the four considered EMS in this study which are: State-based EMS, ECMS, Classical PI EMS, and CDCS strategy in addition to a code that selects the suitable EMS and switches between different strategies during operation to minimize the total consumed energy based on the required load power and the current battery SOC.

For the examined ship *FCS Alsterwasser* which is the first fuel cell passenger ship, an extract of its power requirements during a typical voyage on the Alster, Hamburg, Germany has been measured and published in [296; 20] is shown in Figure 3.15. This power requirement includes the propulsion and auxiliary powers which includes power requirements during cruising, docking, stopping, and acceleration phases of the ship journey. In order to develop the multi-scheme EMS, the ship power requirement is divided into three power modes; low power mode, cruising mode, and high power mode as shown in Figure 3.15. Low power mode includes the stopping phase of the ship voyage and low power requirements during the docking phase. The cruising mode contains the ship power consumption around its cruise speed while the high power mode includes the peak requirements of the ship during acceleration and docking.

Moreover, the current battery SOC affects the calculated powers of the fuel cell and battery systems. Therefore, the battery SOC is also divided into three regions; low, medium, and high SOC regions. Then, a comparison is made between the four studied strategies energy consumption at different initial battery SOC for the three different power modes shown in Figure 3.15 to select the suitable strategy that minimizes the total consumed energy at different operational conditions. By doing this comparison, the suitable strategy that minimizes the total consumed energy is selected at different battery SOC and different power modes for the examined voyage. A code is then developed to implement this comparison in Simulink to select the suitable strategy that minimizes the total consumed energy at different battery SOC and power modes while performing the examined voyage. The developed code allows the hybrid system to use different strategies during the

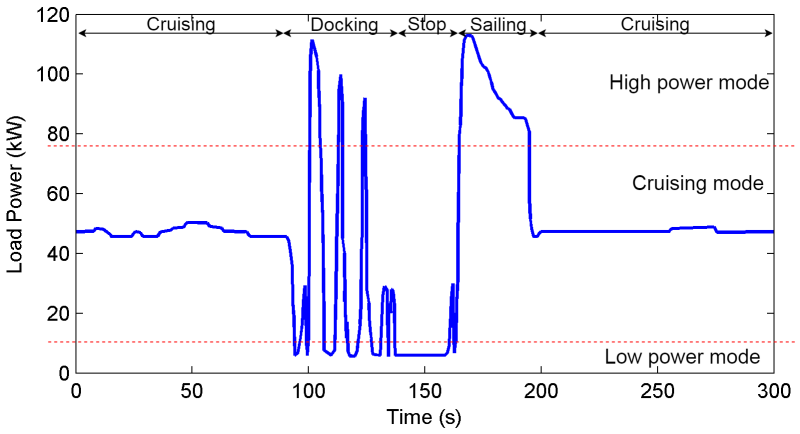

Figure 3.15: Different modes of the FCS Alsterwasser typical power requirements for the multi-scheme EMS development

voyage according to the required load power and current battery SOC as shown in Figure 3.16 in a way that reduces the total consumed energy by the end of the voyage. Simulation parameters and results used to develop this code are presented in the following chapters.

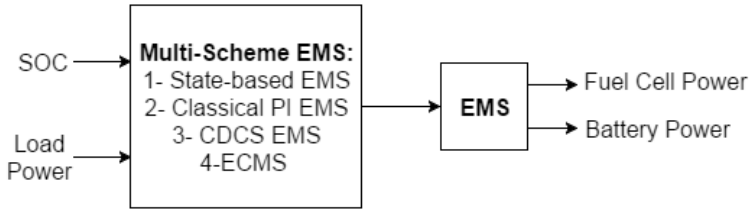

Figure 3.16: Multi-scheme EMS

3.4 Summary

In this chapter the governing equations used in the ship simulator were presented including a literature review about previous ship simulators. Mathematical modelling of the ship calm water resistance using regression analysis equations was made. Two different methods of providing weather data required by the simulator were discussed as it is important for added resistance calculations. Transfer functions were used to simulate 2 and 4-stroke diesel engines because only the engine torque is required by the simulator and different approaches for emissions calculation were also discussed. SimPowerSystems blocks of fuel cell and battery are used in the developed ship simulator to study different architectures of hybrid fuel cell/battery propulsion systems with different degrees of hybridization. Also, the mathematical modelling of DC-DC converters and DC electric motors have been presented. Hydrogen storage calculations have also been taken into consideration as well.

Four different energy management strategies have been presented focusing on the most commonly used EMS which are: State-based, Classical PI, ECMS, and CDCS strategies. Moreover, an improvement to the classical PI strategy has been presented that takes the fuel cell efficiency into consideration as an input to the strategy to increase fuel cell efficiency and reduce its stresses and fuel consumption. A multi-scheme energy managements strategy has been developed for the first time for marine applications with an objective of minimizing the total consumed energy which includes the consumed fuel cell energy as well as the battery depleted energy during operation and the required energy to recharge the battery back to its initial battery SOC. In the next chapter, MATLAB/Simulink implementation of the presented governing equations will be made to develop the ship simulator while Chapters 5 and 6 will contain the results of simulations using the developed ship simulator.

Chapter 4

Ship Simulator

4.1 Introduction

In this chapter, the governing equations used to develop the ship simulator is implemented in the simulation environment. Mathematical equations can be implemented with a graphical programming representation using blocks by Simulink environment. Simulink is a block diagram environment offered together with MATLAB for multi-domain simulation and model-based design developed by MathWorks. Simulink can be used in design, simulation, modelling and analysing systems and it is used in this project to develop the ship simulator. Simulink provides graphical editor and customizable block libraries for managing and modelling systems which can be linear or nonlinear with continuous time, discrete, or hybrid of them.

Simulink can also import MATLAB algorithms into models using MATLAB function blocks. You can build model using Simulink editor and drag predefined blocks from Simulink library into Simulink editor and connect these blocks to establish mathematical relationships between them using signal arrows. Using information of your model, Simulink can simulate the dynamic behaviour of your model using solvers which can be fixed-step or variable-step solvers. Simulink environment provides an appropriate interface for the ship simulator blocks to exchange the required variables between each other. You can analyse the simulation results, visualize the system behaviour and understand it using Simulink debugging tools. Therefore, Simulink is used to simulate ship and its propulsion systems.

Ship propulsion systems modelling and simulation has become a vital tool which can be used at conceptual and detailed design stages for different purposes such as manoeuvring and seakeeping analysis, machinery control development, machinery performance and vibration analysis, studies of equipment health monitoring development, machinery operation training, etc. The governing equations presented in Chapter 3 are implemented

in Simulink environment in this chapter in order to develop a time-domain ship simulator capable of predicting the ship performance with three DOF taking into consideration weather condition and added mass effects. This simulation tool is used to assess the effectiveness of fuel cells as a main source of power for hybrid propulsion systems in addition to investigating the effect of EMS on the performance of these systems as will be discussed in Chapters 5 and 6.

4.2 Overall simulator structure

As shown in Figure 4.1, the overall ship simulator consists of calculation blocks where each block represents a certain component of the ship system such as propeller or performing a certain calculation like the interaction between the ship and the surrounding environment.

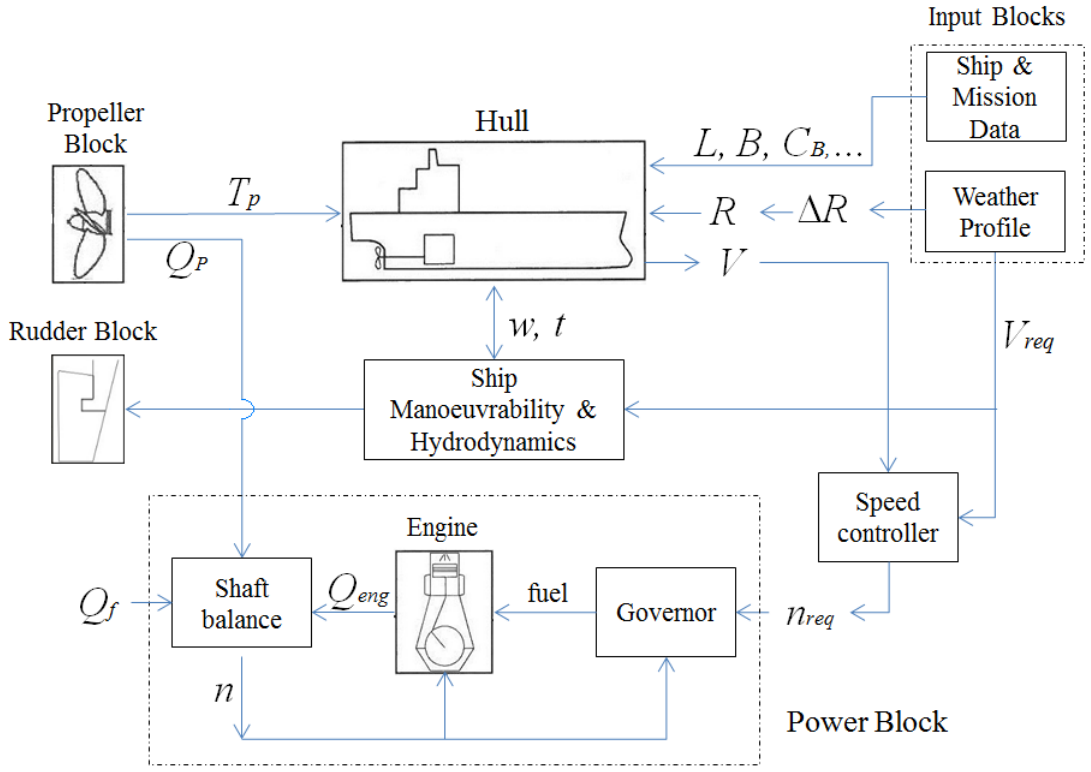

Figure 4.1: Overall ship simulator representation using diesel propulsion system

Two input blocks which are responsible for presenting data about the examined mission and the ship. Data about the mission such as the required speed (V_{req}), the required rotational speed (n_{req}), and the route weather. Data about the ship such as the ship dimensions and its forms' coefficients, propeller characteristics, etc. Then, this data will be used to calculate the ship calm water resistance (R), added resistance due to wind and waves ($\triangle R$) and its hydrodynamics coefficients (w) and (t). Next, these forces are

balanced with the propeller thrust (T_P) to calculate the actual speed of the ship (V) taking into account ship manoeuvrability in three DOF (surge, sway and yaw). The current ship speed is compared with the required speed to control the required propeller rpm using a PID speed controller in the speed controller block. The propeller required power is provided by the power block where the power source can be a 2-stroke, 4-stroke diesel engine, or hybrid fuel cell/battery propulsion system.

In preliminary design stage, the towing tank tests may not have been completed and the final hull form has not been finalized that's why the developed ship simulator could not be more complicated as hull model data may not be available at this stage. In the following sections, each block is discussed in more details. Then, a time step discussion of the developed ship simulator is presented.

4.2.1 Input Data Blocks

In order to perform the simulation, some inputs must be provided to the model by the user who simply will edit an input MATLAB file with the new data. Then, the inputs' values are fed to appropriate output ports automatically and will be passed between other blocks of the ship simulator using Simulink environment. The required input data contains information about the ship, the examined voyage, and the surrounding environment as shown in Table 4.1.

Table 4.1: Ship simulator required inputs

	Inputs
Ship particulars	L_{PP}, L_{WL}, L_{OS}, B, T, T_a, T_f, C_B, D_P, BAR, P/D, Z, Bulbous bow, Number of bosses, brackets, thrusters, rudders. Rudder area & aspect ratio, Lateral & frontal projected areas
Mission data	Required speed or propeller rpm, ship course angle, rudder angle
Environment	BN, weather angle, water temperature& density

Moreover, input data blocks have two options of providing wind speed and direction for the simulation. The user can provide a real wind speed and angle time profiles manually from ship's noon reports or a meteorological database such as NOMADS as discussed in 3.3.2.1 or data can be randomly generated using a developed MATLAB code based on probability theory. In case of limited real weather data, values of BN, wind angle and its corresponding probability can be used by the developed MATLAB code to generate BN and wind angle time profiles during the simulation to be used to calculate added resistance. Figure 4.2 shows an example of randomly generated weather profile. The developed MATLAB code generates BN and wind angle values every time step which can be changed. However, as shown in Figure 4.2, BN value can change from a small value such as 3 to a high value of 8 in one time step which is not realistic. Therefore, multiple runs should be made using different weather profiles to assess the uncertainty in results.

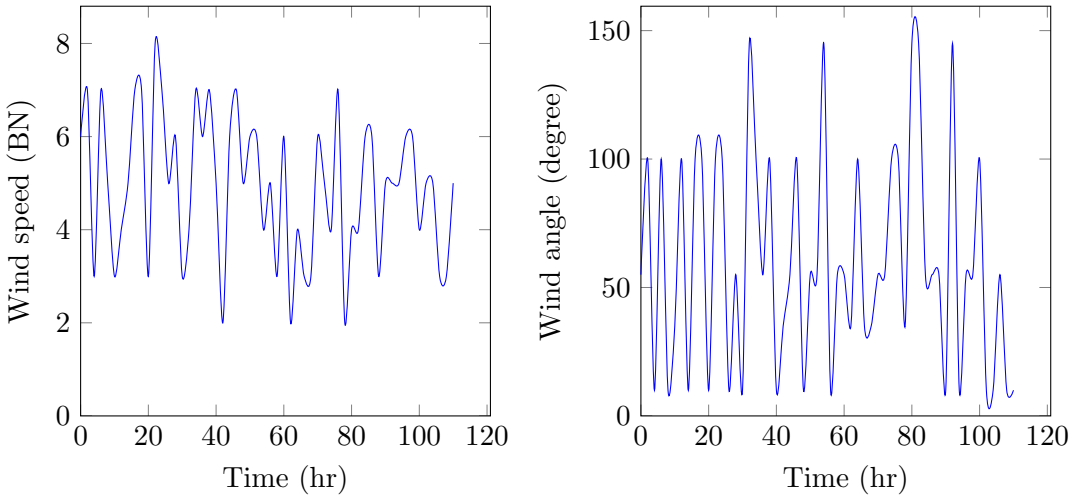

(a) Beaufort Number

(b) wind angle

Figure 4.2: Example of randomly generated weather profile with 2 hours time step

Input blocks can also use two modelling approaches, the forward facing model or the backward facing models. The forward facing model is used if a predefined required power profile is provided by the user. Otherwise, the backward facing model can be used if a required ship speed profile is available and the model calculates the corresponding power [297]. Therefore, two signals are available which are ship speed and the required rpm where one of the two signals is terminated based on the chosen modelling approach using a terminator block. Figure 4.3 shows input blocks where one block is concerned with the ship and the other is about the mission and the surrounding environment.

4.2.2 Hollenbach calm water resistance block:

Because of its modern database, ease of programming, and its wide range of application, Hollenbach regression analysis is selected as discussed in 3.3.1 to be used to calculate calm water resistance of the examined ship. As shown in Table 4.2, it requires less inputs than Holtrop-Mennen method which is required especially in early design stage. Hollenbach approximated the residual resistance in his analysis while the frictional resistance is calculated by the ITTC method but using hollenbach approximation of the ship wetted surface area. Graphical representation of calm water resistance block in Simulink is shown in Figure 4.4.

Table 4.2: Hollenbach calm water resistance block inputs and outputs

Inputs	Outputs
L_{PP}, L_{WL}, L_{OS}, B, T, T_a, T_f, C_B, D_P, Bulbous bow, Number of bosses, brackets, thrusters, rudders. Current ship speed, Water viscosity and density	Mean calm water resistance

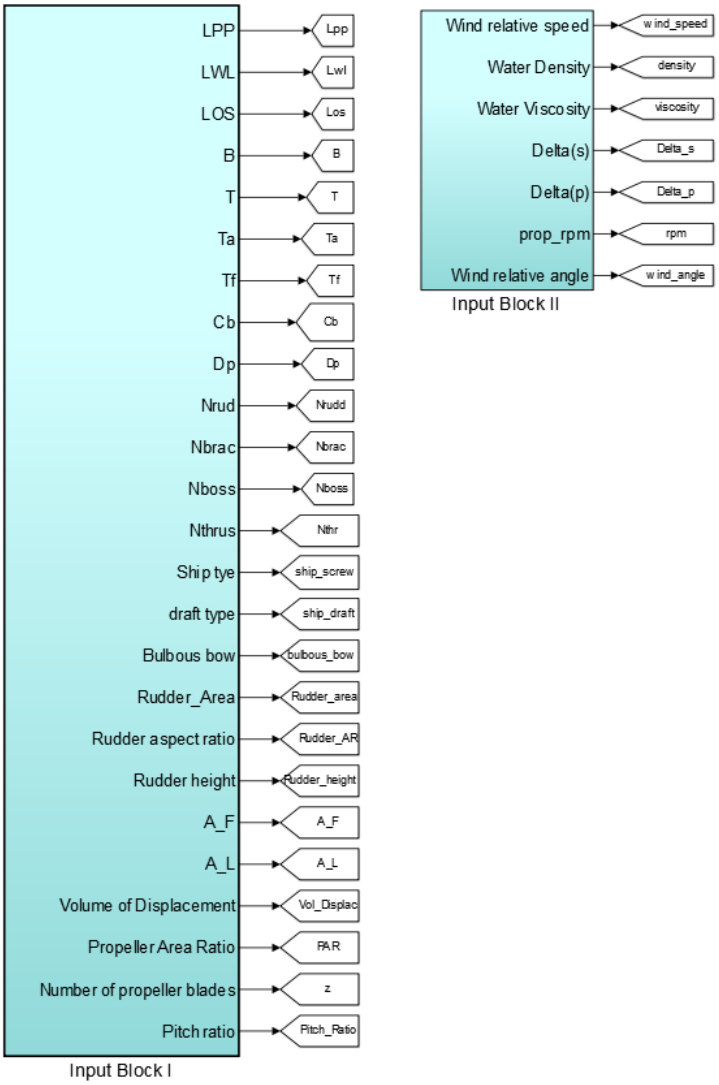

Figure 4.3: Input data blocks in Simulink environment

4.2.3 Added resistance block:

Added resistance block contains Aertsssen's formula as well as Townsin-Kwon method [233] updated by Kwon later in [38] to calculate the added resistance due to wind and waves as discussed in 3.3.2. Added resistance block contains as well Blendermann method of calculating added resistance due to wind and Kreinter's formual to estimate the increase in resistance due to waves. The selection of the used added resistance calculation method will depend on the availability of required weather parameters and the examined voyage duration. The inputs and outputs of added resistance block is shown in Table 4.3 and Figure 4.5 shows the graphical representation of this block in case of using Aertsssen's formula. Results of this block will be verified later in a separate section.

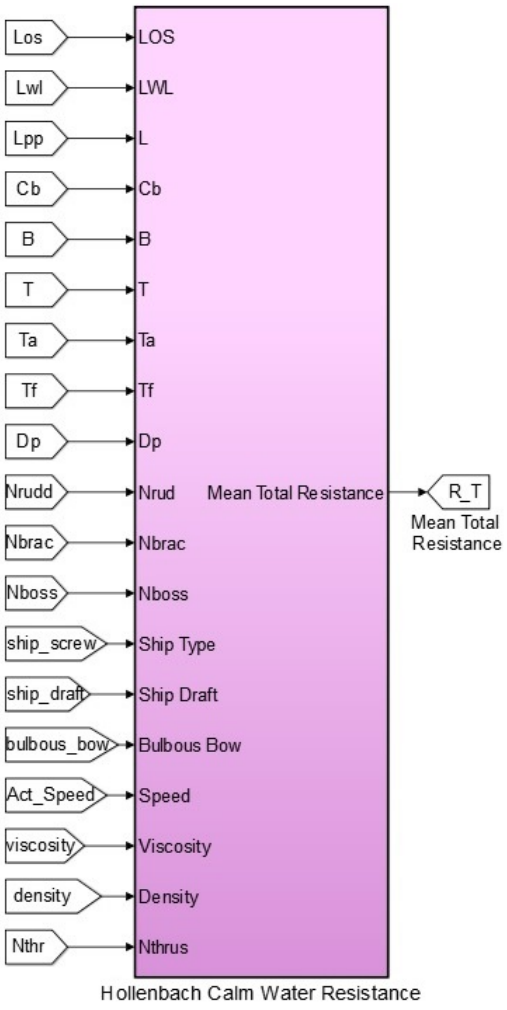

Figure 4.4: Hollenbach calm water resistance block in Simulink environment

Table 4.3: Added resistance block inputs and outputs

Inputs	Outputs
Beaufort number, Wind angle off bow, L_{PP}, B, C_B, γ, R, H_w, ρ_a Frontal projected area & lateral-plane area	Added resistance in X- & Y- directions, Speed loss percentage, and Added resistance percentage

4.2.4 Ship hydrodynamics block:

This block is responsible for representing the interaction between the ship hull and the propeller in terms of wake fraction and thrust deduction. Wake fraction is calculated using Equation 3.33 for single screw ships and Equation 3.29 for twin screw ships where thrust deduction is calculated using Equation 3.34 for single screw ships and Equation 3.36 for twin screw ships. Inputs and outputs of this block is shown in Table 4.4.

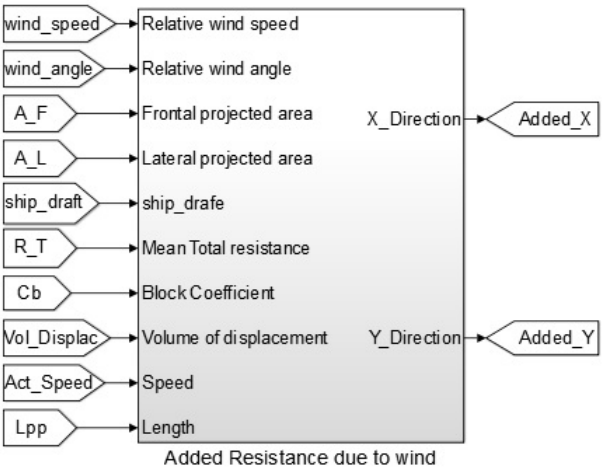

Figure 4.5: Added resistance block in Simulink environment

Table 4.4: Ship hydrodynamics block inputs and outputs

Inputs	Outputs
L_{PP}, B, T, C_B, D_P, Current ship speed Single or twin screw ship	Wake fraction, Thrust deduction

4.2.5 Propeller block:

This block is responsible for calculating propeller thrust and torque using non-dimensional coefficients of thrust and torque for Wageningen B-screw series. Then, the propeller torque and thrust will be used to calculate the delivered and thrust power. The propeller block is developed in a way that allowing to take astern propulsion into consideration which is used for a short period to slow the ship or stop it assuming the same way of torque and thrust calculation but with a negative sign which is not very accurate. The used equations to calculate the propeller thrust and torque coefficients will be verified in a separate section. The inputs and outputs of propeller block is shown in Table 4.5 and graphical representation of this block is shown in Figure 4.6.

Table 4.5: Propeller block inputs and outputs

Inputs	Outputs
D_P, water density, wake fraction, thrust deduction, current speed, rpm	Propeller torque and thrust, Delivered power and thrust power

4.2.6 Manoeuvrability block:

This block is responsible for representing ship manoeuvrability in three DOF which are surge, sway, and yaw for single and twin screw ships. It uses MGM manoeuvrability model which calculate the hydrodynamic forces and moments acting on the ship during voyages taking into consideration the added masses and added resistance in x and y

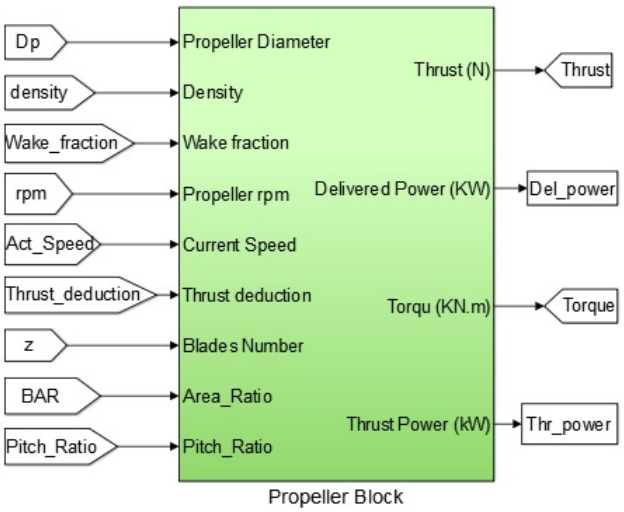

Figure 4.6: Propeller block in Simulink environment

directions. The main output of this block is the ship's speed which can be used then to calculate the travelled distance by the ship.

The resulted current speed from this block is the main input to the next block which is the speed controller block where it is compared to the required ship speed in order to control the propeller speed in case of adopting the backward facing model as discussed in 4.2.1. Table 4.6 shows inputs and outputs of the manoeuvrability block and Figure 4.7 shows its implementation in Simulink.

Table 4.6: Manoeuvrability block inputs and outputs

Inputs	Outputs
L_{PP}, B, T, C_B, D_P, Wake fraction, Propeller Thrust, Rudders height, area and angles, Calm Water Resistance, propeller rpm, Thrust deduction Added resistance in X- & Y- directions, pitch ratio, Water density	Current Speed, Travelled Distance

4.2.7 Speed controller block:

This block is active in case of adopting the backward facing model as discussed in 4.2.1. This block uses the current ship speed calculated by the manoeuvrability block and compare it with the required speed given by the user in the input blocks. The block contains a standard PID controller that calculate the required propeller rotational speed as a function of the error between the required speed and the current speed as shown in Figure 4.8. PID controller is selected due to its simplicity and parameters' few number to be tuned and it has been used successfully in feedback control systems [298].

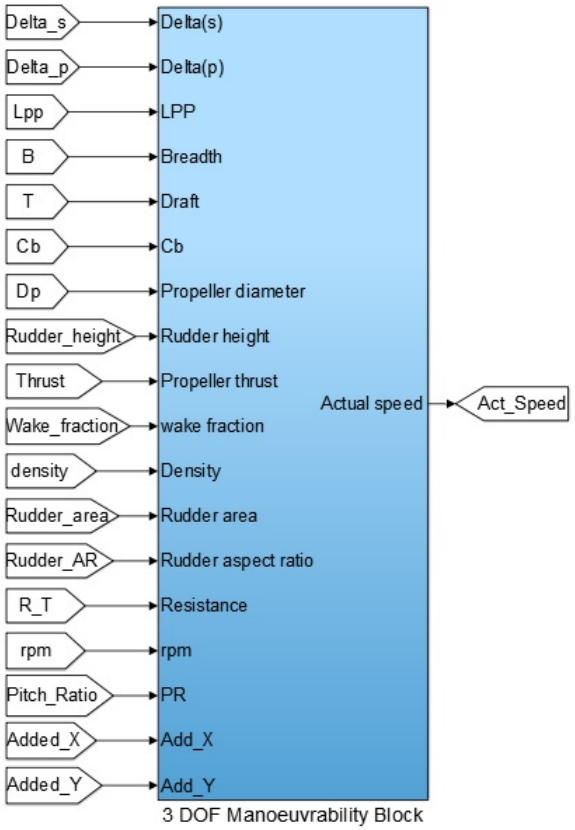

Figure 4.7: Manoeuvrability block in Simulink environment

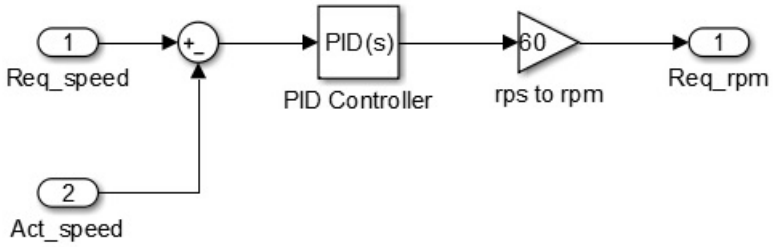

Figure 4.8: Speed block in Simulink environment

4.2.8 Power block:

Different power sources can be used to propel the ship such as diesel engines, turbines, electrochemical devices, or combination of those. The machinery performance analysis is required before deciding what is better which can be done using simulation as will be discussed in the following chapter. In order to have more flexible simulator, the power block is constructed in a way that facilitates the testing of different system configurations with different power sources. The main input of the power block is the required propeller speed to achieve the required ship speed and Table 4.7 shows the inputs and outputs of the power block.

Table 4.7: Power block inputs and outputs

Inputs	Outputs
Required propeller rpm, Propeller torque, SFOC, Number of fuel cell & battery, Inertia of rotating parts, Gear box ratio,	Current propeller rpm, Total fuel consumption, Brake power, Consumed energy, $CO, CO_2, NO_x, N_2O, PM, SO_2$ emissions

The required propeller speed signal is provided by the speed controller block in case of adopting the backward facing model or selected by the ship simulator user in case of adopting the forward facing model as discussed in 4.2.1. This block can represent a conventional mechanical propulsion system where a 2-stroke diesel engine is directly connected to a single screw propeller or a twin screw propulsion system using 4-stroke diesel engines and gearboxes. An example of the four-stroke diesel engine Simulink model is shown in Figure 4.9 where the main input of this model is the required rotational speed n_{req} which is compared with the current rotational speed n and the difference between them is converted into a signal sent to the fuel pump where $\tau_{1..6}$ are time constants for the speed governor, actuator and diesel engine. The output of this model is the engine torque Q_{eng} which is then used with the propeller torque Q_P to calculate the current rotational speed according to Equation 3.59 where I_m is the inertia of the rotating parts including the propeller and added inertia of the water and Q_f is the friction torque. The resulting engine torque and rotational speed are used to calculate the engine power, fuel consumption and emission as discussed in 3.3.6.3. and the consumed energy is calculated as a function of the power using Equation 3.58.

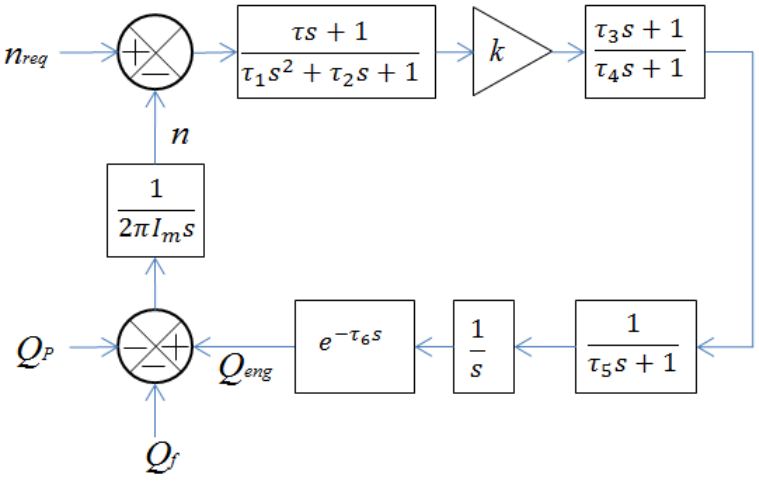

Figure 4.9: Four-stroke diesel engine dynamic model

Hybrid fuel cell propulsion systems can also be represented using the developed ship simulator where battery and fuel cell blocks are also included in the power block which allows the testing of different configurations of electric propulsion such as diesel-electric

propulsion and hybrid fuel cell electric propulsion systems. An example of a hybrid fuel cell/battery propulsion system is shown in Figure 4.10 which consists of DC motor & Controllers subsystem, fuel cell & DC-DC converter subsystem, battery subsystem, and an Energy Management Strategy (EMS) subsystem.

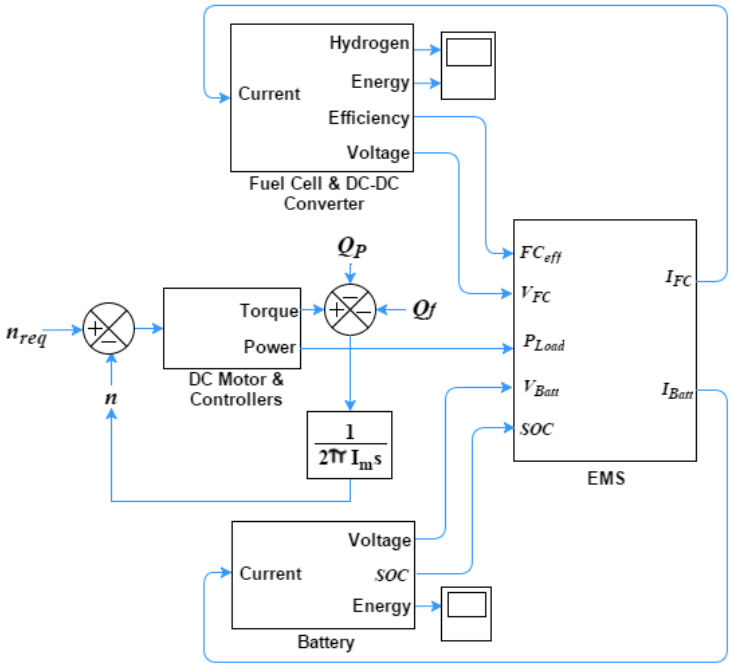

Figure 4.10: Hybrid fuel cell/battery propulsion system model

For hybrid fuel cell propulsion systems, the proper split of the required power P_{Load} between the fuel cell and the battery is a challenging problem which requires a suitable EMS. As illustrated in Figure 4.10, the EMS converts the required load P_{Load} into current and splits it to fuel cell current I_{FC} and battery current I_{Batt}. The main inputs to the EMS subsystem are battery SOC, battery voltage V_{Batt}, fuel cell efficiency FC_{eff}, and voltage V_{FC}. The consumed current by the fuel cell system is then used to calculate the fuel cell hydrogen consumption and energy. The consumed current for the battery system is also used to calculate the depleted cycles and energy to be added to the fuel cell energy to determine the total consumed energy for the examined voyage.

If the required load power is available as in the case study of the first fuel cell passenger ship *FCS Alsterwasser*, a required load power subsystem is added to the power block. The required load power subsystem contains the hybrid propulsion system's required power as shown in Figure 4.11. This power requirement is then fed to the EMS subsystem to be split between the fuel cell and battery systems as discussed earlier.

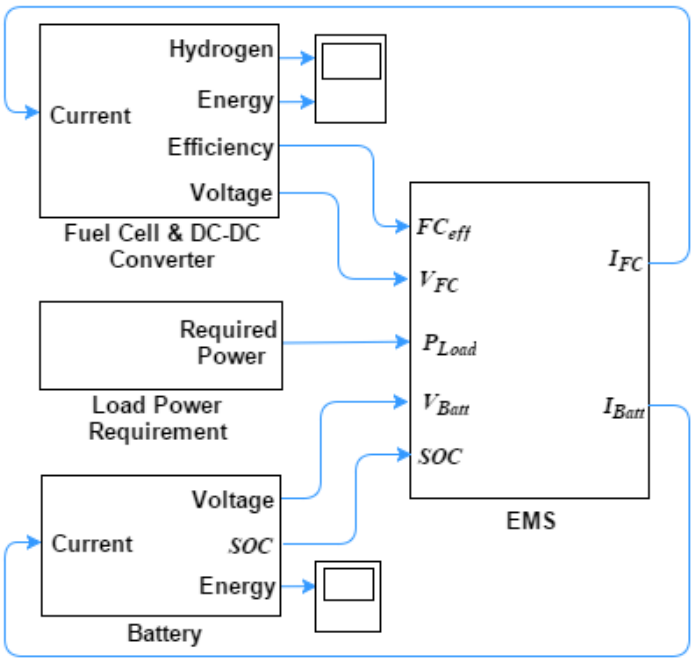

Figure 4.11: *FCS Alsterwasser*'s hybrid fuel cell/battery power system in Simulink environment

After discussing the function of each block, main inputs and outputs, the overall ship simulator representation in Simulink environment is shown in Figure 4.12.

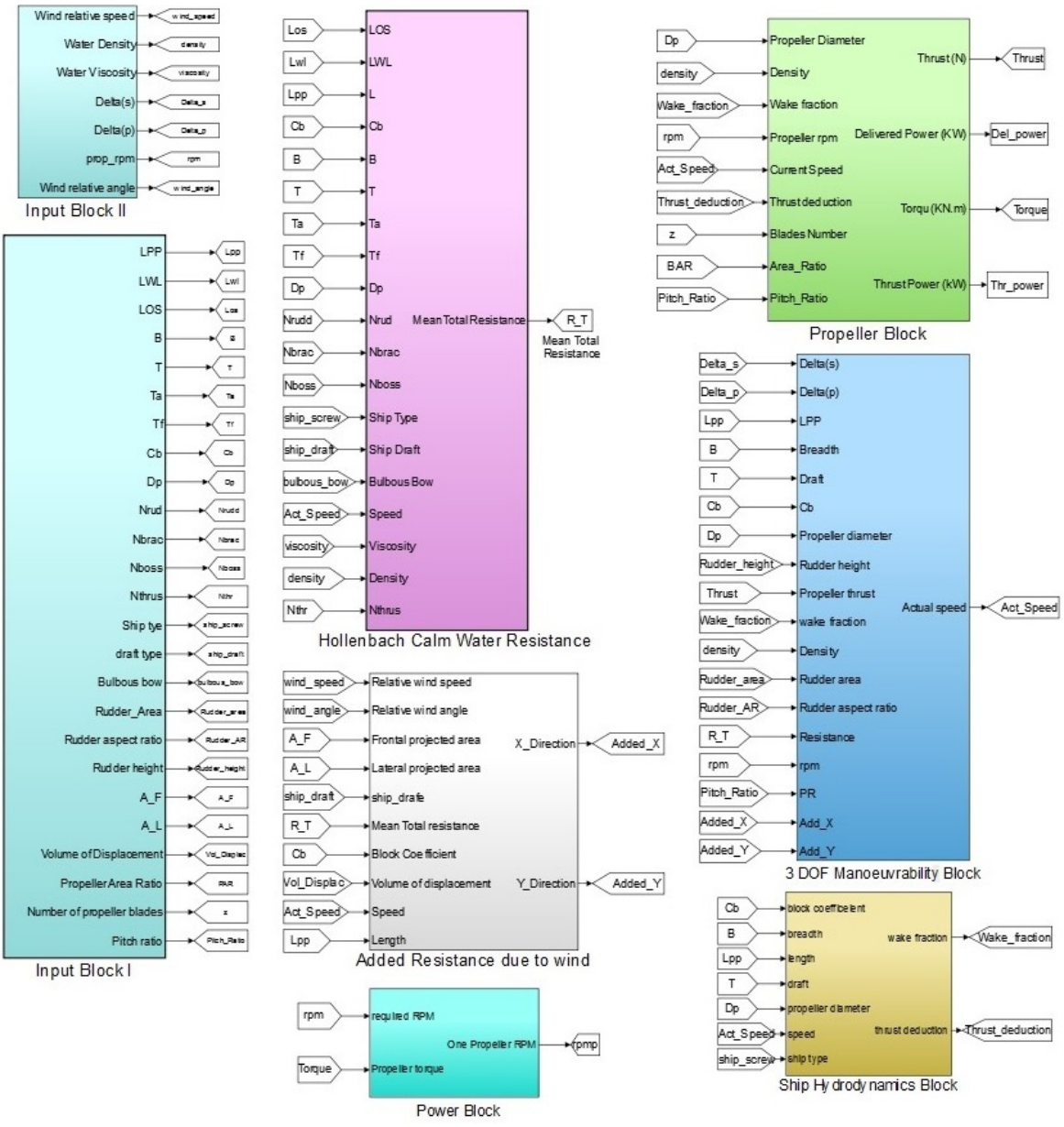

Figure 4.12: Simulink representation of the developed ship simulator

4.2.9 Time Step Discussion

As previously discussed, the total ship system simulator consists of various blocks with different functions, nature and response time. The time response of each block is dictated by the limitations and assumptions of the mathematical model used to describe the system therefore, it is important to define the time step of each block. In order to couple the ship simulator blocks together successfully, a suitable time step should be chosen taking into account the trade-off between accuracy and total simulation time without violating the used mathematical model assumptions and limitations. Moreover, Simulink can couple blocks with different time steps in one model.

Regarding the input blocks, data such as the ship dimensions and form coefficients are constant. Meanwhile, some of the voyage parameters such as the required ship speed or the propeller pitch and speed may change during the simulation. Also, the weather condition parameters during voyages change with time and its time step depends on the source of this data. The required weather parameters can be available in the ship noon reports once or twice per day or it can be extracted from GFS model every 6 hours as discussed earlier in 3.3.2.1. Moreover, the ship may be equipped with measurement devices that keep track of the weather condition during voyages. Therefore, the time step of the input blocks depend on the availability of voyage parameters provided by the simulator user and it is constant for the ship parameters.

For the calm water resistance block, it uses Hollenbach and Holtrop-Mennen methods and both methods use regression to analysis the results of towing tank testing of different models of various ship types statistically. In towing tank tests, measurements of resistance are taken during the constant-velocity phase or at steady forward speed. Therefore, a lookup table is used to determine the ship resistance at each speed or a suitable time step should be used in case of calculating the resistance during the simulation. For regression methods, a simulation time step of one hour can be used [299] with a minimum time step of 1 minute as reported in [210] to calculate the ship resistance in calm water.

The time step of the added resistance block will depend on the used calculation method and the frequency of the available weather parameters used to estimate the added resistance. For example, in Townsin-Kwon method of calculating added resistance due to wind and waves, a fully developed sea condition is assumed where a steady wind blows for a sufficiently long time which is about 2 hours [300]. Therefore, the minimum time step of added resistance calculation should be 2 hours in case of using Kwon's method. By using Blendermann's method of calculating added resistance due to wind, a time step of 5 minutes can be used because the wind energy fluctuation is very small after that time as reported in [301; 302]. Also, the time step of the added resistance block can be 6, 12, or 24 hours depending on the availability of the required weather parameters.

For the estimation of the propeller thrust and torque, approximate equations or polynomials for K_T and K_Q are used which is suitable in early design stage. These equations are fitted for data obtained from testing on series of propellers for different P/D and BAR which were performed with steady inflow and steady rate of propeller revolution in order to achieve reliable results. Therefore, the time step of the propeller block using these approximate equations should be higher than the time delay or time lag of the change in the induced velocity at the propeller (V_i) resulting from a change in the operational state of the propeller such as the blade pitch angle (β) which is called dynamic inflow phenomena [19] as shown in Figure 4.13. The dynamic inflow or wake time constant is calculated as a function of propeller diameter, speed, thrust coefficient, number of blades Z and propeller blade chord c as follows [19]

$$\tau = \frac{(0.637)(\frac{1}{6})D_P}{(\frac{1}{2})(\frac{2}{\pi})^{1/2}K_T^{1/2}D_P n + (\pi/4)Zcn} \tag{4.1}$$

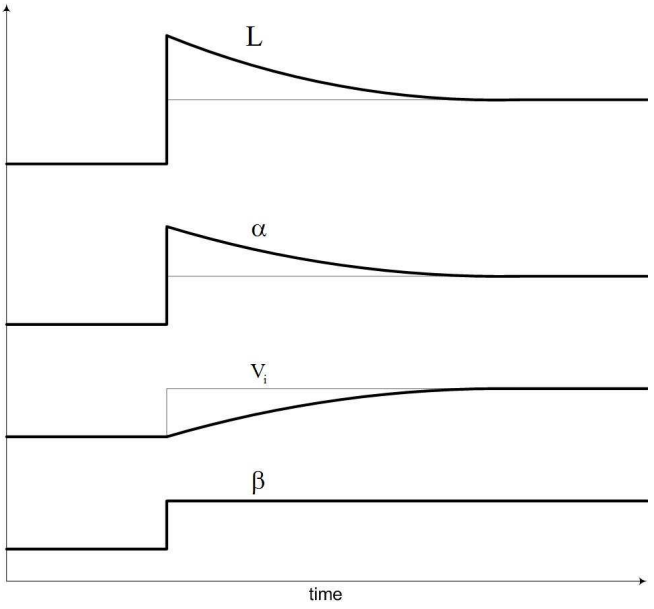

Figure 4.13: The influence of dynamic inflow on the propeller induced velocity (V_i), angle of attack (α), and lift force (L) after a step change in blade pitch angle (β) [19]

Moreover, the used time step for the propeller block should be also higher than the time constant of the propeller load fluctuation to have a steady performance which is less than 1 minute and it can be calculated as a function of inertia of rotating parts, rotational speed and torque as follows [253]

$$\tau_{prop} = \frac{I}{2K_{Q0}N_0} \tag{4.2}$$

Regarding the manoeuvrability block, it uses MGM model which follows a semi-empirical methodology using experimental technique. So, a suitable time step should be used to satisfy the steadiness of the model operational parameters such as model speed during experiments. This time step should be also higher than the rudder lag time or rudder rotational rate whose average value is about 3 degrees per second [303]. In this study the time step of the manoeuvrability block and ship hydrodynamics block will be the same as the time step of the calm water resistance block and the propeller block because these blocks use the same experimental procedure.

For the power block which includes different power sources, in case of using diesel engine models, the minimum time step is one engine cycle order which can be calculated as a function of the engine rotational speed as follows

$$\tau_{diesel} = \text{Crankshaft angle in one cycle}/6/N_{eng} \tag{4.3}$$

where crankshaft angle = 360°for 2-stroke diesel engine and = 720°for 4-stroke diesel engine. Time step of the diesel engine model should also be higher than the summation of time constants in the transfer functions used to model diesel engine dynamics. For fuel cell hybrid propulsion systems, the used fuel cell and battery models can represent both dynamic and steady state performance. These models can take the response time of the fuel cell and battery into consideration which is normally higher than diesel engine response time. These response times should be taken into consideration when choosing a suitable time step of the power block. The fuel cell and battery response times are usually provided by the manufacturer and it depends on the fuel cell or battery type and size. For a 6 kW PEMFC stack as for example, response time is reported to be 10 seconds in [15]. For a 120 kW PEMFC stack, response time is 30 seconds and it can reach 50 seconds as reported in [11]. The response time of batteries, which represents its voltage dynamics, is also reported by its manufacturer. It ranges between 10 seconds as reported in [11] and about 30 seconds as used in [16] meanwhile 20 seconds is used in [304].

Based on the available data, the user should select the suitable time step of each block. However, the selected time step should not violate the minimum time step of these blocks. The minimum time step of each block is related to its function and the used method to perform this function as explained earlier as shown in Table 4.8.

Table 4.8: Minimum time step of the developed ship simulator blocks

Block name	Minimum time step
Inputs	selected by the user or/and constant
Calm water resistance	<1 minute
Added resistance	2 hours using Townsin-Kwon method 5 minutes using Blendermann method
Propeller	<1 minute
Manoeuvrability	<1 minute
Ship hydrodynamics	<1 minute
Power	<1 minute

In conclusion, the range of time step involved in the ship simulator is wide; from sub-seconds for a diesel engine model to a 24 hours time step for added resistance calculation if daily noon reports are used to provide weather data. Simulink allows each block of the developed ship simulator to have its own time step by selecting the option "Treat as atomic unit" as shown in Figure 4.14. Also, Simulink library contains a 'Rate Transition Block' which can be used to handle the transfer of data between blocks with different time steps ensuring data integrity during simulation. In order to study the effect of the used time step size on the simulation results, a sensitivity analysis of different time steps is performed in the next section section.

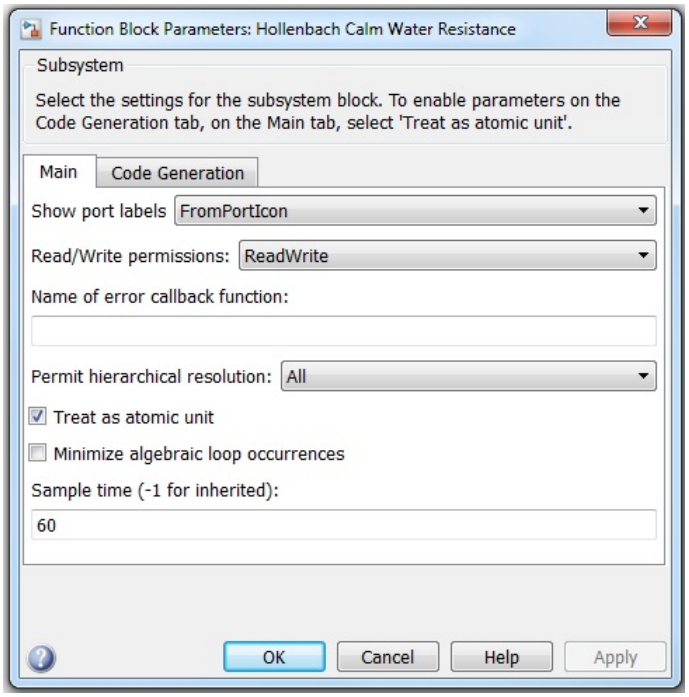

Figure 4.14: Subsystem block dialog of Hollenbach resistance block

4.2.9.1 Sensitivity analysis of time step size

Selecting the time step size of the simulator blocks taking into consideration its dynamic state is important in order to use the ship simulator properly. Different sizes of time step is used in this sensitivity analysis to assess its change effect on the simulation results. The used ship in this analysis is the well-known benchmark tanker ship *Esso Osaka*. The ship specifications used as inputs to the simulation are shown in Table 4.9.

Table 4.9: Specifications of the Esso Osaka tanker ship

L_{PP}	325 m
L_{OS}	339 m
L_{WL}	335 m
B	53 m
T	21.73 m
C_B	0.83
Deadweight (Full load)	278000 tonnes
LCG	10.3 m (aft)
D_P	9.1 m
P/D	0.715
Propeller blade number	5
Propeller area ratio	0.682
Rudder height	8.824 m
Rudder area	119.82 m^2
Rudder aspect ratio	1.539
Number of brackets, thrusters, bosses	0

For setting up the simulation of the examined ship, a real tanker ship voyage between Netherlands (Rotterdam port) and Lithuania (Klaipeda port) is used as an input to the simulation. The examined voyage takes normally about 4 days with an approximate distance of 1114 NM, where the ship's speed and location were saved during the voyage using automatic identification system (AIS) [305] as shown in Figure 4.15.

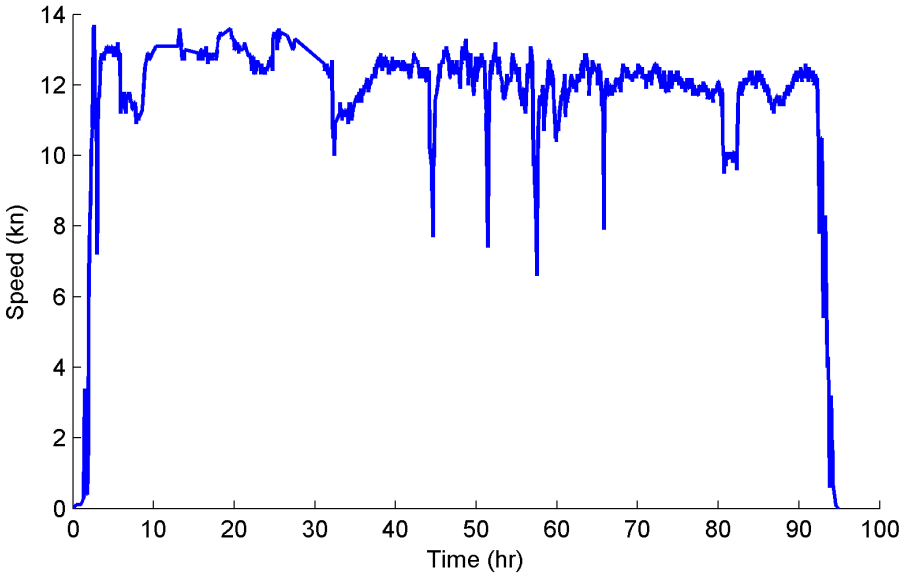

Figure 4.15: AIS ship speed of the examined voyage between Rotterdam and Klaipeda

By using the ship speed profile in Figure 4.15 as an input, the ship simulator is used with different time step sizes to assess its effect on the simulation results in terms of fuel consumption. The ship simulator for this study consists of the two input blocks, the calm water resistance block using Hollenbach's method, the propeller block, the ship hydrodynamics block, and the power block using 2-stroke diesel engine model. Because the used ship speed profile represents the effect of the added resistance as shown in Figure 4.15, the added resistance block is not included in the ship simulator for this study. Time step sizes of 1 minute, 10 minutes, 1 hour, 2 hours, 6 hours, 12 hours, and 24 hours are used for the ship simulator blocks for the same examined voyage and ship. An explicit fixed time step solver is chosen, which is ode8 [306], because this simulation is not a stiff problem and the chosen solver is considered as the most accurate explicit solver type.

Simulation results show that by increasing the time step size of the ship simulator, the simulated fuel consumption decreases as expected because the ship simulator is less able to capture the system changes during the examined voyage using higher time step as shown in Figure 4.16. As shown in Table 4.10, the highest simulated fuel consumption results while using a time step of 1 minute. The differences between the simulated fuel consumption resulting from using time steps of 10 minutes, 1 hour, 2 hours, and 6 hours are less than 5% with reference to the simulated fuel consumption resulting from

using a time step of 1 minute. By using higher time steps of 12 hours and 24 hours, the difference between the simulation results of fuel consumption increase to 6.8% and 13.6% respectively.

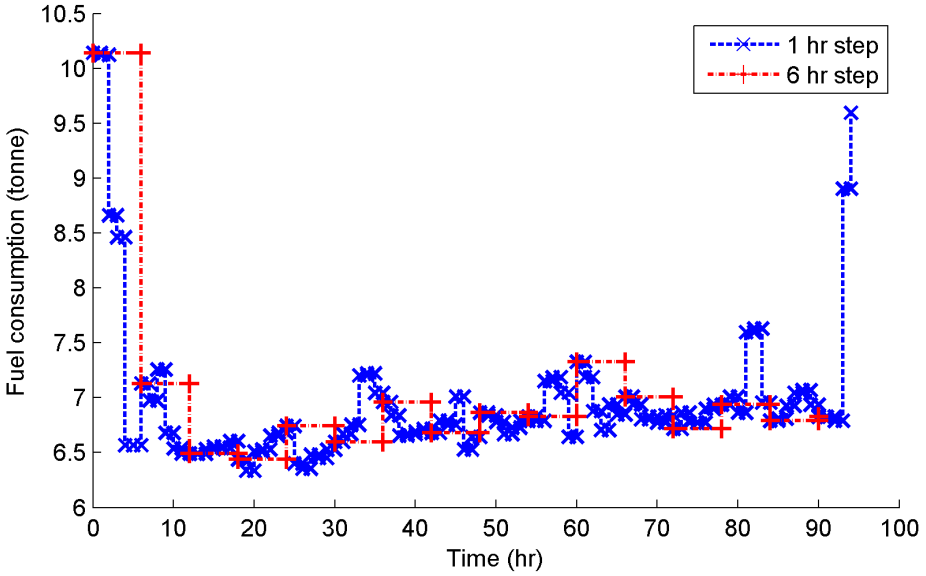

Figure 4.16: Simulated fuel consumption for the examined voyage using time steps of 1 and 6 hours

Table 4.10: Simulated fuel consumption for the examined voyage using different time step sizes

Time step	Simulated fuel consumption (tonne)	Fuel difference (tonne)	Difference percentage (%)
1 minute	659.8		
10 minutes	659.1	0.7	0.1
1 hour	651.6	8.2	1.2
2 hours	650.4	9.4	1.4
6 hours	633.9	25.9	3.9
12 hours	614.9	44.9	6.8
24 hours	569.9	89.9	13.6

In order to study the effect of the time step of the weather input on the simulation results in terms of fuel consumption, another voyage of longer duration is examined for the same tanker ship *Esso Osaka*. The ship is assumed to operate with a constant propeller speed of 95 rpm during the voyage duration of 8 days applying the assumed weather profile shown in Figure 4.17. The ship simulator for this study consists of the two input blocks, the calm water resistance block using Hollenbach's method, the added resistance block using Townsin-Kwon method, the propeller block, the ship hydrodynamics block, and the power block using 2-stroke diesel engine model. For this case study, time steps of 2, 6, 12, and 24 hours are used for the added resistance block while a time step of 1 minute is used for the other blocks using the same ode8 Simulink solver.

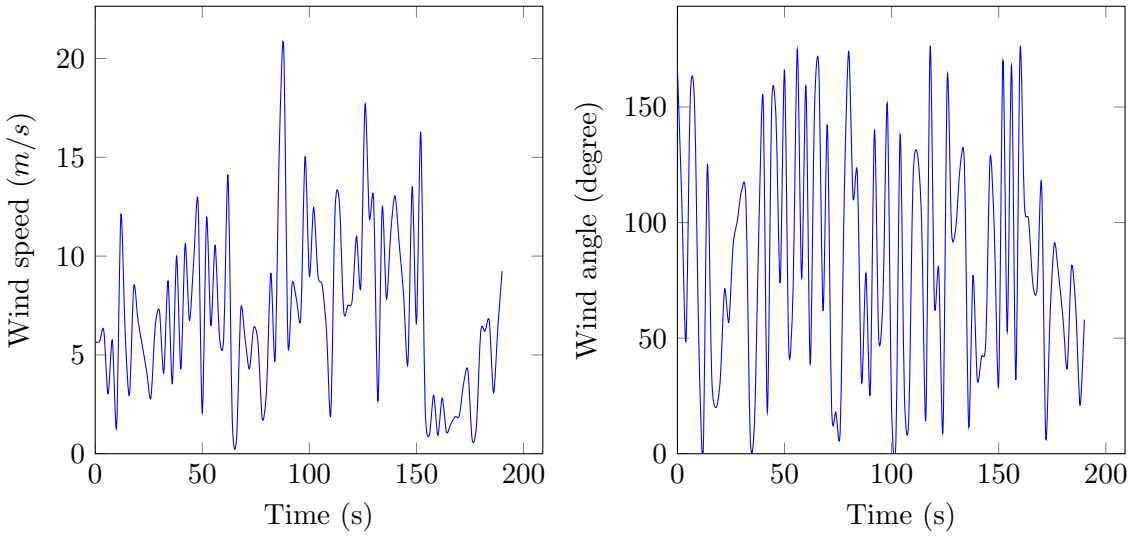

(a) Wind speed

(b) Wind angle

Figure 4.17: Assumed wind speed and direction profile for the examined voyage

As shown in Table 4.11, changing the added resistance calculation time step does not have a considerable effect on the simulated fuel consumption. Also, by increasing the added resistance block time step, the simulated fuel consumption decreases due to the trade-off between simulation time step and accuracy as discussed earlier. An example of the simulation results of the acting forces on the hull during the examined voyage using a time step of 2 hours for the added resistance calculations is shown in Figure 4.18.

Table 4.11: Simulated fuel consumption for the examined voyage using different time step sizes of the added resistance block

Time step (hour)	Simulated fuel consumption (tonne)	Fuel difference (tonne)	Difference percentage (%)
2	970.9		
6	969.8	1.1	0.1
12	967	3.9	0.4
24	966	4.9	0.5

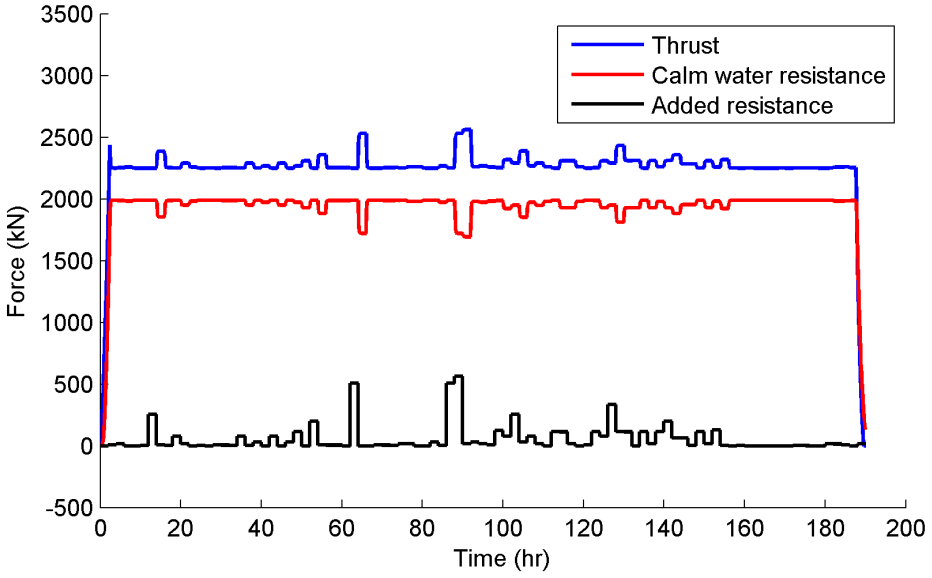

Figure 4.18: Simulated acting forces on the hull during the examined voyage using a time step of 2 hours for added resistance calculations

4.3 Verification and Validation

Judging the goodness of a model should be based on how accurately the results from it correspond to real results which can be done by two steps. Ensuring that the model does the intended calculations correctly which is called model verification and ensuring that the used assumptions are reasonable and the used approximate formulas are suitable with respect to real data which is called model validation.

Verification and validation of the developed ship simulator are made using multiple sources of data because there is no single dataset with the required data. Therefore, four blocks have been verified and validated individually which are calm water resistance block, added resistance block, propeller block, and the power block using state-based strategy for the *FCS Alsterwasser* hybrid fuel cell propulsion system. Also, End-to-End validation has been made for different combination of blocks working together using real ship operational data of the *Esso Osaka* tanker and the *M/S Smyril* ferry as shown in Figure 4.19.

4.3.1 Calm water resistance block

The results of calm water resistance block using Hollenbach and Holtrop-Mennen methods have been validated against experimental results obtained from towing tank naked-hull tests of a 1/60 scale tanker model of a ship with specifications shown in Table 4.12 [307]. Froude's traditional approach [246] has been used to scale up the model resistance and it shows good agreement as shown in Figure 4.20.

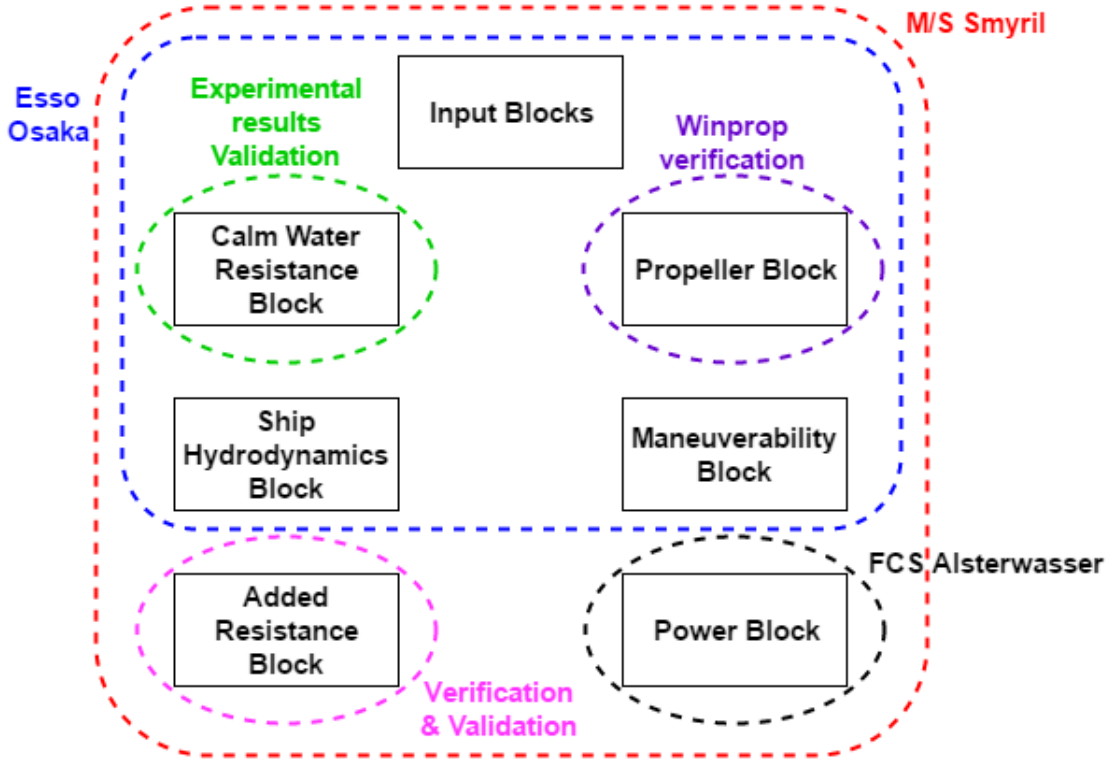

Figure 4.19: Validation and verification approach of the developed ship simulator

Table 4.12: Specifications of the examined Virtue Ice Class vessel [45]

L_{OA}	183.33 m
L_{PP}	174 m
L_{OS}	184 m
B	32.2 m
T	11.02 m
C_B	0.7994
Displacement (Full load)	49969 tonnes
D_P	6 m
BAR	0.55
P/D	0.875
Number of rudders	1
Number of brackets, thrusters, bosses	0

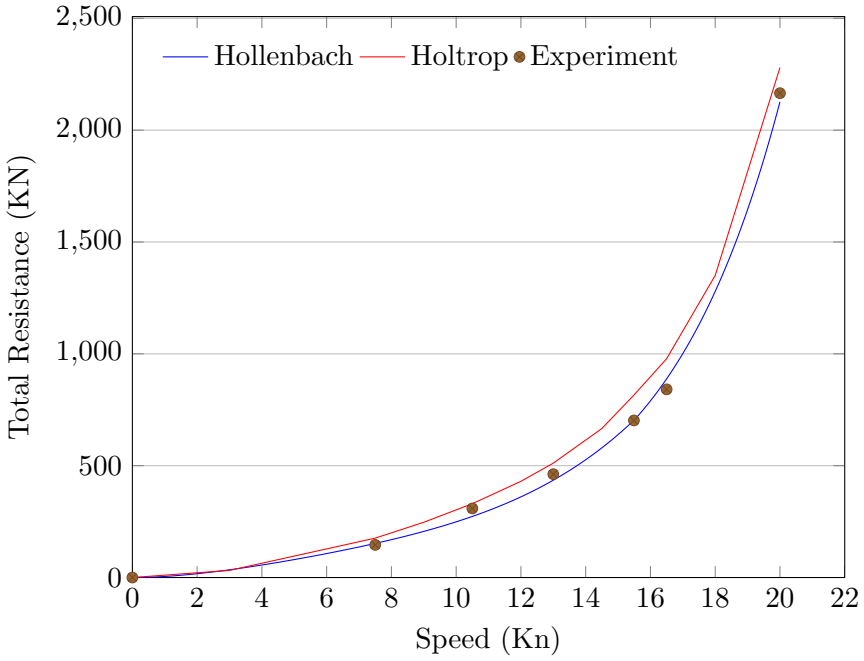

Figure 4.20: Validation of Hollenbach and Holtrop-Mennen calm water resistance methods

The total calm water resistance's components for the examined ship are the residual and frictional resistance calculated by Hollenbach's method as for example as shown in Figure 4.21.

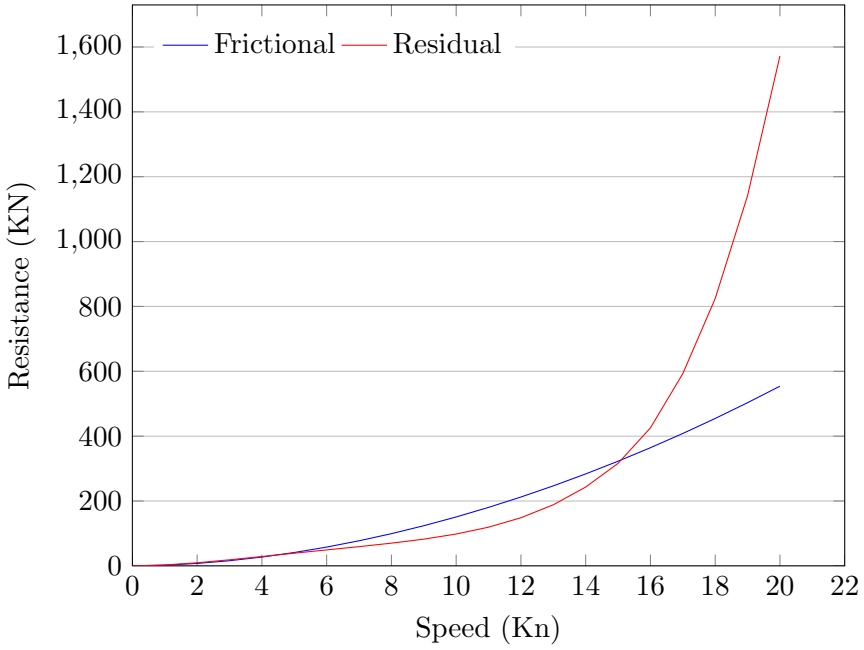

Figure 4.21: Frictional and residual resistance of the examined ship calculated by Hollenbach method

4.3.2 Added resistance block

Verification of the added resistance block is also made where Aertsssen's formulae was used in [246] to calculate the speed loss of a container ship with a length of 200 m, C_B=0.6, displacement=365000 m^3 and Froude number=0.233 and the added resistance block gives the same results as shown in Table 4.13.

Table 4.13: Verification of added resistance block (Aertssen)

Beaufort Number	**Speed loss % [246]**	**Simulation result**
5	6.1	6.09
6	11.9	11.91
7	20.5	20.55
8	34.4	34.36

The same container ship is used to verify the outputs of added resistance block in case of using Townsin-Kwon method and it also gives the same results as predicted as shown in Table 4.14

Table 4.14: Verification of added resistance block (Townsin-Kwon)

Beaufort Number	**Speed loss % [246]**	**Simulation result**
5	5.4	5.39
6	9.7	9.73
7	19.4	19.37
8	39.5	39.52

The added resistance block using Blendermann method is verified well against the computational results published in [234] for a research vessel as shown in Figure 4.22. The main specifications of this ship are: $L_{OA} = 55\ m$, $L_{PP} = 48\ m$, $B = 12.5\ m$, $A_L = 434.8\ m^2$, and $A_F = 160.7\ m^2$.

The added resistance block using Blendermann method is also validated using experimental data from wind tunnel tests of a ferry at the Institute of Naval Architecture, University of Hamburg [308] showing good agreement as shown in Figure 4.23. The ferry dimensions are: $L_{OA} = 161\ m$, $L_{PP} = 144\ m$, $B = 29\ m$, $A_L = 4223.29\ m^2$, and $A_F = 898.21\ m^2$.

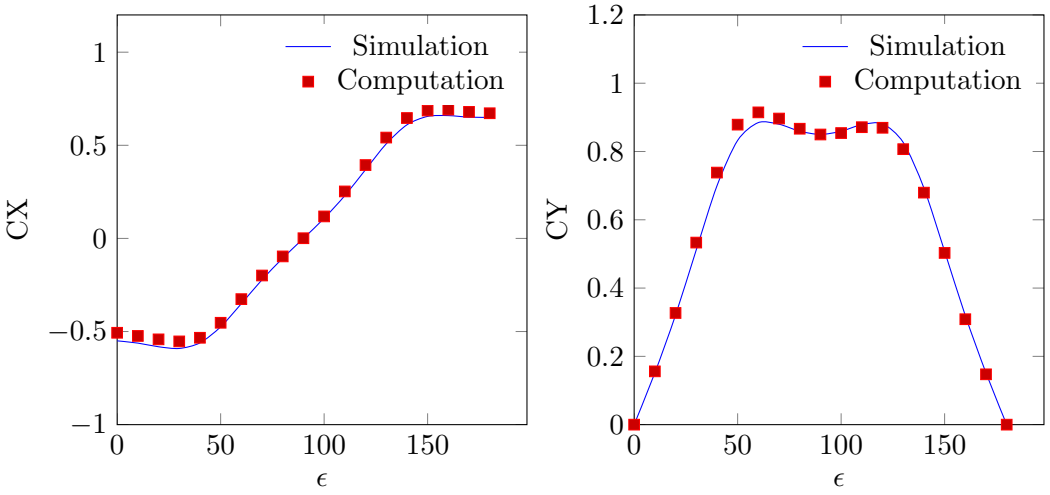

(a) Longitudinal force coefficient

(b) Side force coefficient

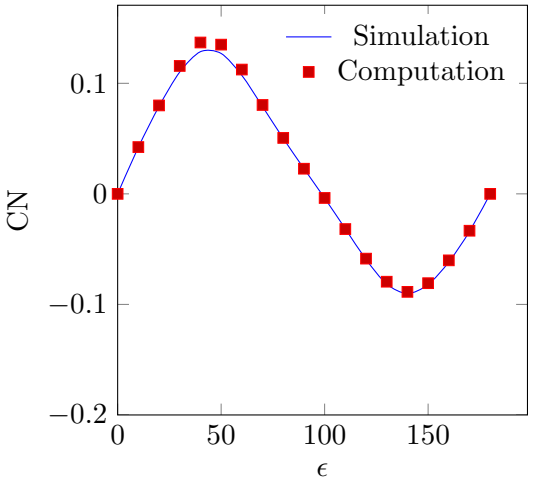

(c) Yawing moment coefficient

Figure 4.22: Verification of Blendermann for a research vessel

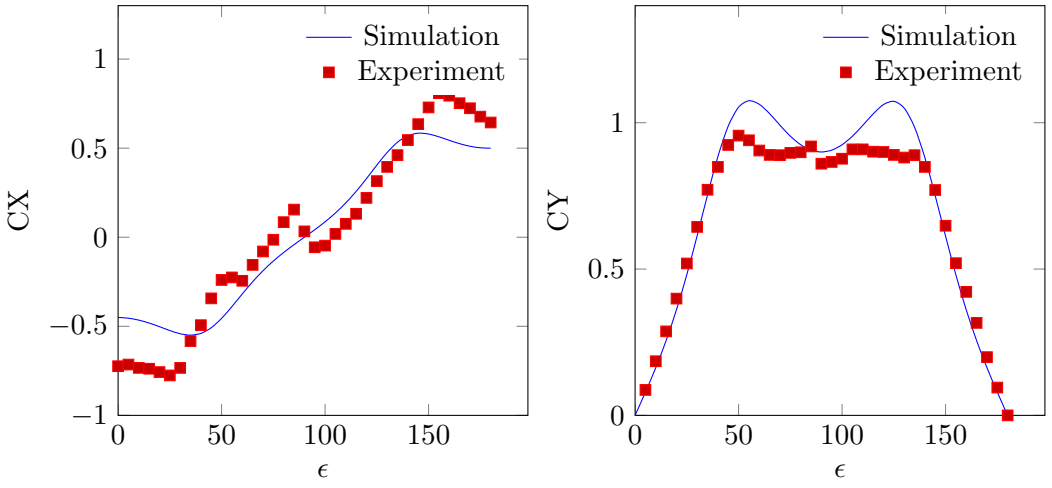

(a) Longitudinal force coefficient

(b) Side force coefficient

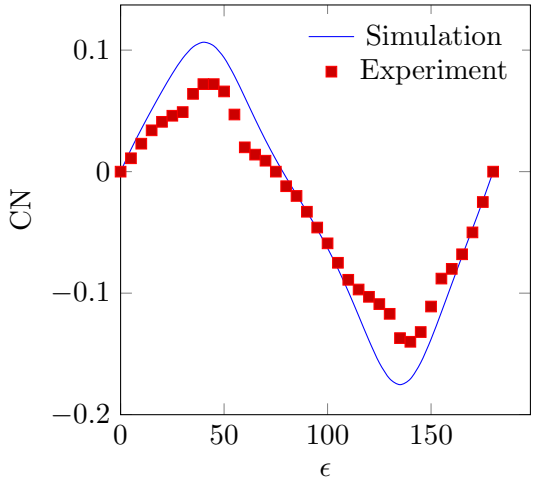

(c) Yawing moment coefficient

Figure 4.23: Validation of Blendermann for a ferry

4.3.3 Propeller block

The approximate Equations 3.39 and 3.40 used in the propeller block to calculate the non-dimensional thrust and torque coefficients for Wageningen B-screw series propeller of the same ship shown in Table 4.12 are verified against values obtained from Winprop software [309] as shown in Figures 4.24 and 4.25 showing good agreement.

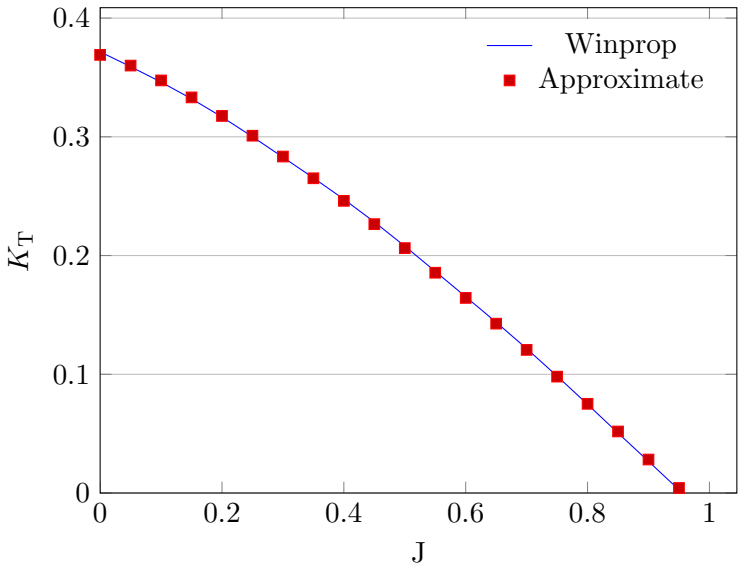

Figure 4.24: Comparison between Winprop and approximate equation to calculate thrust coefficient

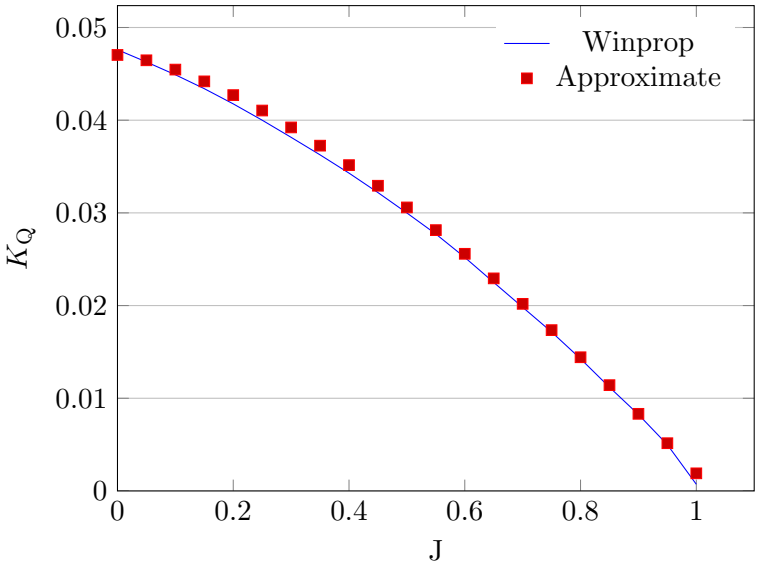

Figure 4.25: Comparison between Winprop and approximate equation to calculate torque coefficient

Moreover, the used polynomials in Equation 3.41 fitted to Wageningen data for calculating the non-dimensional thrust and torque coefficients are also verified against

values obtained from Winprop software for the same propeller as shown in Figures 4.26 and 4.27 showing good agreement as well.

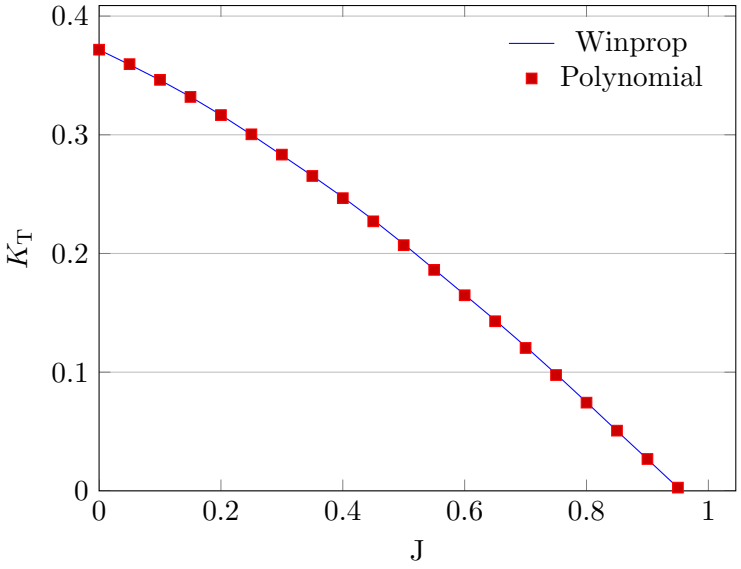

Figure 4.26: Comparison between Winprop and the fitted polynomial to calculate thrust coefficient

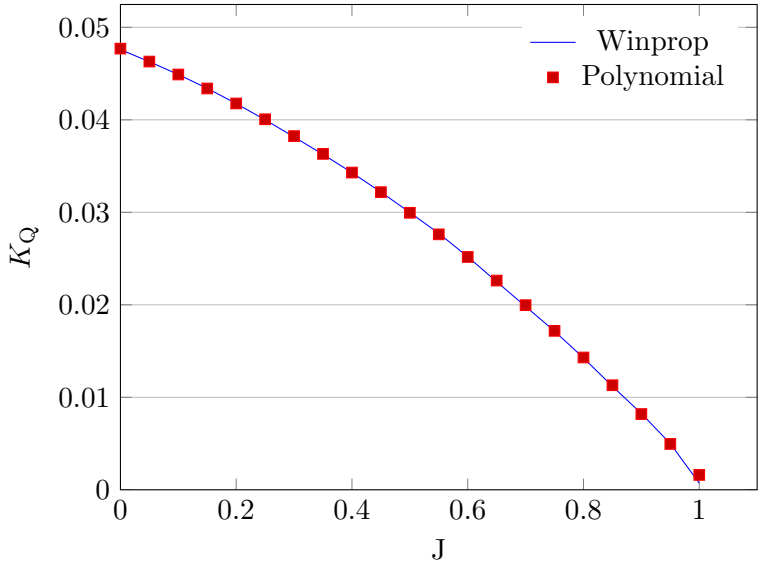

Figure 4.27: Comparison between Winprop and the fitted polynomial to calculate torque coefficient

4.3.4 Power block

For the first fuel cell passenger ship *FCS Alsterwasser*, a part of its typical power requirements has been measured as shown in Figure 3.15. This power has been used as an input in a study to develop a state-based energy management strategy for the ship

hybrid fuel cell/battery propulsion system [20]. The published results in [20] are used to verify the simulation results of the power block.

The hybrid fuel cell/battery propulsion system of this ship consists of two PEMFC modules with a peak power of 48 kW which have proven to be an extremely reliable energy source connected to the DC bus using a boost type unidirectional DC-DC converter to control the voltage. The used converter is composed of an inductor L, a switch S and a diode D as shown in Figure 4.28. A 360 Ah battery is also connected directly to the DC bus to power a 100 kW electric motor. The motor required power is split between the fuel cell and battery systems through the used EMS as shown in Figure 4.29.

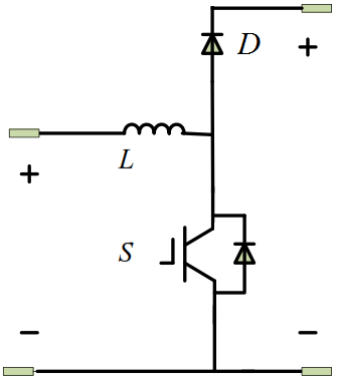

Figure 4.28: Electrical scheme of the fuel cell boost DC-DC converter [20]

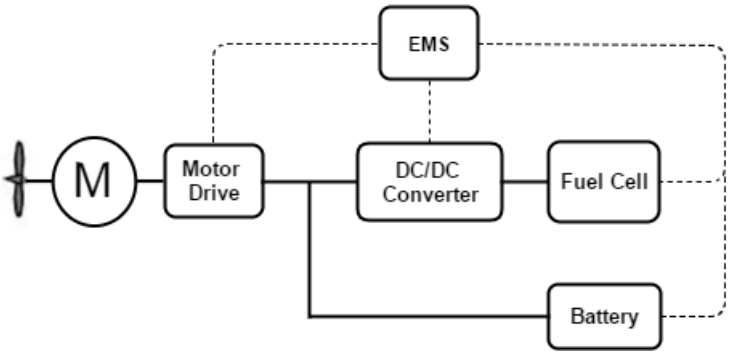

Figure 4.29: Configuration of *FCS Alsterwasser* fuel cell/battery hybrid system

The *FCS Alsterwasser*'s hybrid system is implemented in Simulink as discussed earlier using the mathematical models of PEMFC with a 50 kW nominal power and a lead-acid battery of a 360 Ah capacity, 560 V, and 65 % initial SOC. The EMS developed in [20] is also implemented in Simulink and used with the same power limits of the fuel cell and battery systems to manage the power distribution. The developed state-based strategy splits the required load power between the fuel cell and the battery as shown in Figure 4.30 and Figure 4.31 while Figure 4.32 shows the battery SOC. Figures 4.30 to 4.32 show good agreement between the simulation results and the published results

measured from [20]. The mean difference percentage of fuel cell and battery powers between the simulation and the published results is about 1.1% as shown in Figures 4.30 and 4.31. Regarding the battery SOC, the difference between the simulation results and the published results is approximately 0.11% as shown in Figure 4.32.

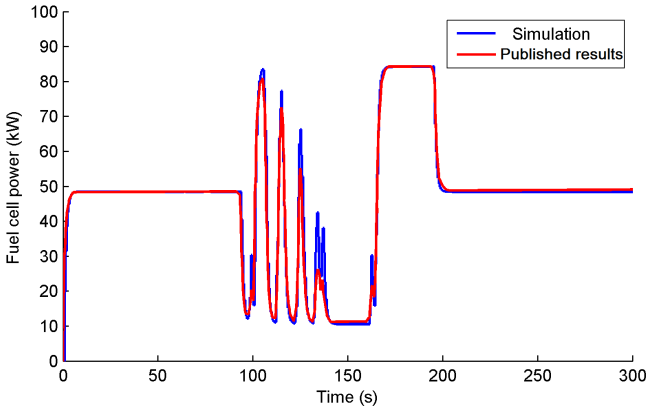

Figure 4.30: Validation of fuel cell power

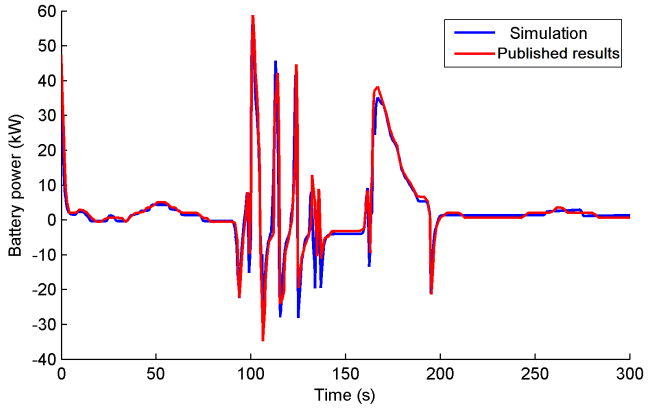

Figure 4.31: Validation of battery power

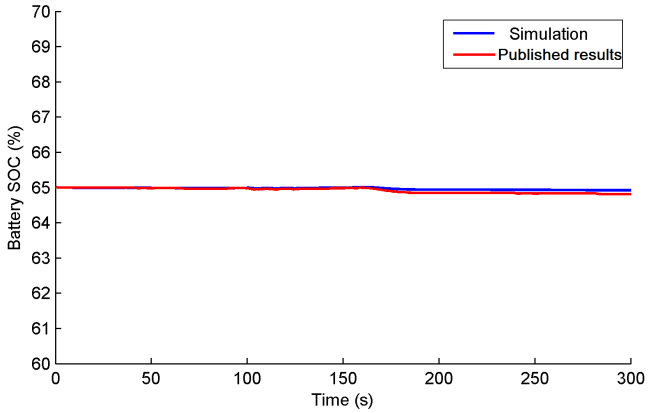

Figure 4.32: Validation of battery SOC

4.3.5 Fuel cell block

The fuel cell block simulation results have been validated against experimental data and real datasheet performance of a 6 *kW* PEMFC *NetStack PS6* with a nominal voltage of 45 *V* showing a good agreement as shown in Figure 4.33 [15]. The error between fuel cell simulation and expected results is in the range of ± 1%.

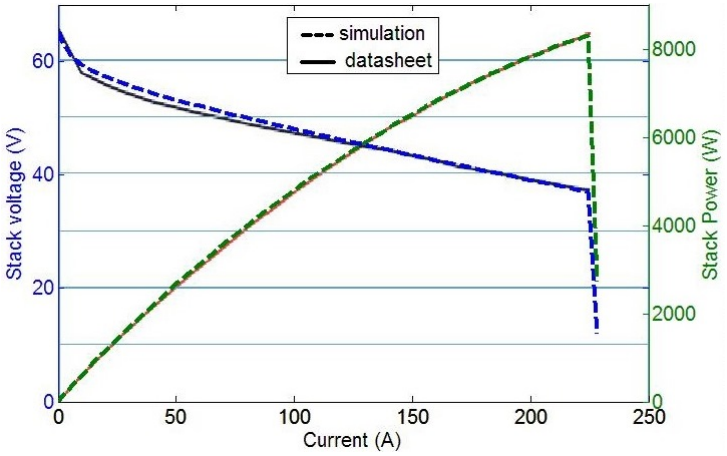

Figure 4.33: Validation of fuel cell block included in the SimPowerSystems toolbox of Simulink [15]

4.3.6 Battery block

The battery block has been also validated against real datasheet of a *Panasonic* battery during a discharge tests at three different current values as shown in Figure 4.34 [16]. The battery model has been also validated against experimental results for four different battery types with a maximum error of 5% however error increase to ± 10% when battery SOC decreases below 20% [275] however it is not recommended to fully discharge a battery.

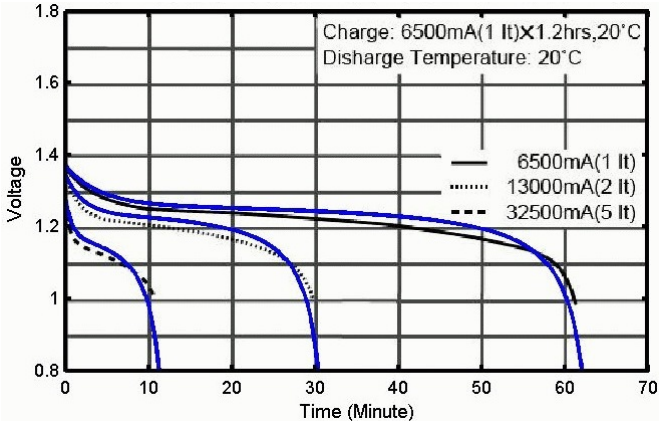

Figure 4.34: Validation of battery block included in the SimPowerSystems toolbox of Simulink [16]

4.3.7 End-to-End Validation

Not only the simulator blocks have been verified and validated individually, but different blocks working as a unit have been validated as well using real ship operational data. Real ship operational data is very confidential and can only be provided by shipping companies and shipyards and because of its sensitivity not many datasets are available so only two validation cases have been made.

4.3.7.1 *Esso Osaka*

One of the well known available dataset which can be used to validate the developed ship simulator is the *'Esso Osaka'* dataset which considered as a benchmark ship by the ITTC for comparing different models of ship manoeuvrability prediction [249]. *Esso Osaka* is a tanker ship with specifications in Table 4.9 and its complete trails results and model tests data are available. An unusual attention to measurement accuracy was taken during the extensive set of trails of this ship.

For this case study, calm water resistance block using Hollenbach's method, propeller block, ship hydrodynamics block, manoeuvrability block and input blocks are put together as shown in Figure 4.35 in order to simulate a starboard circle manoeuvre with 35° rudder angle and the results are compared to the benchmark results in [249]. The simulation time step for this study is chosen to be as small as 1 minute in order to have accurate results taking into account the minimum response time of the used blocks in this validation case according to Table 4.8. Added resistance is assumed to be constant during simulation because simulation time is less than 2 hours and the required weather parameters are not available. Therefore, added resistance block is not used for this case and it is assumed to be 30% of the calm water resistance at service speed [310].

Using data in Table 4.9 with rudder angle of 35° and an initial speed of 10 kn as reported in [249], the turning trajectory and the ship speed are the main outputs of this simulation. Simulation results of the ship turning trajectory is compared to the real turning trajectory of the ship showing good agreement as shown in Figure 4.36. Also, the simulated time history of ship's speed during the turning trajectory is also compared well to the real data as shown in Figure 4.37.

In order to study the impact of the used ship added resistance percentage on the results, different percentages of the calm water resistance at the ship service speed of 17 kn are assumed and used for the same simulation case. The used added resistance percentages are assumed to be constant throughout each simulation case because the case study simulation time is less than the time-step of the added resistance calculations. As shown in Figures 4.38 and 4.39, the ship ends up with a smaller diameter of the turning circle and lower speed by increasing the added resistance percentage.

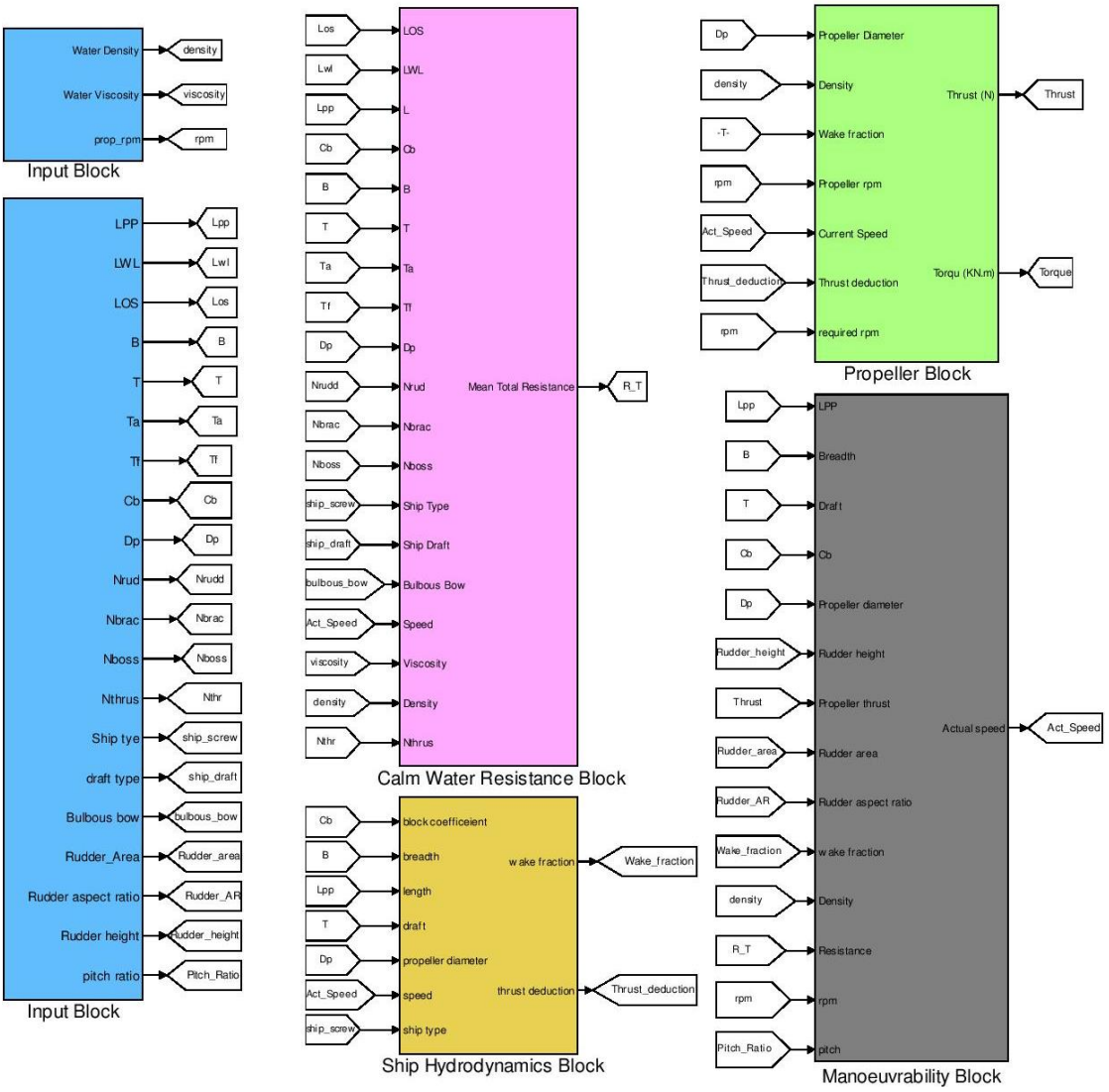

Figure 4.35: Simulink representation for Esso Osaka validation case

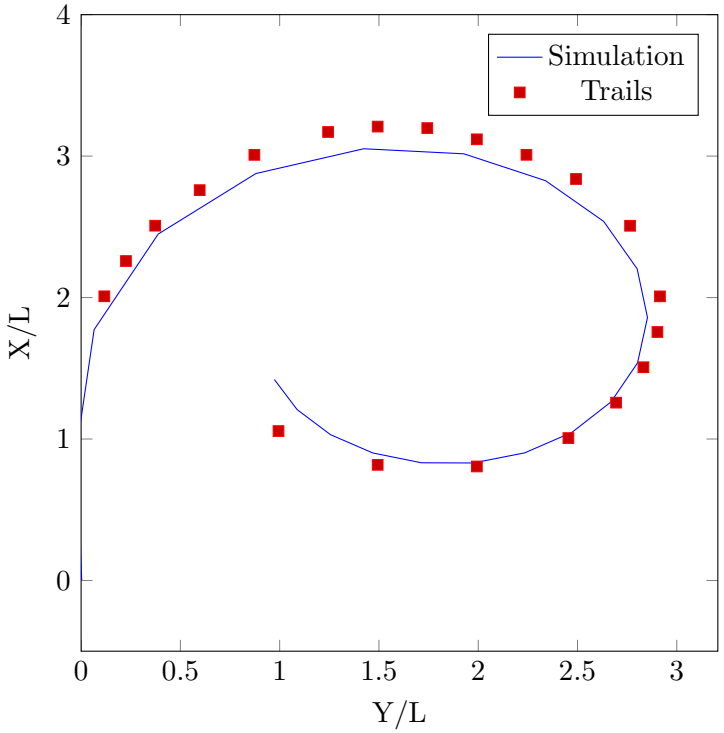

Figure 4.36: Simulated turning trajectory against real turning trajectory

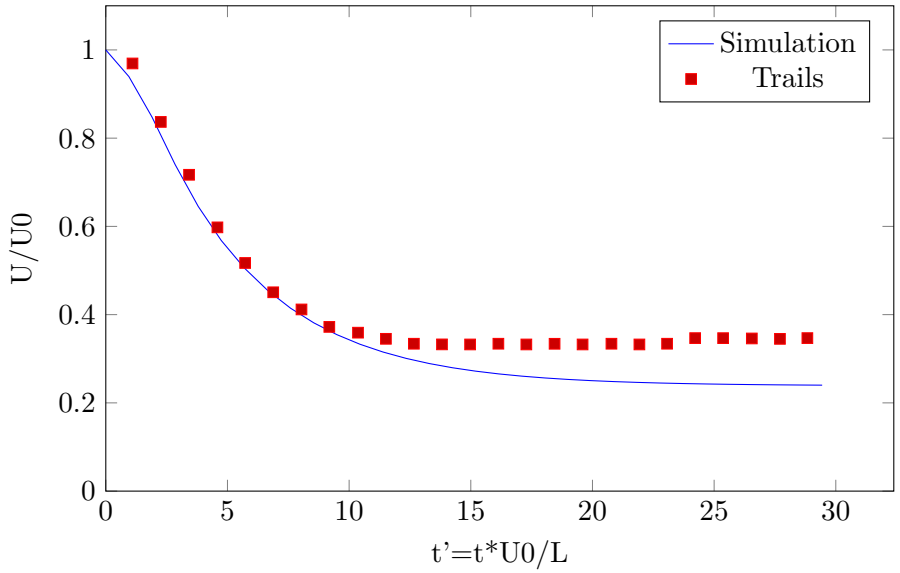

Figure 4.37: Simulated time history of ship's speed against trails values

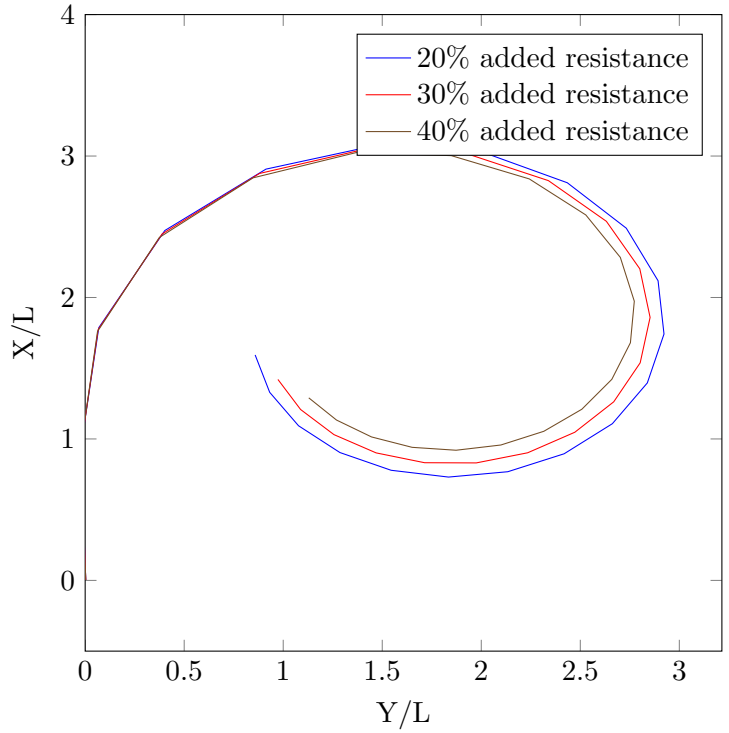

Figure 4.38: Effect of different added resistance percentages on the simulated turning trajectory

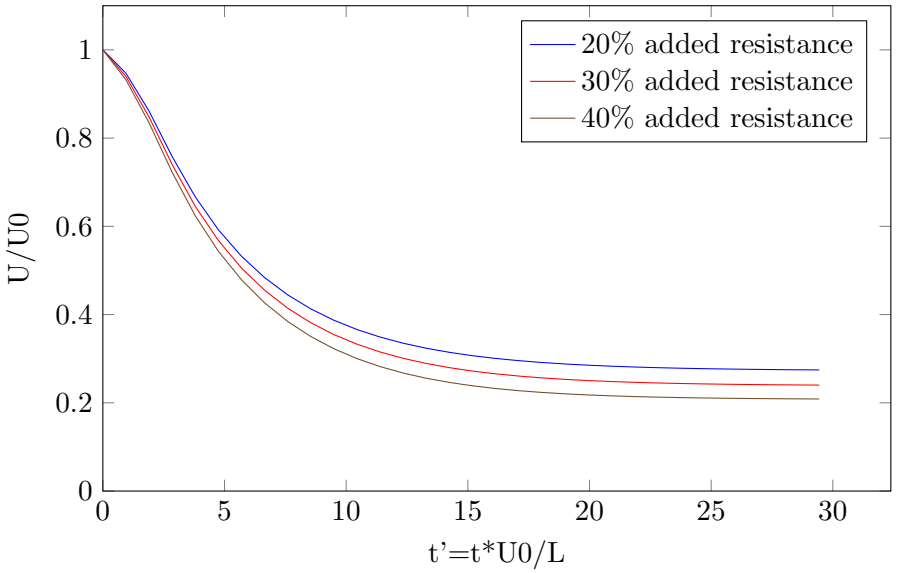

Figure 4.39: Effect of different added resistance percentages on the simulated time history of ship's speed

4.3.7.2 *M/S Smyril*

In order to develop a statistical modelling of ship propulsion system fuel efficiency, real ship operational data were collected onboard the domestic ferry *'M/S Smyril'* for almost two months from 16/2/2010 to 12/4/2010. The data was made available online in [311] to encourage ship's benchmarking. The ship owner is *Strandfaraship Landsins* and the ship works around Faroe Islands from the capital Tórshavn to the southernmost island Suduroy which is a sulphur emission control area. The average crossing time of this voyage is less than two hours sailing, with three or four voyages per day.

The ship specifications are shown in Table 4.15 where a computer system and some additional hardware were installed to measure some of the ship operational variables which included ship speed, latitude and longitude, fuel consumption, fuel density and temperature, relative wind speed and angle, rudder angle, distance to sea surface and propeller pitch while engine speed was considered to be constant and was not measured. Fuel consumption measurements were taken only for main engines, therefore no auxiliary power and fuel consumption are taken into consideration.

Table 4.15: Specifications of the *M/S Smyril* ferry

Passenger capacity	975
Car capacity	970 m / 200 cars
L_{OA}	135 m
L_{WL}	126.1 m
L_{OS}	129.3 m
L_{PP}	123 m
B	22.7 m
T	5.6 m
C_B	0.53
Service speed	21 kn
Main engines	4*3360 kW
Aux. engines	4*515 kW
D_P	4.3 m
Rudder height	4.3 m
Rudder area	11.61 m^2
Rudder aspect ratio	1.593
Number of thrusters & rudders	2

The developed ship simulator is used to simulate the ferry performance during its normal voyage. Then, validation is made using the ship real operational data. For this study, input blocks, calm water resistance block using Hollenbach's method, added resistance block using Blendermann's method, propeller block, ship hydrodynamics block, manoeuvrability block, and power block are the components of the ship simulator for this case as shown in Figure 4.12.

A high accuracy variable step time solver is chosen for this case study which is ode45 [306] because of the differences in the response time of the used blocks of the ship simulator. Time step chosen for this case study is 1 minute as the previous case study for calm water resistance, propeller, and ship hydrodynamics blocks. A time step of 1 second is chosen for the 4-stroke diesel engine model for better accuracy of power requirements and fuel consumption. For the added resistance block, a time step of 5 minutes is chosen for the added resistance due to wind calculation using Blendermann's method while the added resistance due to wave is constant during simulation using Kreinter's formula since voyage time is less than 2 hours.

The power block for this case study contains a 4-stroke diesel engine mathematical model for MAN B&W 7L32/40 engine which runs at constant speed of about 700 rpm which corresponds to the propeller speed of 140 rpm reported by the ship owner company. Specific fuel consumption of the main engines is 186 g/kWh.

Added resistance due to wind is calculated as a function of wind speed and direction as shown in Figure 4.40 using Blendermann's method due to its applicability to ferries.

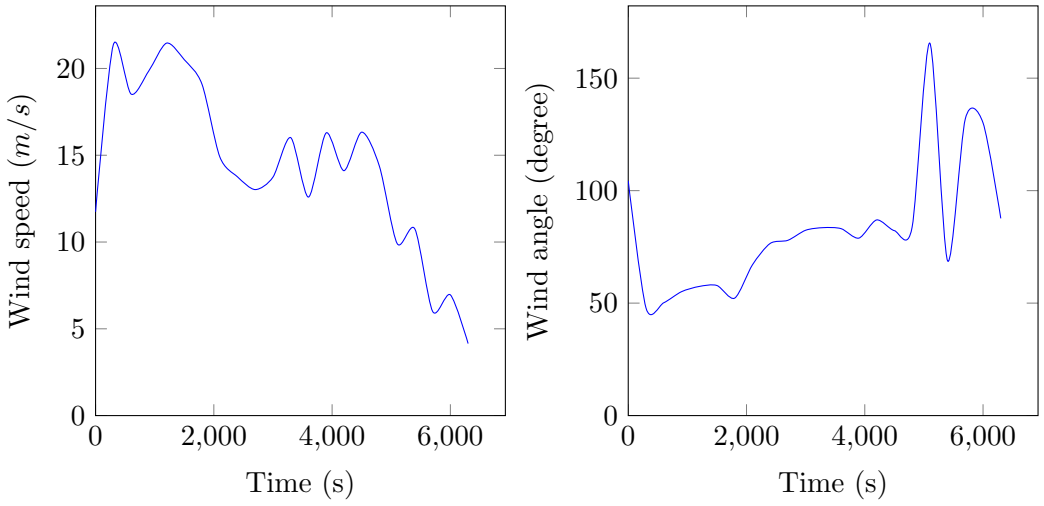

(a) Wind speed

(b) Wind angle

Figure 4.40: Wind speed and direction measurements during the examined voyage

Added resistance due to wave is calculated using Kreinter's formula as recommended by the ITTC. However, in order to improve the estimated results and have more close to reality performance, a noise component is added to the ship speed as follows

$$V = V + \Delta V(\sin(wt)) \tag{4.4}$$

where ΔV is the noise amplitude component equals to 1% of the maximum ship speed as suggested in [193] and w is the noise frequency equals to the dominant frequency of sea

waves during the examined voyage. In order to calculate the dominant frequency during the examined voyage, Fast Fourier Transform (FFT) is used to transform sea surface measurements of the examined voyage shown in Figure 4.41 from the time domain into the frequency domain.

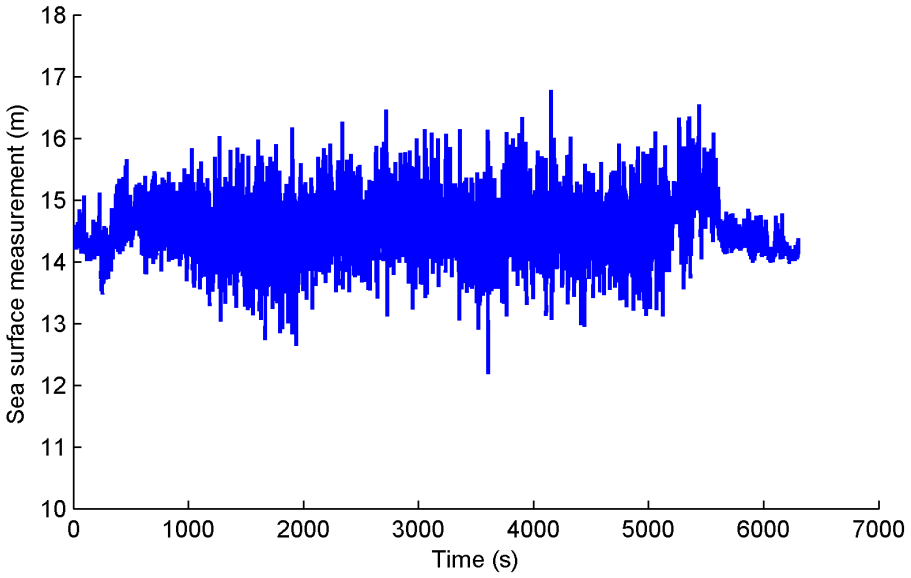

Figure 4.41: Sea surface measurements during the examined voyage

The recorded sea surface measurements during the examined voyage is first processed before using FFT. The average of this measurement is calculated then the amplitude of it is computed as shown in Figure 4.42. The signal sampled in time is then related to the same signal but sampled in frequency using FFT in MATLAB in order to find the dominant frequency.

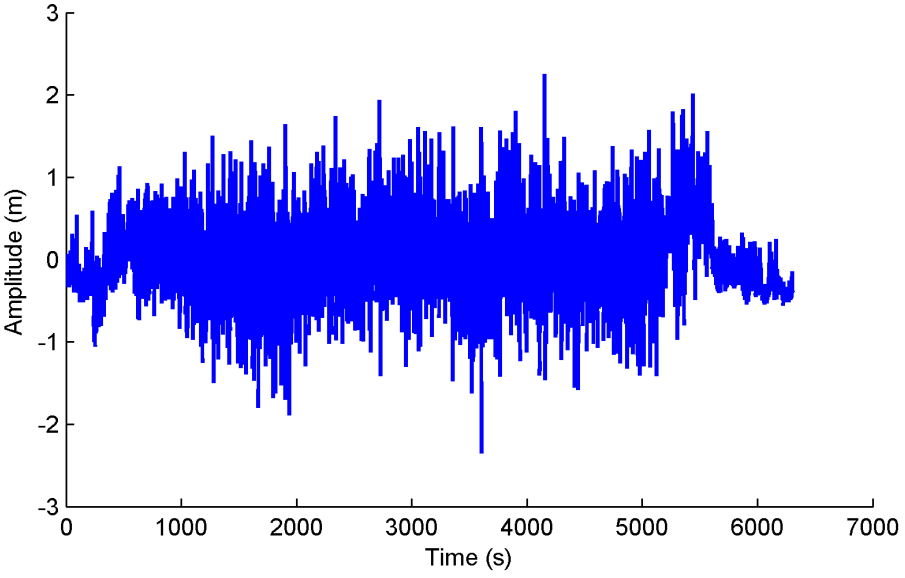

Figure 4.42: Amplitude of sea surface measurements during the examined voyage

Real sea is normally irregular pattern of waves of varying amplitudes and periods therefore, there is no single dominant frequency is resulted using FFT for the examined sea surface measurements as shown in Figure 4.43. Therefore, the total voyage period is split into different time spans and analysed using FFT in order to calculate the average dominant frequency. This analysis results in an average dominant frequency of 0.144 Hz which is then used in Equation 4.4 during the simulation of the examined voyage.

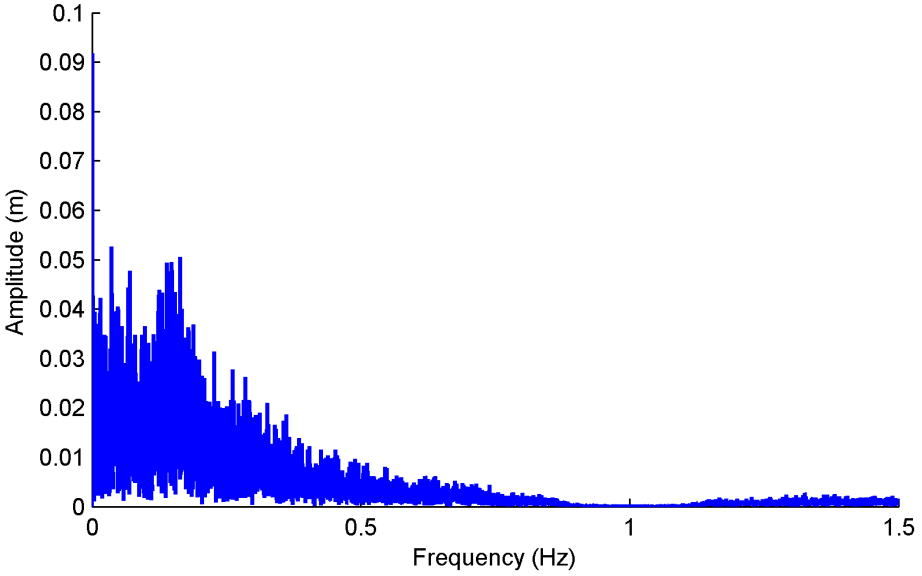

Figure 4.43: FFT analysis results for the examined voyage

Using the ship geometrical particulars, main engines and propeller data in Table 4.15, wind speed and angle shown in Figure 4.40 and rudders angles shown in Figure 4.44 as inputs, the ship performance is simulated during the examined voyage. The main outputs of this simulation are the ship speed and fuel consumption which are compared to the real operational data of the ship as shown in Figures 4.45 and 4.46.

Simulation results of ship's speed and main engines fuel consumption are validated against real operational data of the examined voyage showing good agreement as shown in Figures 4.45 and 4.46 except for the stopping phase of the journey that includes reverse operation of the propellers which could not be captured well by the developed simulator. Two more voyages of the ship in different days of the same route as shown in Figure 4.47 are used to further validate the developed ship simulator.

As shown in Figures 4.48 to 4.51, the simulation results of the ship's speed and fuel consumption are in good agreement with the ship's real operational data. The error between the simulation results and the real fuel consumption is about 5%. This is considered reasonable given the level of uncertainty in the modelling assumptions and acceptable as a basis for comparison.

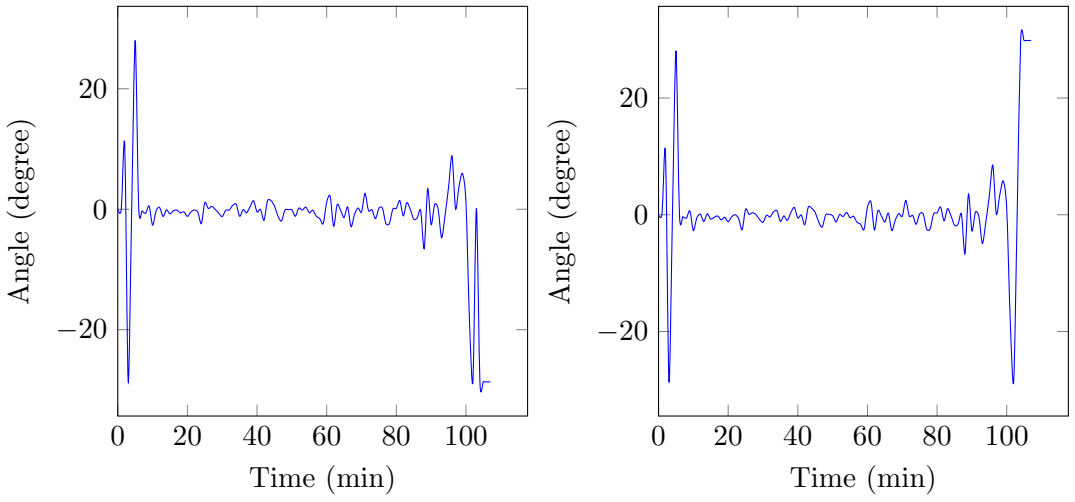

(a) Port rudder

(b) Starboard rudder

Figure 4.44: Port and starboard rudder angles inputs to the simulation

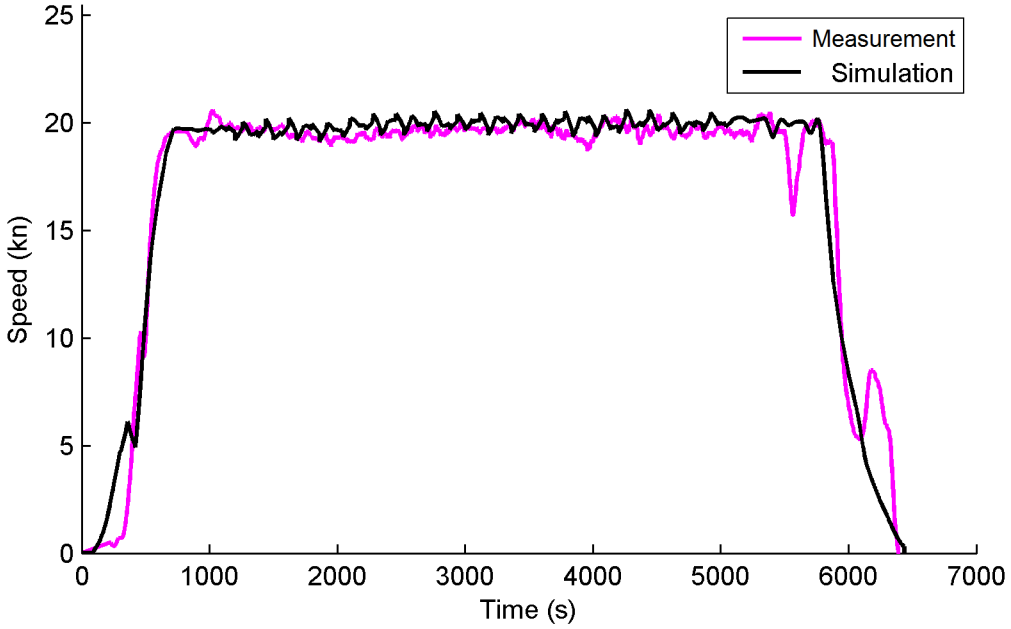

Figure 4.45: Ship speed validation for the examined voyage

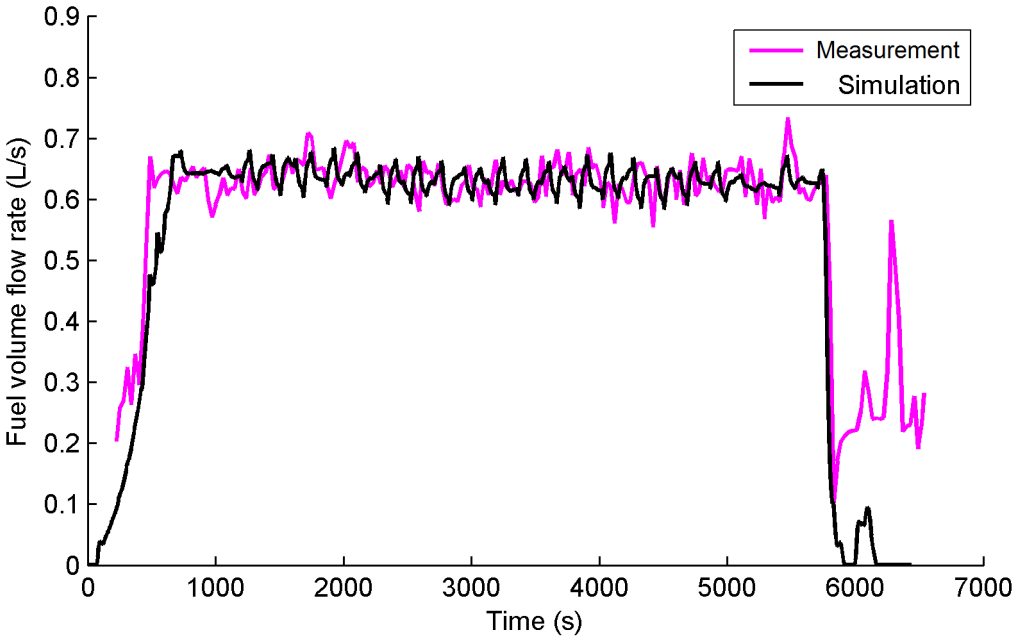

Figure 4.46: Ship fuel volume flow rate validation for the examined voyage

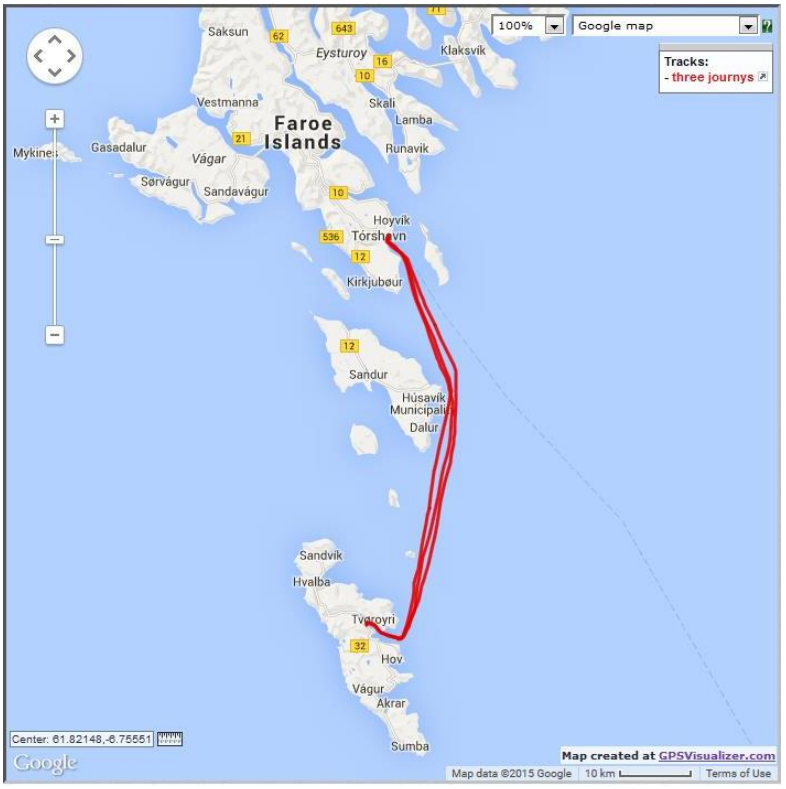

Figure 4.47: Ship voyage route under investigation [21]

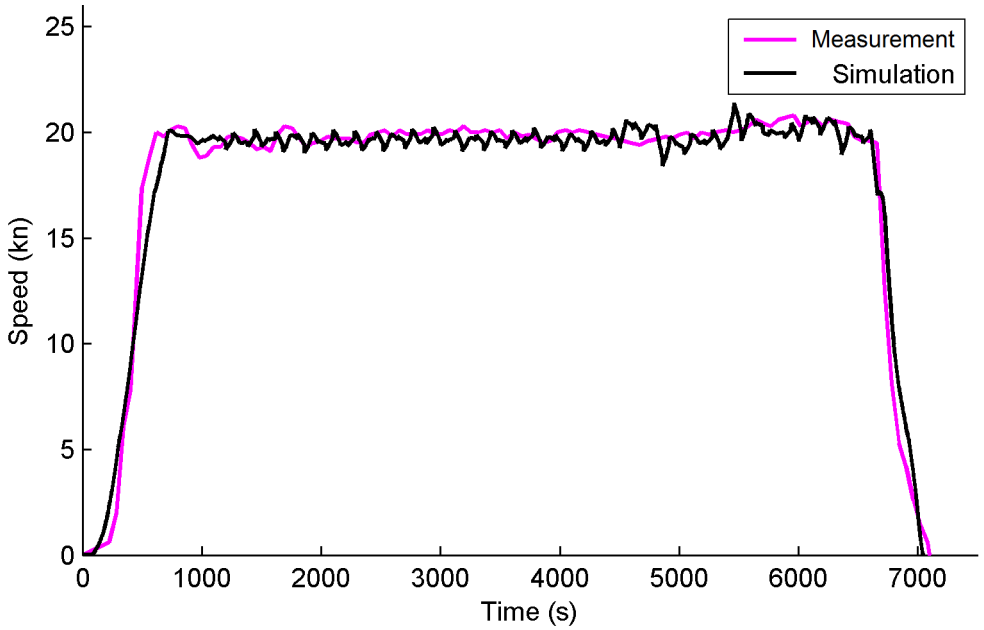

Figure 4.48: Ship speed validation for the second voyage

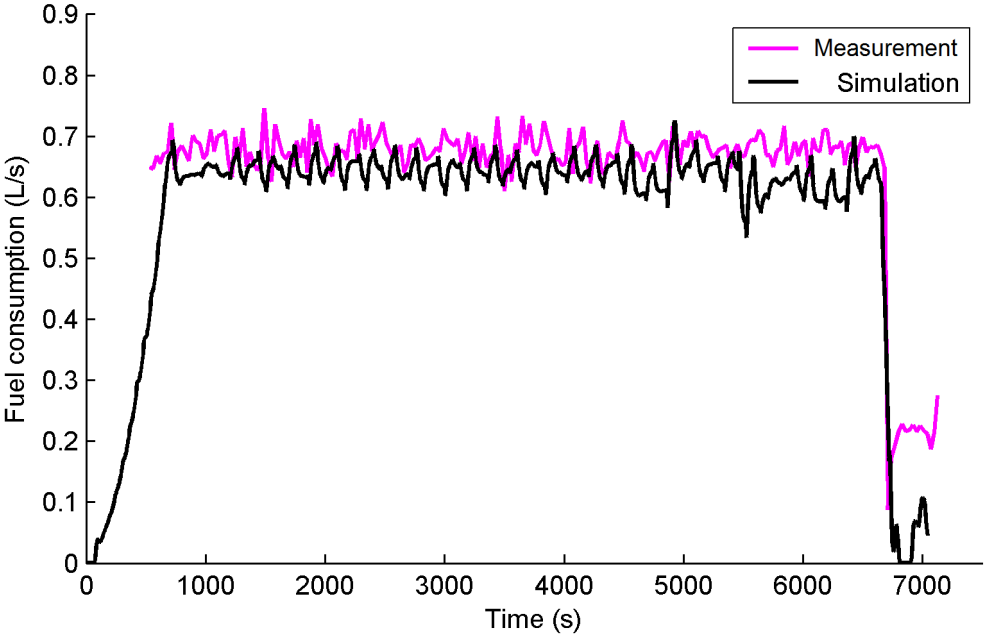

Figure 4.49: Ship fuel volume flow rate validation for the second voyage

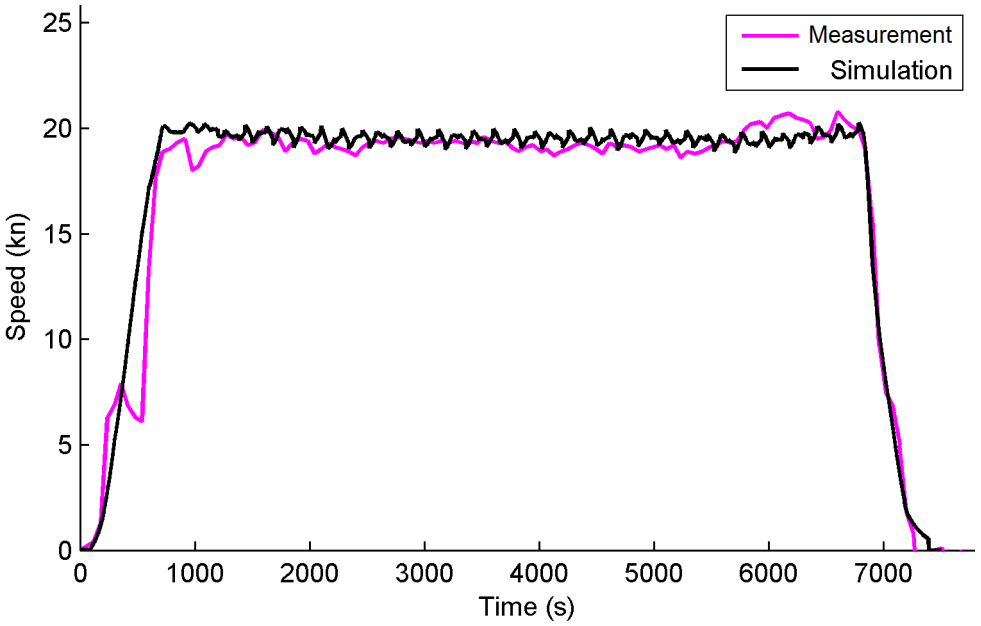

Figure 4.50: Ship speed validation for the third voyage

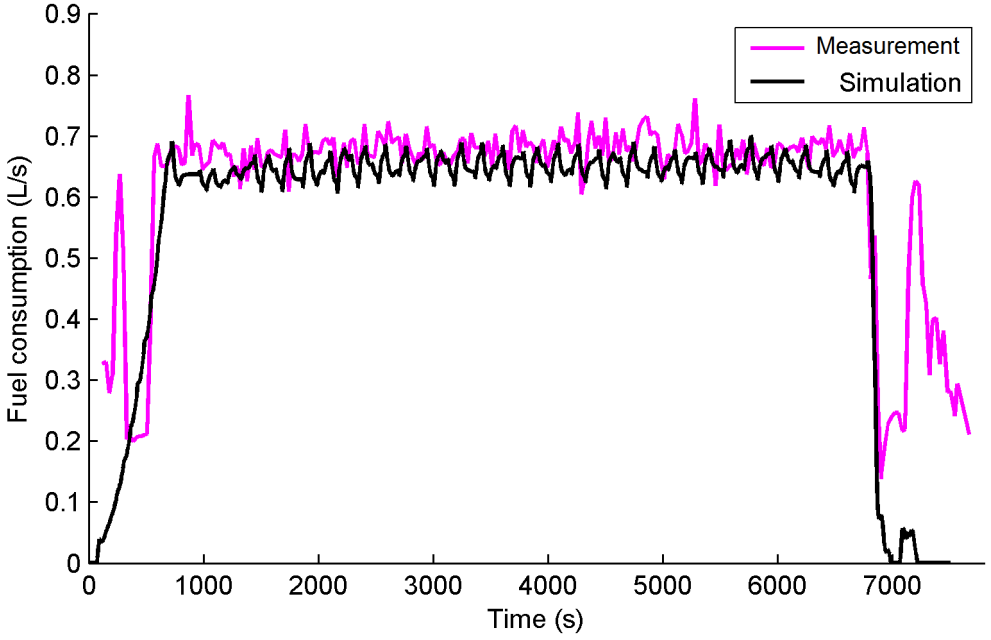

Figure 4.51: Ship fuel volume flow rate validation for the third voyage

4.4 Summary

The implementation of the mathematical equations presented in the Chapter 3 in Simulink environment has been presented in this chapter. The developed ship simulator has been described in this chapter where each block of the simulator is explained showing its function, inputs, outputs and discussing the time step of each block with a performed sensitivity analyses of different time steps. The power block of the developed ship simulator contains different power sources which includes: 2-stroke, 4-stroke diesel engines, fuel cell and battery for the first time.

Verification and validation of the developed ship simulator have been made using data from towing tank tests, wind tunnel tests, Winprop software, and real operational data of three different ships which are: *Esso Osaka*, *M/S Smyril* and *FCS Alsterwasser* where simulation results showed good agreement with the real operational data. Verification and validation of the calm water resistance, added resistance and propeller blocks have been made. Power block verification has been made using real operational data of the first fuel cell passenger ship *FCS Alsterwasser*. Also, validation of fuel cell block, battery block have been presented. Moreover, the overall developed ship simulator has been validated as a unit using real operational data of two different ships which are *Esso Osaka* and *M/S Smyril*.

In the next chapters, the developed ship simulator is used to propose a hybrid fuel cell/battery propulsion system and study different energy management strategies for the *M/S Smyril* and *FCS Alsterwasser*. *M/S Smyril* and *FCS Alsterwasser* are selected due to the availability of their real operational data. Besides, *FCS Alsterwasser* is already fitted with a hybrid fuel cell/battery propulsion system and *M/S Smyril* is a domestic ferry sailing in an emission control area which makes it a possible candidate for using fuel cell hybrid propulsion systems.

Chapter 5

Hybrid Fuel Cell System Sizing

5.1 Introduction

In this chapter, the developed ship simulator is used to propose a hybrid fuel cell/battery electric propulsion system for the domestic ferry *M/S Smyril*. First, a power source sizing methodology is presented to find the optimal sizes of the hybrid fuel cell/battery propulsion system components. Different energy management strategies are used in the sizing optimization study in order to assess the effect of changing the used EMS on the sizing optimization results. Then, the optimal fuel cell/battery hybrid system is compared with the existing diesel propulsion system of the examined ferry using the developed ship simulator. Performance comparison of the two systems is made in terms of first cost, fuel cost, maintenance cost, emissions, system weight and volume. Different energy management strategies are compared for the optimal fuel cell battery combination in terms of operational stresses, hydrogen consumption, and total energy consumption. Moreover, sensitivity analyses of the initial battery SOC, fuel and hydrogen prices are also made.

5.2 Sizing optimization

The adoption of hybrid fuel cell propulsion systems has the potential to reduce the negative environmental impacts of shipping. Among the various fuel cell technologies available, PEMFC is considered the most promising because of its solid electrolyte, high efficiency, low operating temperature, quick start-up, high power density, low noise, and zero emission. In order to improve the hybrid system dynamics and efficiency, batteries are considered as the main energy storage device used to hybridize fuel cell propulsion systems. Therefore, a hybrid fuel cell/battery propulsion system is proposed for the *M/S Smyril* using the developed ship simulator. *M/S Smyril* is a domestic ferry sailing

in an emission control area which makes the ship a possible candidate for using fuel cell hybrid propulsion systems. Also, its real operational data is available and it has been used to validate the ship simulator for three different voyages as reported in Chapter 4.

The proposed hybrid fuel cell/battery system is studied using the ship simulator and it consists of a fuel cell system with a DC-DC converter to control the power generated by the fuel cell modules. A battery system is also used as a supplement to the fuel cell system. Both systems provide the electric motors with the required power through the motor drive to propel the ship through the same gearboxes and propellers of the ship's conventional diesel propulsion system to keep changes to a minimum as shown in Figure 5.1. Based on the torque and speed requirements of the ship, four DC motors are selected to replace the four diesel engines of the ferry conventional propulsion system with the specifications in Table 5.1.

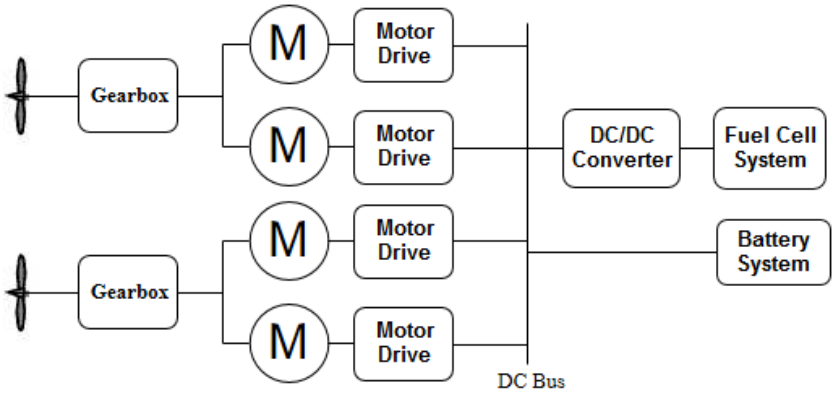

Figure 5.1: Proposed hybrid fuel cell propulsion system

Table 5.1: DC motor specifications [46; 47]

Weight	4950 kg/motor
Size	11.519 m^3/motor
Cost	\$52/kW
Annual maintenance cost	10% of first cost
Controller cost	25,000 \$/unit

Power source sizing plays an important role in hybrid fuel cell systems since it affects its performance, fuel consumption, and its first and operational costs. Most of the sizing studies reported in the literature have the objectives of minimizing the system cost [312; 313] or the system fuel consumption and operational cost [314; 188] or the sum of them [315; 316; 18]. Also, sizing objectives include maximizing the overall efficiency of the hybrid system [317; 318]. For marine applications, lifetime of ships is around 20 years which makes fuel cell and battery maintenance and replacements costs essential elements to be taken into consideration in the optimal sizing problem. Consequently, a power source sizing methodology is proposed for the examined ship with an objective of minimizing the hybrid fuel cell system first cost plus the operational cost taking maintenance and replacement costs of fuel cell and battery systems into consideration.

Based on the ferry power requirement during its real voyage, different combinations of fuel cell and battery modules are modelled and used to power the ship using the developed total ship system simulator in order to select the optimal combination according to the sizing objective considering the regular voyage of the ferry. As illustrated in Table 4.15, the examined ferry is equipped with four four-stroke diesel engines for propulsion driving two propellers through two gearboxes as shown in Figure 5.2.

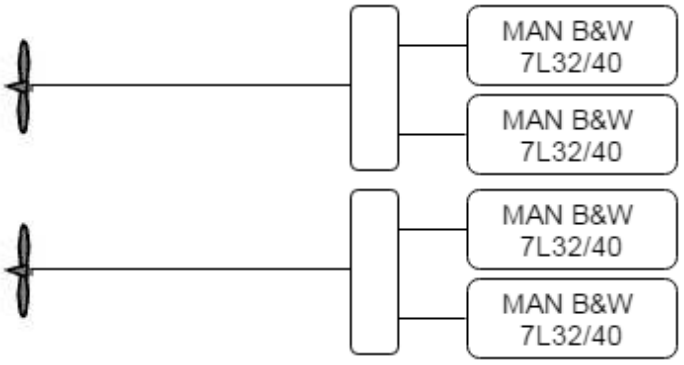

Figure 5.2: M/S Smyril diesel propulsion system configuration

The developed ship simulator can supply a breakdown of the forces acting on the hull as well as the consumed power during the ship's voyage as shown in Figures 5.3 and 5.4 for the first validated voyage as discussed in 4.3.7.2. This allows the analysis of the ship performance and its propulsion system during the examined voyage.

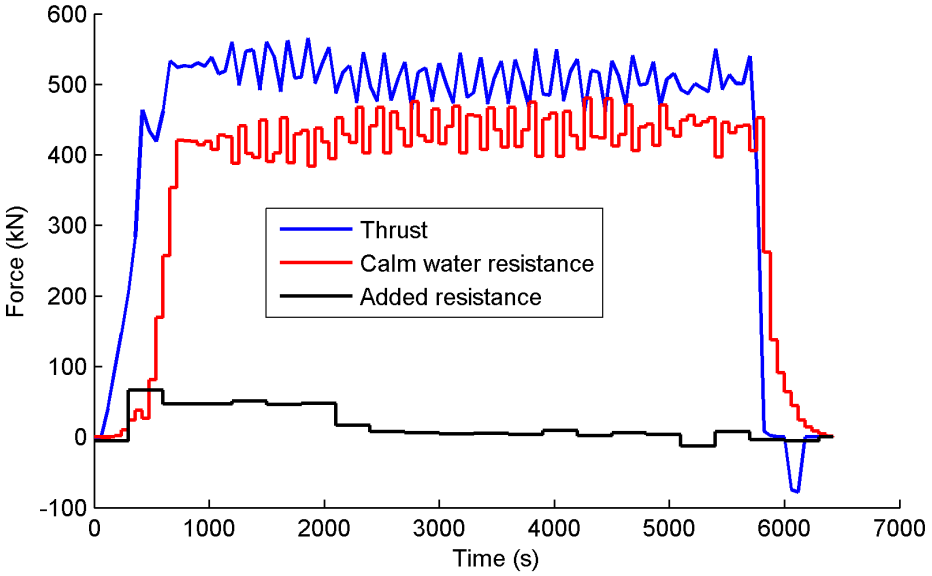

Figure 5.3: Acting forces on the hull during the ferry examined voyage

The brake power developed by the engines is the highest as shown in Figure 5.4 which is transmitted through the shaft and gearbox to the propeller. Because of the shaft efficiency, the brake power is reduced and becomes delivered power. The propeller uses the developed power to generate the thrust power which is less than the delivered power

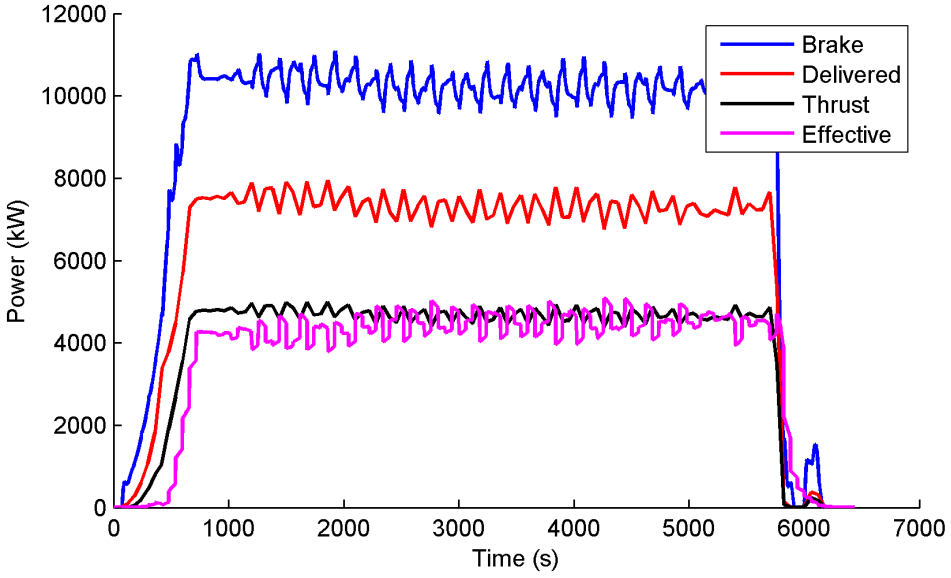

Figure 5.4: Consumed power breakdown during the ferry examined voyage

because of the propeller efficiency. The effective power is also calculated as a function of calm water resistance and ship speed. The consumed brake power during the voyage shown in Figure 5.4 can be used to select the required sizes of the fuel cell and battery of the hybrid system.

According to the consumed brake power displayed in Figure 5.4 during the examined voyage, different combinations of fuel cell and battery modules are suggested using off-the-shelf components wherever possible. The fuel cell system is sized to supply an average required power to reduce its stresses and fuel consumption while the battery system is used as a supplement. The sizing objective function is to minimize the system total cost ($Cost_{Tot}$) which includes the first cost ($Cost_{fir}$) and the operational cost ($Cost_{ope}$) taking into consideration maintenance ($Cost_{main}$) and replacement costs ($Cost_{rep}$) of fuel cell and battery systems as follows:

$$\underset{x}{\text{minimize}} \begin{cases} Cost_{Tot} = Cost_{fir} + Cost_{ope} \\ Cost_{fir} = FC + Batt + motor + Tank_{H_2} \\ Cost_{ope} = Cost_{H_2} + Cost_{main} + Cost_{rep} \end{cases} \tag{5.1}$$

The system first cost includes the costs of the fuel cell system (FC), battery system ($Batt$), electric motors and its controllers, and the hydrogen tank cost ($Tank_{H_2}$). The operational cost of the system includes the fuel cost ($Cost_{H_2}$) plus the maintenance and replacement costs of fuel cell and battery systems as illustrated in Equation 5.1. The decision variables of the optimization problem in Equation 5.1 are the number of fuel cell and battery modules.

Based on the ferry brake power requirements shown in Figure 5.4, the number of fuel cell modules changes from 143 to 168 modules considering its nominal power rating and taking efficiencies of the motor drive and DC-DC converter into consideration assuming a constant efficiency of 95% of both [114]. The used PEMFC system is $NedStackPS50$ and its main specifications are shown in Table 5.2. Figure 5.5 shows the used PEMFC model characteristics of voltage and power versus current.

Table 5.2: Specifications of NedStack PS50 module [48]

Net rated nominal power	50-72 kW
Net rated peak power	120 kW
Output voltage	630 V
Resistance	0.664 Ω
Efficiency	55-57 %
Mass	600 kg
Volume	0.672 m^3
Expected life	20,000 h
First cost	235.51 \$/kW [319]
Replacement cost	30% of first cost [320]
Annual maintenance cost	50 \$/kW [320]

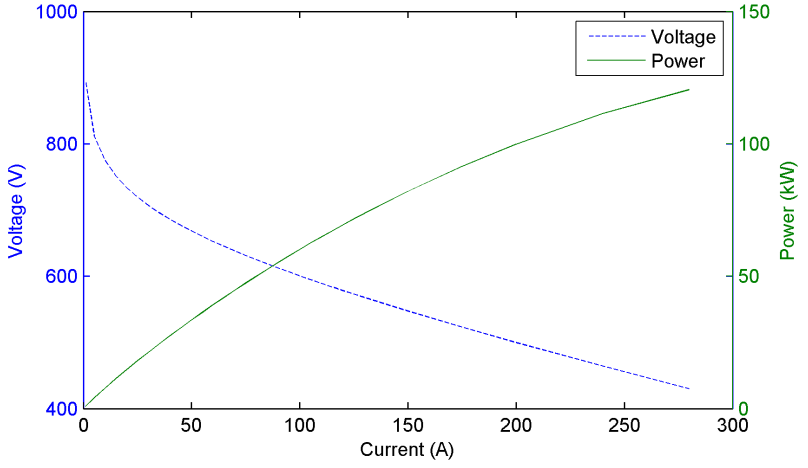

Figure 5.5: Fuel cell voltage and power versus current

The number of battery modules changes from 2 to 6 modules using lithium-ion battery packs of 500 Ah capacity which will be used as a supplement to the fuel cell system and its main features are shown in Table 5.3. Lithium-ion batteries have been selected due to its several advantages over other battery types such as the higher energy and power densities as detailed in Table 2.4 which is required for marine transportation applications. Moreover, Lithium-ion batteries have higher efficiency and are more durable [321; 274]. Also, its voltage does not fall considerably during discharging the battery discharge as shown in Figure 5.6.

Table 5.3: Lithium-ion battery pack specifications [49]

Standard capacity	500 Ah
Output voltage	600 V
Resistance	0.0156 Ω
Standard C-rate	0.2C
Maximum C-rate	2.5C
Cycle life	2000 cycle
Mass	2800 kg
Volume	2.29 m^3
First cost	1000 \$/kWh [274]
Replacement cost	27.63 \$/kWh [321]
Annual maintenance cost	21 \$/kW [321]

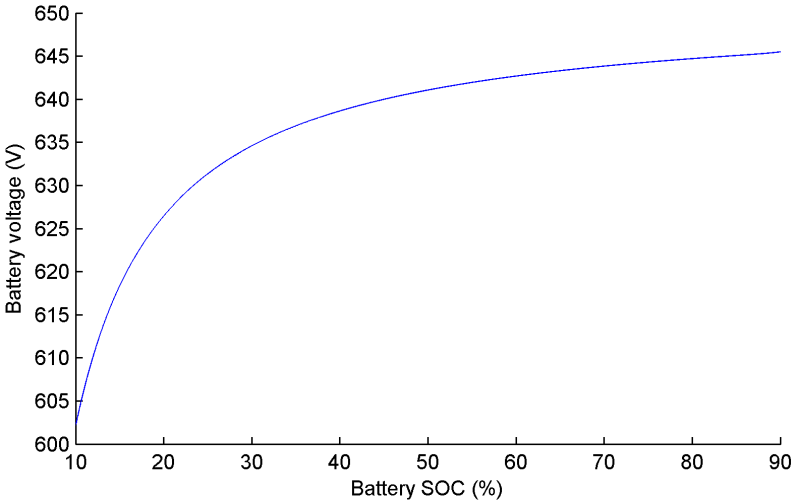

Figure 5.6: Battery voltage versus SOC at 0.2C discharge rate

5.3 Simulation parameters

Different sizes of the fuel cell and battery systems combinations are modelled and used to power the ship for the same examined voyage using the developed ship simulator assuming the same ship trim and displacement using different fuel cell/battery combinations. The distribution of the ship required propulsion power between the fuel cell system and the battery system is controlled through the energy management strategy. Since the hybrid fuel cell system performance depends on the used EMS, the most four common strategies are used to split the required power between the fuel cell and battery systems for the studied fuel cell and battery systems combinations for the sake of investigating the effect of the used energy management strategy on the sizing optimization output. The used strategies are: the state-based, classical PI, CDCS, and ECMS strategies. Using these strategies for different fuel cell and battery systems combinations, simulation results include hydrogen consumption, energy consumption, number of fuel cell operational hours, and number of the battery consumed cycles.

Hydrogen consumption of the examined voyage is then used to calculate the daily fuel cost considering four voyages per day. Number of fuel cell operational hours and battery consumed cycles are used to calculate the total replacement cost of the fuel cell and battery systems during the ship lifetime assumed to be 20 years. Moreover, the hybrid system first cost and maintenance cost for different combinations of the fuel cell and battery systems are calculated according to its power sizes as shown in Tables 5.2 and 5.3. Then, the total replacement cost, first cost and maintenance cost of different fuel cell and battery combinations are compared on daily basis assuming 300 operational days per year, in addition to the daily hydrogen cost, in order to obtain the optimal size of the fuel cell and battery systems according to Equation 5.1.

The same fuel cell and battery mathematical models are used with the same initial conditions and operating limits for different fuel cell/battery combinations using different strategies of energy management. Regarding the fuel cell system, operational limits have been used to avoid operating at poor efficiency region which are: fuel cell minimum power of 5 kW, maximum power of 120 kW, and an optimum power value of 50 kW, the same as the nominal power of the used PEMFC model as described in Table 5.2. The efficiency of the DC-DC converters and motor drives are set to 95% [114]. Regarding the battery, a normal SOC of 70% is chosen as an initial condition for different strategies as suggested in [322]. For the classical PI EMS, a reference value of the battery SOC of 60% is selected as recommended by automotive industry designers [280]. The battery SOC controller in the PI based strategy is tuned manually for the examined voyage and the P and I gains are 500 and 0.5 respectively. For the ECMS, SOC_H and SOC_L are set to 80% and 30% [323] and the battery threshold value for the CDCS strategy is 30% [324]. The SOC constant μ is set to 0.6 to balance the battery SOC during the examined driving cycle using the ECMS as reported in [17; 293]. The battery C-rate limits are 0.2C and 2.5C as recommended by the battery manufacturer [49].

5.4 Simulation results

Hydrogen consumption of different fuel cell and battery combinations clearly depends on the used energy management strategy as shown in Figure 5.7. In order to compare different strategies fairly, the calculated hydrogen consumption shown in Figure 5.7 includes the fuel cell system hydrogen consumption during the examined voyage in addition to the consumed hydrogen used to charge the battery system back to its initial battery SOC towards the end of the examined voyage. As illustrated in Figure 5.7, increasing the number of fuel cell blocks results in reducing the hydrogen consumption using different strategies. This can be justified by the fact that using more fuel cells means that less energy is depleted from the battery system which reduce the hydrogen consumption and energy losses in recharging the battery back to its initial SOC. Moreover, increasing the number of fuel cell blocks helps in avoiding the operation

in a poor efficiency region and maintaining higher efficiency of the fuel cell system which reduce its hydrogen consumption. As shown in Figure 5.7(d), CDCS strategy has lower hydrogen consumption than other strategies for different fuel cell and battery combinations due to its prioritizing of the battery system energy consumption.

According to Figure 5.7, a hydrogen tank with specifications shown in Table 5.4 will be sufficient for the ferry daily operation considering 4 voyages per day. In this study, hydrogen is assumed to be refuelled daily and stored as a cryogenic liquid in a tank as suggested in [272] for marine transportation applications.

Table 5.4: Liquid hydrogen tank specifications [50]

Capacity	4000 kgH_2
Gravimetric density	0.142 kgH_2/kg
Volumetric density	70.8 kgH_2/m^3
Cost	$650,000

Regarding the first and maintenance costs of different fuel cell and battery combinations, it can be calculated according to the values in Tables 5.1 to 5.4. First cost includes the fuel cell and battery blocks first costs, electric motors and its controllers, and hydrogen tank first costs as shown in Figure 5.8. Maintenance costs of the fuel cell and battery systems are also calculated according to its power sizes in Tables 5.2 and 5.3 as shown in Figure 5.9. As expected, using more fuel cell and battery blocks increase the first and maintenance costs of the hybrid system as shown in Figures 5.8 and 5.9. The calculated first and maintenance costs are then distributed over the life of the ship assuming 20 years lifetime operating 300 days yearly.

The used energy management strategy affects the replacement costs of the fuel cell and battery systems. This is because the dynamic behaviour of the hybrid system is controlled through the used EMS which decides the operational condition and time of the fuel cell and battery systems. Expected lifetime of the fuel cell is about 20000 hr while the battery cycle life is about 2000 cycles as reported by the manufacturers as shown in Tables 5.2 and 5.3. As anticipated, increasing the number of battery blocks reduces the number of fuel cell operational time and consumed battery cycles which results in increasing the operational lifetime of the fuel cell and battery modules using different strategies as shown in Figure 5.10. Therefore, replacement cost is lower for fuel cell/battery combinations with higher battery blocks number as shown in Figure 5.11. Figure 5.11 presents the total replacement costs of the fuel cell and battery systems during the ship's lifetime assumed to be 20 years using different strategies. However, increasing battery blocks number will increase the hybrid system first cost as shown in Figure 5.8.

The effect of increasing the number of battery blocks is not significant while using CDCS strategy. Also, different fuel cell/battery combinations have lower operational life and have higher maintenance cost using CDCS strategy compared to other strategies as can

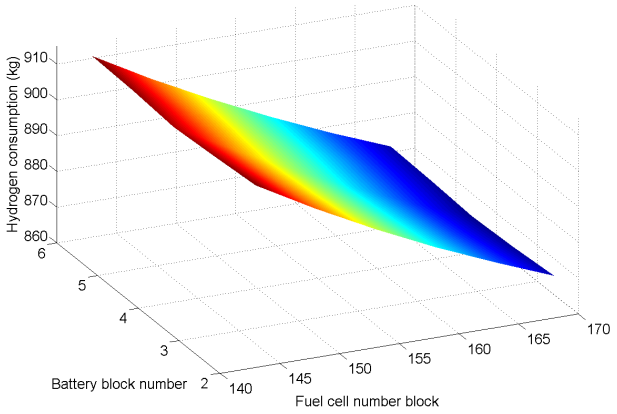

(a) State-based strategy

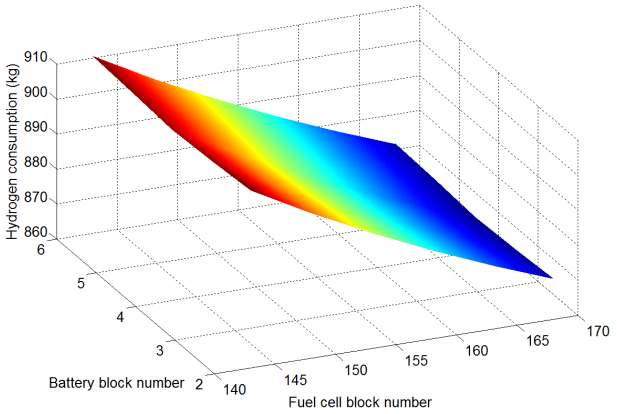

(b) Classical PI strategy

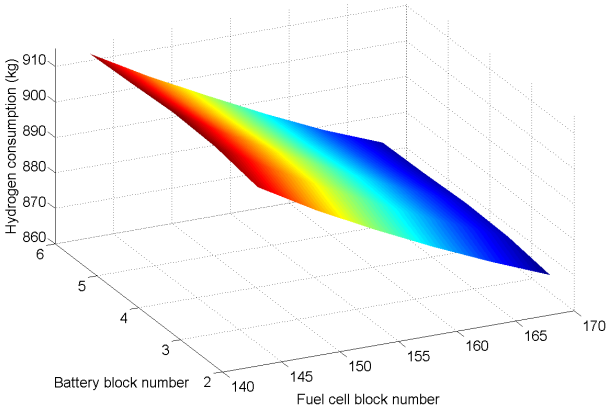

(c) ECMS

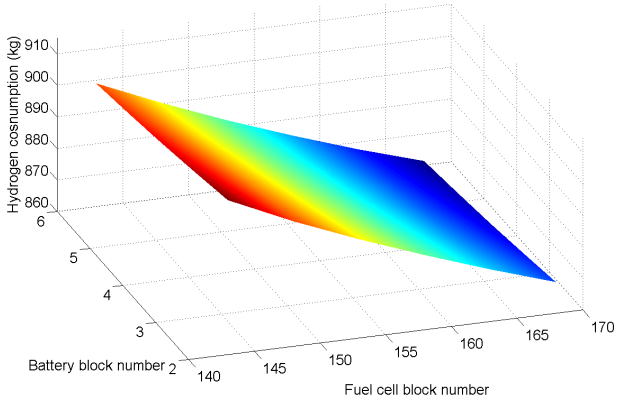

(d) CDCS strategy

Figure 5.7: Hydrogen consumption during the examined voyage for different fuel cell/battery combinations using different strategies

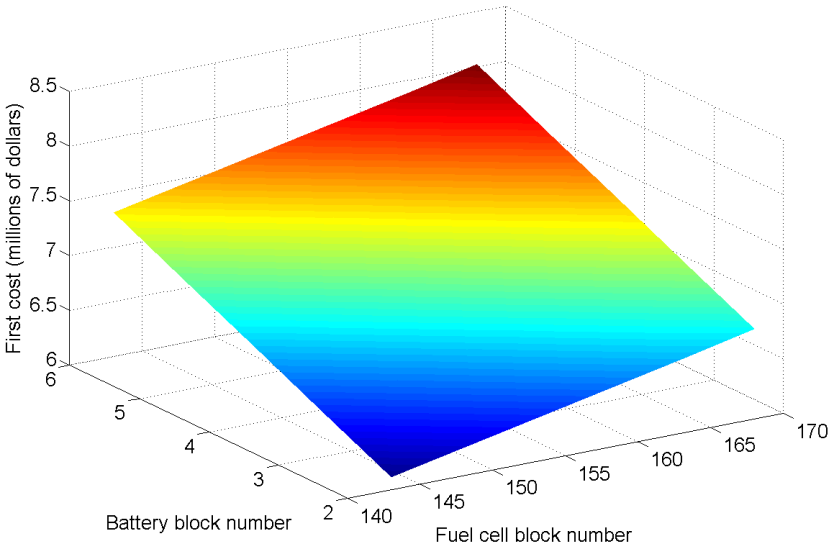

Figure 5.8: First cost of different fuel cell/battery combinations

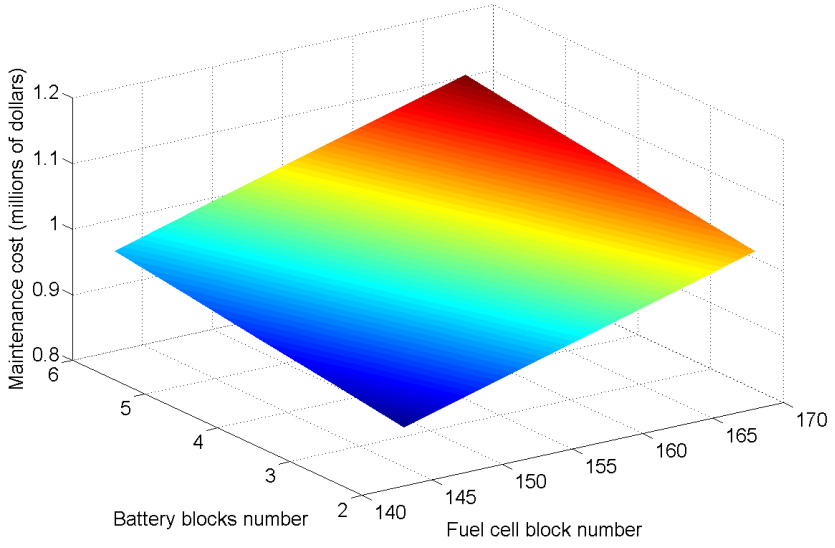

Figure 5.9: Annual maintenance costs of different fuel cell/battery combinations

be seen from Figures 5.10 and 5.11. This is due to the fact that CDCS strategy prioritizes the battery power usage which rapidly consumes the battery cycles and increase the fuel cell operational hours in order to charge the battery back to its initial SOC which reduces the operational life of the fuel cell and battery modules and increases its total replacement cost.

Comparing the total considered costs according to Equation (5.1) for different fuel cell/battery combinations, the optimal combination that gives the minimum daily total cost is different for the four studied strategies of energy management. It is 158 fuel cell and 4 battery blocks using the state-based as shown in Table 5.5. By using the classical PI strategy, the optimal combination is 163 fuel cell and 3 battery blocks as shown in Table 5.6. 158 fuel cell and 2 battery blocks combination gives the the minimum

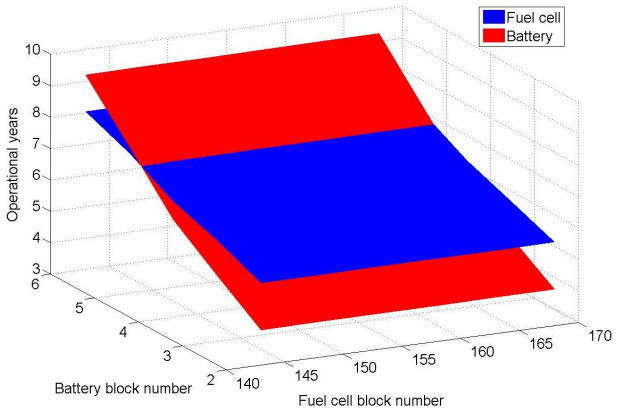

(a) State-based strategy

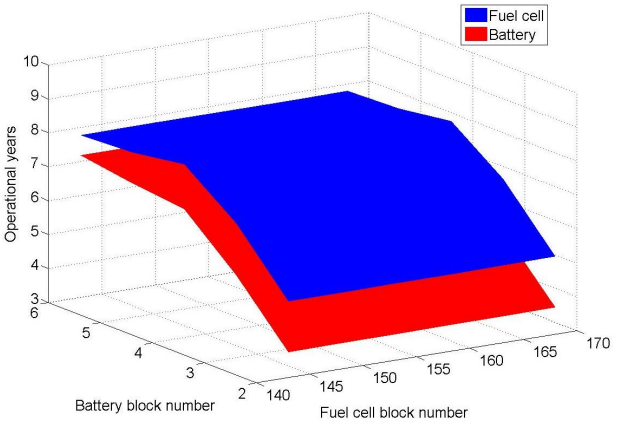

(b) Classical PI strategy

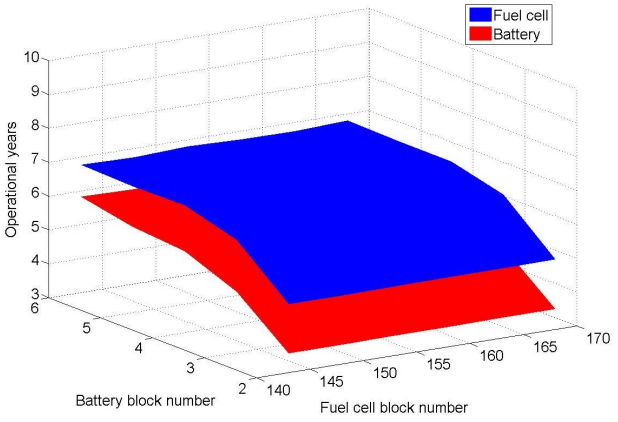

(c) ECMS

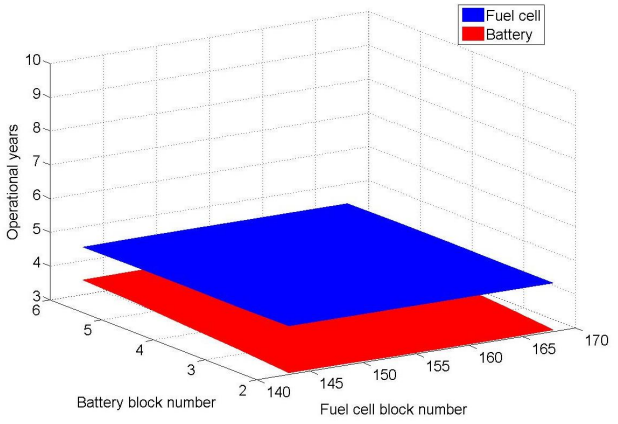

(d) CDCS strategy

Figure 5.10: Fuel cell and battery operational years of different combinations using different strategies

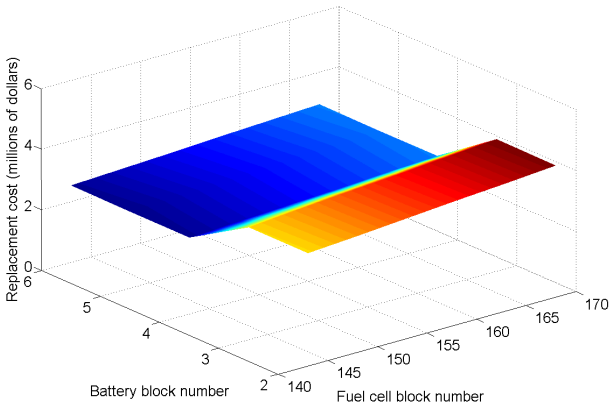

(a) State-based strategy

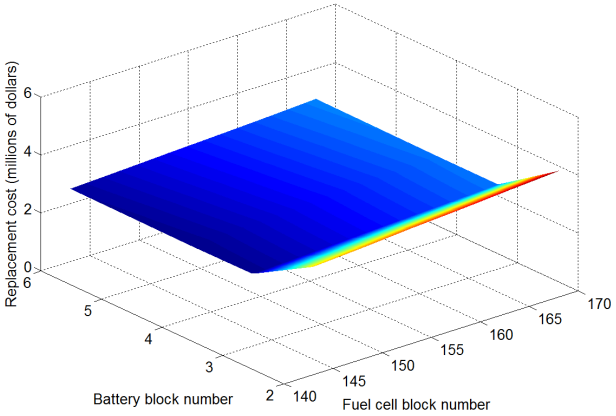

(b) Classical PI strategy

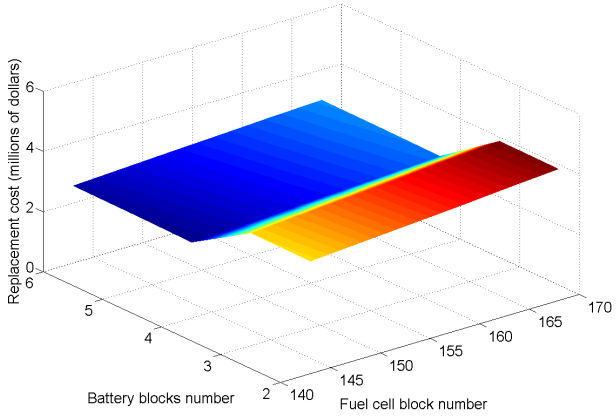

(c) ECMS

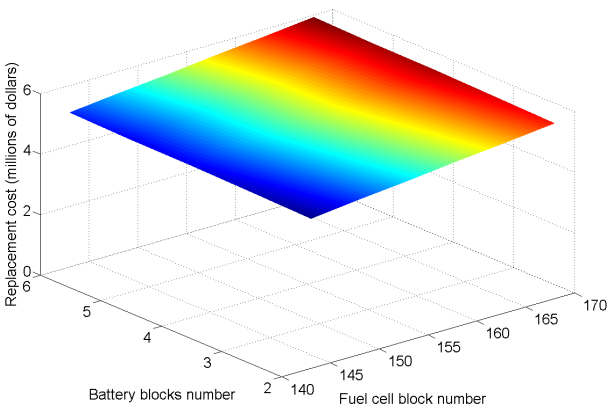

(d) CDCS strategy

Figure 5.11: Total replacement cost of different fuel cell/battery combinations using different strategies

daily total cost using ECMS as shown in Table 5.7. Meanwhile, 153 fuel cell and 2 battery blocks combination is the optimal in case of using the CDCS strategy as shown in Table 5.8.

Table 5.5: Daily total cost of the hybrid system for different fuel cell/battery combinations using state-based strategy

Fuel cell blocks number	Battery blocks number				
	2	3	**4**	5	6
143	$22,172	$22,256	$22,146	$22,263	$22,382
148	$22,138	$22,223	$22,106	$22,223	$22,342
153	$22,120	$22,205	$22,083	$22,199	$22,317
158	$22,115	$22,200	**$22,072**	$22,188	$22,305
163	$22,122	$22,208	$22,073	$22,189	$22,306
168	$22,140	$22,225	$22,085	$22,199	$22,316

Table 5.6: Daily total cost of the hybrid system for different fuel cell/battery combinations using classical PI strategy

Fuel cell blocks number	Battery blocks number				
	2	**3**	4	5	6
143	$22,170	$22,125	$22,271	$22,360	$22,457
148	$22,136	$22,082	$22,225	$22,314	$22,411
153	$22,118	$22,054	$22,195	$22,285	$22,382
158	$22,113	$22,040	$22,180	$22,270	$22,367
163	$22,121	**$22,038**	$22,176	$22,266	$22,364
168	$22,138	$22,047	$22,183	$22,274	$22,371

Table 5.7: Daily total cost of the hybrid system for different fuel cell/battery combinations using ECMS strategy

Fuel cell blocks number	Battery blocks number				
	2	3	4	5	6
143	$22,164	$22,315	$22,227	$22,319	$22,415
148	$22,130	$22,279	$22,183	$22,277	$22,373
153	$22,112	$22,259	$22,154	$22,249	$22,351
158	**$22,108**	$22,253	$22,140	$22,234	$22,332
163	$22,115	$22,258	$22,138	$22,232	$22,329
168	$22,133	$22,274	$22,146	$22,240	$22,343

As can be observed in Tables 5.5 to 5.8, the used EMS affects the resulting optimal fuel cell/battery combination. However, the difference between the daily total cost of the resulting optimal fuel cell/battery combinations using different strategies is about 1.2%. This small difference can be justified by the fact that the ship operational profile does not have a lot of variation in speed and power requirements which minimizes the effect of using different strategies. Moreover, the energy required to charge the battery system back to its initial SOC is taken into consideration. Consequently, changing the used EMS does not affect the daily total cost of the hybrid system considerably. To

Table 5.8: Daily total cost of the hybrid system for different fuel cell/battery combinations using CDCS strategy

Fuel cell blocks number	Battery blocks number				
	2	3	4	5	6
143	$22,342	$22,397	$22,458	$22,517	$22,588
148	$22,316	$22,373	$22,435	$22,495	$22,567
153	**$22,305**	$22,364	$22,428	$22,489	$22,562
158	$22,308	$22,368	$22,433	$22,496	$22,570
163	$22,323	$22,384	$22,450	$22,514	$22,589
168	$22,348	$22,410	$22,477	$22,542	$22,617

conclude, according to the sizing objective of minimizing the hybrid power system first cost plus the operational cost taking maintenance and replacement costs of fuel cell and battery systems into consideration, the optimal fuel cell/battery combination is 163 fuel cell blocks combined with 3 battery blocks using the classical PI EMS. This combination is compared later with the conventional diesel propulsion system of the ferry.

5.4.1 Sensitivity analysis of Hydrogen price

Fuel cost represents the highest percentage of ships operational costs. Regarding the total costs shown in Tables 5.5 to 5.8, it is dominated by the hydrogen fuel cost with more than 70% as shown in Figure 5.12. Meanwhile, maintenance cost percentage is about 15% of the considered total cost while the first cost and replacement cost percentages are about 5% and 3% respectively. Therefore, a sensitivity analysis is performed to study the effect of different hydrogen prices on the resulting optimal fuel cell/battery combination. Hydrogen price depends on how it is produced where solar systems costs more than coal gasification systems of hydrogen production. The reported results to this point corresponds to a hydrogen price of 4.823 $\$/kg$ generated by wind energy [325]. The examined ship operating area is around Faroe Islands where a great potential for the exploitation of wind energy is there. Therefore, building a hydrogen generation and fuelling facility using wind power for hybrid fuel cell ships would be an optimal solution towards the green ship design.

As shown in Figure 5.7, increasing the number of fuel cell blocks results in reducing the hydrogen consumption. Consequently, at higher hydrogen prices, the optimal fuel cell/battery combination tends to have more fuel cell blocks with the same battery blocks number to reduce the hydrogen consumption because of its high price. At lower hydrogen prices, the optimal fuel cell/battery combination will have less fuel cell blocks with the same battery blocks number using different strategies. For the classical PI strategy as for example, at a higher hydrogen price of 6.3 $\$/kg$, the optimal fuel cell/battery combination will be 168 fuel cell plus 3 battery blocks as shown in Table 5.9. Meanwhile,

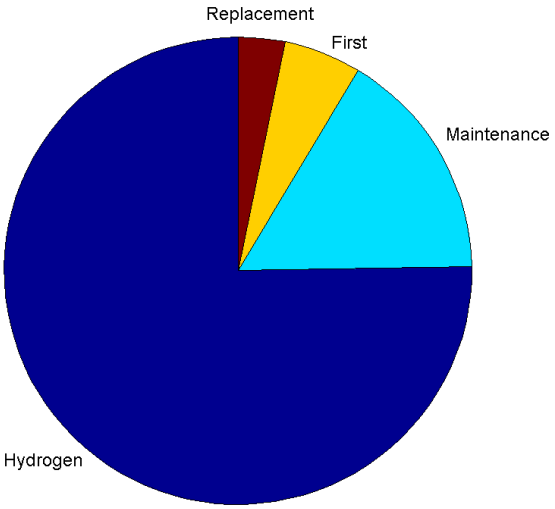

Figure 5.12: Breakdown of the considered total daily cost of the proposed hybrid fuel cell system

at a lower hydrogen price of 2.35 $\$/kg$, the optimal fuel cell/battery combination is 143 fuel cell plus 3 battery blocks as shown in Table 5.10.

Table 5.9: Daily total cost of the hybrid system for different fuel cell/battery combinations using classical PI strategy

Fuel cell blocks number	Battery blocks number				
	2	**3**	4	5	6
143	\$27,549	\$27,522	\$27,682	\$27,765	\$27,860
148	\$27,461	\$27,423	\$27,579	\$27,664	\$27,758
153	\$27,393	\$27,344	\$27,498	\$27,583	\$27,678
158	\$27,343	\$27,284	\$27,435	\$27,521	\$27,616
163	\$27,308	\$27,239	\$27,389	\$27,474	\$27,569
168	\$27,286	**\$27,208**	\$27,355	\$27,442	\$27,536

Hydrogen price = 6.3 $\$/kg$

Table 5.10: Daily total cost of the hybrid system for different fuel cell/battery combinations using classical PI strategy

Fuel cell blocks number	Battery blocks number				
	2	**3**	4	5	6
143	\$13,163	**\$13,089**	\$13,212	\$13,310	\$13,411
148	\$13,221	\$13,139	\$13,261	\$13,358	\$13,459
153	\$13,286	\$13,196	\$13,317	\$13,414	\$13,516
158	\$13,358	\$13,260	\$13,380	\$13,477	\$13,579
163	\$13,436	\$13,329	\$13,448	\$13,546	\$13,648
168	\$13,519	\$13,404	\$13,522	\$13,620	\$13,722

Hydrogen price = 2.35 $\$/kg$

5.4.2 Comparison with conventional propulsion system

As detailed in Table 4.15, the examined ship is equipped with 4 diesel engines with weight and size of 42 tonnes and 68.25 m^3 each according to its manufacturer. Comparing the optimal fuel cell/battery combination of 163 fuel cell and 3 battery blocks to the conventional diesel propulsion system of the examined ship, weight and size saving percentages of 7.3% and 18.6% respectively can be achieved by using the hybrid fuel cell/battery propulsion system as shown in Figure 5.13. The calculated weight and size of the hybrid fuel cell/battery system include the weight and size of the daily hydrogen tank, the electric motors and its controllers in addition to the weight and size of the fuel cell and battery modules. This saving of weight and size can be used for additional passenger rooms or private cars which makes the proposed fuel cell system more feasible. On the other hand, the first cost of the proposed hybrid system is higher than the diesel engines by about 81% as shown in Figure 5.14 because of the high current initial cost of fuel cells.

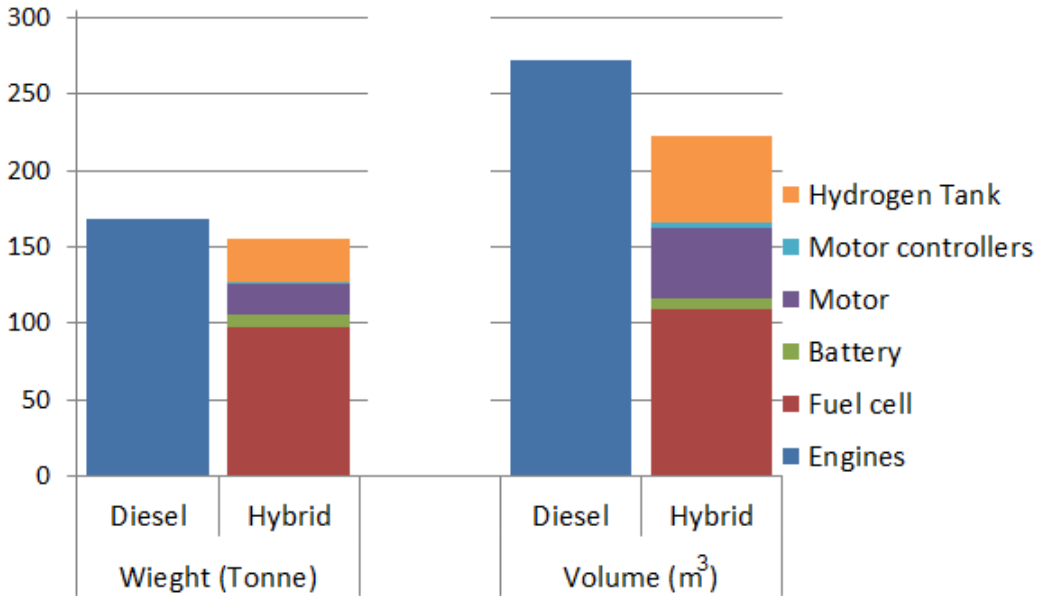

Figure 5.13: Proposed hybrid fuel cell/battery system weight and size comparison to the conventional diesel system

Due to the absence of any moving parts, the maintenance cost of fuel cells is lower than diesel engines. Using low cost and mid-range cost estimations of the annual fuel cell maintenance cost of 20 and 27 $\$/kW$ respectively [320], the maintenance cost of the fuel cell modules of the proposed hybrid system is lower than the maintenance cost of the conventional diesel engines assuming diesel maintenance cost of 0.01 $\$/kWh$ as shown in Figure 5.15. Using the high cost estimation of the annual fuel cell maintenance cost of 50 $\$/kW$, the fuel cell maintenance cost will be higher than maintenance cost of the diesel engines. The difference between high and low cost estimates of fuel cell maintenance cost is about considering fuel cell as a mature technology, assuming fuel

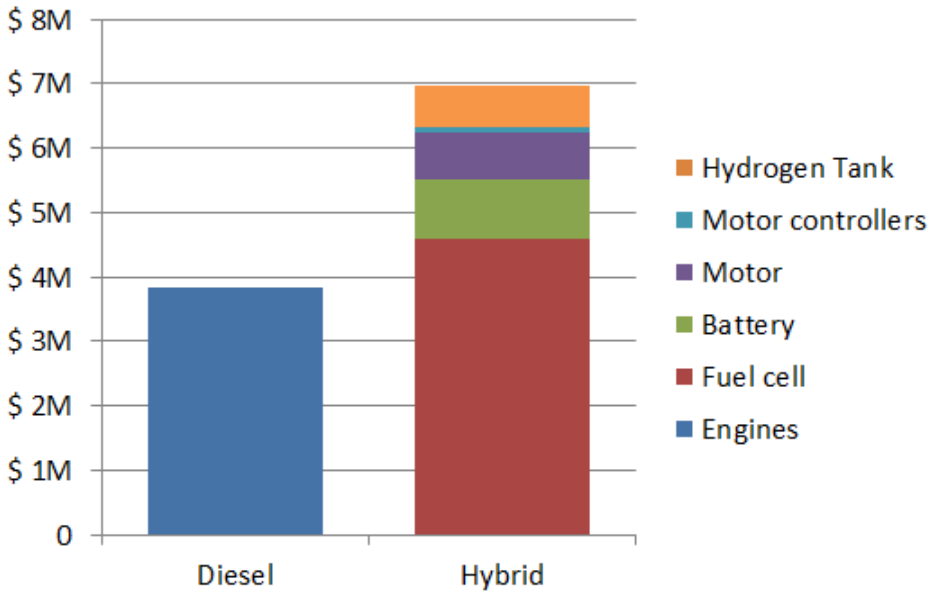

Figure 5.14: Proposed hybrid fuel cell/battery system first cost comparison to the conventional diesel system

cell mass production, and the size of application. Low cost estimates consider fuel cell as a mature technology, used in large-scale applications and produced in large amounts which reduces its maintenance cost. On the other hand, high cost estimates consider fuel cell as a new technology and uses costs of the first-generation installations. Meanwhile, mid-range cost is the expected cost of the near future. By taking the annual maintenance costs of the electric motors and batteries into consideration, the annual maintenance cost of the diesel engines is lower than the proposed hybrid fuel cell/battery system using mid-range and high cost estimates of fuel cell maintenance. Figure 5.15 displays the annual maintenance cost of the four diesel engines of the examined vessel compared to the annual maintenance cost of the fuel cell and battery modules in addition to the electric motors of the proposed hybrid fuel cell system.

Moreover, hydrogen price is still higher than the diesel fuel which makes the fuel cost of the hybrid fuel cell/battery system higher. Also, as oil price has been dropping recently, more economic pressure is increasing on the clean energy investment. However, using hydrogen as a fuel can result in less emissions and saving in the environmental damages caused by using diesel fuel which can be converted into cost saving. Without taking into consideration the environmental damage cost resulting from using diesel oil, the average hydrogen cost has more than two-fold increase compared to the diesel oil for the examined voyage. By taking the environmental damage cost into consideration, hydrogen cost is higher than marine diesel oil (MDO) by about 46% for the examined voyage as shown in Figure 5.16, assuming a marine fuel cost of 0.41 $\$/kg$.

Due to the high efficiency of fuel cells, the efficiency of the energy flow using the proposed hybrid fuel cell system is approximately the same as the efficiency of the conventional

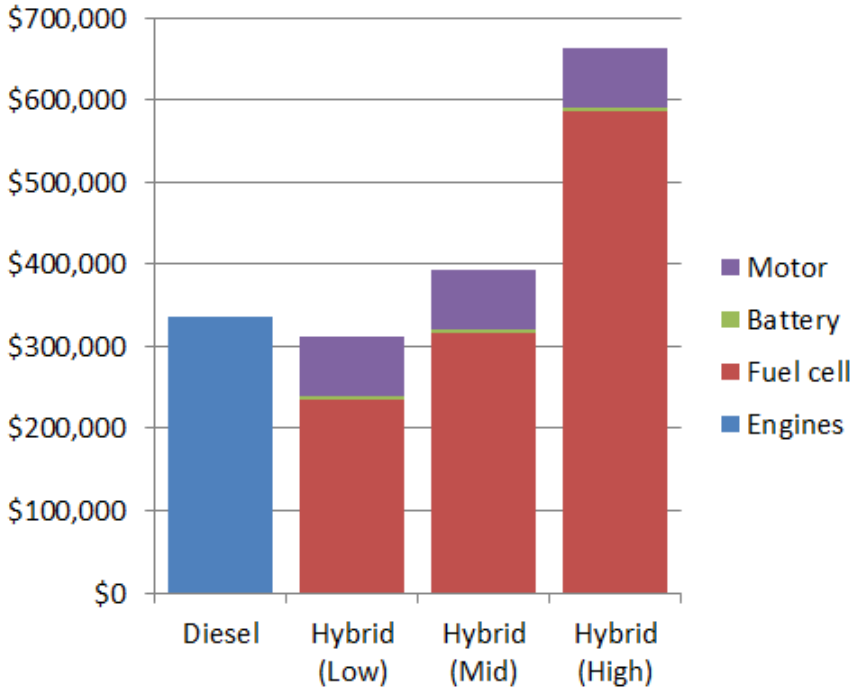

Figure 5.15: Proposed hybrid fuel cell/battery annual maintenance cost comparison to the conventional diesel system

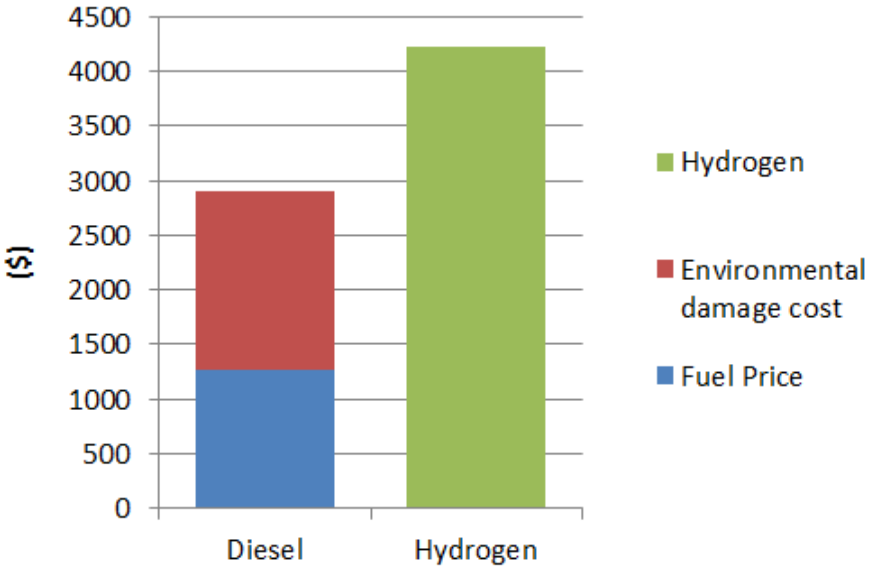

Figure 5.16: Fuel cost comparison for the examined voyage

diesel system. As shown in Figure 5.17, at rated load, an overall efficiency of about 47% can be achieved using the hybrid fuel cell system. For part load operation, the efficiency of the proposed hybrid fuel cell system would be higher than the conventional diesel system because diesel engines fuel consumption is higher at part load. However, the conventional diesel system is less complex than the proposed hybrid fuel cell system.

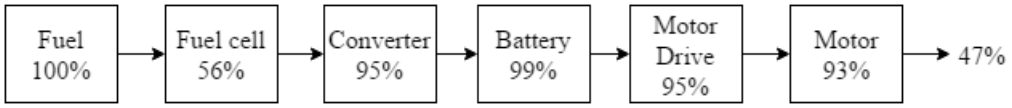

Figure 5.17: Energy flow diagram of the proposed hybrid fuel cell/battery system

Regarding ship emissions for the examined voyage, by using the fuel-based emissions factors in Table 3.6, the emissions of the examined ship per voyage using its conventional diesel propulsion system is about 9.8 tonnes of CO_2, 22.8 kg of CO, 172.5 kg of NO_X, 30.8 kg of SO_2, and 3.4 kg of PM. These emissions are compared to zero pollutant emissions from hydrogen fuelled fuel cell. Also, noise level is reduced from a level of 105 dB(A) using diesel engines to a level of 65 dB(A) using fuel cells. This results in increasing the passengers comfort level and reduces the need for sound insulation systems which will increase the weight saving percentage of using hybrid fuel cell system and make it more feasible compared to diesel engines.

5.4.2.1 Impact of varying fuel prices

The comparison between the proposed hybrid fuel cell propulsion system and the conventional diesel propulsion system is highly sensitive to the used prices of hydrogen and MDO. Regarding hydrogen, its price varies greatly according to its method of production and transportation, its pressure, state, and volume. Different studies and scenarios of hydrogen future can be found in the literature [325; 326]. Hydrogen prices are expected to decline with time; even so these scenarios are different depending on the expected progress of hydrogen production and transportation methods as well as the society commitment to use hydrogen as a new fuel. Figure 5.18 illustrates hydrogen production cost from wind energy in three cases which declines with time due to the reduction of electrolyzer and compressor costs on the mid term (to 2020) and long term (to 2030) [325].

Oil prices trend can also change with time. After the recent drop of oil prices, three potential scenarios of low, medium and high oil prices can be seen as shown in Figure 5.19 which all increases with time but with different rates. Therefore, a sensitivity analysis is carried out for the three different paths of oil prices shown in Figure 5.19 and the average expected hydrogen price from Figure 5.18.

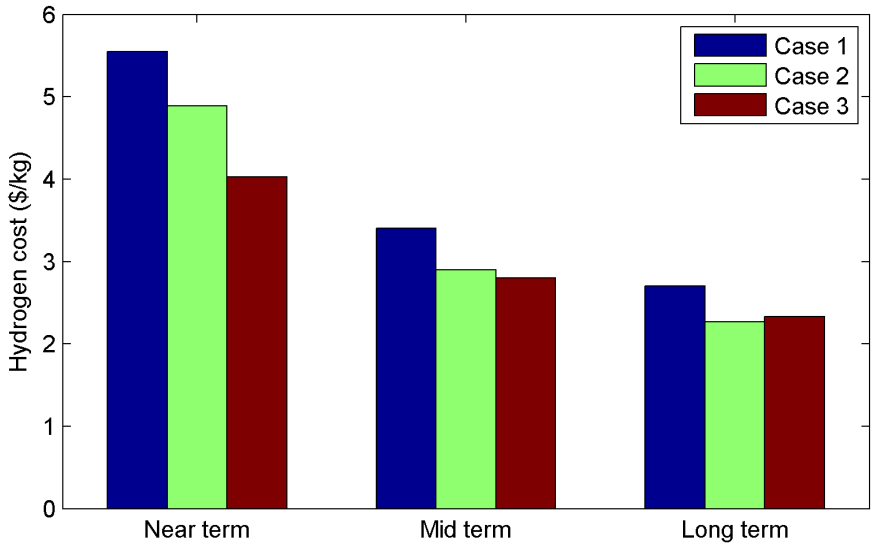

Figure 5.18: Cost per kg of hydrogen generated from wind energy for near, mid, and long terms

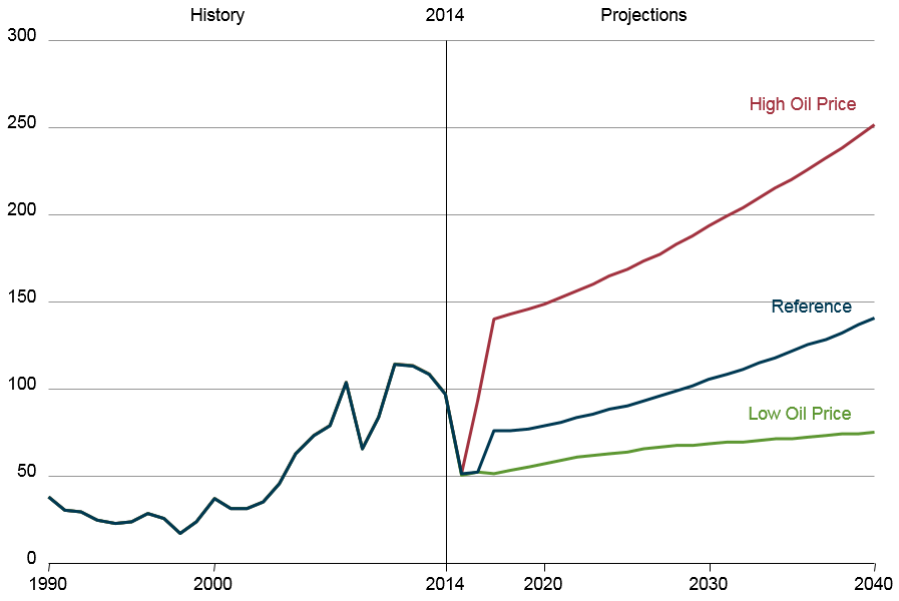

Figure 5.19: Oil price paths during 1990-2040 in $/barrel [22]

For an average mid term hydrogen price of 3.03 $/kg, the hydrogen fuel cost for the examined voyage would be less than the diesel oil by about 17%, 24%, or 33% as shown in Figure 5.20 assuming low, medium, and high MDO prices of 0.5, 0.6, and 0.75 $\$/kg$ respectively. On the long term, hydrogen price is expected to decline more meanwhile oil price is expected to increase which increase the attractiveness of hydrogen powered hybrid fuel cell propulsion systems.

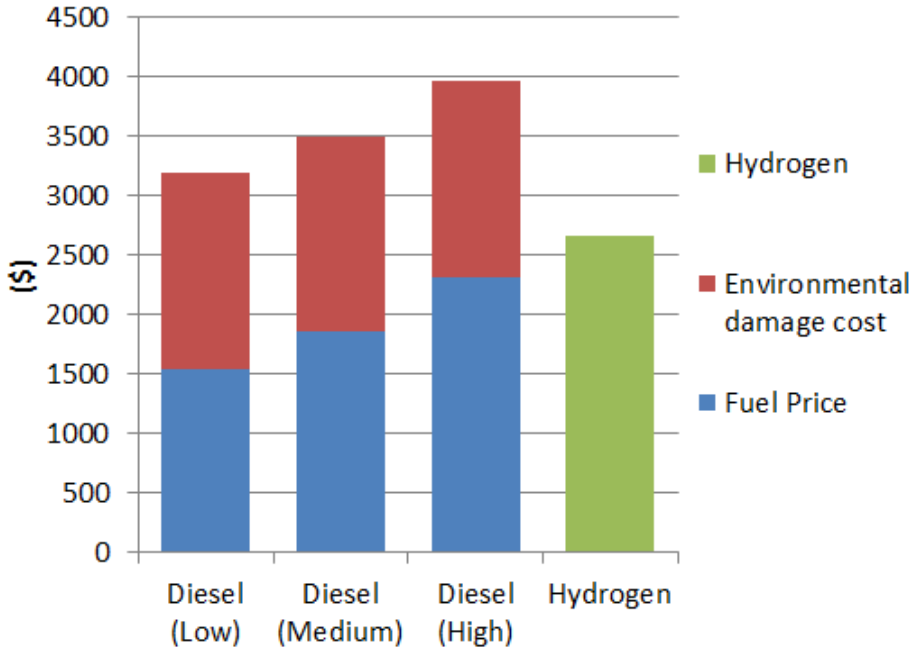

Figure 5.20: Mid term hydrogen fuel cost compared to low, medium, and high MDO cost for the examined voyage

5.4.3 Stress analysis

Operational stresses on the fuel cell and battery systems play a key role in the durability and lifetime of the hybrid propulsion system. The used strategy to manage the power split between the fuel cell and battery systems has a great effect on these stresses. Therefore, a stress analysis is performed for the optimal fuel cell/battery combination of 163 fuel cell and 3 battery blocks using different strategies for three cases of starting with high, normal, and low initial battery SOC of 85%, 70%, and 35% respectively. The instantaneous power from the fuel cell and battery systems during the examined voyage are decomposed into low frequency and high frequency components using Haar wavelet transform as suggested in [17]. Then, the standard deviation of the high frequency component is calculated to have a good indication of the stresses on the fuel cell and battery for the examined voyage. The time required to recharge the battery back to its initial battery SOC is not included because batteries are recharged at constant rate which affects the stress results using the adopted approach. Also, the time required to recharge the battery back to its initial battery SOC is already taken into consideration in the replacement and maintenance cost of the hybrid system as discussed earlier.

As listed in Table 5.11, the operational stress on the fuel cell system doesn't change considerably since it provides the average required power during the voyage. Regarding the operational stress on the battery system, it becomes higher in case of starting with high initial battery SOC. This can be justified by the fact that, at higher initial battery SOC, more energy is available in the battery system to be used which increases the

battery stress. At high and normal initial battery SOC of 85% and 70%, state-based EMS has the lowest fuel cell and battery operational stresses. Also, CDCS strategy results in the highest battery stress because it prioritize the battery power usage. However, at low initial battery SOC of 35%, CDCS strategy has the lowest battery stress because it maintains the battery SOC around its reference value of 30% which is close to the low initial battery SOC. Meanwhile, other strategies have approximately the same fuel cell and battery stresses because it tends to recharge the battery to increase its SOC which increases the battery stress compared to the CDCS strategy.

Table 5.11: Fuel cell and battery systems operational stresses indicator using different strategies at initial battery SOC of 85% and 35%

Initial battery SOC	85%		70%		35%	
	Fuel cell	Battery	Fuel cell	Battery	Fuel cell	Battery
State-based	5236	599	5243	579	5273	516
Classical PI	5342	825	5355	684	5274	516
ECMS	5342	885	5374	768	5281	517
CDCS	5298	1110	5330	975	5322	450

5.4.4 Power distribution using different EMS

In order to have a closer look on how each EMS splits the required load power between the fuel cell and the battery systems, the optimal fuel cell/battery combination of 163 fuel cell and 3 battery blocks is used to power the ship using different strategies for the examined voyage. The hybrid fuel cell/battery system is used to power the ship during the voyage. Then, the fuel cell system is used to charge the battery system back to its initial SOC in order to have fair comparison between different strategies. Consequently, the simulation time is not the same for different strategies. A high initial battery SOC as well as a low initial battery SOC are used to further investigate each strategy performance.

5.4.4.1 Results at high initial battery SOC of 85%

At high initial battery SOC of 85%, the state-based strategy tends to discharge the battery system as shown in Figure 5.21 in order to reach a normal battery SOC while the fuel cell system supplies the average required power. By adopting the classical PI strategy, whose main objective is to maintain the battery SOC at its reference value of 60%, more energy is depleted from the battery system until it reaches 60% then it maintains this value during the voyage as can be seen in Figure 5.22. Because the classical PI strategy depletes more energy from the battery system, it requires more time to recharge the battery back to its initial SOC and it consumes more hydrogen as indicated in Figure 5.25.

Using ECMS which transforms the battery electrical energy consumption into an equivalent hydrogen consumption, more battery power is used during the voyage and a battery SOC of around 55% is realised which increases its simulation time as shown in Figure 5.23. CDCS strategy prioritizes the battery system power usage until battery SOC reaches its threshold value of 30% as shown in Figure 5.24. As a result, CDCS has the lowest hydrogen consumption as illustrated in Figure 5.25 but it requires more time to charge the battery back to its initial SOC. As can be seen in Figure 5.25, the variance in hydrogen fuel consumption caused by using different EMS does not exceed 1% because of taking the required energy to recharge the battery system back to its initial SOC into consideration in addition to the nature of the ship operational profile which does not vary significantly.

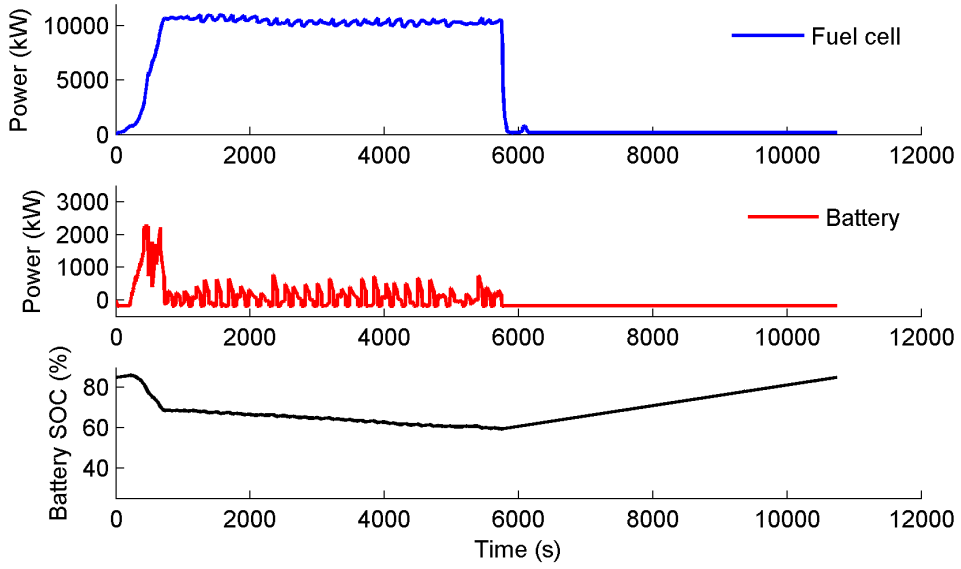

Figure 5.21: Fuel cell and battery powers and SOC using state-based strategy for a battery initial SOC of 85%

5.4.4.2 Results at low initial battery SOC of 35%

At low initial battery SOC of 35%, simulation time of different strategies is lower than the simulation time in case of high initial battery SOC because less energy and time is required to recharge the battery back to its initial SOC. For the same examined voyage, the state-based, classical PI, and ECMS strategies tend to charge the battery system to increase its SOC after the acceleration phase of the voyage as shown in Figures 5.26 to 5.28. Therefore, their hydrogen consumption are very similar to each other as shown in Figure 5.30. Meanwhile, CDCS strategy maintains the SOC around its threshold value of 30% during the voyage and the fuel cell system supplies more power which is why more hydrogen is consumed using CDCS strategy as shown in Figure 5.30.

The hydrogen fuel consumption difference resulting from using different strategies is still below 1% for the examined voyage as shown in Figure 5.30. Also, by comparing

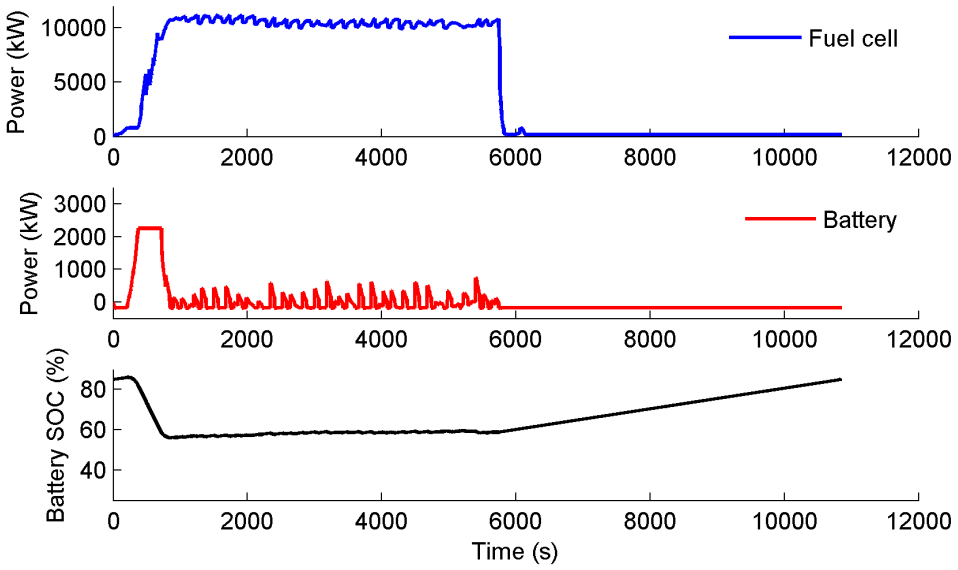

Figure 5.22: Fuel cell and battery powers and SOC using classical PI strategy for a battery initial SOC of 85%

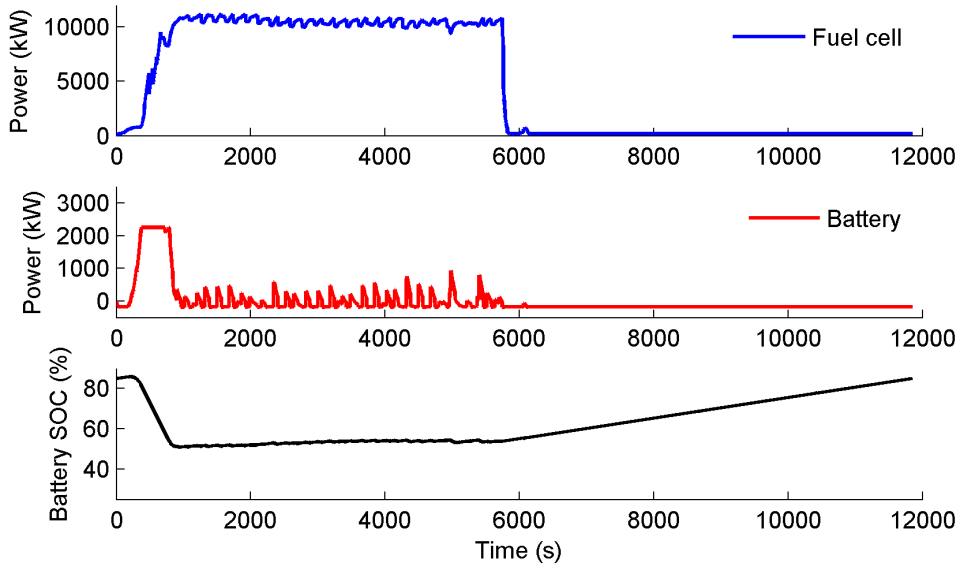

Figure 5.23: Fuel cell and battery powers and SOC using ECMS strategy for a battery initial SOC of 85%

Figure 5.25 to Figure 5.30, more hydrogen is consumed by different strategies because less battery energy is available while starting with low initial battery SOC.

5.4.5 Sensitivity analysis of different initial battery SOC

Different values of initial battery SOC have been used for different strategies to show its effect on the hydrogen consumption and total consumed energy of the fuel cell and battery systems for the examined voyage. Figure 5.31 summarises the total hydrogen consumption of the ship during the examined voyage using different strategies at different

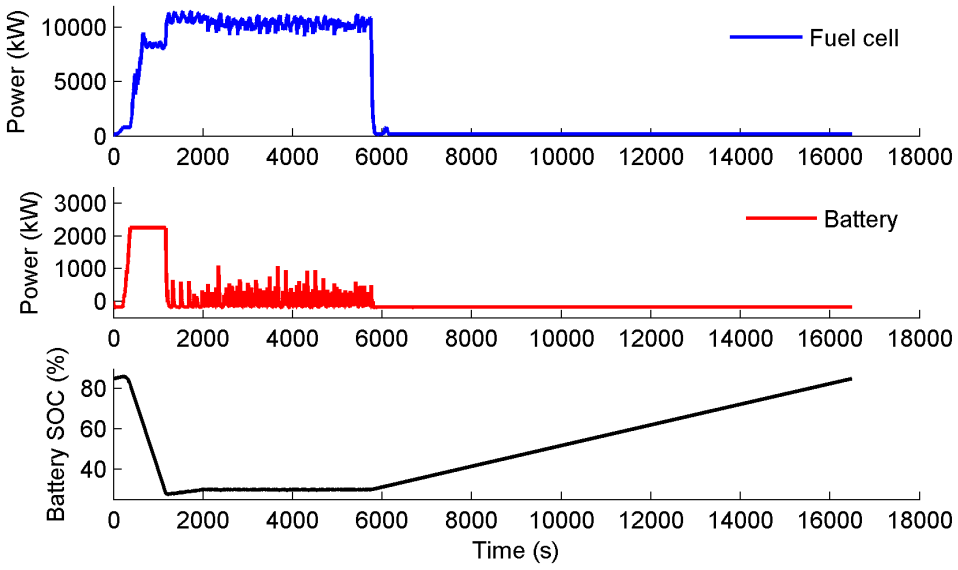

Figure 5.24: Fuel cell and battery powers and SOC using CDCS strategy for a battery initial SOC of 85%

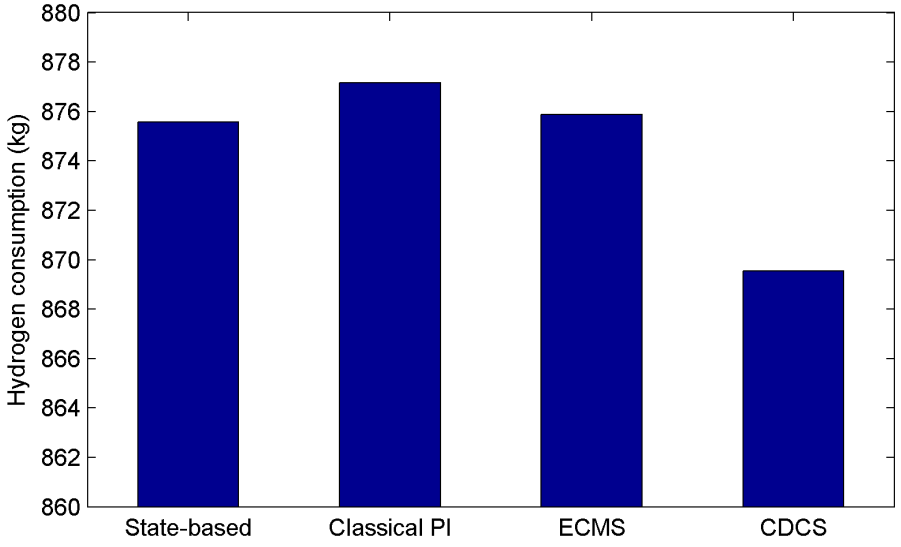

Figure 5.25: Hydrogen consumption using different strategies for a battery initial SOC of 85%

initial battery SOC. Due to prioritizing battery energy, CDCS strategy has the lowest fuel consumption starting with high and normal initial battery SOC. However, by starting with low initial battery SOC of 40% or less, CDCS tends to use more power from the fuel cell system to maintain the battery SOC at its threshold value of 30%. Therefore, CDCS strategy consumes more fuel than other strategies in case of starting with low initial SOC. Also, the fuel consumption of the state-based, classical PI, and ECMS strategies in case of starting with low initial battery SOC are approximately the same because they all tend to recharge the battery. Meanwhile, differences between the fuel consumption using theses strategies are higher in case of starting with high

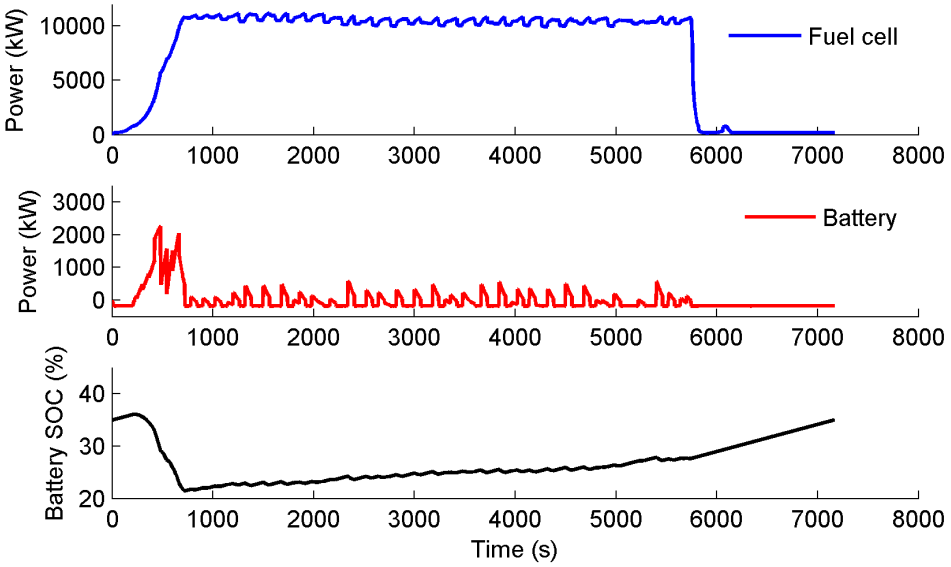

Figure 5.26: Fuel cell and battery powers and SOC using state-based strategy for a battery initial SOC of 35%

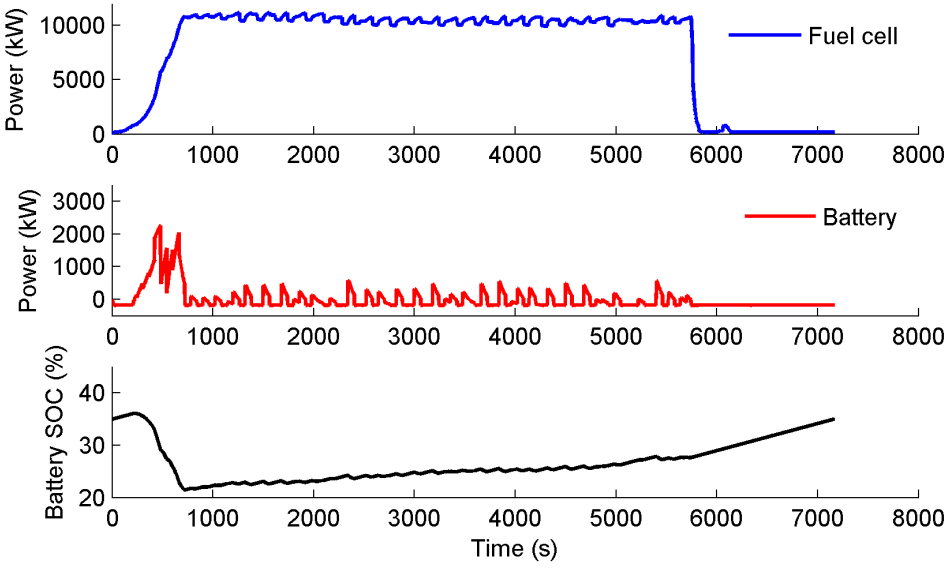

Figure 5.27: Fuel cell and battery powers and SOC using classical PI strategy for a battery initial SOC of 35%

initial battery SOC. This is justified by the fact that, in case of starting with low initial battery SOC, these strategies have the same goal of increasing the battery SOC. On the other hand, by starting with high initial battery SOC, each strategy has a different battery SOC target (i.e. 60% for the classical PI strategy). Moreover, the difference between the highest and lowest hydrogen consumption using different strategies is below 1% regardless of the initial battery SOC.

The difference between the highest and lowest total consumed energy of the hybrid fuel cell/battery system is also below 1% regardless of the initial battery SOC as shown in Figure 5.32. This difference is higher in case of starting with high initial battery

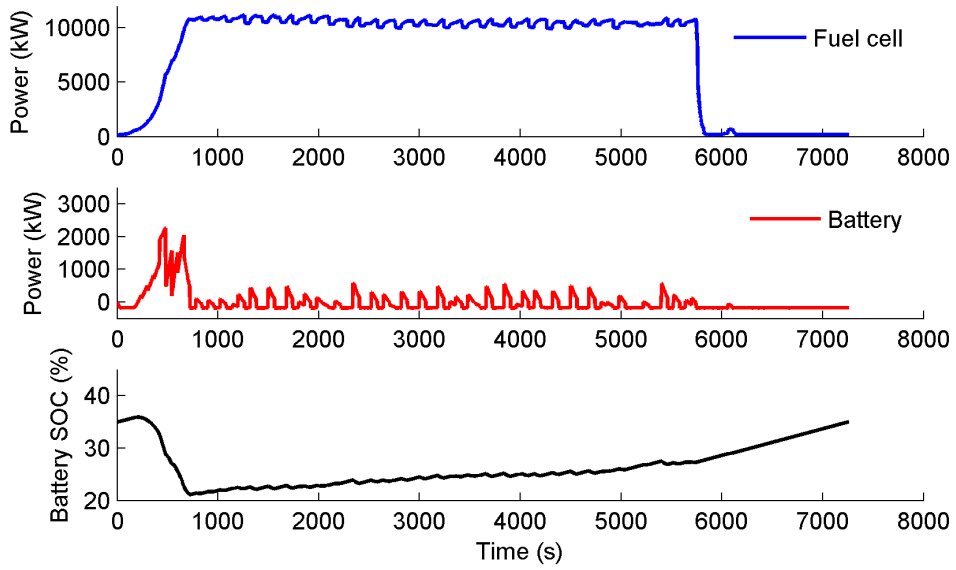

Figure 5.28: Fuel cell and battery powers and SOC using ECMS strategy for a battery initial SOC of 35%

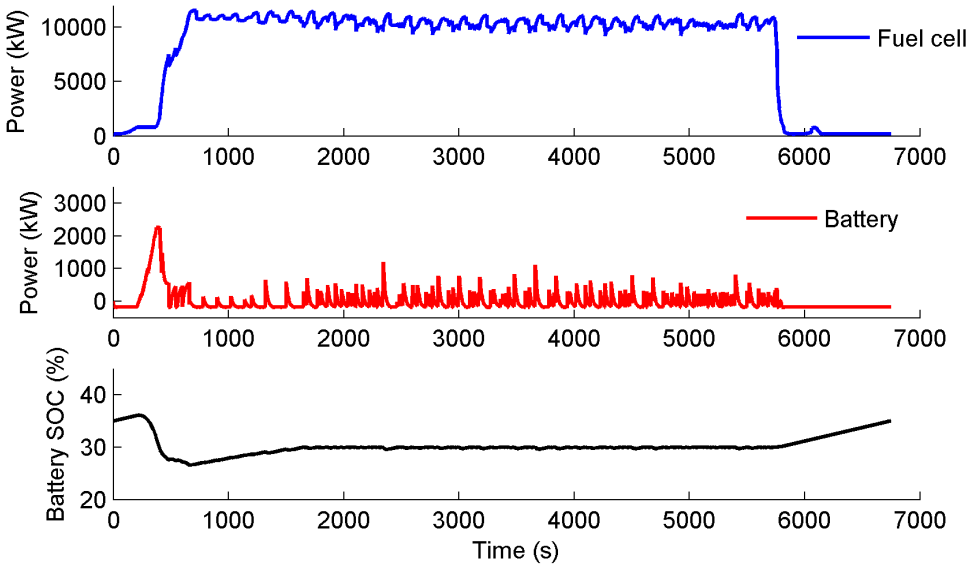

Figure 5.29: Fuel cell and battery powers and SOC using CDCS strategy for a battery initial SOC of 35%

SOC since each strategy uses the battery available power in different ways. Meanwhile, the total energy consumption is quite similar if the battery system starts with low initial battery SOC because different strategies tend to recharge the battery in the case of starting with low initial battery SOC. Furthermore, at high initial battery SOC, state-based strategy has lower energy consumption than CDCS strategy, although CDCS strategy results in less fuel consumption at higher initial battery SOC as shown in Figure 5.31. This is because the total consumed energy shown in Figure 5.32 includes the consumed energy from the fuel cell and battery systems. Meanwhile, hydrogen consumption shown in Figure 5.31 gives indication about the consumed energy from

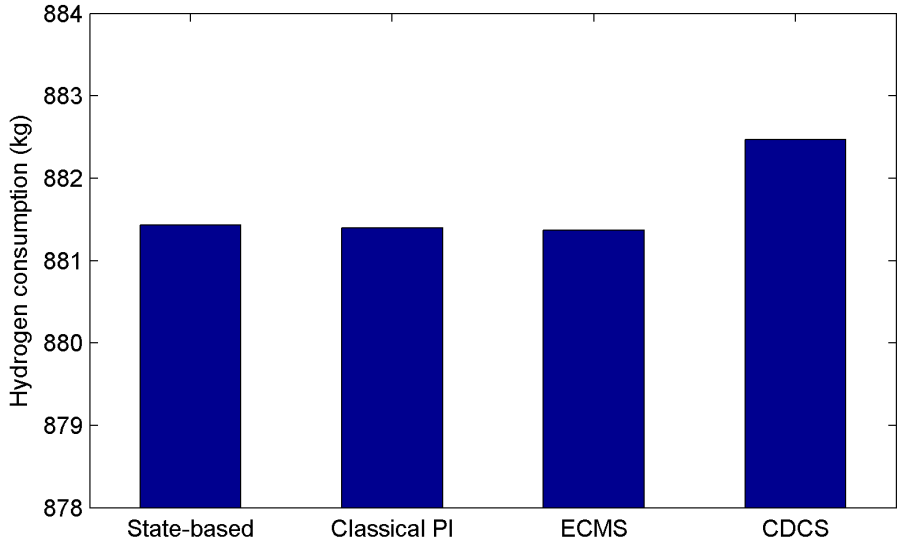

Figure 5.30: Hydrogen consumption using different strategies for a battery initial SOC of 35%

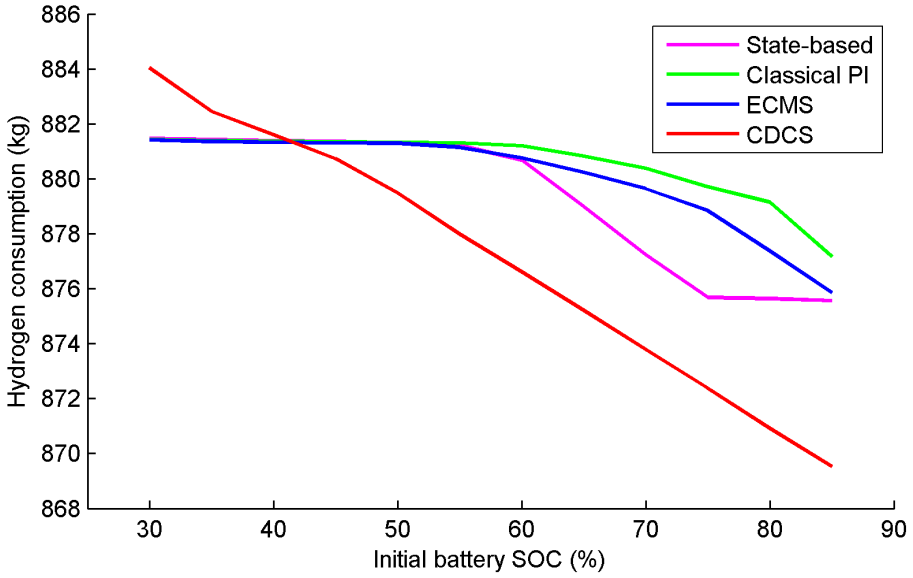

Figure 5.31: Hydrogen consumption using different strategies at different battery initial SOC

only the fuel cell system.

The small differences in the consumed hydrogen and energy using different strategies are owing to the small variation in the ship operational speed and consumed power during its voyage in addition to taking the battery recharging energy into consideration. In order to identify the effect of taking the battery recharging into consideration on the consumed hydrogen and energy, the sensitivity analysis of different initial battery SOC is repeated without considering the consumed hydrogen and energy to recharge the battery back to its initial SOC as shown in Figures 5.33 and 5.34.

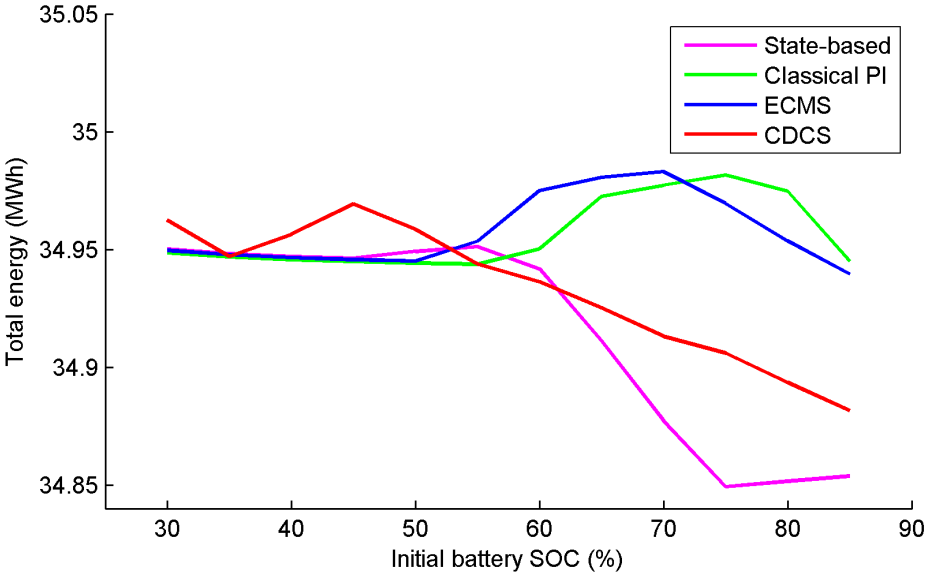

Figure 5.32: Total consumed energy using different strategies at different battery initial SOC

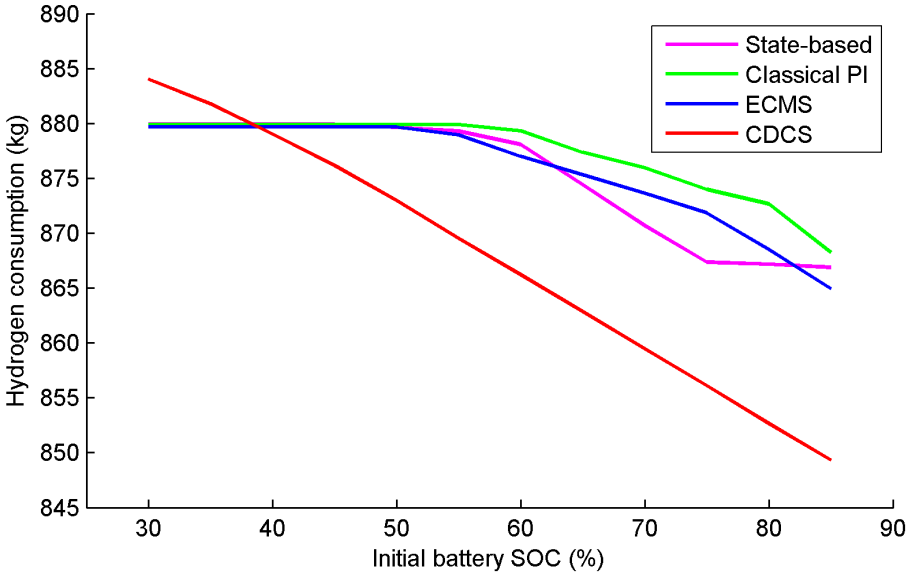

Figure 5.33: Hydrogen consumption using different strategies at different battery initial SOC without taking battery recharging into consideration

Without taking the required hydrogen and energy of battery recharging into consideration, CDCS strategy still has the lowest hydrogen consumption but the saving percentage between different strategies in terms of hydrogen consumption increases from 0.88% to 2.23% at an initial battery SOC of 85% as for example as shown in Figure 5.33. Regarding the total energy consumption, CDCS strategy tends to have the lowest energy consumption as shown in Figure 5.34 in case of not taking the battery recharging energy into consideration and the saving percentage between different strategies also increases from 0.3% to 1.5% at an initial battery SOC of 85%. The saving percentages of hydrogen and energy consumption increase as a result of not taking the battery

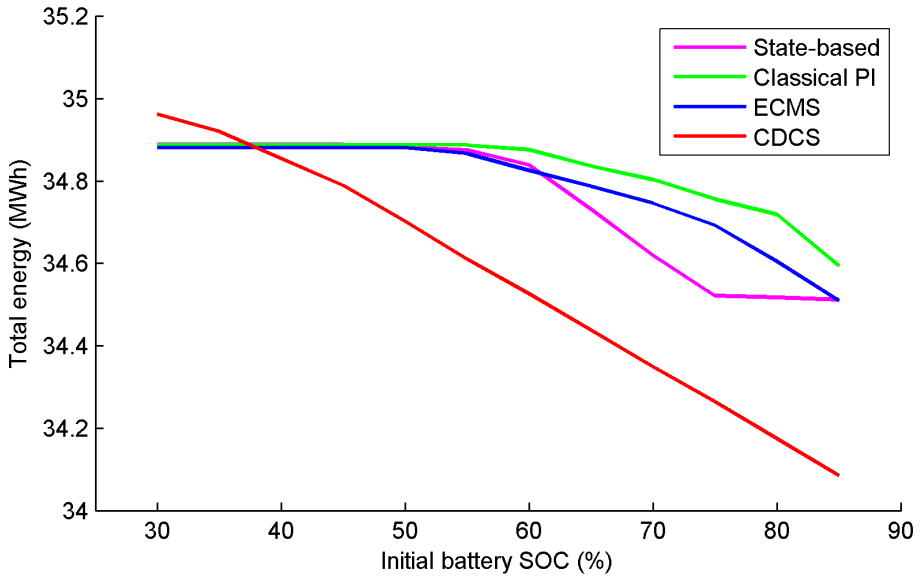

Figure 5.34: Total consumed energy using different strategies at different battery initial SOC without taking battery recharging into consideration

recharging time into consideration which includes the electrical losses resulting from the fuel cell converter while recharging the batteries. To investigate the effect of the examined ship operational profile on the energy and hydrogen consumption using different strategies, two sensitivity studies are performed using different ship operational profiles in the next section.

5.4.6 Results using different ship operational profile

The examined ship *M/S Smyril* sails between the capital Tórshavn to the southernmost island Suduroy at an approximately constant speed of 20 kn. The proposed hybrid fuel cell/battery propulsion system has been studied using four different EMS to manage the power distribution for the examined voyage. However, the results show that the consumed hydrogen and total energy are approximately the same using different strategies regardless of the battery initial SOC. These results could be attributed to the examined ship operational profile which does not have significant variation in power requirements as shown in Figure 5.4. Therefore, different ship operational profiles are assumed and studied in order to determine the effect of the studied ship operational profile on the simulation results.

5.4.6.1 Slow steaming operation

The first assumed ship operational profile will be dominated by two speeds of 10 and 20 kn as shown in Figure 5.35 in contrast to the real operational profile of the examined ship which has one main speed of 20 kn as shown in Figures 4.45, 4.48 and 4.50. It is

assumed that the ship reduces its speed because of running in a slow steaming mode to reduce its fuel consumption. Then, the proposed hybrid fuel cell/battery system is used to perform the assumed operational profile employing the four studied EMS to manage the required power split. The calculated hydrogen and energy consumption also include the hydrogen and energy consumption used to recharge the battery back to its initial battery SOC for the purpose of comparing different strategies fairly. Moreover, different initial battery SOC are used for the assumed operational profile case study in order to study its effect on the simulation results.

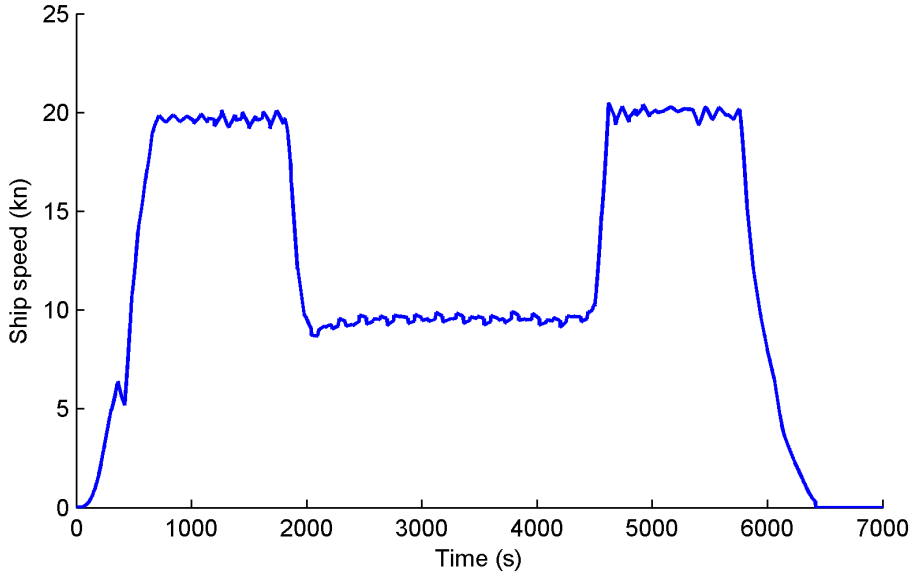

Figure 5.35: Ship speed of the assumed operational profile

It can be noted that the results in Figures 5.36 and 5.37 for the assumed operational profile are generally similar to those in Figures 5.31 and 5.32 for the real ship operational profile using different strategies and starting with different initial battery SOC. However, comparing Figure 5.36 and Figure 5.37 of the assumed operational profile with Figure 5.31 and Figure 5.32 show that changing the used EMS has more effect in terms of the consumed fuel and energy for the assumed operational profile than the ship's real low varying operational profile. As for example, at high initial battery SOC of 85%, changing the used EMS from state-based strategy to CDCS strategy can result in a hydrogen fuel consumption saving of 1.24% in the case of the assumed operational profile. Meanwhile, only 0.88% fuel saving percentage can be achieved by changing the used EMS for the original ship operational profile starting with the same initial battery SOC as shown in Figure 5.25. This percentage becomes higher in case of not considering the hydrogen and energy required to recharge the battery back to its initial SOC as discussed earlier. These results indicate that changing the used EMS has more effect for ships with more varying operational profile due to the different handling of each EMS to the power requirement variation.

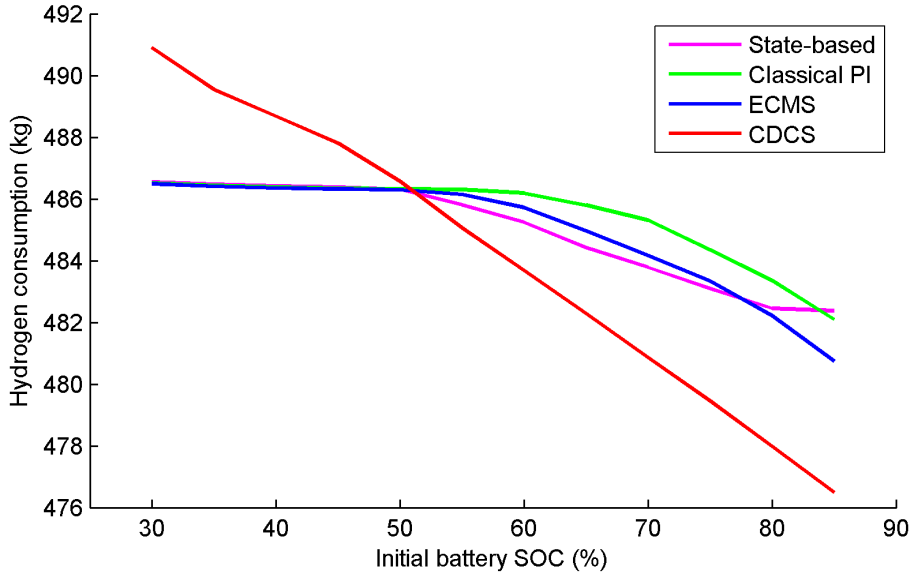

Figure 5.36: Hydrogen consumption using different strategies at different battery initial SOC for the assumed operational profile

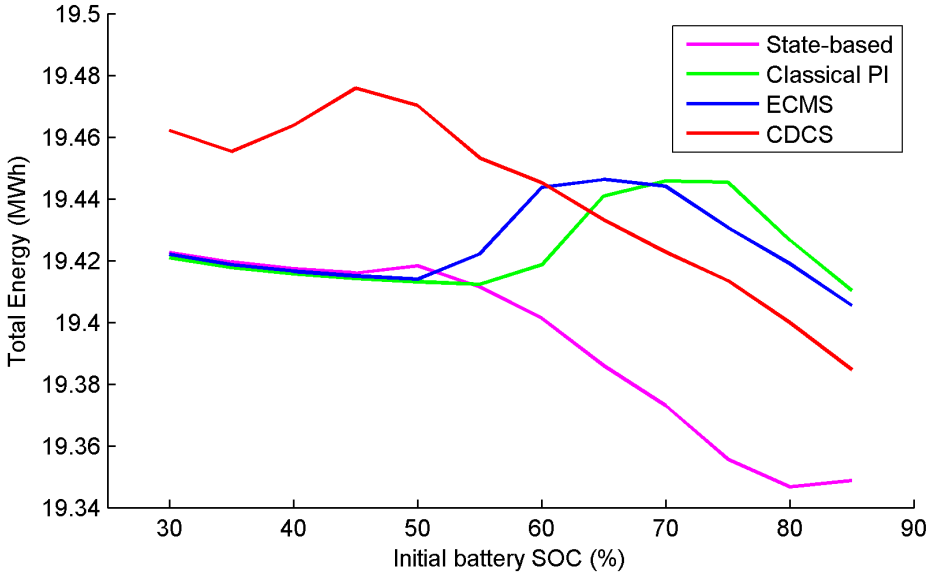

Figure 5.37: Total consumed energy using different strategies at different battery initial SOC for the assumed operational profile

5.4.6.2 Day & night operation

Another sensitivity study using a different ship operational profile with more variation is performed for the examined ship using the developed ship simulator. Figure 5.38 shows the typical ship speed of a similar ferry in the Baltic Sea between Stockholm (Sweden) and Mariehamn (The Åland Islands) for a Day & night ferry operation extracted from [327]. The voyage under study starts with departing from Stockholm port at 6 pm then the ship sails through Stockholm archipelago and Sea of Åland. By midnight, the ship stops in the Sea of Åland until 4 am and it starts to sail again for about 3 hours arriving at Mariehamn port at 7 am. Then, the ship stays at Mariehamn port for about 1 hour before sailing again to Stockholm port with a total cruise time of 22 hour.

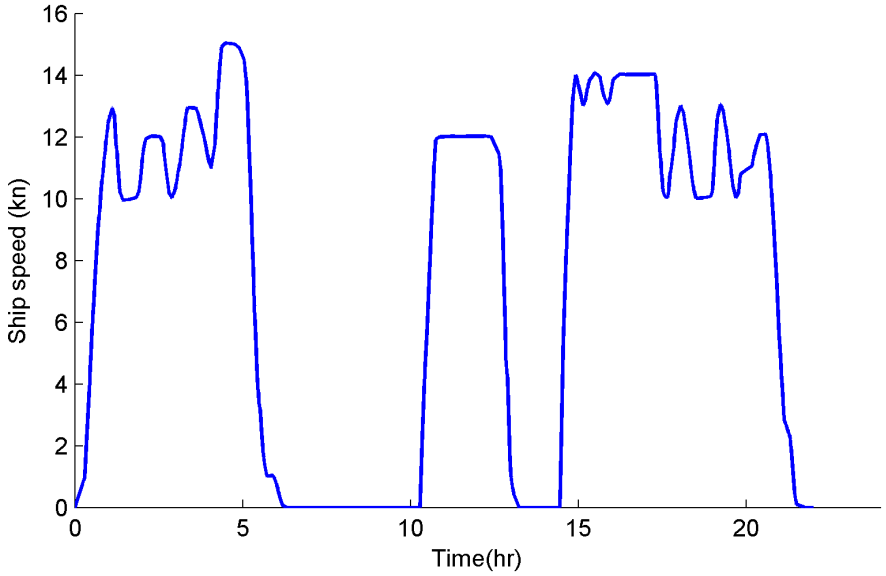

Figure 5.38: Typical ship speed in the Baltic Sea between Stockholm (Sweden) and Mariehamn (The Åland Islands)

The ship speed shown in Figure 5.38 is used as an input to the simulation of the proposed hybrid fuel cell/battery combination of the examined ship *M/S Smyril* in calm water condition with 1 DOF simulation using different EMS to further study the applicability and suitability of different energy management systems for ships with significant variation in speed and power requirements. Using the simulation parameters in Section 5.3 for different EMS, simulation results show that CDCS strategy results in lower energy and hydrogen consumption than other strategies. Moreover, by changing the used EMS from state-based to CDCS strategy, a hydrogen fuel consumption saving of 6% can be achieved as shown in Figure 5.39 at an initial battery SOC of 85% for the studied ship speed in Figure 5.38.

Because the battery initial SOC may affect the performance of the hybrid fuel cell system using different EMS, different values of the initial battery SOC are used. As shown in Figures 5.40 and 5.41, using CDCS strategy results in the lowest hydrogen and energy

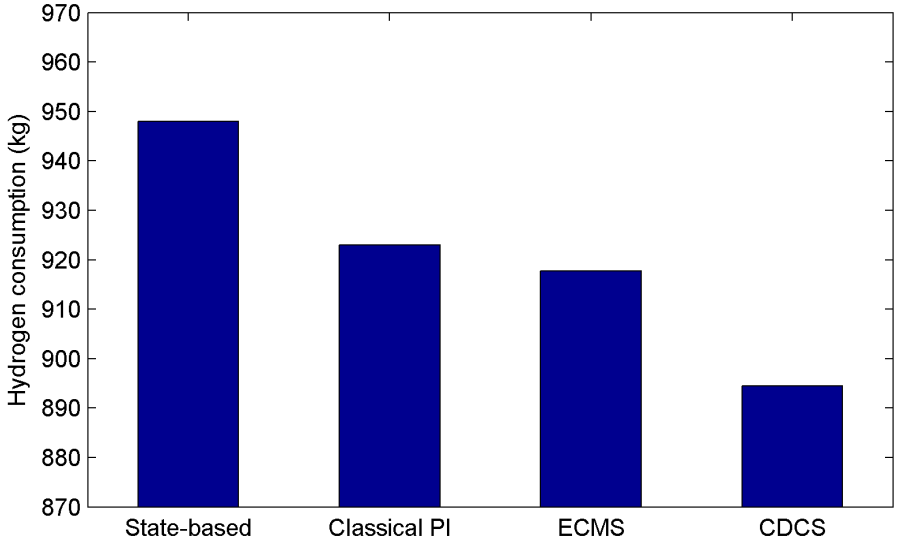

Figure 5.39: Hydrogen consumption using different strategies for the examined day & night operation in calm water at an initial battery SOC of 85%

consumptions for the examined ship speed profile starting with different initial battery SOC. It can be also noted that the hydrogen and energy consumptions increase when starting with lower initial battery SOC because of the less available battery energy. The hydrogen consumption saving percentage of using CDCS strategy compared to the state-based strategy varies between 6% and 4.5% as shown in Figure 5.40. Also, the energy consumption saving percentage of using CDCS strategy compared to the state-based strategy varies between 2.8% and 2.4% according to the initial battery SOC as shown in Figure 5.41. These results are in line with the previous studies showing that changing the used EMS has more effect for ships with more variation in the required power and speed.

In addition to the initial battery SOC, the weather condition is also investigated as a parameter that can affect the results. Two weather profiles are assumed as shown in Figure 5.42 representing the average weather in summer when wind speed changes between 4.5 and 5.4 m/s and winter when wind speed changes between 6.4 and 9.2 m/s [328]. The assumed weather profiles are used to calculate the added resistance due to wind and waves using Townsin and Kwon method with a time step of 2 hours. Then, the calculated added resistance is applied to the ship while performing the same examined voyage in Figure 5.38 using different strategies of energy management and starting with different initial battery SOC as well.

Simulation results of the examined voyage after taking into consideration the added resistance due to wind and waves show that CDCS strategy still results in the lowest hydrogen and energy consumption at different initial battery SOC. Meanwhile, state-based EMS results in the highest hydrogen and energy consumption as shown in Figures 5.43 to 5.46. The difference in hydrogen consumption by using the CDCS

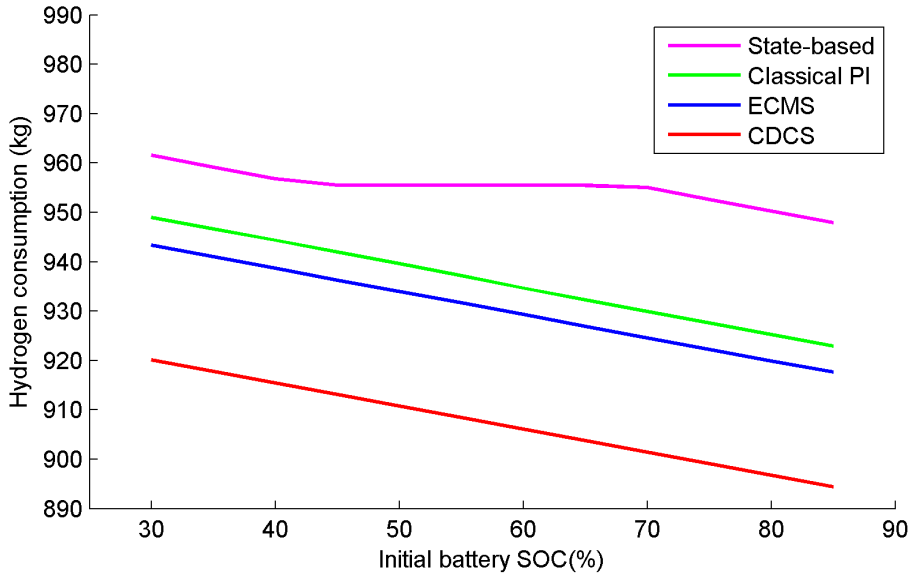

Figure 5.40: Hydrogen consumption using different strategies for the examined day & night operation in calm water at different initial battery SOC

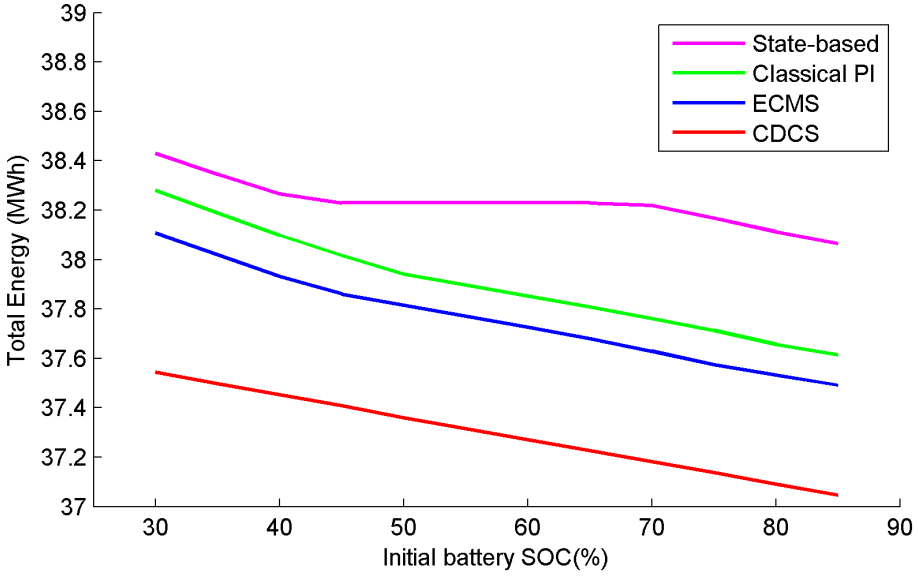

Figure 5.41: Total consumed energy using different strategies for the examined day & night operation in calm water at different initial battery SOC

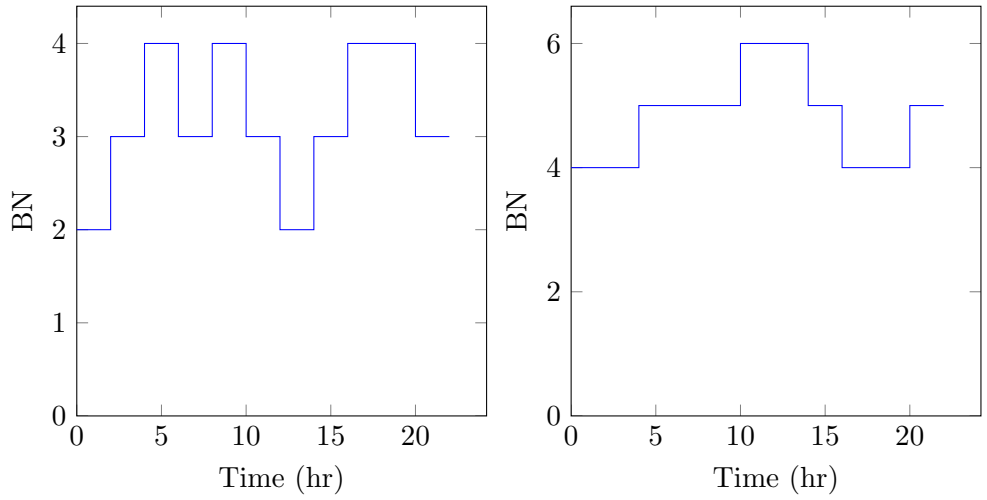

(a) Summer wind speed (b) Winter wind speed

Figure 5.42: Assumed Beaufort Number profiles for the examined Baltic Sea voyage

strategy compared to the state-based strategy varies between 5.7% and 2.9% as shown in Figures 5.43 and 5.45. Moreover, The difference in energy consumption using CDCS strategy compared to the state-based strategy varies between 2.6% and 1.7% depending on the initial battery SOC and weather condition as shown in Figures 5.44 and 5.46. It can be also observed that hydrogen and energy consumptions using the average summer wind speed in Figures 5.43 and 5.44 are lower than the hydrogen and energy consumptions using the average winter wind speed in Figures 5.45 and 5.46 as expected due to the increase in the added resistance.

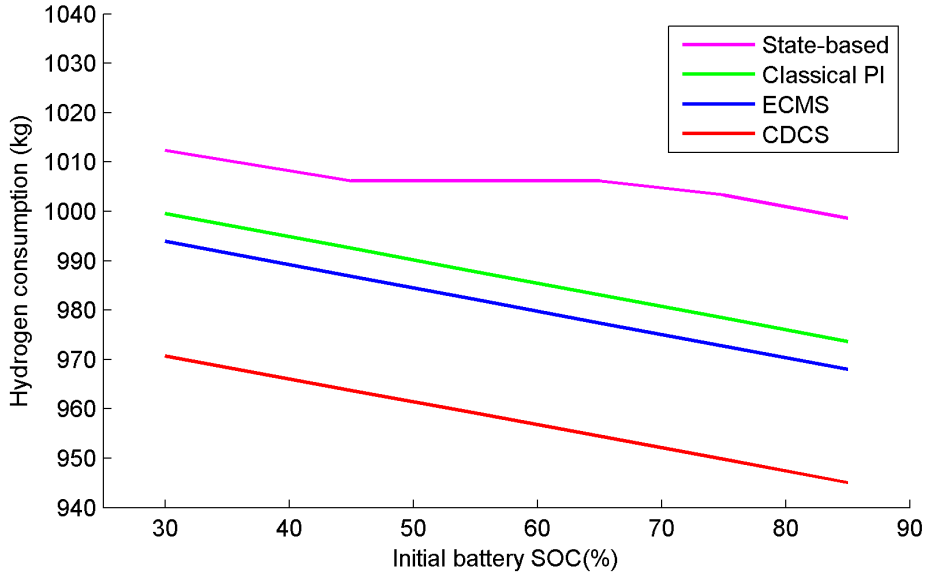

Figure 5.43: Hydrogen consumption using different strategies for the examined day & night operation assuming summer operation at different initial battery SOC

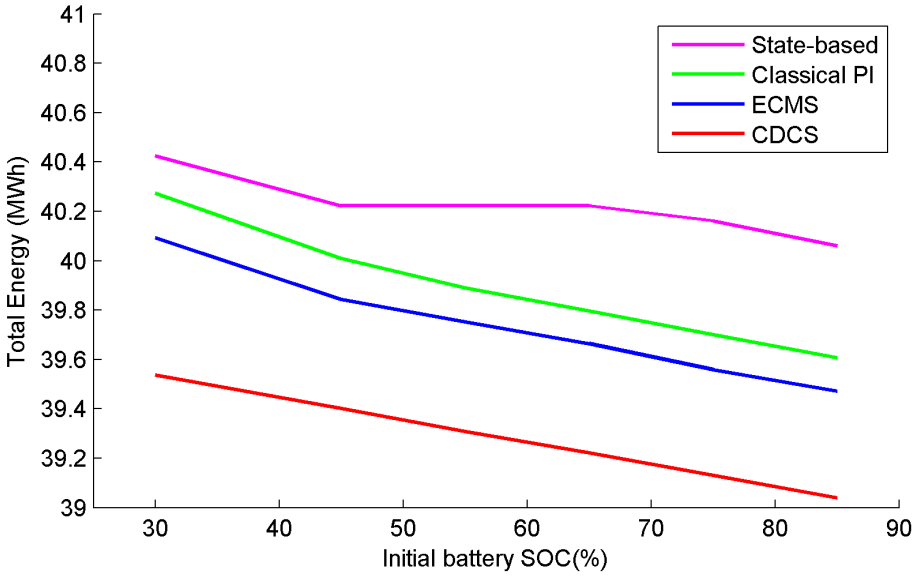

Figure 5.44: Total consumed energy using different strategies for the examined day & night operation assuming summer operation at different initial battery SOC

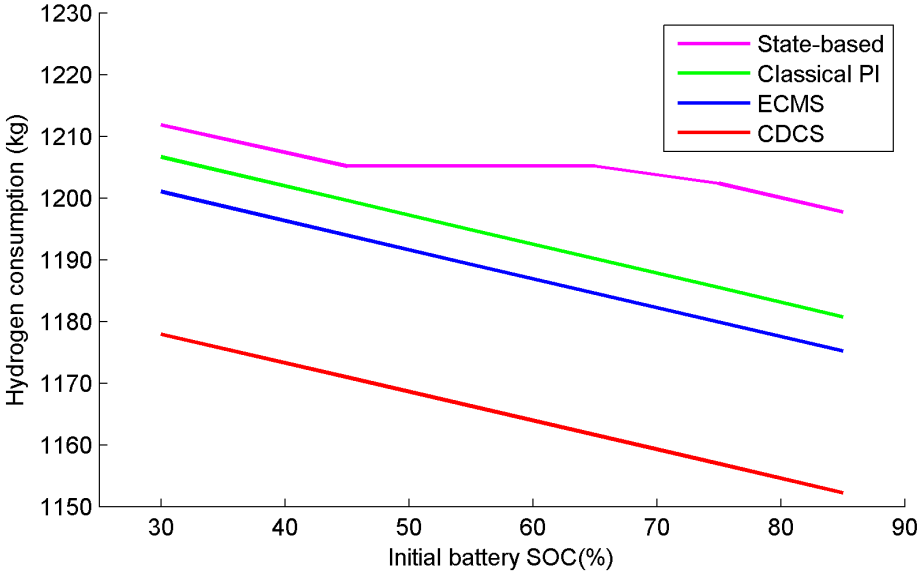

Figure 5.45: Hydrogen consumption using different strategies for the examined day & night operation assuming winter operation at different initial battery SOC

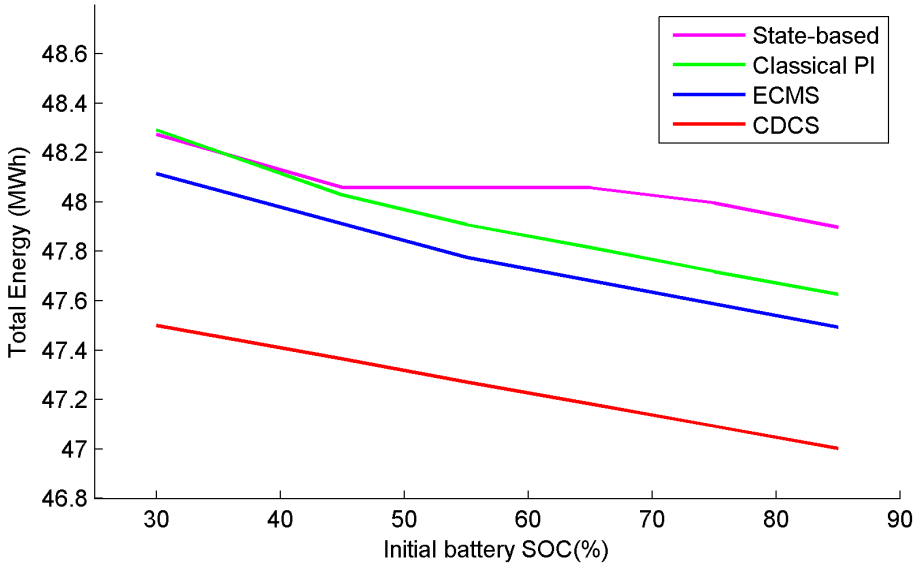

Figure 5.46: Total consumed energy using different strategies for the examined day & night operation assuming winter operation at different initial battery SOC

As explained earlier, CDCS strategy results in the lowest hydrogen consumption due to its prioritizing of the battery energy. Therefore, the investigated parameters in this study include the battery minimum SOC or the SOC threshold. Two more minimum values of the battery SOC of 35% and 40% are used and simulation results are compared with the simulation results of using a minimum battery SOC of 30% which has been used so far for different cases. This change affects the ECMS and CDCS strategies because they split the required power between the fuel cell and battery systems as a function of the minimum battery SOC. Meanwhile, the classical PI and state-based strategies are not affected by changing the minimum battery SOC because they have different battery SOC targets (i.e. 60% for the classical PI strategy) as discussed in Chapter 3. For calm water condition and at an initial battery SOC of 85%, simulation results of the examined voyage show that hydrogen and energy consumptions of the ECMS and CDCS strategies increase by increasing the minimum value of the battery SOC as shown in Figures 5.47 and 5.48. This can be justified by the fact that increasing the battery SOC threshold value will reduce the available battery energy which increases the used fuel cell energy and hydrogen consumption. Therefore, the hydrogen consumption difference between CDCS and state-based strategies falls from 6% using minimum battery SOC of 30% to 5.4% and 4.9% using minimum battery SOC of 35% and 40% respectively as shown in Figure 5.47. The energy consumption difference between CDCS and state-based strategies also decreases from 2.8% using minimum battery SOC of 30% to 2.5% and 2.3% using minimum battery SOC of 35% and 40% respectively as shown in Figure 5.48.

The sensitivity study also includes the investigation of the battery C-rate as a parameter that can affect the performance of the hybrid system using different strategies of energy management. Battery C-rate is a measure of the battery charging or discharging rate

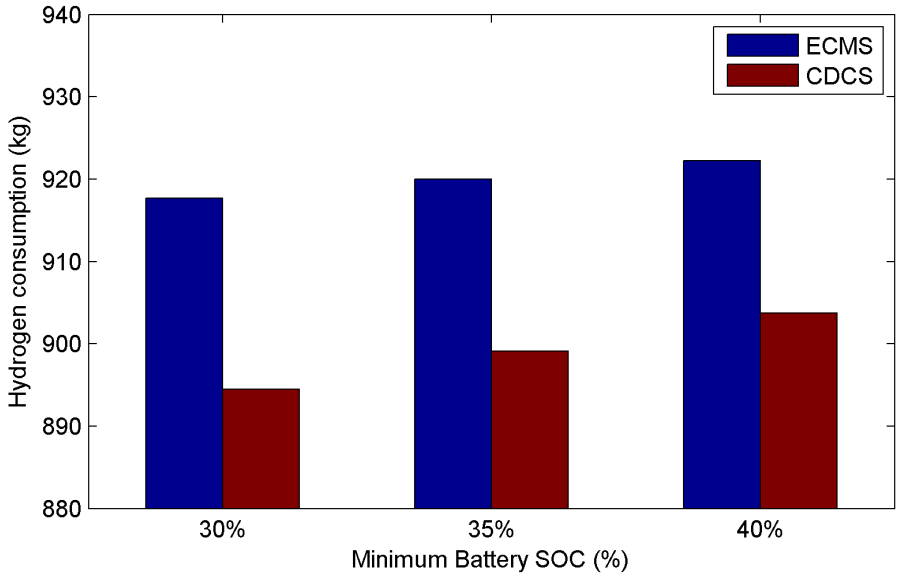

Figure 5.47: Hydrogen consumption of the ECMS and CDCS strategies for the examined day & night operation in calm water using different values of minimum battery SOC

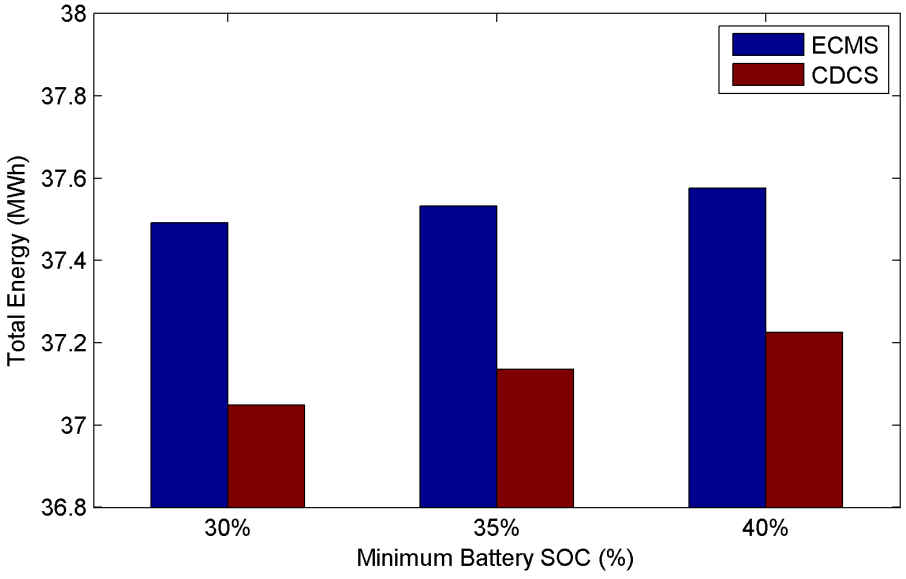

Figure 5.48: Total consumed energy of the ECMS and CDCS strategies for the examined day & night operation in calm water using different values of minimum battery SOC

relative to its maximum capacity and it affects the battery time of charge or discharge. The standard C-rate of the used battery system is 0.2C as listed in Table 5.3 according to its manufacturer. For the same examined voyage at an initial battery SOC of 85% assuming calm water condition, using a lower battery C-rate of 0.1C for different strategies results in reducing the total consumed energy and hydrogen consumption by the hybrid system. Meanwhile, by increasing the battery C-rate to 0.3C, the hydrogen and energy consumptions increase using different strategies as shown in Figures 5.49 and 5.50. This is because the higher the battery C-rate, the quicker the battery charges or discharges which increases the number of consumed battery cycles and the electrical losses of the hybrid system during the examined voyage.

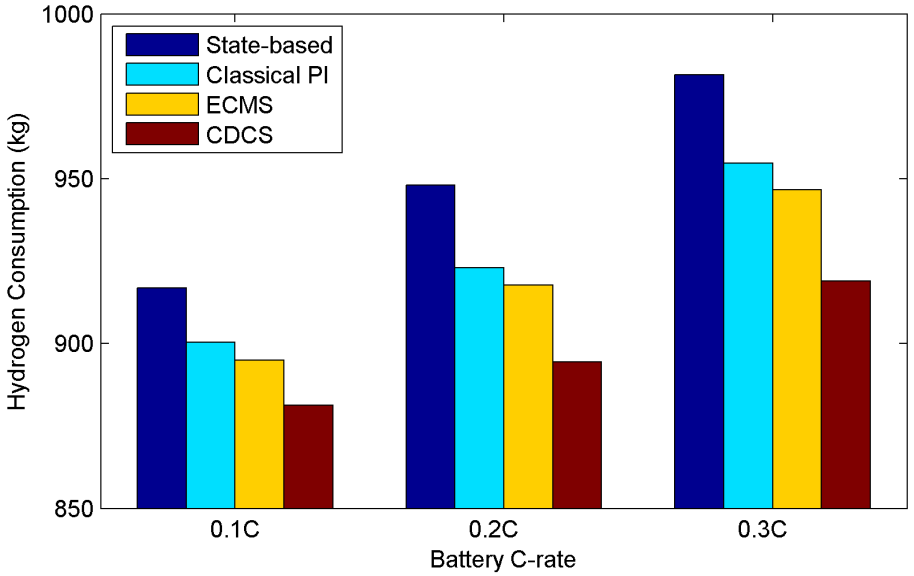

Figure 5.49: Hydrogen consumption using different strategies for the examined day & night operation in calm water using different battery C-rate

As shown in Figures 5.49 and 5.50, CDCS strategy still results in lower hydrogen and energy consumptions compared to other strategies using different battery C-rate. However, it should be noted that changing the used EMS is more effective at higher battery C-rate. The hydrogen consumption saving percentages of using CDCS strategy compared to the state-based strategy are 4%, 6% and 6.8% using battery C-rate of 0.1C, 0.2C, and 0.3C respectively. Also, the energy consumption saving percentages of using CDCS strategy compared to the state-based strategy are 1.9%, 2.8%, and 3.1% using battery C-rate of 0.1C, 0.2C, and 0.3C respectively. This can be justified by the fact that at higher battery C-rate, more instantaneous battery energy is available for different strategies to be used which increase its effect of reducing the hydrogen consumption.

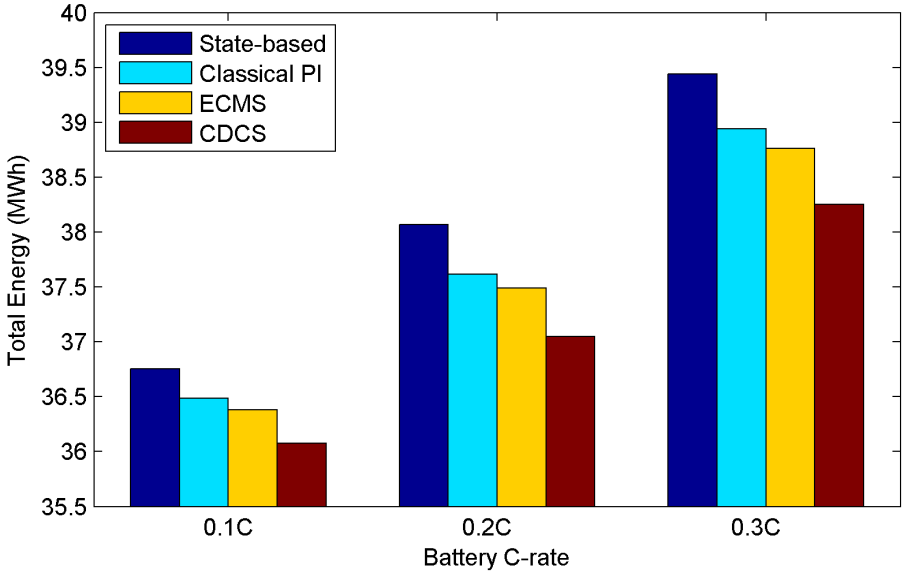

Figure 5.50: Total consumed energy using different strategies for the examined day & night operation in calm water using different battery C-rate

5.5 Summary

This chapter demonstrated the efficiency of the developed total ship simulator. It has been used to propose a hybrid fuel cell/battery propulsion system for the examined ferry *M/S Smyril*. In order to find the optimal fuel cell battery combination of the proposed hybrid system, a sizing optimization study has been performed which included the investigation of six different fuel cell sizes and five different battery sizes which have been modelled and used to power the ship using the developed simulator. For the studied fuel cell battery combinations, four different energy management strategies have been used for the ship required power splitting between the fuel cell and battery systems during the examined voyage which are: state-based, classical PI, ECMS, and CDCS strategies for the purpose of investigating the effect of changing the used EMS on the resulting optimal fuel cell battery combination. The objective of the sizing optimization study has been enhanced by taking the replacement and maintenance costs of the fuel cell and battery systems into consideration in addition to the hybrid system first cost and hydrogen consumption cost.

Results of the power source sizing study revealed that the used EMS affects the resulting optimal fuel cell battery combination for the same examined voyage where the optimal fuel cell battery combination was different for each EMS. However, the difference between the different optimal fuel cell battery combinations in terms of total costs was less than 1%. There are two reasons for this small difference in the total cost of different optimal fuel cell battery combinations which are taking the required energy to recharge the battery back to its initial battery SOC into consideration and the small variation in the ship operational speed and consumed power during the voyage. Simulation results

revealed also that the total cost of different fuel cell battery combinations is dominated by hydrogen fuel cost. Therefore, a sensitivity analysis was performed on the effect of hydrogen prices on the resulting fuel cell battery combination.

According to the objective of the sizing study of minimizing the hybrid system first and operational costs, the optimal fuel cell battery combination consists of 163 fuel cell blocks combined with 3 battery blocks. The resulted combination is considered optimal for the examined voyage and sub-optimal for the ferry since a single real voyage is used in this study. Since the available operational dataset of the examined ship covers less than two months of operation, a representative driving cycle could not be generated. However, the ferry operates with constant propeller and engine speeds which reduces the risk of sub-optimization. Also, the optimal fuel cell battery combination uses the same gearboxes and propellers of the conventional diesel propulsion system in order to keep changes to a minimum. Comparing this combination with the conventional diesel engines of the examined ship showed that weight and size savings of 7.3% and 18.6% can be achieved by using the hybrid fuel cell battery system instead of the ship conventional system. However, the first cost of the hybrid system is higher than the conventional diesel system by 81%. The maintenance cost of the fuel cell system is lower than diesel engines maintenance cost. However, by taking the maintenance cost of the batteries and electrical motors into consideration, maintenance cost of the diesel engines become lower. Moreover, hydrogen fuel cost is higher than marine diesel oil which increases the operational cost of the ship. A sensitivity analysis of hydrogen and MDO prices on the mid and long term projections reported that hydrogen would be cheaper and more attractive than MDO especially by taking the environmental damage caused from using oil into consideration. Also, using hydrogen as a fuel results in zero pollutant emissions which was compared with over 10 tonnes of emissions using the conventional diesel propulsion system. Furthermore, noise levels are reduced from about 105 dB(A) using diesel engines to about a level of 65 dB(A) using fuel cells which helps in saving more weight and increasing the luxury level of the ship.

For the same optimal fuel cell battery combination, a detailed insight into the power split manner between the fuel cell and battery systems using different energy management strategies was provided using the developed ship simulator. The power distribution between the hybrid system components using different EMS has been explained and the effect of different initial battery SOC has been also studied in terms of hydrogen and energy consumption and operational stresses on the fuel cell and battery systems. Simulation results of the examined voyage around Faroe Islands showed that using CDCS strategy has the lowest hydrogen consumption meanwhile state-based strategy has the lowest total energy consumption and results in the lowest fuel cell and battery operational stresses for the examined voyage starting with normal battery SOC of 70%. However, the difference between different EMS in terms of hydrogen and total energy consumption was small regardless of the initial battery SOC. Consequently, two

sensitivity analyses on the effect of the ship operational profile were performed using the optimal fuel cell/battery combination. An assumed ship operational profile which contained more variation in the ship speed and power assuming slow steaming operation was used as an input to the simulation of the optimal fuel cell/battery combination using different EMS. Although the ship speed changed between 20 kn and 10 kn for the assumed slow steaming operation case, the difference in terms of hydrogen consumpion using different strategies was still low at a level of 1.24% compared to 0.88% for the original operational profile.

Another real ship speed profile of a day & night ferry around Baltic Sea was used in a sensitivity study to further study the effect of changing the used strategy of energy management for ships with more variation in power requirements. The sensitivity study included the investigation of the weather condition effect, the battery initial SOC, the battery threshold value, and battery C-rate for different strategies. Results revealed that changing the used EMS has more effect in terms of hydrogen and energy consumption for ships with operational profiles that have significant variations in its speed and power requirements. The hydrogen consumption saving resulted from changing the used energy management strategy for the examined day & night ferry operational profile ranged between 6.8% and 2.9% depending on the operational battery parameters and weather condition. The variation of the used simulation parameters were presented for clarification purposes. In order to appropriately discuss the effect of the ship operational profile speed and power variations, another passenger ship with real operational profile that has more fluctuations is studied in the next chapter using the ship simulator.

Chapter 6

Comparative Study and Development of Energy Management Strategies

6.1 Introduction:

In the previous chapter it was concluded that changing the used energy management strategy does not have considerable effect on the consumed fuel and energy for ships with negligible fluctuations in the speed and power requirements. In this chapter, the world's first hydrogen fuel cell passenger ship *FCS Alsterwasser* is studied using the developed ship simulator. *FCS Alsterwasser* operates around Hamburg, Germany on Lake Alster, HafenCity, the River Elbe and the inner city waterways for round and charter trips which is why its operational profile has significant speed and power fluctuation. The typical ship power requirement, which has been made publicly available, is used as an input to the simulations of different energy management strategies in order to compare between them and study the effect of changing the used strategies on the consumed fuel and energy consumption of the examined ship. Different strategies are compared to each other in terms of consumed energy and fuel, fuel cell efficiency, battery SOC, operational cost and stresses. This comparison is then used to develop a multi-scheme EMS in addition to the introduction of an improvement to the classical PI controller based EMS.

6.2 Ship data

This chapter uses the world's first hydrogen fuel cell passenger vessel *FCS Alsterwasser* as a case study. This vessel was developed in Germany as part of the ZEMSHIPS project

funded by the European Union life program [175; 165; 296]. The total project budget was €5.5 million, of which €2.4 million was co-funded by the EU-Life program [69]. A hydrogen filling station has been also built by Linde Group as part of this project. The ship has been classified by the Germanischer Lloyd and its main particulars are shown in Table 6.1.

Table 6.1: Specifications of the FCS Alsterwasser passenger vessel

Capacity	100 passengers
Length	25.5 m
Breadth	5.36 m
Depth	2.65 m
Draft	1.33 m
Displacement	72 tonnes
Top speed	8 kn
Powering	2 PEMFC of 48 kW each 360 $Ah/560\ V$ lead-gel battery

As detailed in Table 6.1, this ship is equipped with two PEMFC systems which have proven to be an extremely reliable energy source connected to the DC bus using a boost type unidirectional DC-DC converter to control the voltage. A lead-gel battery system is also connected directly to the DC bus to deliver the propulsion power to a 100 kW electric motor as shown in Figure 4.29. The vessel is also equipped with twelve hydrogen tanks at a pressure of 350 bar and a hydrogen weight of 50 kg which is sufficient for two or three days of operation without refuelling [175]. The required time for filling the hydrogen tanks is about twelve minutes [69].

An extract of the power requirements for a typical voyage on the Alster, Hamburg, Germany has been measured and published in [296; 20]. This power requirement includes propulsion and auxiliary power and it shows power requirements during cruising, docking, stopping, and acceleration phases of the ship journey. The data measured from [20] as shown in Figure 3.15 starts with a cruising time of about 90 seconds, the vessel then enters a docking phase lasting 45 seconds. The vessel is alongside for 25 seconds. Finally the vessel starts to sail again and reaches its cruising speed after an acceleration time of about 35 seconds, giving 300 seconds total time for the manoeuvre.

Based on the typical power consumption shown in Figure 3.15, the power consumption of a complete voyage from Finkenwerder to Landungsbrucken has been extrapolated as shown in Figure 6.1. Duration of the full journey is about 1 hour as shown in Table 6.2 with 4 stops between the two destinations as shown in Figure 6.2 [23]. In order to cover a daily vessel operation of 8 hours, the developed load power requirement displayed in Figure 6.1 has been repeated for 8 times in order to be used as an input to the simulation as will be described in the following sections.

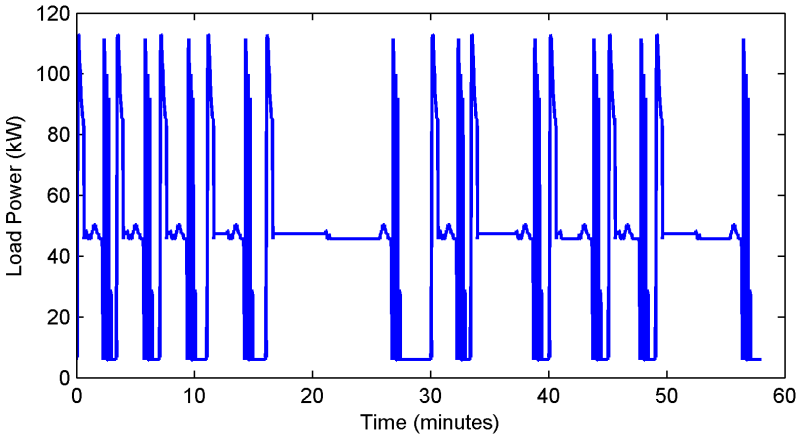

Figure 6.1: Developed power requirement of a real full voyage between Finkenwerder and Landungsbrucken

Table 6.2: Finkenwerder - Landungsbrucken time table in minutes [23]

Landungsbrucken	0	Finkenwerder	30
Altona	3	Bubendey-Ufer	33
Dockland	7	Neumuhlen	40
Neumuhlen	11	Dockland	45
Bubendey-Ufer	16	Altona	49
Finkenwerder	28	Landungsbrucken	58

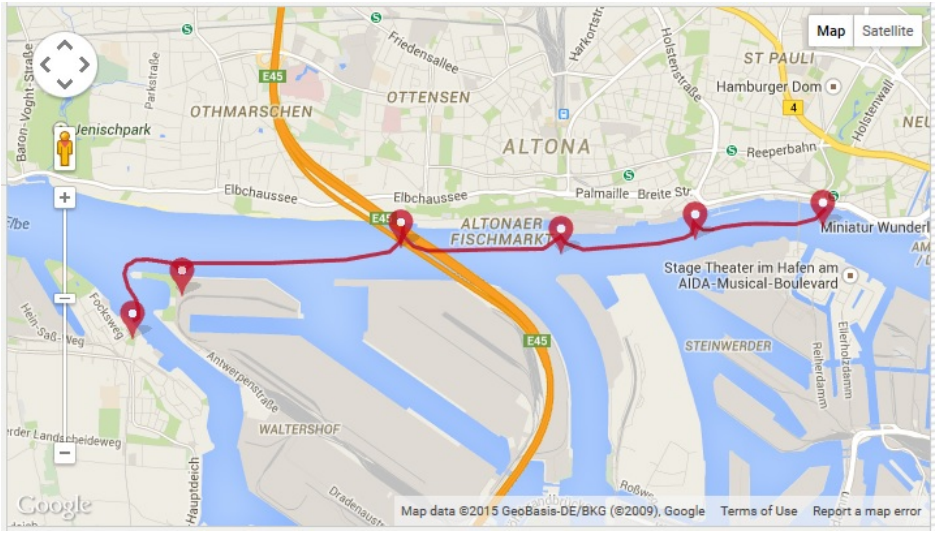

Figure 6.2: The examined vessel route [23]

6.3 Simulation parameters

The *FCS Alsterwasser*'s hybrid fuel cell/battery propulsion system is modelled and implemented in Simulink as discussed earlier in Chapter 4. As illustrated in Figure 4.11, the developed daily load power requirements of the examined ship is used as an input through the load power requirement subsystem to the EMS subsystem. The required

power is then converted into current and split between the fuel cell and battery systems by the used EMS in the EMS subsystem. The required currents are then drained from the fuel cell and battery subsystems to supply the ship's required power. The EMS subsystem includes the four studied strategies which are: the state-based, classical PI, ECMS, and CDCS strategies. A performance comparison is made between these strategies in terms of fuel cell hydrogen consumption and efficiency, battery SOC, total consumed energy, operational cost and stresses seen by each power source. To compare these strategies appropriately, the same fuel cell and battery models are used with the same initial conditions for different strategies. For this study, the same preset PEMFC Simulink model with a nominal power of 50 kW is used which is sufficient to provide the average load required power shown in Figure 3.15. A boost type unidirectional DC-DC converter is used to connect the fuel cell to the DC bus assuming the efficiency of the converter to be 95% [114]. A 360 Ah lead-gel battery which is a lead-acid battery type with a voltage of 560 V and constant internal resistance of 0.0156 Ω is also modelled and used. Figure 6.3 plots the battery voltage versus its SOC.

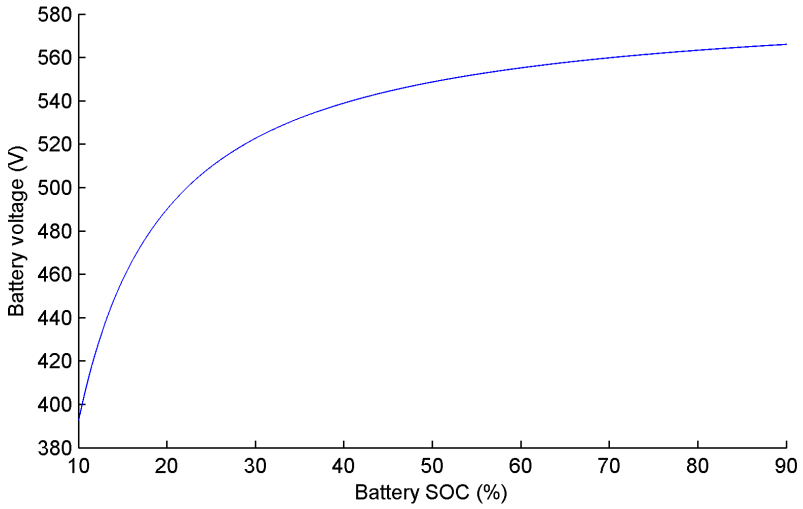

Figure 6.3: Battery voltage versus SOC at 0.2C discharge rate

For the classical and improved PI EMS, a reference value of the battery SOC of 60% is selected as recommended by automotive industry designers [280]. Regarding the reference value of fuel cell efficiency for the proposed PI EMS, the nominal efficiency of the used PEMFC model is 55% [270; 48] which can increase at part loads [114] as shown in Figure 3.11. Therefore, a higher fuel cell efficiency than 55% is selected as a reference value of fuel cell efficiency for the proposed PI EMS which is 60%. The P and I gains of the battery SOC PI controllers are 50000 and 1 for the classical PI EMS and 200 and 0.0001 for the proposed PI EMS respectively. For the ECMS, SOC_H and SOC_L are set to 80% and 30% [323] and the battery threshold value for the CDCS strategy is 30% [324]. The SOC constant μ is set to 0.6 to balance the battery SOC during the examined driving cycle using the ECMS as reported in [17; 293; 295]. A minimum power limit of 5 kW, a maximum power of 80 kW, as suggested in [20], and an optimum power

of 50 kW, the same as the nominal power of the used PEMFC model as described in Table 5.2, are used to avoid operating the fuel cell at poor efficiency region. The battery C-rate limits are 0.3C and 2C as recommended by the battery manufacturer [20]. Also, a normal battery SOC of 65% is used as an initial condition for different strategies.

6.4 Simulation results

The performance of the hybrid fuel cell propulsion system of the ship has been investigated using different energy management strategies. Figures 6.4 and 6.5 represent fuel cell and battery powers using different strategies for the examined voyage. Each strategy decides the power split between the fuel cell and battery systems as discussed in 3.3.7.5 according to the required load power, operational limit points of the fuel cell and battery, battery SOC, and fuel cell efficiency. Also, fuel cell and battery powers are within the minimum and maximum limits using different strategies. As can be found in Figure 6.4, CDCS strategy operates the fuel cell at its minimum power until the battery SOC reaches its threshold value as shown in Figure 6.6 while the battery provides most of the required load as reported in Figure 6.5. The classical PI EMS also uses the battery power until its SOC reaches its reference value of 60%. The improved PI EMS discharges the battery energy as well to attain the required battery SOC reference value but more gradually than the classical PI EMS due to the use of fuel cell efficiency as an input. Using the fuel cell efficiency as an input in the improved PI strategy results in reducing the fuel cell power fluctuation compared to other strategies as can be seen in Figure 6.4 which reduces its hydrogen consumption and operational stress as discussed later in the following sections. The state-based strategy results in less fuel cell and battery power fluctuations as well due to taking the optimum fuel cell and battery powers into consideration.

Considering the developed 8 hours voyage, the hydrogen consumption of the examined ship depends considerably on the used EMS. As expected, CDCS strategy has the lowest hydrogen consumption due to its prioritizing of the battery energy usage as shown in Figure 6.7. Also, the ECMS strategy has lower hydrogen consumption than other strategies because it uses more energy from the battery to minimize the equivalent hydrogen consumption of the hybrid system. State-based strategy results in the highest hydrogen consumption because the simulation starts with a normal battery SOC. Therefore, the fuel cell supplied mostly the required load power or works at its optimum power value. The improved PI strategy has lower hydrogen consumption than the classical PI and the state-based strategies by 1.3% and 5.1% respectively.

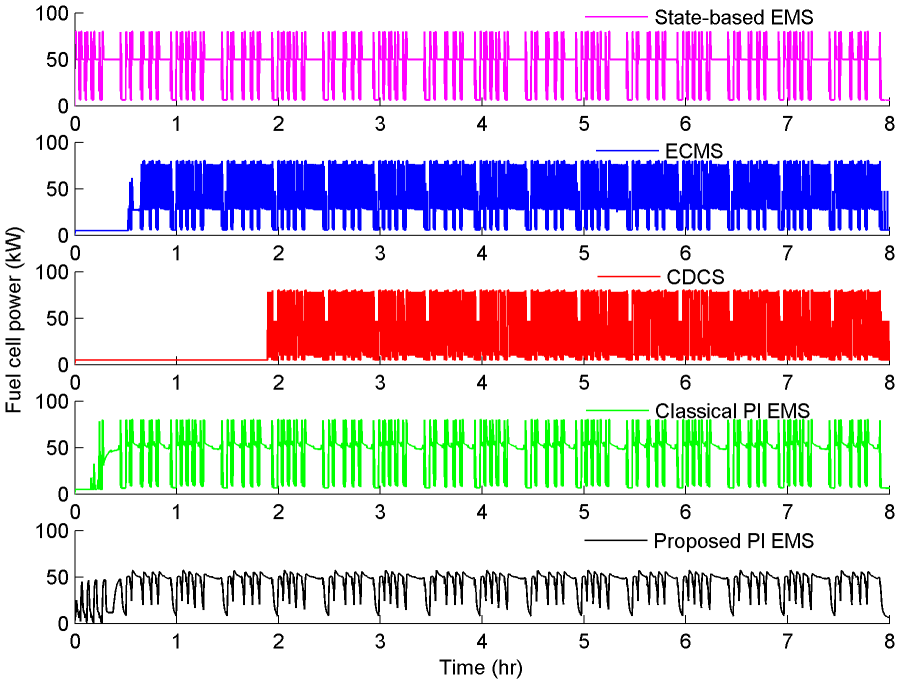

Figure 6.4: Fuel cell power during the examined voyage using different strategies

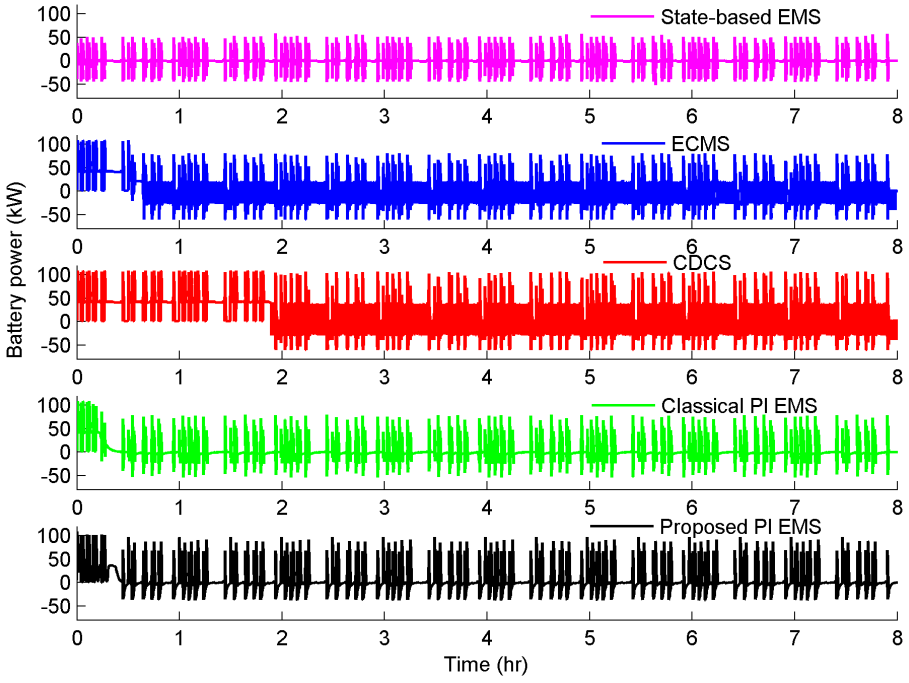

Figure 6.5: Battery power during the examined voyage using different strategies

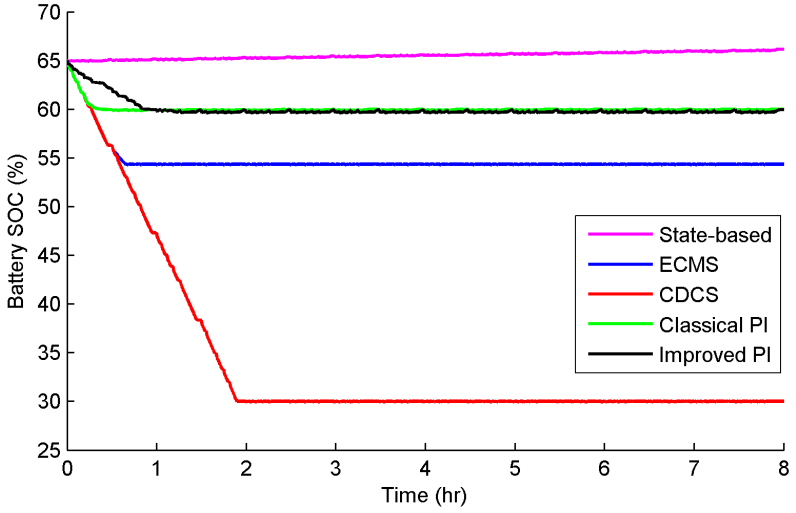

Figure 6.6: Battery SOC during the examined voyage using different strategies

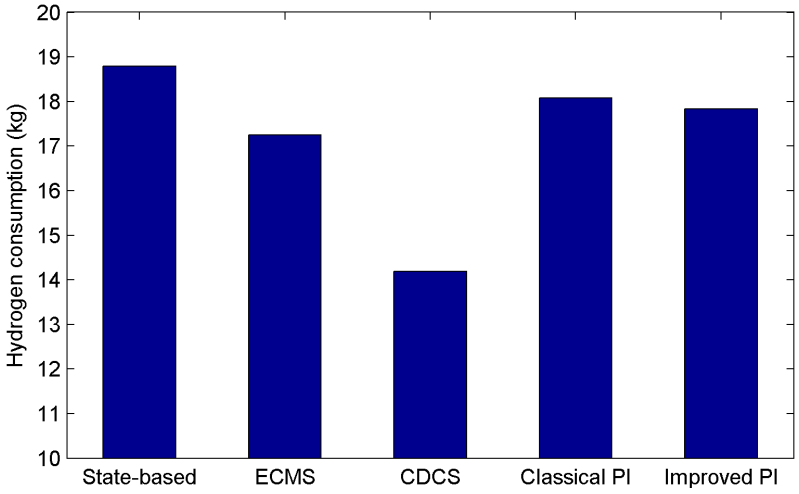

Figure 6.7: Hydrogen consumption using different strategies for the examined voyage

6.4.1 Improved PI EMS

One reason for the improved PI strategy hydrogen saving over the classical PI and state-based strategies is the use of fuel cell efficiency as an input to the EMS which maintains the fuel cell efficiency around 55% or higher in case of adopting the proposed PI EMS while fuel cell efficiency can be lower than 50% using other strategies as illustrated in Figure 6.8.

It can be observed from Figure 6.8 that the fuel cell efficiency is constant at the start of the journey using CDCS strategy because the fuel cell system works constantly at its minimum power due to prioritizing the battery power until it reaches its threshold value of 30% as shown in Figure 6.6. In order to compare fuel cell stack efficiency properly during the 8 hours driving cycle using different strategies, the mean, standard deviation (SD), and coefficient of variation of fuel cell efficiency are calculated. As listed in Table

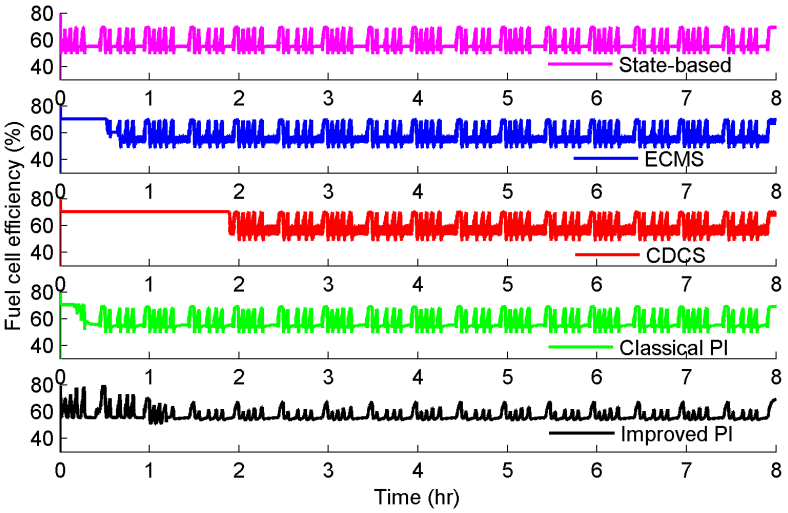

Figure 6.8: Fuel cell stack efficiency during the examined voyage using different strategies

6.3, the improved PI EMS has the lowest average value of fuel cell efficiency. However, the SD and coefficient of variance of the improved PI EMS are significantly lower by 21% and 22% respectively compared to the state-based EMS, 36% and 36% respectively compared to the ECMS, 44% and 42% respectively compared to the CDCS strategy, and 28% and 30% respectively compared to the classical PI EMS. This means less variability and high stability of fuel cell efficiency during the examined load cycle [329] which means less stress on the fuel cell stack and results in longer lifetime and saving in hydrogen consumption.

Table 6.3: Mean, standard deviation, and coefficient of variation of fuel cell stack efficiency comparison using different strategies

	Mean (%)	SD (%)	Coefficient of variation
State-based	57.4	5.3	0.09
ECMS	58.9	6.6	0.11
CDCS	61.5	7.5	0.12
Classical PI	57.9	5.8	0.10
Improved PI	57.2	4.2	0.07

6.4.1.1 Sensitivity analysis of fuel cell efficiency reference value

In order to study the effect of the selected reference value of fuel cell efficiency on the performance of the improved PI EMS, a sensitivity analysis is performed. Different values of fuel cell efficiency are used as reference values for the proposed PI EMS to calculate the hydrogen consumption saving percentage using the improved PI EMS compared to other strategies for the examined 8 hours of operation as shown in Figure 6.9.

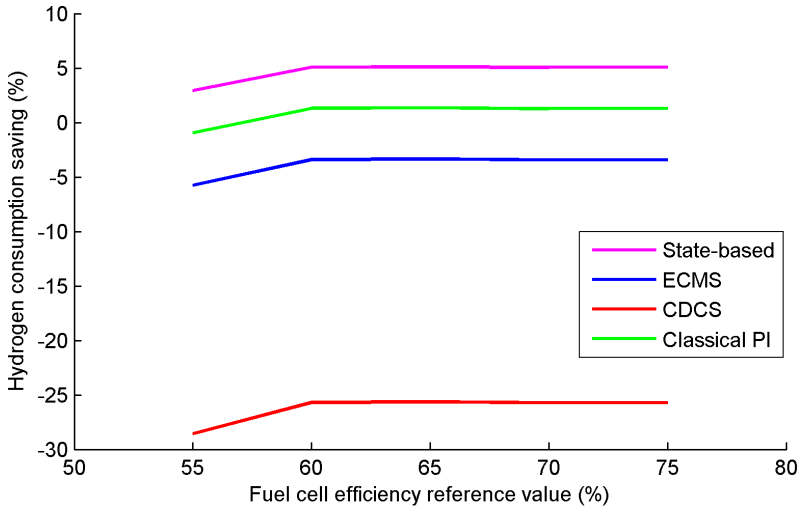

Figure 6.9: Fuel cell efficiency reference values effect on the hydrogen consumption saving percentage of the improved PI strategy compared to other strategies

As shown in Figure 6.9, fuel cell efficiency reference value starts from the fuel cell stack nominal efficiency of 55%. By increasing the fuel cell efficiency reference value, the hydrogen consumption saving percentage of the improved PI strategy increases until 65% where it starts to level off. This levelling off is expected because higher fuel cell efficiency is achieved in the low load region as shown in Figure 3.11 where it is difficult to operate the fuel cell because of the vessel required power and the fuel cell and battery operational limits. Therefore, the optimum reference value of fuel cell efficiency for the improved PI EMS that gives the lowest hydrogen consumption is 65% for the examined full driving cycle of 8 hours. The hydrogen consumption saving percentages of the proposed PI EMS using the optimum reference value of fuel cell efficiency of 65% are 5.11% and 1.4% compared to the state-based and classical PI strategies respectively. However, ECMS and CDCS strategies have lower hydrogen consumption than the improved PI EMS by 3.4% and 25.6% respectively as shown in Figure 6.9.

As explained earlier, using fuel cell efficiency as an input to the improved PI as proposed helps in reducing the fuel cell hydrogen consumption and operational stress which results in prolonging its lifetime. In the following section, the improved PI EMS is compared to other strategies in terms of the operational stresses on the fuel cell and battery systems.

6.4.1.2 Stress analysis

The lifetime of the hybrid fuel cell/battery system, reliability and durability depend mainly on the intended application and the stress on each power source of the hybrid system. Since fuel cells have shorter life and higher maintenance and replacement costs compared to batteries, more focus is now on extending the lifetime of fuel cells [330; 331]. Reducing fuel cell operational stresses can significantly help in extending its lifetime and

reducing its fuel consumption. Therefore, in this study it is proposed to take fuel cell efficiency into consideration by the EMS in order to avoid operating the fuel cell away from high efficiency region.

The approach suggested in [17] to determine the stress on the fuel cell and the battery is used in this study. This approach uses Haar wavelet transform to decompose the instantaneous power from the fuel cell and battery into approximation coefficients which contains the low frequency components of the power and detail coefficients which contain the high frequency components [332]. The standard deviation of the high frequency components can give a good indication of the stress on each power source of the hybrid fuel cell/battery system for the examined mission profile. As shown in Table 6.4, the improved PI EMS has the lowest fuel cell stress while it has higher battery stress than other strategies as a result of the trade-off issue between the stresses on the fuel cell and the battery except for the CDCS strategy that has the highest fuel cell and battery stresses. Moreover, the improved PI EMS has lower hydrogen consumption and more use of the battery energy than the state-based and classical PI strategies. Meanwhile, CDCS has the lowest hydrogen consumption as shown in Figure 6.7. For the examined power requirements, changing the used strategy from state-based EMS to CDCS can result in a hydrogen consumption saving of 23% which confirms the strong effect of the used EMS on the hybrid fuel cell systems for ships with high variation in power requirements. An overall performance comparison of the proposed PI EMS is presented in Table 6.4 using the optimum reference value of the fuel cell efficiency of 65% for the improved PI EMS as discussed earlier.

Table 6.4: Overall performance comparison

	State-based	ECMS	CDCS	Classical PI	Improved PI
Fuel cell stress	29.26	37.92	42.37	31.69	19.94
Battery stress	15.85	29.92	40.61	19.18	32.81
Hydrogen consumption (kg)	18.79	17.25	14.49	18.07	17.83
Battery SOC (%)	65–66.11	65–54.35	65–30	65–59.99	65–59.95

6.4.1.3 Total energy & cost analysis

Another reason for the hydrogen consumption saving achieved by the improved PI EMS over the state-based and the classical PI strategies is that the improved PI EMS tends to use more power from the battery than the state-based and the classical PI strategies as shown in Figure 6.6. For the same reason, using the CDCS strategy results in the lowest hydrogen consumption as explained earlier. Therefore, in order to have a fair comparison between different strategies, the total consumed energy and operational cost during the examined driving cycle should be calculated and compared. The total consumed energy includes the fuel cell and battery consumed energy during the voyage

as well as the required energy to charge the battery back to its initial battery SOC assuming charging efficiency of 88% [333] using shore-shared (or shore-side) energy. The shore-shared external power source is used to recharge the battery system during night instead of using the fuel cell in order to reduce the fuel cell operational time and increase its lifetime. Also, the calculated operational cost includes hydrogen cost and the cost of charging the battery back to its initial SOC.

As illustrated in Figure 6.10, the classical PI and state-based strategies have the lowest total energy consumption. Meanwhile, the ECMS strategy has the highest total energy consumption. Although ECMS strategy has low hydrogen consumption, its total energy consumption is high because of its use of battery energy and the wasted energy during the battery recharging. On the other hand, the state-based strategy has the lowest battery depleted energy and it doesn't need to be recharged after the examined voyage since the battery final SOC is approximately the same as the initial SOC as can be seen in Figure 6.6. Regarding the improved PI EMS, it has lower total energy consumption than the ECMS by 1.1% and it has approximately the same total energy consumption as the CDCS strategy. However, the improved PI EMS has higher total energy consumption than the classical PI and state-based strategies by 2.1% and 1.5% respectively.

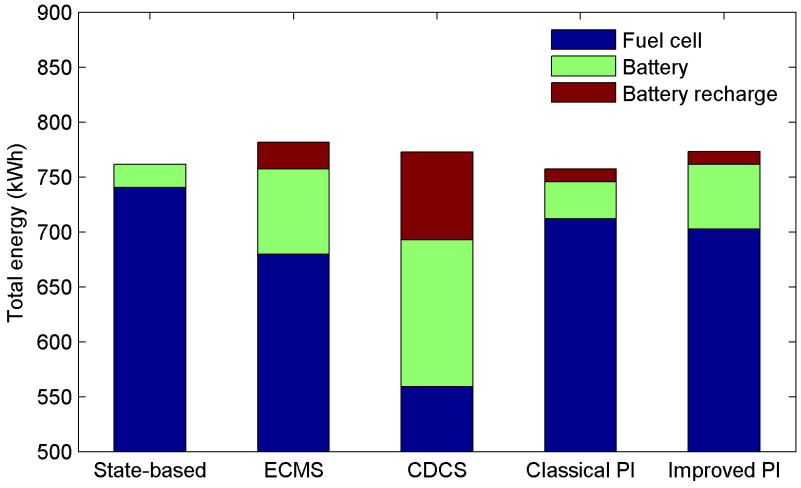

Figure 6.10: Comparison of the total consumed energy during the examined voyage using different strategies

Regarding the operational cost which includes hydrogen cost and battery recharging cost using different strategies, it is dominated by hydrogen cost as can be noticed in Figure 6.11. Also, the improved PI EMS has the lowest operational cost compared to other strategies. Using the optimum reference value of the fuel cell efficiency of 65%, the improved PI EMS has lower operational cost than the CDCS, state-based, classical PI, and ECMS strategies by 2.1%, 1.5%, 1.3%, and 0.9% respectively for the examined daily operation of the ship. As can be found in Figure 6.11, although CDCS strategy has the lowest hydrogen cost, it has the highest daily operational cost because of the higher battery recharging cost compared to other strategies. These results are a function of

the used energy prices hence, a sensitivity analysis of energy prices is performed in the following section.

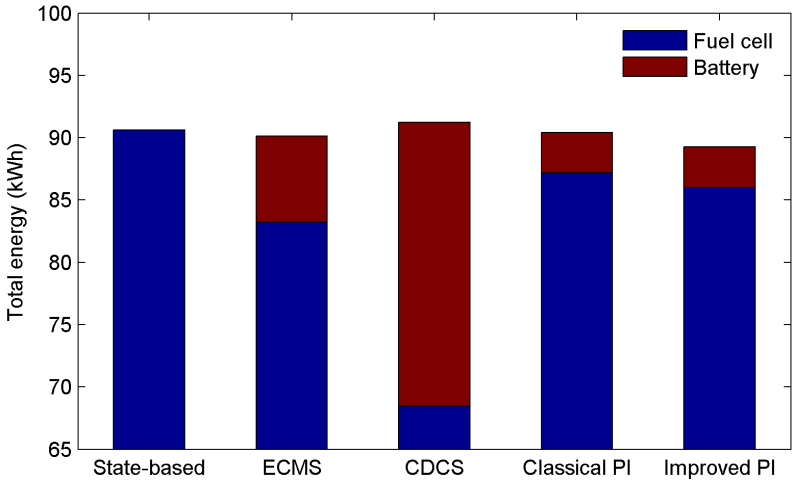

Figure 6.11: Comparison of the operational cost during the examined voyage using different strategies

6.4.1.4 Sensitivity analysis of energy prices

The reported cost saving percentages to this point corresponds to a a wind generated hydrogen cost of 4.823 $\$/kg$ [325] and an average electricity price of 0.284 $\$/kWh$ for the battery recharging using shore-shared (or shore-side) energy [334]. The prices of hydrogen and electricity vary spatially and temporally depending on their used production method. In order to study the impact of varying energy prices on the operational cost saving percentages, an energy price ratio (β) is used and it can be calculated as follows

$$\beta = \frac{\text{Price of Hydrogen per kWh}}{\text{Price of Electricity per kWh}} \tag{6.1}$$

Assuming an energy content of 39.4 kWh/kg for the hydrogen, the energy price ratio β equals 0.43 using the assumed energy prices. Different values of β are assumed and its impact on the operational cost saving percentages of adopting the improved PI EMS compared to other strategies is shown in Figure 6.12 where higher values of β means that hydrogen becomes more expensive relative to fixed electricity prices [284].

Two key observations can be made from Figure 6.12; firstly, the operational cost saving percentages of the improved PI EMS compared to the state-based and the classical PI strategies become higher for higher values of β. This is due to the fact that the improved PI strategy has lower hydrogen consumption than the the state-based and the classical PI strategies. Therefore, at higher values of β the total operational cost becomes more dominated by the hydrogen cost. Meanwhile, the operational cost saving percentages

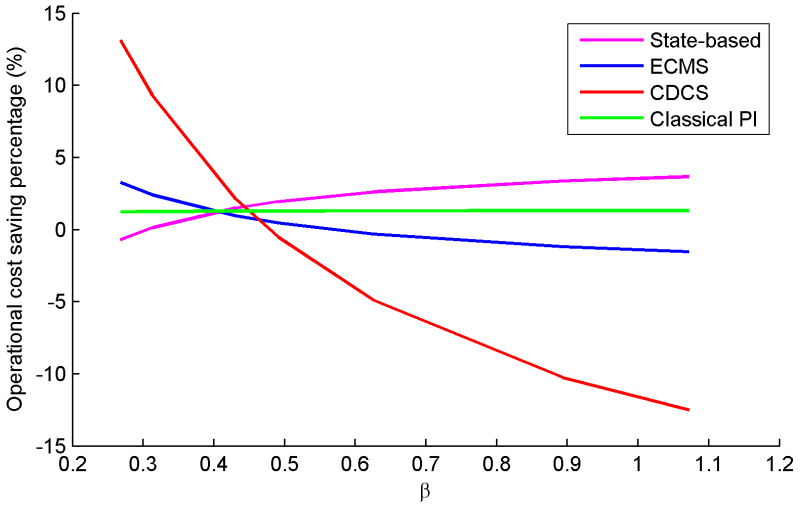

Figure 6.12: Impact of energy price ratio on operational cost saving percentages of adopting the improved PI EMS compared to other strategies at an initial battery SOC of 65%

of the improved PI EMS compared to the ECMS and CDCS strategies become lower for higher values of β. Secondly, the cost saving percentage of the improved PI EMS compared to the CDCS strategy is more significant at lower β values. This is because at lower β values, the battery recharging cost percentage of the total cost increases and CDCS results in the highest battery usage compared to other strategies. However, at higher β values which means higher hydrogen prices, the total cost becomes dominated by the hydrogen cost. Consequently, the total operational cost saving of the improved PI EMS over CDCS strategy is negative at higher β values since CDCS has the lowest hydrogen consumption. Moreover, the improved PI strategy has lower operational cost than the classical PI strategy at different β values.

6.4.1.5 Sensitivity analysis of initial battery SOC

The reported saving percentages of the improved PI EMS in terms of operational cost, hydrogen and energy consumption can be affected by the initial battery SOC. Therefore, different initial battery SOC values are used for the examined load cycle in order to study its effect on the results of using different strategies. It is apparent that the hydrogen consumption of the hybrid propulsion system becomes higher for lower initial battery SOC using different strategies because of the less available battery energy which increases the hydrogen consumption. As shown in Figure 6.13, the improved PI EMS has lower hydrogen consumption than the classical PI EMS at different initial battery SOC with saving values varies between 1.3% to 1.4%. Also, the ECMS and CDCS strategies have lower hydrogen consumption than the improved PI strategies at different initial battery SOC with saving values varies between 3.4% to 4.4% for the ECMS and 26% to 28.6% for the CDCS. Compared to the state-based strategy, the improved PI strategy has

14.3% lower hydrogen consumption at high initial battery SOC of 80%. However, this percentage starts to decrease at lower initial battery SOC until it becomes negative at an initial battery SOC of 50% where the state-based EMS has lower hydrogen consumption than the improved PI EMS by 6.9%. This can be justified by the fact that, at an initial battery SOC of 50% the improved PI EMS tends to charge the battery until it reaches a SOC of 60% which is the battery SOC reference value of the improved PI EMS. Meanwhile, the state-based EMS consider the initial battery SOC of 50% as a normal battery SOC as can be seen in Table 3.8.

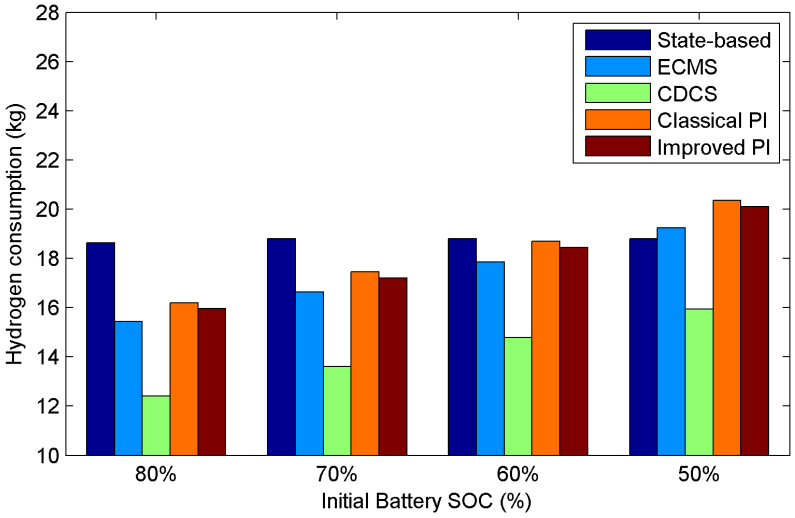

Figure 6.13: Hydrogen consumption of the hybrid propulsion system using different strategies at different initial battery SOC

Regarding the total energy consumption of the hybrid propulsion system, it also becomes higher for lower initial battery SOC using different strategies since less battery energy is available as shown in Figure 6.14. The total energy consumption includes the battery depleted energy during the voyage and the battery recharging energy to its initial SOC in addition to the fuel cell consumed energy. Although the improved PI EMS has lower hydrogen consumption than the classical PI EMS at different initial battery SOC, it has higher total energy consumption than the classical PI EMS with values varies between 1.1% and 2.2% after taking the battery energy into consideration. Moreover, the classical PI EMS has the lowest energy consumption compared to other strategies provided that the initial battery SOC is higher or equal to 60% which is the same SOC reference value to be maintained by both PI based strategies. By starting with an initial battery SOC below 60%, the classical PI as well as the improved PI strategies will have higher energy consumption than other strategies because the fuel cell system tends to supply the required load power in addition to charging the battery until it reaches its reference value of 60% as recommended. For low initial battery SOC, the state-based and CDCS strategies have lower total energy consumption than other strategies as shown in Figure 6.14.

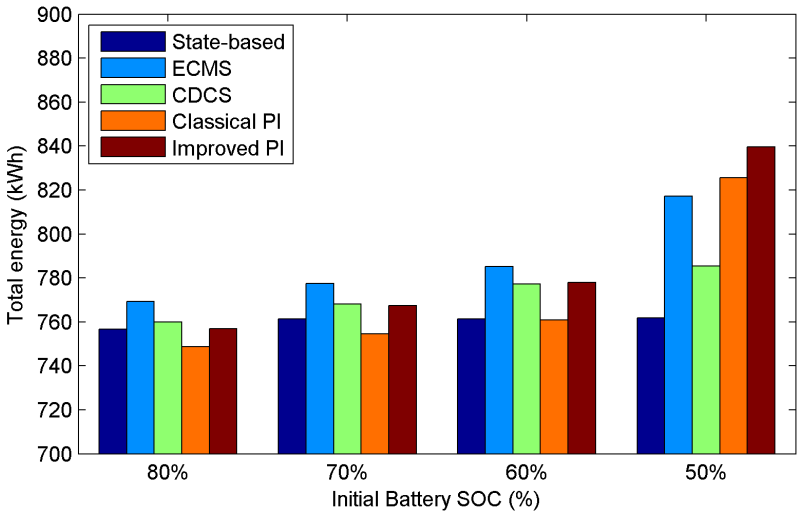

Figure 6.14: Total energy consumption of the hybrid propulsion system using different strategies at different initial battery SOC

Due to the hydrogen consumption saving of the improved PI EMS over the classical PI strategy as shown in Figure 6.13, the improved PI strategy has less operational cost of the hybrid system than the classical PI strategy by 1.5% starting with an initial battery SOC of 80% and by 1.3% starting with an initial SOC of 50%, 60%, and 70% as shown in Figure 6.15. This can be justified by the fact that the total cost is dominated by hydrogen price. Also, the improved PI EMS has the same or lower operational cost than other strategies provided that the initial battery SOC is higher or equal to 60% which is the battery threshold value for the PI based strategies. The results shown in Figure 6.15 is sensitive to the energy prices as discussed in Section 6.4.1.4. Therefore, the same analysis of starting with different initial battery SOC is made for higher and lower β values which corresponds to hydrogen prices of 7 and 3 \$/kg respectively as shown in Figures 6.16 and 6.17.

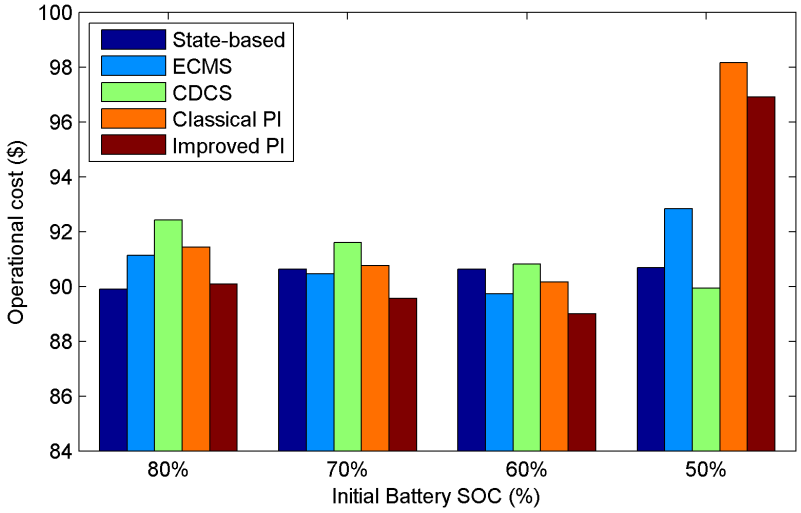

Figure 6.15: Operational cost of the hybrid propulsion system using different strategies at different initial battery SOC

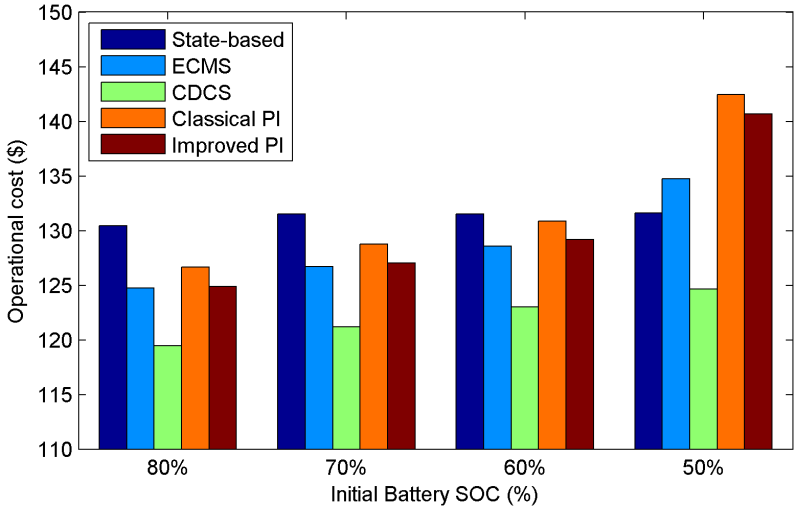

Figure 6.16: Operational cost of the hybrid propulsion system using different strategies at different initial battery SOC for hydrogen price of 7 $/kg

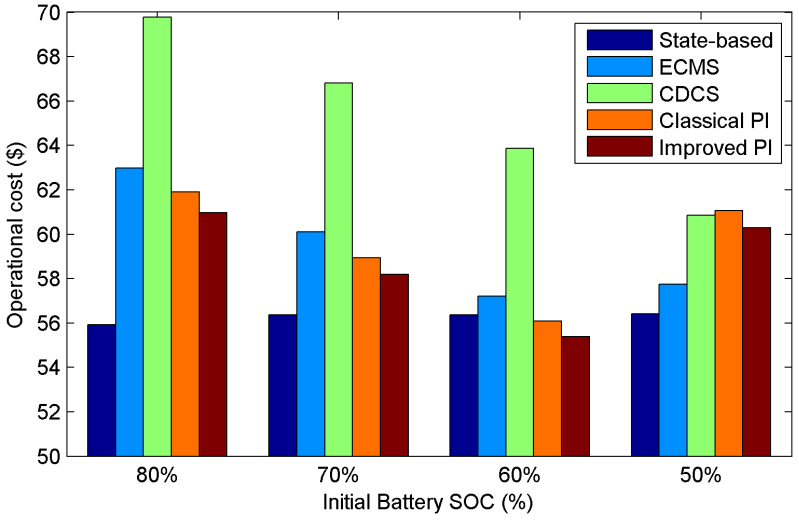

Figure 6.17: Operational cost of the hybrid propulsion system using different strategies at different initial battery SOC for hydrogen price of 3 $/kg

Since using CDCS strategy results in the lowest hydrogen consumption, the effect of hydrogen price is more pronounced for CDCS strategy. As shown in Figure 6.16, at higher hydrogen prices, the total operational cost is dominated by the fuel cost hence, CDCS strategy has the lowest operational cost at different initial battery SOC compared to other strategies because it has the lowest hydrogen consumption. On the other hand, at lower hydrogen prices, CDCS strategy has the highest operational cost because CDCS has the highest battery recharging cost compared to other strategies as shown in Figure 6.11 and the total operational cost is less dominated by the fuel cost. Also, the proposed PI EMS has lower operational cost than the classical PI EMS at different initial battery SOC for different hydrogen prices.

Regarding the improved PI EMS, it could be concluded that using fuel cell efficiency

as an input to the classical PI EMS as proposed can reduce the stresses on the fuel cell which prolongs its lifetime and results in a saving of its hydrogen consumption. Simulation results show that the improved PI EMS has the least fuel cell stress and lower hydrogen consumption than the state-based and classical PI strategies by 5.11% and 1.4% respectively with more use of the battery energy. Moreover, the improved PI EMS has lower hydrogen consumption and operational cost than the classical PI EMS using different initial battery SOC and for different hydrogen prices. However, ECMS and CDCS strategies have lower hydrogen consumption than other strategies but with the loss of more battery energy. By taking the battery discharged energy into consideration to have fair comparison between different strategies, the improved PI EMS has lower total energy consumption than the ECMS and CDCS strategies while it has higher total energy consumption than the classical PI and the state-based strategies which reduces the energy efficiency of the ship. In order to increase the energy efficiency of the ship, a multi-scheme EMS with an objective of minimizing the total consumed energy is developed as described in the next section.

6.4.2 Multi-scheme EMS

6.4.2.1 Multi-scheme EMS development

The use of a multi-scheme EMS has been proposed for hybrid fuel cell propulsion systems since different strategies have different objectives. For the world's first hydrogen fuel cell passenger ship *FCS Alsterwasser*, a multi-scheme EMS is developed in this study for the first time with an objective of minimizing the total consumed energy for the sake of increasing the energy efficiency of the ship as discussed in 3.3.7.5. The developed multi-scheme EMS contains the four examined strategies which are: the state-based, ECMS, CDCS, and the classical PI strategies and it switches between these strategies during operation according to a code that selects the suitable EMS according to the required load power and battery SOC. In order to develop this code, the four considered strategies are compared at three different power levels of about 6, 48 and 90 kW starting with different initial battery SOC. The three power levels are chosen in accordance with the examined ship operational profile shown in Figure 6.1 to represent the low, cruising, and high power requirements of the ship during its voyage. At each power level, simulations are performed starting with different initial battery SOC to decide which strategy consumes the lowest energy. The considered energy consumption includes the fuel cell and battery energy consumption and the required energy to recharge the battery back to its initial SOC in order to have a fair comparison between different strategies.

For the examined ship cruising mode of 48 kW power requirement, and at a high initial battery SOC of 80% as for example, the total energy consumption of the hybrid fuel cell/battery propulsion system has been investigated using different strategies

as shown in Figure 6.18 which indicates that the classical PI EMS results in lower energy consumption than the the state-based, ECMS, and CDCS strategies by 8.1%, 0.04% and 0.04% respectively. The state-based EMS regulates the fuel cell to provide the required power which results in the high energy consumption. Meanwhile, other strategies tend to discharge the battery but with different SOC target (i.e. 30% for the CDCS strategy) therefore, they results in approximately the same energy consumption. However, classical PI EMS has the lowest energy consumption and operational stresses as shown in Table 6.4.

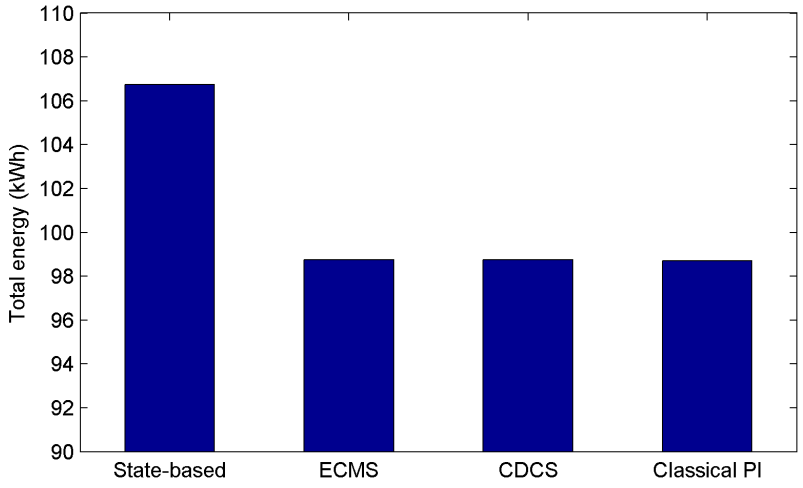

Figure 6.18: Total energy consumption comparison for the *FCS Alsterwasser* cruising mode using different strategies at an initial battery SOC of 80%

Comparing the four considered strategies for the examined ship low power mode of 6 kW power requirement for another example and at a medium SOC of 45% shows that CDCS strategy results in the lowest energy consumption as illustrated in Figure 6.19. This is because state-based, ECMS, and classical PI strategies uses the fuel cell to supply the required load and recharge the battery while CDCS strategy uses more energy from the battery than other strategies to reach its threshold value of 30%. By doing this analysis for different power modes and starting with different initial battery SOC, the strategy that results in the least energy consumption can be identified for each operation condition. This comparison is then used to develop the multi-scheme EMS as shown in Figure 6.20.

Using the multi-scheme EMS in the case of starting with high initial battery SOC as for example, the multi-scheme EMS uses the classical PI EMS until the battery SOC decreases to the medium SOC region. Then, the ECMS and CDCS strategies are used instead of the classical PI as shown in Figure 6.20. This is because the classical PI EMS consumes more energy than the ECMS and CDCS strategies at the medium SOC region since the classical PI EMS maintains the battery SOC around a reference value of 60%. Eventually, as shown in Figure 3.16, the battery SOC in addition to the required load power are used as inputs to the the developed code of the multi-scheme EMS to select

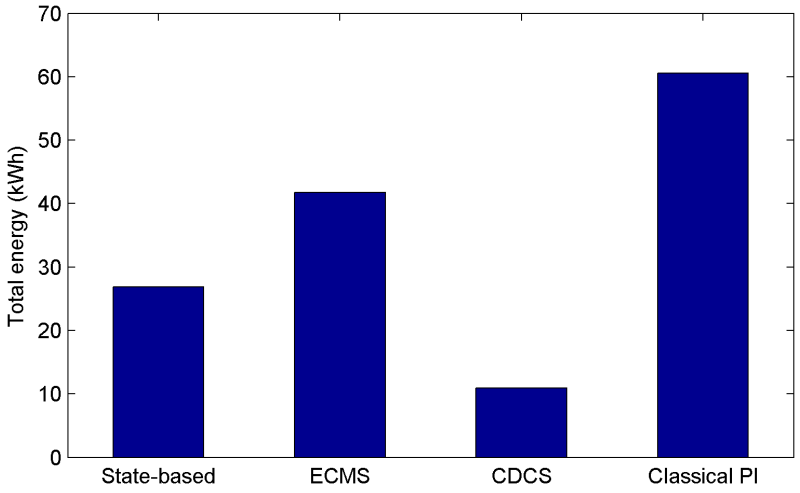

Figure 6.19: Total energy consumption comparison for the *FCS Alsterwasser* low power mode using different strategies at an initial battery SOC of 45%

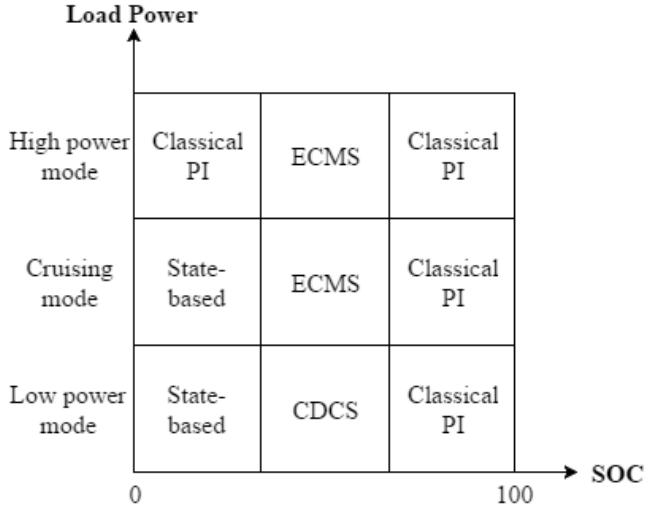

Figure 6.20: Developed code of the multi-scheme EMS

the suitable EMS during the voyage that splits the required power between the fuel cell and battery systems in order to have less total energy consumption than the resulting consumption from using any single strategy of them during the whole voyage as shown in the following section.

6.4.2.2 Multi-scheme EMS results

Considering the same 8 hours working cycle of the ship and using the same simulation parameters detailed earlier, simulation results show that the developed multi-scheme EMS has less energy consumption than the state-based, ECMS, CDCS, and the classical PI strategies by 1.4%, 3.9%, 2.8%, and 0.8% respectively as shown in Figure 6.21. This indicates that changing the used EMS during the voyage can be better than using a single EMS and result in an energy saving.

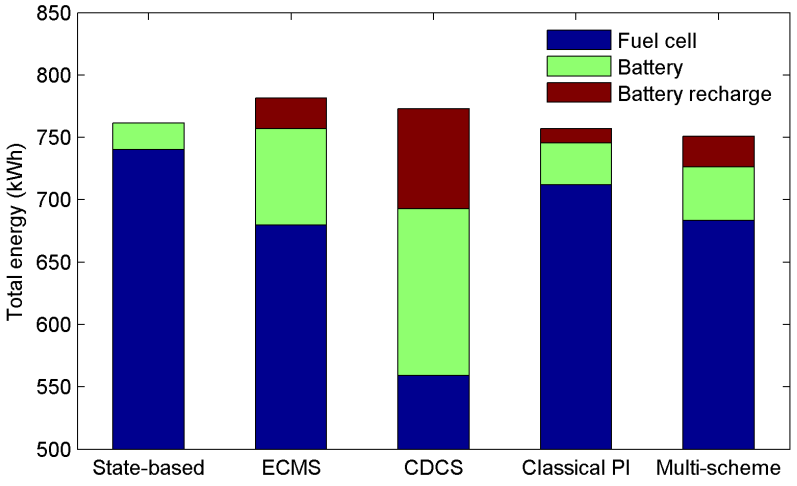

Figure 6.21: Multi-scheme EMS total consumed energy compared to other strategies for the examined working cycle

The developed multi-scheme EMS uses different strategies during the voyage as shown in Figure 6.20 according to the required load power and the battery SOC. As can be noticed in Figures 6.22 and 6.23 the similarity between the multi-scheme EMS and other strategies in splitting the required power between the fuel cell and battery systems since the multi-scheme EMS switches between different strategies to manage the power distribution.

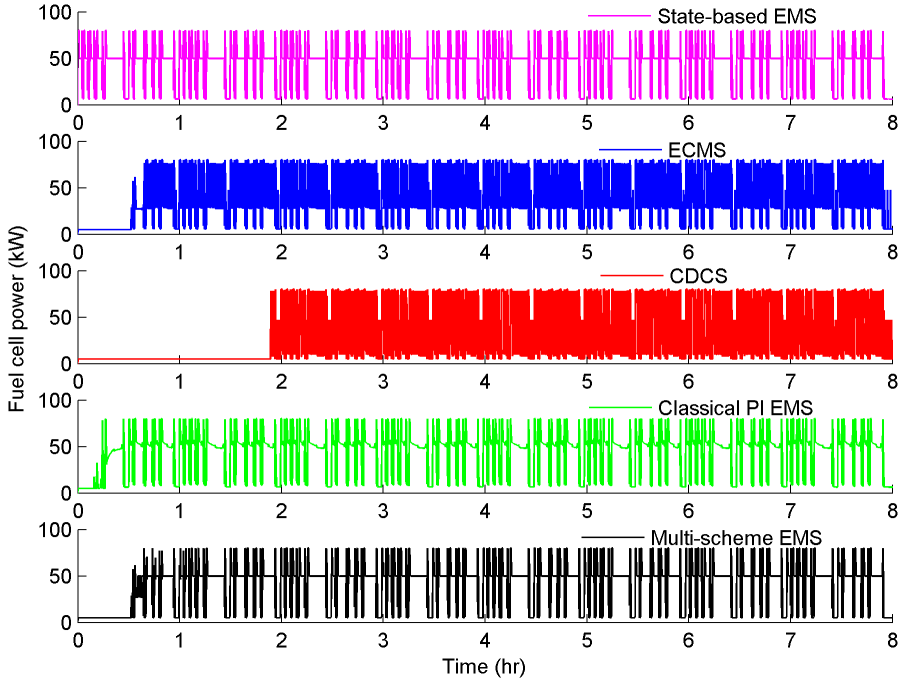

Figure 6.22: Multi-scheme EMS fuel cell power compared to other strategies during the examined voyage

Regarding the fuel cell hydrogen consumption, CDCS strategy still consumes less hydrogen than other strategies as expected since it uses more battery energy as shown in

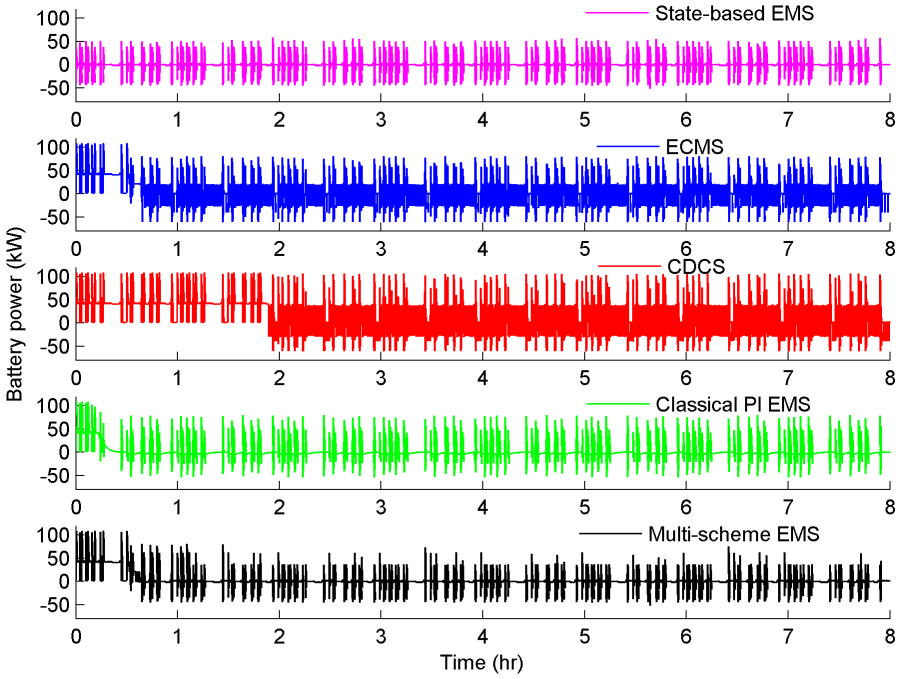

Figure 6.23: Multi-scheme EMS battery power compared to other strategies during the examined voyage

Figure 6.24. Figure 6.25 plots the ship hydrogen consumption using different strategies for the examined daily working cycle. The developed multi-scheme EMS has lower hydrogen consumption than the state-based and classical PI strategies by 7.7% and 4% respectively. However, it has higher hydrogen consumption than the ECMS and CDCS strategies by 0.6% and 22.2% respectively.

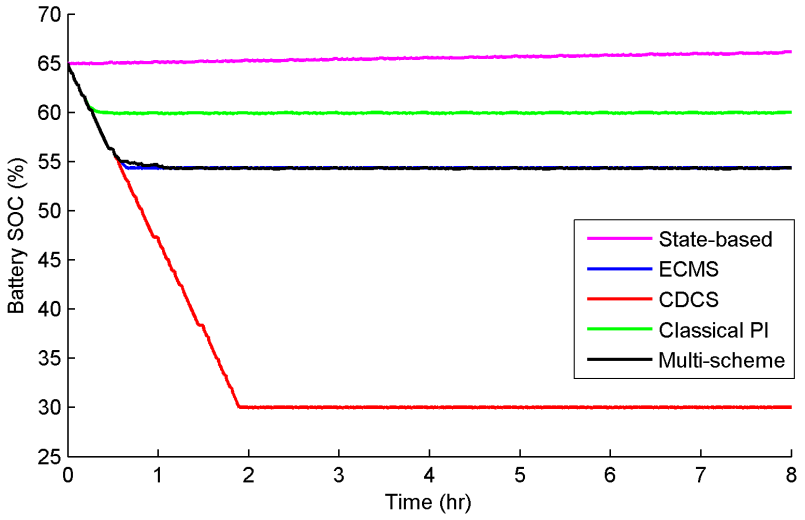

Figure 6.24: Battery SOC during the examined working cycle

As shown in Figure 6.24, at an initial battery SOC of 65%, the developed multi-scheme EMS discharges the battery energy in a similar way to the ECMS which makes the hydrogen consumption of both of them very close as reported by Figure 6.25. The

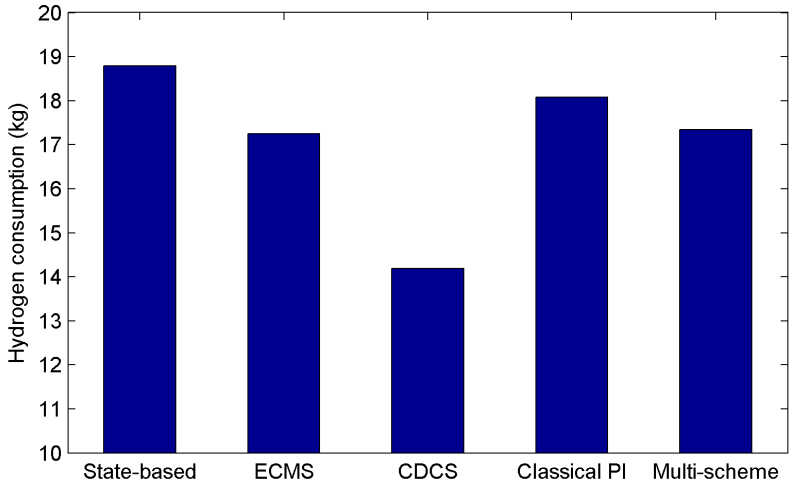

Figure 6.25: Multi-scheme EMS hydrogen consumption compared to other strategies for the examined working cycle

classical PI and CDCS strategies tend to discharge the battery energy until it reaches its reference value at 60% and 30% respectively. Meanwhile, the state-based strategy regulates the fuel cell to provide most of the power since the battery SOC is not high to be discharged therefore it has higher hydrogen consumption as shown in 6.25.

Regarding the hybrid system's operational cost, the multi-scheme EMS has approximately the same operational cost as other strategies as shown in Figure 6.26. The multi-scheme EMS results in a cost saving of 0.7% and 0.02% compared to the CDCS and state-based strategies respectively. However, the total cost of the multi-scheme EMS is slightly higher than the ECMS and classical PI strategies by 0.5% and 0.2% respectively. These results are sensitive to the used energy prices as well as the initial battery SOC as discussed in the following sections.

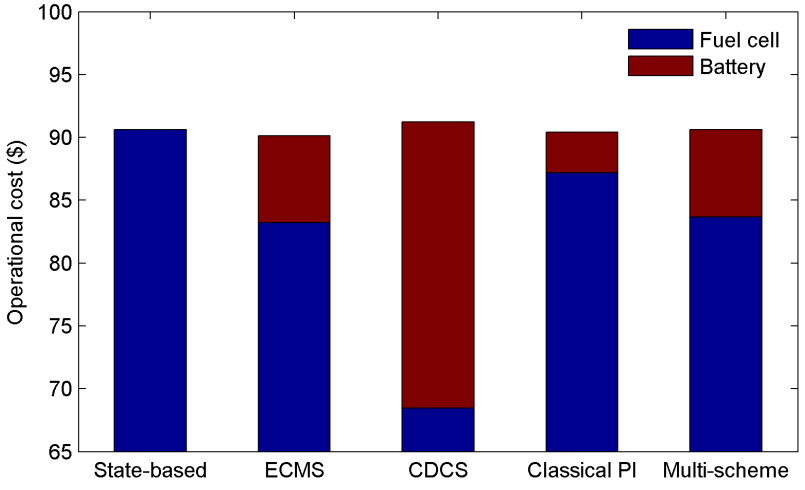

Figure 6.26: Multi-scheme EMS operational cost compared to other strategies for the examined working cycle

6.4.2.3 Impact of varying energy prices

As discussed earlier, the cost saving percentages reported in Figure 6.26 depends on the used prices of the hydrogen and energy used to recharge the battery back to its initial SOC. Therefore, different values of the energy price ratios β are used in order to assess the impact of varying the energy prices on the operational cost saving percentages of the developed multi-scheme EMS compared to other strategies as can be seen in Figure 6.27 where higher values of β means that hydrogen becomes more expensive relative to fixed electricity prices.

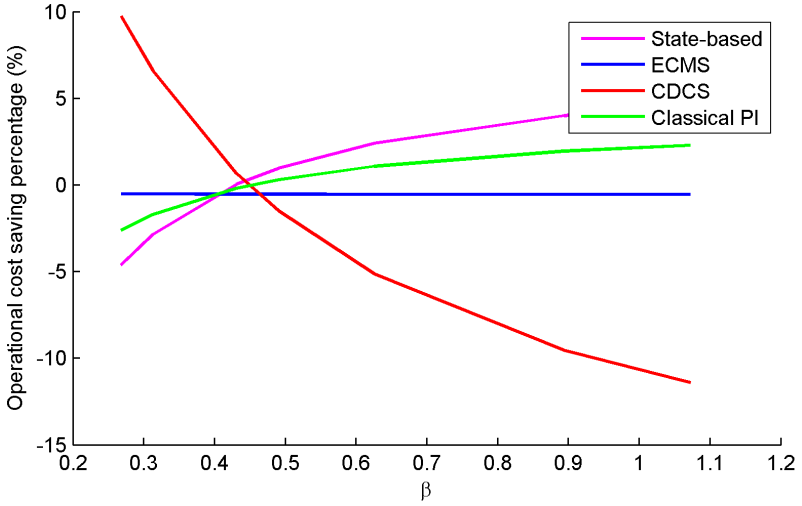

Figure 6.27: Impact of energy price ratio on operational cost saving percentage of the developed multi-scheme EMS compared to other strategies at initial battery SOC of 65%

The results shown in Figure 6.27 are associated with two factors; the hydrogen consumption saving of the multi-scheme EMS compared to other strategies and the percentages of the hydrogen and battery recharging costs from the total operational cost. Since the developed multi-scheme and ECMS strategies have approximately the same hydrogen consumption, ECMS strategy has less operational cost than the developed multi-scheme EMS by less than 1% at different β values as shown in Figure 6.27. Compared to the state-based and classical PI strategies, the developed multi-scheme EMS has higher operational cost at low β values. For higher β values, the operational cost resulting from using the developed multi-scheme EMS becomes lower than those resulting from using the state-based and classical PI strategies. This is justified by the fact that the developed multi-scheme EMS has lower hydrogen consumption than the state-based and classical PI strategies. On the other hand, the multi-scheme EMS has lower operational cost than CDCS strategy at low β values and higher operational cost than CDCS strategy at high β values. It can be noticed that, operational cost saving percentages of the developed multi-scheme EMS compared to CDCS strategy is more sensitive to β than other strategies. This is because using CDCS strategy results in the least hydrogen consumption and consequently the highest battery recharging cost.

6.4.2.4 Impact of different initial battery SOC

The reported saving percentages of the developed multi-scheme EMS in terms of total consumed energy, cost and hydrogen consumption can be affected by the initial conditions of the battery SOC. Therefore, different values of battery initial SOC have been used for the same examined voyage to study the impact of this parameter on the resulted saving percentages of the developed multi-scheme EMS. As detailed in Figure 6.28, the developed multi-scheme EMS has lower energy consumption than the four examined strategies at different initial battery SOC. The maximum energy saving percentage is 8% compared to the classical PI EMS while the minimum energy saving percentage is 0.3% compared to the state-based EMS and both values at an initial battery SOC of 50%.

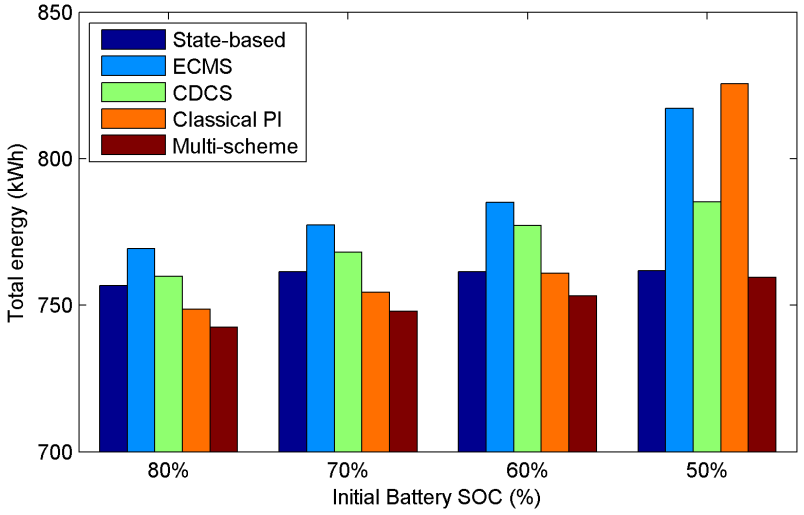

Figure 6.28: Impact of different initial battery SOC on total consumed energy saving percentage of the developed multi-scheme EMS compared to other strategies

As can be seen from Figure 6.29, using CDCS strategy results in the lowest hydrogen consumption at different initial battery SOC due to the fact that CDCS supplies the required load power from the battery system whenever possible. Compared to other strategies, the developed multi-scheme EMS has lower hydrogen consumption than the state-based and classical PI strategies at different initial battery SOC. A hydrogen consumption saving of 16.7% can be achieved by using the developed multi-scheme EMS instead of the state-based strategy at an initial battery SOC of 80%. Also, the developed multi-scheme EMS has lower hydrogen consumption than the ECMS strategy by 2.6% at an initial battery SOC of 50% and it has approximately the same hydrogen consumption of the ECMS at an initial battery SOC of 80%, 70%, and 60%. However, the developed multi-scheme EMS has higher hydrogen consumption than the CDCS strategy by 25%, 23.1%, 21.4%, and 17.5% at an initial battery SOC of 80%, 70%, 60%, and 50% respectively.

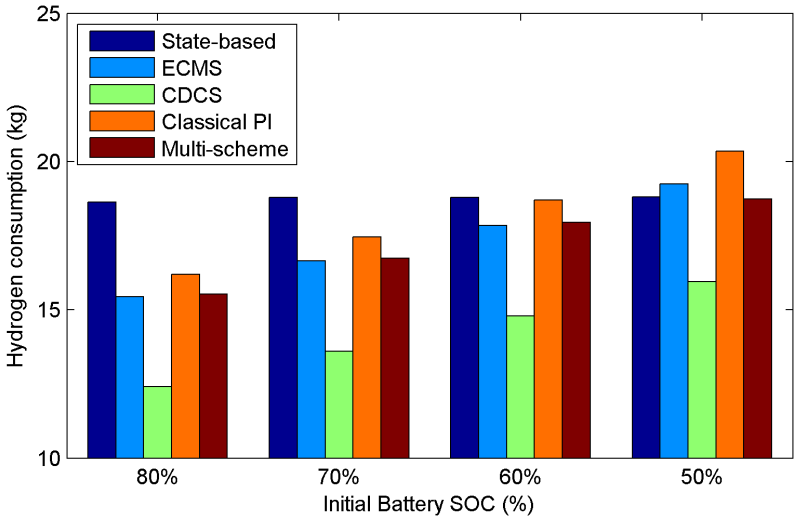

Figure 6.29: Impact of different initial battery SOC on hydrogen consumption of the developed multi-scheme EMS compared to other strategies

Regarding the operational cost saving percentage, the developed multi-scheme EMS can result in a saving of 7.9% compared to the classical PI EMS using an initial battery SOC of 50%. However, the developed multi-scheme EMS can have higher operational cost than the state-based EMS by 1.9% using an initial battery SOC of 80%. In case of starting with normal initial battery SOC between 60% and 70%, the difference between the developed multi-scheme EMS and other strategies in terms of operational cost is less than 1% as shown in Figure 6.30.

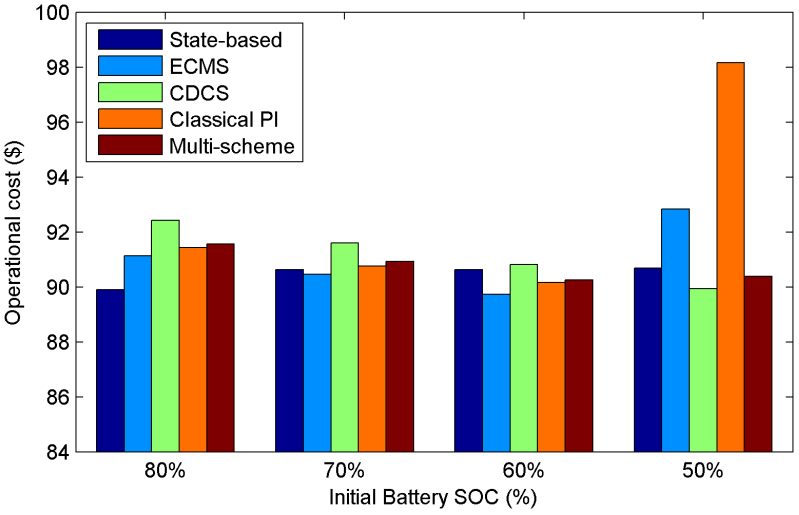

Figure 6.30: Impact of different initial battery SOC on the operational cost of the developed multi-scheme EMS compared to other strategies

As mentioned earlier, the used energy prices can influence the operational cost calculation. Therefore, the impact of different initial battery SOC on the operational cost of the developed multi-scheme EMS comparison with other strategies is reinvestigated at different β values which corresponds to hydrogen prices of 7 and 3 \$/kg. At higher

hydrogen prices, the strategies that result in hydrogen consumption saving has lower operational cost as shown in Figure 6.31. It can be noticed that Figure 6.31 is in consistent with Figure 6.29 and this is because of the dominance of fuel cost over the operational cost of the hybrid system using higher hydrogen prices. As discussed earlier, CDCS strategy is more affected by the hydrogen price because it results in the least hydrogen consumption. So, using CDCS strategy results in the least operational cost of the hybrid system at higher hydrogen prices as shown in Figure 6.31. Meanwhile, CDCS strategy results in the highest operational cost compared to other strategies at lower hydrogen prices as shown in Figure 6.32.

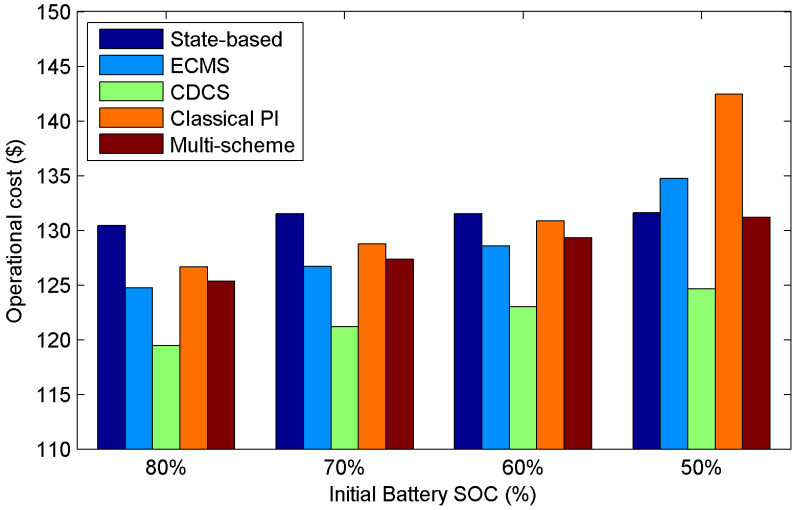

Figure 6.31: Impact of different initial battery SOC on the operational cost of the developed multi-scheme EMS compared to other strategies for hydrogen price of 7 $/kg

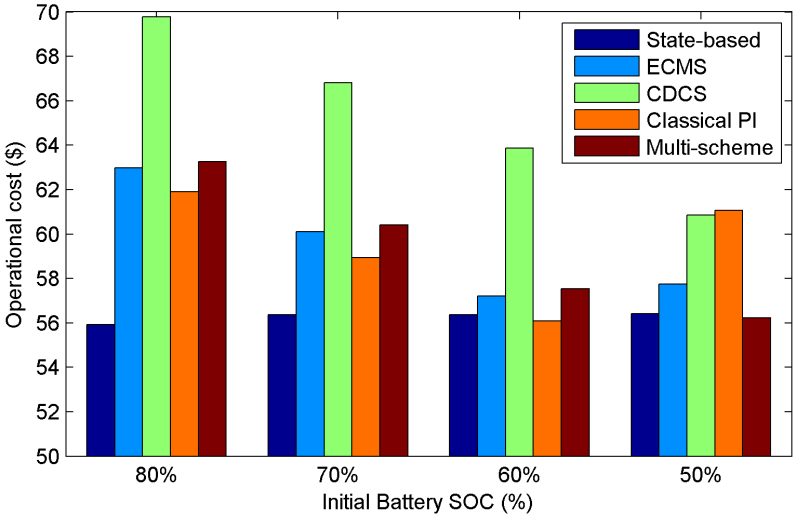

Figure 6.32: Impact of different initial battery SOC on the operational cost of the developed multi-scheme EMS compared to other strategies for hydrogen price of 3 $/kg

At higher hydrogen prices, the developed multi-scheme EMS has lower operational cost than the state-based and classical PI strategies starting with different initial battery SOC due to its hydrogen consumption saving. The developed multi-scheme EMS also has lower operational cost than the ECMS strategy at an initial battery of 50% and it has approximately the same operational cost of the ECMS starting with an initial battery SOC of 80%, 70%, and 60%. However, CDCS strategy has lower operational cost than the developed multi-scheme EMS starting with different initial battery SOC as shown in Figure 6.31. On the other hand, the developed multi-scheme EMS will have higher operational cost than the state-based, classical PI, and ECMS strategies at initial battery SOC of 80%, 70%, and 60% while it will have lower operational cost than other strategies at initial battery SOC of 50% in case of lower hydrogen prices as shown in Figure 6.32. This is because at lower hydrogen prices, the percentage of the battery recharging cost increases compared to its percentage at higher hydrogen prices.

It is evident from the results to this point that switching between different energy management strategies during ship operation using the developed multi-scheme EMS can result in an energy saving starting with different initial battery SOC and can reduce the operational cost of the hybrid system in some cases. However, will changing the used EMS during ship operation increase the operational stresses on the fuel cell and battery systems? A stress analysis is performed to compare the operational stresses resulted from using the multi-scheme EMS to other strategies in the following section.

6.4.2.5 Stress analysis

An analysis of the stresses seen by each power source is performed to investigate the effect of changing the used energy management strategy during the voyage by the proposed multi-scheme strategy on the fuel cell and battery systems. Using the same Haar wavelet transform based approach described earlier, changing the used EMS during the voyage by the multi-scheme EMS doesn't increase the stresses on the fuel cell and battery systems. As can be found in Table 6.5, the fuel cell and battery stresses are lower using the developed multi-scheme EMS than the ECMS and CDCS strategies. However, it provides slightly higher stresses on the fuel cell and battery systems than the state-based and the classical PI strategies.

Table 6.5: Overall performance comparison of different energy management strategies for the examined voyage at an initial battery SOC of 65%

	State-based	ECMS	CDCS	Classical PI	Multi-scheme
Fuel cell stress	29.26	37.92	42.37	31.69	32.03
Battery stress	15.85	29.92	40.61	19.18	22.49
Hydrogen consumption (kg)	18.79	17.25	14.19	18.07	17.35
Battery SOC (%)	65 – 66.11	65 – 54.35	65 – 30	65 – 59.99	65 –54.33

6.5 Summary

The influence of the ship operational profile's nature on the performance of hybrid fuel cell was investigated in this chapter. The first hybrid fuel cell passenger ship *FCS Alsterwasser* which has an operational profile with significant speed and power variations was used as a case study in order to study the effect of changing the used energy management strategy on the hybrid system performance. Results showed that the efficiency and performance of fuel cell hybrid systems depend considerably on the used energy management strategy which is responsible for splitting the required power between the different components of the hybrid system. Moreover, the effect of the used EMS is higher for ships whose operational profile has more variations in the required power and speed.

In this chapter, we first proposed an improved PI energy management strategy for marine applications that takes fuel cell efficiency into consideration as an input to the original PI EMS. The proposed strategy has been studied for the first fuel cell passenger vessel showing better performance than other strategies in terms of fuel cell stress and having lower hydrogen consumption than the state-based and the classical PI strategies. For a full driving cycle of 8 hours, a performance comparison using different strategies has been made in terms of total consumed energy, total cost, battery state of charge, fuel cell efficiency, hydrogen consumption, and the operational stresses seen by each power source. The total consumed energy included the required energy to recharge the battery back to its initial SOC in addition to the consumed battery and fuel cell energies during the examined driving cycle. Simulation results showed that a daily hydrogen saving of 5.1% and 1.3% compared to the state-based and the classical PI strategies respectively can be achieved by adopting the proposed PI strategy with no additional first cost or hardware changes. This study has contributed towards a publication [335].

Moreover, taking fuel cell efficiency into consideration as an input to the energy management strategy as proposed in this study has contributed in better fuel cell performance during operation and less stress on the fuel cell stack which prolongs its lifetime and resulted in less hydrogen consumption. Also, using the improved PI EMS can result in lower operational cost than other strategies. Since these results are sensitive to the used parameters, sensitivity analysis of the initial battery SOC and the energy prices were performed. On the other hand, the total energy consumption using the the improved PI EMS was higher than the original PI EMS using different initial battery SOC which reduces the energy efficiency of the ship. Therefore, a multi-scheme EMS with an objective of minimizing the total consumed energy was developed in this chapter as well.

A novel multi-scheme EMS that contains four different strategies was developed and compared to other strategies in this chapter. The objective of the developed multi-scheme EMS is to reduce the total consumed energy of the ship for the sake of

increasing ship energy efficiency. The performance comparison was made as well in terms of the total consumed energy, operational cost, hydrogen consumption, battery SOC, and operational stresses on the fuel cell and battery systems. Simulation results showed that the developed multi-scheme EMS has lower energy consumption than other strategies while starting with different initial battery SOC with and the energy saving percentage can be as much as 8%. In the case of starting with a normal initial battery SOC of 65%, using the developed multi-scheme EMS can result in a hydrogen consumption saving of 7.7% and 4% compared to the state-based and classical PI strategies but it has higher hydrogen consumption saving than the CDCS strategy by 22.2% and the approximately the same hydrogen consumption of the ECMS strategy. Furthermore, the developed multi-scheme EMS has nearly the same operational cost of other strategies. Sensitivity analyses of different energy prices and initial battery SOC have been also made for the developed multi-scheme EMS. A stress analysis was also performed to investigate the effect of changing the used EMS on the performance of the fuel cell and battery systems which showed that changing the used EMS using the developed multi-scheme EMS does not increase the operational stresses on the fuel cell and battery systems. This study has also contributed towards a publication [336].

Chapter 7

Conclusions

The potential of hybrid fuel cell propulsion systems for marine applications was investigated in this work using numerical simulation in order to reduce ship emissions and noise from global shipping. Mathematical modelling and simulation of the whole ship system were accomplished allowing a detailed investigation of different power sources including fuel cells to assess its effectiveness and compare it to conventional diesel systems economically and environmentally. The developed ship simulator, which is a time-domain quasi-steady three degree of freedom ship simulator, offered significant aid in proposing a hybrid fuel cell/battery propulsion system for the case study *M/S Smyril* through investigating different fuel cell/battery combinations. The proposed hybrid fuel cell propulsion system clearly demonstrated its ability of providing the ship with the required power to perform its intended voyage. In addition, the proposed hybrid fuel cell system showed potential in terms of weight and size savings compared to conventional diesel systems. However, with the current costs associated with fuel cells and hydrogen, conventional diesel systems are still more economically feasible. Also, the developed ship simulator was used to study different strategies of energy management and compare between them which includes the presenting of an improvement to the classical PI controller based EMS in addition to the development of a novel multi-scheme EMS for the first time for marine applications. Savings up to 8% and 16.7% of energy and hydrogen consumption respectively were demonstrated for a hybrid fuel cell propulsion system through adopting the developed multi-scheme EMS. The following conclusion can be made as a result of this work:

- Among the different fuel cell technologies available, PEMFC is considered as the optimal technology to be used for marine applications. This is due to its advantages drawn from review of literature such as solid electrolyte, high efficiency even at low loads, low operating temperature, quick start-up, high power density, low noise, and zero emissions as discussed in Chapter 2.

- The used building block modular approach has simplified the ship simulator development and can enable its improvement for future studies. It has also increased the flexibility of the simulator by providing the ability to switch between constant-speed and constant-rpm modes of ship operation. Moreover, different power sources can be used for the ship propulsion.

- Regarding the calm water resistance, both Hollenbach and Holtrop-Mennen methods provided close agreement with the experimental results. However, it is recommended to use Hollenbach method due to its relatively modern database and because it requires less input parameters.

- Based on the presented verification and validation studies, it was shown that the developed ship simulator can provide good prediction of the ship speed and fuel consumption. Validation and verification of individual blocks have been made as well as end-to-end validations of the total ship simulator. Real ship operational data of the tanker ship *'Esso Osaka'*, the passenger ship *FCS Alsterwasser* and the ferry *'M/S Smyril'* have been used to validate the total ship simulator showing good agreement. Also, numerical results and experimental results from towing tank and wind tunnel tests have been compared well with simulator results. For the *M/S Smyril*, simulation results of speed and fuel consumption volume flow rate were in good agreement with the real operational data. The error between the simulation results and the real fuel consumption was about 5% which is considered reasonable given the level of uncertainty in the modelling assumptions and acceptable as a basis for comparison.

- The developed total ship simulator showed its capability of investigating different fuel cell and battery combinations as well as using different energy management strategies in the sizing optimization study performed to propose a hybrid fuel cell/battery propulsion system for the *M/S Smyril*. It can be used, therefore, to design fuel cell based hybrid systems with different hybrid ratio using different strategies of energy management.

- The developed simulator can also be used to assess the effectiveness of different EEDI and SEEMP measures such as slow steaming, voyage execution, and hybrid electric fuel cell propulsion system showing the advantages and disadvantages in terms of voyage time, fuel consumption, emissions, machinery weight and volume, etc. which contributed towards a publication in [337].

- As highlighted in Chapter 5, the used strategy of energy management affects the resulting optimal fuel cell/battery combination where the four used strategies resulted in four different fuel cell battery combinations in the performed sizing optimization study. However, the difference between these combinations in terms of total cost according to the sizing objective was less than 1%. This is linked to the nature of the ship operational profile which has small variation in speed

and power requirements as shown by parametric studies using two different ship operational profiles.

- The performed sizing study revealed that increasing the number of fuel cell blocks for the hybrid fuel cell system results in reducing the hydrogen consumption. However, this will increase the capital cost of the hybrid system.

- Sensitivity studies of different hydrogen prices highlight that the selection of the fuel cell blocks number is greatly affected by the hydrogen cost. This is because hydrogen cost dominates the total cost of the optimal hybrid fuel cell/battery propulsion system, accounting for over 70% of the cost. Therefore, at higher hydrogen prices, the optimal fuel cell/battery combination tends to have more fuel cell blocks.

- Maintenance and replacement costs of the fuel cell and battery systems should be included in the sizing optimization cost function because of the relatively high cost and short life of fuel cells compared to the conventional power sources. For the proposed fuel cell/battery combination, maintenance and replacement costs accounts for about 18% of the total considered cost in the sizing study.

- Hybrid fuel cell power systems can result in weight and size saving compared to conventional diesel engines. Regarding the examined ship *M/S Smyril*, the proposed optimal fuel cell/battery combination has lower weight and size by 7.3% and 18.6% compared to the conventional diesel engines taking into consideration the required weight and size of the daily hydrogen tank, electric motors and controllers of the proposed hybrid system.

- More than 10 tonnes of emissions emitted by the conventional diesel engines of the examined ship *M/S Smyril* per voyage can be eliminated through using the proposed hybrid fuel cell system. Moreover, less noise levels are achieved using fuel cells which reduces the need for sound insulation systems and increase the passengers comfort levels.

- With the current technology price of PEMFC, the first cost and maintenance cost of hybrid fuel cell systems still higher than conventional diesel systems. However, with mass production of fuel cells and the R&D current focus on improving the fuel cell design and membrane materials and using more cost-effective catalyst materials, this will reduce fuel cell's first and maintenance costs and make it more cost competitive with conventional power sources.

- By taking into consideration the environmental damage cost caused by using diesel oil, hydrogen can be competitive as a marine fuel with diesel oil especially hydrogen generated from petroleum fuels. In this project, it is assumed that hydrogen is produced from wind energy in order to have a real zero-emission solution. As a result, the hybrid fuel cell system fuel cost was higher than the conventional

diesel system for the examined voyage because recent hydrogen price is still higher than marine diesel oil. In the mid and long terms, hydrogen generated by wind energy will be more competitive with diesel oil due to reduction of electrolyzer and compressor costs. Using oil and hydrogen prices projection, fuel cost of the hybrid fuel cell system would be less than the fuel cost of the conventional diesel system in the mid term considering the environmental damage cost.

- The comparative analysis of different energy management strategies demonstrated that energy and fuel consumption of hybrid fuel cell systems are clearly affected by the used EMS for ships with high variation in power requirements. As shown for *FCS Alsterwasser*, changing the used strategy can reduce the hydrogen consumption by about 23%.

- A sensitivity analysis of different initial battery SOC has been performed which showed that CDCS strategy results in the lowest hydrogen consumption of hybrid fuel cell systems. However, CDCS can result in high fuel cell and battery operational stresses.

- Using fuel cell efficiency as an input to the classical PI controller based EMS can improve its performance by operating the fuel cell more at high efficiency region [335]. Results in Chapter 6 showed that the improved PI EMS has better performance than other strategies in terms of fuel cell operational stress which increases its lifetime. Operational cost saving ranging from 0.9 to 2.1% for the improved PI EMS was demonstrated. Moreover, the improved PI EMS has lower hydrogen consumption than the original PI EMS with saving values varies between 1.3% to 1.4% starting with different initial battery SOC.

- Using multi-scheme EMS can reduce the hydrogen and energy consumption of hybrid fuel cell/battery propulsion systems of ships that have significant variation in its power demand. A new approach to design an energy efficient multi-scheme EMS was presented in Chapter 6 which contributed towards a publication [336]. For the examined ship *FCS Alsterwasser*, a maximum energy and hydrogen saving percentages of 8% and 16.7% respectively can be achieved using the developed multi-scheme EMS.

- It was also found that changing the used strategy during the examined voyage through the developed multi-scheme EMS will not increase the operational stresses on the fuel cell and battery systems.

- Furthermore, the developed multi-scheme resulted in nearly the same operational cost as other strategies starting with different initial battery SOC as shown by the performed sensitivity analyses.

7.1 Novelty

This thesis investigated the effectiveness of fuel cells as a main source of power for hybrid propulsion systems of marine transportation applications considering the current status of fuel cell technology and providing further insight into the effect of energy management strategies on the performance of these systems. The performance of the classical PI controller based energy management strategy was improved in this study by using fuel cell efficiency as an input to the strategy controller in order to improve the fuel cell performance and reduce its hydrogen consumption and operational stress to extend its lifetime which considers as the most technically challenging barrier to the widespread usage of fuel cell systems. The project also proposed a new approach of designing more efficient multi-scheme EMS for marine applications that have significant variation in its power demand for the first time. The novel multi-scheme EMS was presented with an objective of minimizing the energy consumption in order to increase the energy efficiency of the examined ship with no additional first cost, operational stresses or hardware changes. The effect of the used energy management strategy on the sizing optimization output of hybrid fuel cell systems was also investigated. Moreover, the cost function of the sizing optimization study was enhanced by taking the replacement and maintenance costs of the fuel cell and battery systems into consideration.

In order to conduct this investigation, a flexible three degree of freedom quasi-study total ship system simulator was built using building block modular approach to facilitate ship system modelling and simulation. The developed time domain simulation tool is able to simulate the performance of ships with both mechanical or electrical propulsion systems utilizing different power sources which includes conventional two and four-stroke diesel engines, fuel cells and batteries. Also, the simulation tool can switch between constant-speed and constant-rpm modes of ship operation. Furthermore, this simulation tool provides a framework for future studies involving simulation of ship systems. It can be used to design fuel cell based power systems and assess its performance with different topologies, hybrid ratio, and energy management strategies which can be done for different ship types and different operational profiles. The simulator also has the potential to test different EEDI and SEEMP measures such as slow steaming, voyage execution, trim/draft changing, etc.

7.2 Future Work

Different areas have been identified for further investigation as follows:

- It was evident from the results that the hybrid fuel cell system performance and energy consumption depend considerably on the used EMS and the

ship operational profile. Therefore, it would be beneficial to conduct experimental work using ship models in order to study different types of energy management strategies and different ship operational profiles. Different manoeuvres can also be performed to prove that hybrid fuel cell systems are capable of meeting the IMO requirements but care should be taken with the scaling-up issue.

- Since electricity and heat are the outputs of PEM fuel cell operation, different heat recovery systems such as organic Rankine cycle should be proposed and optimized to get higher efficiency of the system through cogeneration and trigeneration systems.
- Future work should also focus on the demonstration of hybrid fuel cell propulsion system for marine transportation applications. A coastal area such as Southampton would be a perfect location for a hybrid fuel cell ferry to create an eco-friendly transportation service. The route would be around Itchen River where it is important to have less emission and noise which can provided by fuel cell operation. A hydrogen filling station may also be part of this project which will solve the issue of hydrogen bunkering for the ship. However, to successfully develop this project, more in-depth economical and technical studies are essential.
- The developed total ship system simulator can assist further studies of other EEDI and SEEMP measures suggested by the IMO to increase the energy efficiency of ships such as weather routing, voyage execution, waste heat recovery, trim and draft optimization, etc. These studies may require upgrading the used manoeuvrability model to four or six DOF. Also, using more advanced diesel engine models is proposed to accurately represent the engine behaviour required for investigating SEEMP measures such as waste heat recovery option. Different propeller types should also be considered and added to the simulator to extend the applicability of the ship simulator. Moreover, developing a MATLAB code to download the required weather parameters form online sources such as GFS database and fed it into the simulation environment automatically in case that this data is not available. It is also proposed to study different ship types with the develop simulator but more real ship operational data will be required for the validation.

7.3 Concluding Remark

Based on the findings of this research project, the concept of zero emission ships can be achieved using hybrid fuel cell systems using hydrogen generated from clean energy sources as a fuel. It is just a matter of time until fuel cell first cost decreases and hydrogen storage technologies improve, so it is believed that hybrid fuel cell power trains will have higher market share.

References

[1] "Review of maritime transport 2016," tech. rep., United Nations Conference on Trade and Development (UNCATD), 2016.

[2] "Lloyds register fairplay, world fleet statistics 1900-2010," tech. rep.

[3] *Reduction of GHG Emissions From Ships - Third IMO GHG Study 2014*. London, UK: International Maritime Organization (IMO), July 2014.

[4] "Energy and climate change - world energy outlook special report," tech. rep., International Energy Agency IEA, France, 2015.

[5] "U.S. energy information administration, independent statistics and analysis." `http://www.eia.gov/dnav/pet/hist_xls/RBRTEa.xls`, 2015.

[6] "CO_2 emissions from fuel combustion highlights," tech. rep., International Energy Agency IEA, Paris, 2016.

[7] J. Larminie and A. Dicks, *Fuel Cell Systems Explained*. John Wiley & Sons Ltd,, second ed., 2003.

[8] B. Cook, "Introduction to fuel cells and hydrogen technology," *Engineering Science and Education Journal*, 2002.

[9] D. Hart, F. Lehner, R. Rosa, and J. Lewis, "The fuel cell industry review 2015," tech. rep., E4tech, 2015.

[10] "Fuel cell system cost - 2012," *DOE Fuel Cell Technologies Program Record*, September 2012.

[11] P. Thounthong, S. Ra and B. Davat, "Energy management of fuel cell/battery/supercapacitor hybrid power source for vehicle applications," *Journal of Power Sources*, vol. 193, no. 1, pp. 376 – 385, 2009.

[12] B. Oleksiy, K. Masashi, and N. Shigeru, "Dynamics of diesel engine in the framework of ship propulsion plant," in *Conference proceedings,*

the Japan Society of Naval Architects and Ocean Engineers, vol. 8, pp. 335–338, May 2009.

[13] M. Jefferson, P. L. Zhou, and G. Hindmarch, "Analysis by computer simulation of a combined gas turbine and steam turbine (COGAS) system for marine propulsion," *Journal of Marine Engineering and Technology*, vol. 2, no. 1, pp. 43–53, 2003.

[14] K. U. Hollenbach, "Estimating resistance and propulsion for single-screw and twin-screw ships," *Ship Technology Research*, vol. 45, pp. 72–76, 1998.

[15] "Fuel cell stack." `http://uk.mathworks.com/help/physmod/sps/powersys/ref/fuelcellstack.html`. Accessed on: 18/11/2014.

[16] "Battery." `http://uk.mathworks.com/help/physmod/sps/powersys/ref/battery.html`. Accessed on: 18/11/2014.

[17] S. Motapon, L.-A. Dessaint, and K. Al-Haddad, "A comparative study of energy management schemes for a fuel-cell hybrid emergency power system of more-electric aircraft," *Industrial Electronics, IEEE Transactions on*, vol. 61, no. 3, pp. 1320–1334, 2014.

[18] L. Xu, M. Ouyang, J. Li, F. Yang, L. Lu, and J. Hua, "Optimal sizing of plug-in fuel cell electric vehicles using models of vehicle performance and system cost," *Applied Energy*, vol. 103, pp. 477–487, 2013.

[19] J. W. Stettler, *Steady and unsteady dynamics of an azimuthing podded propulsor related to vehicle maneuvering*. PhD thesis, Massachusetts Institute of Technology, 2004.

[20] J. Han, J.-F. Charpentier, and T. Tang, "An energy management system of a fuel cell/battery hybrid boat," *Energies*, vol. 7, pp. 2799–2820, 2014.

[21] "GPS visualizer." `http://www.gpsvisualizer.com/`. Accessed on: 25/7/2014.

[22] EIA, "International energy outlook 2016," tech. rep., U.S. Energy Information Administration, May 2016.

[23] `http://www.hadag.de/english/`. Accessed on: 25/4/2015.

[24] N. Acomi and O. C. Acomi, "Improving the voyage energy efficiency by using EEOI," *Procedia - Social and Behavioral Sciences*, vol. 138, pp. 531–536, 2014.

[25] "IMO secretariat, main events in IMO's work on limitation and reduction of greenhouse gas emissions from international shipping." `http://www.imo.org/OurWork/Environment/PollutionPrevention/AirPollution/Documents/Main%20events%20IMO%20GHG%20work%20-%20October%202011%20final.pdf`, October 2011.

[26] A. Kirubakaran and R. N. Shailendra Jain, "A review on fuel cell technologies and power electronic interface," *Renewable and Sustainable Energy Reviews*, vol. 13, pp. 2430–2440, 2009.

[27] K. Sopian and W. R. W. Daud, "Challenges and future developments in proton exchange membrane fuel cells," *Renewable Energy*, vol. 31, pp. 719–727, 2006.

[28] S. Srinivasan, *Fuel Cell From Fundamentals to Applications*. Springer, 2006.

[29] D. J. L. Brett, P. Aguiar, N. P. Brandon, R. N. Bull, R. C. Galloway, G. W. Hayes, K. Lillie, C. Mellors, C. Smith, and A. R. Tilley, "Concept and system design for a ZEBRA batteryintermediate temperature solid oxide fuel cell hybrid vehicle," *Journal of Power Sources*, vol. 157, no. 2, pp. 782 – 798, 2006.

[30] D. Linden and T. B. Reddy, eds., *Handbook of Batteries*. McGraw-Hill, third ed., 2002.

[31] R. C. Galloway and C.-H. Dustmann, "ZEBRA battery - material cost availability and recycling," in *International Electric Vehicle Symposium (EVS-20)*, (Long Beach, California), November 2003.

[32] B. L. Norris, J. Newmiller, and G. Peek, "NAS® battery demonstration at american electric power, a study for the DOE energy storage program," tech. rep., Sandia National Laboratories, March 2007.

[33] H. L. Ferreira, R. Garde, G. Fulli, W. Kling, and J. P. Lopes, "Characterisation of electrical energy storage technologies," *Energy*, vol. 53, pp. 288–298, 2013.

[34] C. Vartanian and N. Bentley, "A123 systems' advanced battery energy storage for renewable integration," in *Power Systems Conference and Exposition (PSCE), 2011 IEEE/PES*, pp. 1–6, March 2011.

[35] S. McCluer and J.-F. Christin, "Comparing data center batteries, flywheels, and ultracapacitors," *White Paper*, vol. 65, 2008.

[36] K. U. Hollenbach, "Beitrag zur abschätzung von widerstand und propulsion von ein- und zweischraubenschiffen im vorentwurf," Tech. Rep. 588, Institut Für Schiffbau Der Universit´at Hamburg, 1997.

[37] G. Aertssen, "Service performance and trails at sea," *Report of Performance Committee, 12th ITTC*, p. 210:214, 1969.

[38] Y. J. Kwon, "Speed loss due to added resistance in wind and waves," *The Naval Architect*, pp. 14–16, March 2008.

[39] J. S. Carlton, *Marine Propellers and Propulsion*. Elsevier Ltd., 2007.

[40] F. Geos, "Wind and wave frequency distributions for sites around the british isles, offshore technology report," tech. rep., Southampton Oceanography Centre, 2001.

[41] Ø. Buhaug, J. Corbett, Ø. Endresen, V. Eyring, J. Faber, S. Hanayama, D. Lee, D. Lee, H. Lindstad, A. Markowska, *et al.*, "Second IMO GHG study 2009," *International Maritime Organization (IMO) London, UK*, vol. 20, 2009.

[42] Q. Cai, D. J. L. Brett, D. Browning, and N. P. Brandon, "A sizing-design methodology for hybrid fuel cell power systems and its application to an unmanned underwater vehicle," *Journal of Power Sources*, vol. 195, pp. 6559 – 6569, 2010.

[43] A. Züttel, "Materials for hydrogen storage," *Materials Today*, vol. 6, no. 9, pp. 24–33, 2003.

[44] G. Griffiths, D. Reece, P. Blackmore, M. Lain, S. Mitchell, and J. Jamieson, "Modeling hybrid energy systems for use in AUV′s," *Proc. Unmanned Untethered Submersible Technology*, 2005.

[45] "Virtue ice class vessels." `http://www.bp.com/en/global/bp-shipping/about-bp-shipping/who-we-are/our-fleet/virtue-class-overview/virtue-class.html`. Accessed on: 15/10/2014.

[46] "Development of a hybrid fuel cell ferry," tech. rep., John J. McMullen Associates, Incorporated, August 2003.

[47] "ABB DC motors catalog." `http://aac-eg.net/images/DC_motors_DMI_catalog_low%20res.pdf`, 2011.

[48] "NedStack PS50 product data." `http://www.fuelcellmarkets.com/content/images/articles/ps50.pdf`. Accessed on: 10/02/2016.

[49] "Lithium-ion specifications." `http://optimum-china.en.alibaba.com/product/437274726-212297973/rechargeable_HEV_EV_bus_battery_pack_of_lifepo4_600v_500ah.html`. Accessed on: 10/02/2016.

[50] C. Yang and J. Ogden, "Determining the lowest-cost hydrogen delivery mode," *International Journal of Hydrogen Energy*, vol. 32, no. 2, pp. 268–286, 2007.

[51] D. C. Bose, *Principles of Management and Administration*. PHI Learning Pvt. Ltd., second ed., September 2012.

[52] "Shipping statistics and market review," tech. rep., Institute of Shipping Economics and Logistics, Bremen, Germany, 2012.

[53] K. Ware, "Assessment of the impacts of shipping on the marine environment," tech. rep., Monitoring and Assessment Series OSPAR Commission, 2009.

[54] S. Kollamthodi, C. Brannigan, M. Harfoot, I. Skinner, C. Whall, L. Lavric, R. Noden, D. Lee, vind Buhaug, K. Martinussen, R. Skejic, I. Valberg, J. C. Brembo, V. Eyring, and J. Faber, *Greenhouse gas emissions from shipping: trends, projections and abatement potential:Final Report*. No. 4, September 2008.

[55] A. Numata, T. Kumagai, Y. Nagae, and S. Osafune, "Increase of thermal efficiency and reduction of NO_x emissions in DI diesel engines," *Technical Review*, vol. 38, pp. 136–140, October 2001.

[56] C. D. Holmes, M. J. Prather, and G. C. M. Vinken, "The climate impact of ship NO_x emissions: an improved estimate accounting for plume chemistry," *Atmospheric Chemistry and Physics*, vol. 14, pp. 6801–6812, 2014.

[57] V. Eyring, H. W. Köhler, J. van Aardenne, and A. Lauer, "Emissions from international shipping: 1. the last 50 years," *Journal of Geophysical Research*, vol. 110, p. 19842012, 2005.

[58] "Air emissions & EMSA overview." `http://www.emsa.europa.eu/implementation-tasks/environment/air-pollution/149-air-pollution/96-air-emissions.html`. Accessed on: 24/08/2014.

[59] V. Matthias, I. Bewersdorff, A. Aulinger, and M. Quante, "The contribution of ship emissions to air pollution in the north sea regions," *Environmental Pollution*, vol. 158, pp. 2241–2250, 2010.

[60] "Sulphur regulations: bad for jobs and the environment," *Maritime UK*, October 2012.

[61] A. Badino, D. Borelli, T. Gaggero, E. Rizzuto, and C. Schenone, "Control of airborne noise emissions from ships," in *International Conference on Advances and Challenges in Marine Noise and Vibration (MARNAV)*, (Glasgow, Scotland, UK), pp. 21–29, September 2012.

[62] "Code on noise levels on board ships, 2014 edition."

[63] "Work programme of the committee and subsidiary bodies, minimizing the introduction of incidental noise from commercial shipping operations into the marine environment to reduce potential adverse impacts on marine life," June 2008.

[64] "Implementing a ship energy efficiency management plan (SEEMP) - guidance for shipowners and operators," tech. rep., Lloyd's Register, June 2012.

[65] "EEDI tests and trials for EMSA," tech. rep., DELTAMARIN, December 2009.

[66] P. P. Edwards, V. L. Kuznetsov, W. I. David, and N. P. Brandon, "Hydrogen and fuel cells: towards a sustainable energy future," *Energy policy*, vol. 36, no. 12, pp. 4356–4362, 2008.

[67] Z. Karni, R. Willigan, C. Artze, M. Badal, W. Gordon, , J. Halder, R. Levesque, and W. Forsyth, "Comparative life cycle costs of fuel cells and other propulsion systems," Tech. Rep. CG-D-19-00, U.S. Coast Guard Research and Development Center, January 2000.

[68] G. Sattler, "Fuel cells going on-board," *Journal of Power Sources*, vol. 86, pp. 61–67, 2000.

[69] J. J. de Troya, C. lvarez, C. Fernez-Garrido, and L. Carral, "Analysing the possibilities of using fuel cells in ships," *International Journal of Hydrogen Energy*, vol. 41, no. 4, pp. 2853 – 2866, 2016.

[70] S. Sortland, "Hybrid propulsion system for anchor handling tug supply vessels," *Wärtsila Technical Journal*, vol. 1, pp. 45–48, 2008.

[71] E. K. Dedes, D. A. Hudson, and S. R. Turnock, "Assessing the potential of hybrid energy technology to reduce exhaust emissions from global shipping," *Energy Policy*, vol. 40, pp. 204–218, 2012.

[72] L. Jun and W. Liming, "The research of propulsion system matching calculation of hybrid diesel and wind propulsion ship," in *Mechanic*

Automation and Control Engineering (MACE), 2010 International Conference on, pp. 4085–4088, June 2010.

[73] M. C. D. de Baldasano, F. J. Mateos, L. R. NRivas, and T. J. Leo, "Conceptual design of offshore platform supply vessel based on hybrid diesel generator-fuel cell power plant," *Applied Energy*, vol. 116, pp. 91–100, 2014.

[74] C. P. Casson, C. J. Wood, D. J. Bricknell, K. Daffey, and R. Partridge, "Power and propulsion for the new global combatant," 2006.

[75] S.-Y. Kim and S.-K. Sul, "Integrated power system of high speed destroyer for increased fuel-efficiency and power-reliability," in *Electric Machines Technology Symposium*, May 2012.

[76] S. De Breucker, E. Peeters, and J. Driesen, "Possible applications of plug-in hybrid electric ships," in *Electric Ship Technologies Symposium, 2009. ESTS 2009. IEEE*, pp. 310–317, April 2009.

[77] G. Shu, Y. Liang, H. Wei, H. Tian, J. Zhao, and L. Liu, "A review of waste heat recovery on two-stroke IC engine aboard ships," *Renewable and Sustainable Energy Reviews*, vol. 19, pp. 385–401, 2013.

[78] J. Huang, L. Lin, Y. Wang, J. Qin, A. P. Roskilly, L. Li, T. Ouyang, and Y. Yu, "Experimental study of the performance and emission characteristics of diesel engine using direct and indirect injection systems and different fuels," *Fuel Processing Technology*, vol. 92, no. 7, pp. 1380–1386, 2011.

[79] G. Benvenuto and U. Campora, "Performance prediction of a faulty marine diesel engine under different governor settings," in *International Conference on Marine Research and Transportation*, (Italy), June 2007.

[80] V. Lamaris and D. Hountalas, "A general purpose diagnostic technique for marine diesel engines – Application on the main propulsion and auxiliary diesel units of a marine vessel," *Energy Conversion and Management*, vol. 51, no. 4, pp. 740–753, 2010.

[81] "Frequently asked questions from marine engine owners and rebuilders about epas marine remanufacture program," *United States Environmental Protection Agency (EPA)*, February 2009.

[82] A. M. El-Nashar, "Cogeneration for power and desalination – state of the art review," *Desalination*, vol. 134, no. 1, pp. 7–28, 2001.

[83] N. A. Odeh and T. T. Cockerill, "Life cycle analysis of UK coal fired power plants," *Energy Conversion and Management*, vol. 49, no. 2, pp. 212–220, 2008.

[84] A. Ragheb and M. Ragheb, "Wind turbine gearbox technologies," *Fundamental and Advanced Topics in Wind Power*, pp. 189–206, June 2011.

[85] F. Barbir, *PEM fuel cells: theory and practice*. Academic Press, 2013.

[86] A. K. Ådnanes, *Maritime electrical installations and diesel electric propulsion*. ABB, 2003.

[87] H. Grimmelius, P. de Vos, M. Krijgsman, and E. van Deursen, "Control of hybrid ship drive systems," in *10th International Conference on Computer Applications and Information Technology in the Maritime Industries (COMPIT), Berlin, downloadable at www.compit.info*, 2011.

[88] M. Oka, K. Hiraoka, and K. Tsumura, "Development of next-generation LNGC propulsion plant and hybrid system," *Mitsubishi Heavy Industries Technical Review*, vol. 41, no. 6, 2004.

[89] R. Alvarez, P. Schlienger, and M. Weilenmann, "Effect of hybrid system battery performance on determining CO_2 emissions of hybrid electric vehicles in real-world conditions," *Energy Policy*, vol. 38, pp. 6919–6925, November 2010.

[90] P. Thounthong, V. Chunkag, P. Sethakul, S. Sikkabut, S. Pierfederici, and B. Davat, "Energy management of fuel cell/solar cell/supercapacitor hybrid power source," *Journal of Power Sources*, vol. 196, pp. 313–324, 2011.

[91] J. Cho, H.-S. Kim, and K. Min, "Transient response of a unit proton-exchange membrane fuel cell under various operating conditions," *Journal of Power Sources*, vol. 185, no. 1, pp. 118–128, 2008.

[92] Y. M. Welaya, M. M. E. Gohary, and N. R. Ammar, "A comparison between fuel cells and other alternatives for marine electric power generation," *International Journal of Naval Architecture and Ocean Engineering*, vol. 3, no. 2, pp. 141 – 149, 2011.

[93] L. K. C. Tse, S. Wilkins, N. McGlashan, B. Urban, and R. Martinez-Botas, "Solid oxide fuel cell/gas turbine trigeneration system for marine applications," *Journal of Power Sources*, vol. 196, pp. 3149–3162, 2011.

[94] E. Carlson, P. Kopf, J. Sinha, S. Sriramulu, and Y. Yang, "Cost analysis of PEM fuel cell systems for transportation," tech. rep., National Renewable Energy Laboratory, September 2005.

[95] R. Remick and D. Wheeler, "Molten carbonate and phosphoric acid stationary fuel cells: Overview and gap analysis," tech. rep., National Renewable Energy Laboratory, September 2010.

[96] P. Garcia, L. M. Fernandez, C. A. Garcia, and F. Jurado, "Fuel cell-battery hybrid system for transport applications," in *International Conference on Electrical Machines and Systems ICEMS*, November 2009.

[97] K. Subramanyan, U. M. Diwekar, and A. Goyal, "Multi-objective optimization for hybrid fuel cells power system under uncertainty," *Journal of Power Sources*, vol. 132, pp. 99–112, 2004.

[98] M. W. Ellis, M. R. V. Spakovsky, and D. J. Nelson, "Fuel cell systems: Efficient, flexible energy conversion for the 21st century," *Proceedings of the IEEE*, vol. 89, no. 12, pp. 1808–1818, 2001.

[99] C. K. Dyer, "Fuel cells for portable applicatlons," *Fuel Cells Bulletin*, no. 42, pp. 8–9, 2002.

[100] K. Akiyama, S. Matsumoto, A. Miyasaka, and T. Shodai, "An air-breathing single cell small proton exchange membrane fuel cell system with ab5-type metal hydride and an ultra-low voltage input boost converter," *Journal of Power Sources*, vol. 186, pp. 37–44, 2009.

[101] C. W. Blake and C. H. Rivkin, "Stationary fuel cell application codes and standards: Overview and gap analysis," tech. rep., National Renewable Energy Laboratory, September 2010.

[102] P. Britz and N. Zartenar, "PEM-fuel cell system for residental applications," *Fuel Cells*, vol. 4, no. 4, pp. 269–275, 2004.

[103] T. Mahlia and P. Chan, "Life cycle cost analysis of fuel cell based cogeneration system for residential application in malaysia," *Renewable and Sustainable Energy Reviews*, vol. 15, pp. 416–426, 2011.

[104] Z. Yu, J. Han, and X. Cao, "Investigation on performance of an integrated solid oxide fuel cell and absorption chiller tri-generation system," *International Journal of Hydrogen Energy*, vol. 36, pp. 12561–12573, 2011.

[105] S. Ma, J. Wang, Z. Yan, Y. Dai, and B. Lu, "Thermodynamic analysis of a new combined cooling, heat and power system driven by solid oxide fuel cell based on ammoniawater mixture," *Journal of Power Sources*, vol. 196, pp. 8463–8471, 2011.

[106] A. Mai, B. Iwanschitz, U. Weissen, R. Denzler, D. Haberstock, V. Nerlich, J. Sfeir, and A. Schuler, "Status of hexis SOFC stack development and the galileo 1000 N micro-CHP system," in *216th Electrochemical Society (ECS) Meeting*, (Vienna), October 2009.

[107] K. Föger, "Commercialisation of CFCLs residential power station - *blugen*^{TM}," in *Proceedings of 9th European Fuel Cell Forum*, (Lucerne), 2010.

[108] A. Liu and Y. Weng, "Performance analysis of a pressurized molten carbonate fuel cell/micro-gas turbine hybrid system," *Journal of Power Sources*, vol. 195, pp. 204–213, 2010.

[109] L. Carrette, K. A. Friedrich, and U. Stimming, "Fuel cells - fundamentals and applications," *Fuel Cells*, vol. 1, no. 1, pp. 5–39, 2001.

[110] N. Sammes, R. Bove, and K. Stahl, "Phosphoric acid fuel cells: Fundamentals and applications," *Current Opinion in Solid State and Materials Science*, vol. 8, pp. 372–378, 2004.

[111] A. Emadi, Y. J. Lee, and K. Rajashekara, "Power electronics and motor drives in electric, hybrid electric, and plug-in hybrid electric vehicles," *IEEE Transactions On Industrial Electronics*, vol. 55, no. 6, pp. 2237–2245, 2008.

[112] S. Jemeï, D. Hissel, M.-C. P, and J. M. Kauffmann, "A new modeling approach of embedded fuel-cell power generators based on artificial neural network," *IEEE Transactions On Industrial Electronics*, vol. 55, pp. 437–447, January 2008.

[113] B. Huang, Y. Qi, and M. Murshed, "Solid oxide fuel cell: Perspective of dynamic modeling and control," *Journal of Process Control*, vol. 21, pp. 1426–1437, 2011.

[114] E. . G. Technical Services, "Fuel cell handbook (seventh edition)," tech. rep., November 2004. Contract No.DE-AM26-99FT40575.

[115] J. T. Pukrushpan, A. G. Stefanopoulou, and H. Peng, "Control of fuel cell breathing," *IEEE Control Systems Magazine*, pp. 30–46, April 2004.

[116] A. Kazim, "Economical and environmental assessments of proton exchange membrane fuel cells in public buildings," *Energy Conversion and Management*, vol. 42, pp. 763–772, 2001.

[117] S. Shaffer, "Delphi SOFC development update," in *2008 SECA Annual Review Meeting*, (Pittsburgh), 2008.

[118] A. Choudhury, H. Chandra, and A. Arora, "Application of solid oxide fuel cell technology for power generation – a review," *Renewable and Sustainable Energy Reviews*, vol. 20, pp. 430–442, April 2013.

[119] A. R. Miller, J. Peters, B. E. Smith, and O. A. Velev, "Analysis of fuel cell hybrid locomotives," *Journal of Power Sources*, vol. 157, pp. 855–861, 2006.

[120] A. Miller, K. Hess, D. Barnes, and T. Erickson, "System design of a large fuel cell hybrid locomotive," *Journal of Power Sources*, vol. 173, pp. 935–942, 2007.

[121] "Fuel cell vehicle world survey 2003," tech. rep., Breakthrough Technologies Institute, Washington, D.C., February 2004.

[122] R. Zaetta and B. Madden, "Hydrogen fuel cell bus technology state of the art review," tech. rep., 2011.

[123] "The fuel cell industry review," tech. rep., Fuel Cell Today, 2012.

[124] K. J. Karimi, "Future aircraft power systems- integration challenges," in *The Boeing Company*, 2007.

[125] J. W. Pratt, L. E. Klebanoff, K. Munoz-Ramos, A. A. Akhil, D. B. Curgus, and B. L. Schenkman, "Proton exchange membrane fuel cells for electrical power generation on-board commercial airplanes," tech. rep., Sandia National Laboratories, May 2011.

[126] A. Hajizadeh, A. H. Shahirinia, and D. C. Yu, "Power control of autonomous hybrid diesel generator/ fuel cell marine power system combined with energy storage," in *2012 IEEE International Conference on Power and Energy (PECon)*, (Malaysia), December 2012.

[127] Y. H. Li, S. S. Choi, and S. Rajakaruna, "An analysis of the control and operation of a solid oxide fuel-cell power plant in an isolated system," *IEEE Transactions on Energy Conversion*, vol. 20, pp. 381–387, June 2005.

[128] "Marine applications for fuel cell technology - a technical memorandum," Tech. Rep. OTA-TM-O-37, U.S. Congress, Office of Technology Assessment, February 1986.

[129] R. Lawton, J. Bash, and S. Barnett, "Marine applications of fuel cells," in *OCEANS '02 MTS/IEEE*, vol. 3, pp. 1784–1790, 2002.

[130] S. Allen, E. Ashey, D. Gore, J. Woerner, and M. Cervi, "Marine applications of fuel cells-a multi-agency research program," *Naval Engineers Journal*, vol. 110, pp. 93–106, January 1998.

[131] M. Krcum, A. Gudelj, and Z. Juric, "Fuel cells for marine application," in *46th International Symposium Electronics in Marine ELMAR-2004*, (Croatia), pp. 491–495, June 2004.

[132] C. Georgescu and E. Mamut, "A study concerning the possibilities for using fuel cells systems for maritime propulsion," *Romanian Journal of Physics*, vol. 51, no. 1-2, pp. 49–56, 2006.

[133] M. Altmann, W. Weindorf, and M. Weinberger, "Life cycle analysis results of fuel cell ships-recommendations for improving cost effectiveness and reducing environmental impacts," tech. rep., July 2004.

[134] S. Alkaner and P. Zhou, "A comparative study on life cycle analysis of molten carbon fuel cells and diesel engines for marine application," *Journal of Power Sources*, vol. 158, pp. 188–199, 2006.

[135] E. Ovrum and G. Dimopoulos, "A validated dynamic model of the first marine molten carbonate fuel cell," *Applied Thermal Engineering*, vol. 35, pp. 15–28, 2012.

[136] C. A. Frangopoulos and L. G. Nakos, "Development of a model for thermoeconomic design and operation optimization of a PEM fuel cell system," *Energy*, vol. 31, pp. 1501–1519, 2006.

[137] N. Benyahia, N. Benamrouche, and T. Rekioua, "Modeling, design and simulation of fuel cell modules for small marine applications," in *International Conference on Electrical Machine ICEM*, pp. 1989–1995, 2012.

[138] P. Beckhaus, M. Dokupil, A. Heinzel, S. Souzani, and C. Spitta, "On-board fuel cell power supply for sailing yachts," *Journal of Power Sources*, vol. 145, pp. 639–643, 2005.

[139] L. Luckose, H. L. Hess, and B. K. Johnson, "Fuel cell propulsion system for marine applications," *Electric Ship Technologies Symposium ESTS*, pp. 574–580, 2009.

[140] T. Leo, J. Durango, and E. Navarro, "Exergy analysis of PEM fuel cells for marine applications," *Energy*, vol. 35, no. 2, pp. 1164 – 1171, 2010. ECOS 2008 21st International Conference, on Efficiency, Cost, Optimization, Simulation and Environmental Impact of Energy Systems.

[141] J. Sun, J. Stebe, and C. Kennell, "Feasibility and design implications of fuel cell power for sealift ships," *Naval Engineers Journal*, vol. 3, pp. 87–102, 2010.

[142] V. Tsourapas, A. Stefanopoulou, and J. Sun, "Dynamics, optimization and control of a fuel cell based combined heat power (CHP) system for shipboard applications," in *2005 American Control Conference*, (USA), pp. 1993–1998, June 2005.

[143] K. Astróm, E. Fontell, and S. Virtanen, "Reliability analysis and initial requirements for fc systems and stacks," *Journal of Power Sources*, vol. 171, pp. 46–54, 2007.

[144] B. gang San, P. lin Zhou, and D. Clealand, "Dynamic modeling of tubular SOFC for marine power system," *Journal of Marine Science and Application*, vol. 9, pp. 231–240, 2010.

[145] D. F. Waters and C. P. Cadou, "Modeling a hybrid rankine-cycle/fuel-cell underwater propulsion system based on aluminume-water combustion," *Journal of Power Sources*, vol. 221, pp. 272–283, 2013.

[146] F. Ghirardo, M. Santin, A. Traverso, and A. Massardo, "Heat recovery options for onboard fuel cell systems," *International Journal of Hydrogen Energy*, vol. 36, pp. 8134–8142, 2011.

[147] B. J. Crowe, "Fuel cells - a survey," tech. rep., Technology Utilisation Office, NASA, January 1973.

[148] V. P. McConnell, "Now, voyager? the increasing marine use of fuel cells," *Fuel Cells Bulletin*, pp. 12–17, May 2010.

[149] Z. Karin, N. Leavitt, T. Costa, and R. Grijalva, "Marine fuel cell market analysis," tech. rep., U.S. Coast Guard Research and Development Center, September 1999.

[150] G. Weaver and S. Barrett, "Marine applications of fuel cell technology," *Fuel Cells Bulletin*, pp. 11–12, January 2003.

[151] R. M. Privette, T. A. Flynn, M. A. Perna, R. Holland, S. Rahmani, C. Woodburn, S. W. Scoles, and R. C. Watson, "2.5 MW PEM fuel cell system for navy ship service power," tech. rep., National Energy Technology Laboratory, 1999.

[152] A. D. Nickens, "Electric power sources for the navy and marine corps," tech. rep., Office of Naval Researchs-Fuel Cell Programs.

[153] E. House, "U.S. navy shipboard fuel cell program." U.S. Maritime Administration Workshop on Maritime Energy and Clean Emissions, Washington, DC, January 2002.

[154] "Fuel cell power plant experience naval applications." US Department of Energy/ Office of Naval Research Shipboard Fuel Cell Workshop, Washington, DC, March 2011.

[155] "Fossil energy-developed fuel cell technology being adapted by navy for advanced unmanned undersea vehicles." `http://energy.gov/fe/articles/fossil-energy-developed-fuel-cell-technology-being-adapted-navy`. Accessed on: 30/10/2014.

[156] "Hydrogen house." `http://hydrogenhouseproject.org/`. Accessed on: 14/10/2016.

[157] "New clermont project." `http://green.rpi.edu/archives/ncp/`. Accessed on: 30/10/2014.

[158] R. Baumert and D. Epp, "Hydrogen storage for fuel cell powered underwater vehicles," in *Proceedings of OCEANS '93*, vol. 2, pp. 166–171, October 1993.

[159] "Hydrogenesis." `http://www.bristolhydrogenboats.co.uk/`. Accessed on: 31/10/2014.

[160] "Ups systems yacht wins race with onboard fuel cell," *Fuel Cells Bulletin*, p. 5, February 2010.

[161] "Vento di sardegna." `http://www.fuelcelltoday.com/news-archive/2012/june/efoy-comfort-fuel-cell-powers-boat-in-twostar-transatlantic-race`. Accessed on: 31/10/2014.

[162] "Hallin marine 2." `http://www.fuelcelltoday.com/news-archive/2012/august/fuel-cell-to-power-equipment-on-board-ocean-rowing-boat-during-world-record-attempt`. Accessed on: 31/10/2014.

[163] M. Cropper, "Opening doors to fuel cell commercialisation, fuel cells in ocean-going yachts," *Fuel Cell Today*, pp. 1–5, March 2004.

[164] W. Harnfel, "Deepc: The new deep water AUV generation," in *ASME 2003 22nd International Conference on Offshore Mechanics and Arctic Engineering*, vol. 3, (Mexico), pp. 713–721, June 2003.

[165] F. Vogler and G. Wúrsig, "Fuel cells in maritime applications challenges, chances and experiences," in *The 4th International Conference on Hydrogen Safety (ICHS)*, 2011.

[166] "Nemo h2." `http://www.lovers.nl/co2zero/`. Accessed on: 30/10/2014.

[167] "Annual report," tech. rep., Wärtsila, 2010.

[168] "e4ships." `http://www.e4ships.de/e4ships-home.html`. Accessed on: 31/10/2014.

[169] "Sunfire 50 kw SOFC for ship-integrated fuel cell project in germany," *Fuel Cells Bulletin*, vol. 2015, no. 11, pp. 3 – 4, 2015.

[170] B. Árnason and T. I. Sigfússon, "Iceland - a future hydrogen economy," *International Journal of Hydrogen Energy*, vol. 25, pp. 389–394, 2000.

[171] F. Vogler and G. Wúrsig, "New developments for maritime fuel cell systems," in *Proceedings of the 18th World Hydrogen Energy Conference (WHEC)*, pp. 445–453, May 2010.

[172] E. Fontes, E. Nilsson, and P. Bosander, "The nordic fuel cell effort," *Refocus*, vol. 2, pp. 24–28, September 2001.

[173] T. Maeda, S. Ishiguro, K. Yokoyama, K. Hirokawa, A. Hashimoto, Y. Okuda, and T. Tani, "Development of fuel cell AUV "URASHIMA"," *Mitsubishi Heavy Industries, Ltd. Technical Review*, vol. 41, no. 6, 2004.

[174] J.-F. Affolter, T. Wankewycz, and J. Davison, "Compact hydrogen fuel cell solution for recreational fishing boats," in *International Conference on Ecologic Vehicles and Renewable Energies*, (Monaco), 2007.

[175] C. H. Choi, S. Yu, I.-S. Han, B.-K. Kho, D.-G. Kang, H. Y. Lee, M.-S. Seo, J.-W. Kong, G. Kim, J.-W. Ahn, S.-K. Park, D.-W. Jang, J. H. Lee, and M. Kim, "Development and demonstration of PEM fuel-cell-battery hybrid system for propulsion of tourist boat," *International Journal of Hydrogen Energy*, vol. 41, no. 5, pp. 3591 – 3599, 2016.

[176] "Nyk super eco ship 2030." `http://www.nyk.com/english/csr/envi/ecoship/`. Accessed on: 30/10/2014.

[177] "Green flagship." `www.2wglobal.com/www/pdf/Green_Flagship.pdf`. Accessed on: 30/10/2014.

[178] F. Rohde, "The future of the fehmarn link," *Germanischer Lloyd nonstop*, no. 3, pp. 10–13, 2012.

[179] "Scotland plans fuel cell ferry, could run on green hydrogen," *Fuel Cells Bulletin*, p. 3, January 2013.

[180] "CMR prototech plans first hydrogen ferry in norway, with fuel cells," *Fuel Cells Bulletin*, vol. 2016, no. 5, pp. 3 –, 2016.

[181] "Climate change: Impacts, vulnerabilities and adaptation in developing countries," tech. rep., United Nations Framework Convention on Climate Change (UNFCCC), 2007.

[182] G. D. Jong and P. Corrignan, "Guidelines for the safe application of fuel cell systems on ships," in *Annual Marine Propulsion Conference*, (London), March 2009.

[183] "Rules for classification and construction, additional rules and guidelines, machinery installations, guidelines for the use of fuel cell systems on board of ships and boats," tech. rep., Germanischer Lloyd, 2003.

[184] J. Baker, "New technology and possible advances in energy storage," *Energy Policy*, vol. 36, pp. 4368–4373, 2008.

[185] C. Naish, I. McCubbin, O. Edberg, and M. Harfoot, "Outlook of energy storage technologies," tech. rep., Policy Department, Economic and Scientific Policy, February 2008.

[186] D. A. Scherson and A. Palencsár, "Batteries and electrochemical capacitors," *The Electrochemical Society Interface*, vol. 15, no. 1, pp. 17–22, 2006.

[187] A. F. Burke, "Batteries and ultracapacitors for electric, hybrid, and fuel cell vehicles," *Proceedings of the IEEE*, vol. 95, pp. 806–820, April 2007.

[188] E. Tazelaar, Y. Shen, P. Veenhuizen, T. Hofman, and P. van den Bosch, "Sizing stack and battery of a fuel cell hybrid distribution truck," *Oil & Gas Science and Technology–Revue d'IFP Energies nouvelles*, vol. 67, no. 4, pp. 563–573, 2012.

[189] C.-S. N. Shiau, C. Samaras, R. Hauffe, and J. J. Michalek, "Impact of battery weight and charging patterns on the economic and environmental benefits of plug-in hybrid vehicles," *Energy Policy*, vol. 37, p. 26532663, 2009.

[190] Z. Bazari and T. Longva, "Assessment of IMO mandated energy efficiency measures for international shipping," tech. rep., October 2011.

[191] W. Droste, "Dynamic simulation of propulsion system," in *WEGEMT 12th Graduate School: Propulsion Systems*, (London, UK), 1989.

[192] M. Blanke, R. Izadi-zamanabadi, and T. F. Lootsma, "Fault monitoring and re-configurable control for a ship propulsion plant," *International*

Journal of Adaptive Control and Signal Processing, vol. 12, pp. 671–688, 1998.

[193] R. Izadi-Zamanabadi and M. Blanke, "A ship propulsion system as a benchmark for fault-tolerant control," *Control Engineering Practice*, vol. 7, pp. 227–239, 1999.

[194] C. Bonivento, A. Paoli, and L. Marconi, "Fault-tolerant control of the ship propulsion system benchmark," *Control Engineering Practice*, vol. 11, pp. 483–492, 2003.

[195] G. Benvenuto, S. Brizzolara, and M. Figari, "Simulation of the propulsion system behaviour during ship standard manoeuvres," in *Proceedings of the 8th International Symposium on Practical Design of Ships and Other Floating Structures (PRADS 2001)*, (Shangai), 2001.

[196] W. Shi, H. Grimmelius, and D. Stapersma, "Analysis of ship propulsion system behaviour and the impact on fuel consumption," *International shipbuilding progress*, vol. 57, no. 1-2, pp. 35–64, 2010.

[197] P. J. M. Schulten, *The interaction between diesel engines, ship and propellers during manoeuvring.* TU Delft, Delft University of Technology, 2005.

[198] A. Ircani, M. Martelli, M. Viviani, M. Altosole, C. Podenzana-Bonvino, and D. Grassi, "A simulation approach for planing boats propulsion and manoeuvrability," *International Journal of Small Craft Technology, Transactions RINA*, vol. 158, 2016.

[199] G. A. Livanos, G. N. Simotas, G. G. Dimopoulos, and N. P. Kyrtatos, "Simulation of marine diesel engine propulsion system dynamics during extreme maneuvering," in *ASME 2006 Internal Combustion Engine Division Spring Technical Conference (ICES2006)*, (Aachen, Germany), May 2006.

[200] U. Campora and M. Figari, "Numerical simulation of ship propulsion transients and full-scale validation," *Proceedings of the Institution of Mechanical Engineers, Part M: Journal of Engineering for the Maritime Environment*, vol. 217, no. 1, pp. 41–52, 2003.

[201] N. P. Kyrtatos, P. Theodossopoulos, G. Theotokatos, and N. Xiros, "Simulation of the overall ship propulsion plant for performance prediction and control," in *Proceedings of the Marpower '99 conference*, (Newcastle-upon-Tyne, UK), March 1999.

[202] M. Altosole and M. Figari, "Effective simple methods for numerical modelling of marine engines in ship propulsion control systems design," *Journal of Naval Architecture and Marine Engineering*, vol. 2, pp. 129–147, December 2011.

[203] N. P. Kyrtatos and V. Lambropoulos, "Modular simulation of marine propulsion systems using an engineering building block approach," in *Proceedings of ISME 6th International Symposium on Marine Engineering*, (Tokyo, Japan), 2000.

[204] G. Theotokatos and V. Tzelepis, "A computational study on the performance and emission parameters mapping of a ship propulsion system," *Proceedings of the Institution of Mechanical Engineers, Part M: Journal of Engineering for the Maritime Environment*, 2013.

[205] D. Trodden, A. Murphy, K. Pazouki, and M. Woodward, "The use of a ship simulator as a tool for exhaust gas emission estimation," in *MARSIM 2015*, (Newcastle upon Tyne, UK), September 2015.

[206] U. Campora, M. Figari, M. Martelli, S. Vignolo, M. Viviani, and M. Ratto, "Propulsion plant simulation for fast military vessels," in *Proceedings of HSMV 2011-9 th Symposium on High Speed Marine Vehicles*, May 2011.

[207] A. Ouroua, J. R. Jackson, J. H. Beno, R. C. Thompson, and E. Schroeder, "Modeling and simulation of electric ships power system components and their interaction," in *Proceedings of the 2007 Summer Computer Simulation Conference SCSC*, (San Diego, California, USA), July 2007.

[208] J. F. Hansen, A. K. Adnanes, and T. I. Fossen, "Mathematical modelling of diesel-electric propulsion systems for marine vessels," *Mathematical and Computer Modelling of Dynamical Systems*, vol. 7, no. 1, pp. 1–33, 2001.

[209] Y. Guo, H.-Y. Zheng, B.-L. Wang, and A.-D. Shen, "Design of ship electric propulsion simulation system," in *Proceedings of the Fourth International Conference on Machine Learning and Cybernetics*, (Guangzhou), August 2005.

[210] E. Dedes, *Investigation of hybrid systems for diesel powered ships*. PhD thesis, University of Southampton, 2013.

[211] C. Xie, C. Zhang, and J.-Y. J. Chang, "Research on simulation of ship electric propulsion system with flywheel energy storage system," *Microsystem Technologies*, vol. 17, pp. 1161–1167, 2011.

[212] R. Hebner, J. Herbst, and A. Gattozzi, "Large scale simulations of a ship power system with energy storage and multiple directed energy loads," in *Grand Challenges in Modeling & Simulation (GCMS)*, (Ottawa, Canada), pp. 430–435, July 2010.

[213] W. Froude, "Experiments on the surface-friction experienced by a plane moving through water," *Report of the British Association for the Advancement of Science*, vol. 42, pp. 118–125, 1872.

[214] V. Bertram, *Practical Ship Hydrodynamics.* Elsevier Ltd., second ed., 2012.

[215] A. S. Sabit, "Regression analysis of the resistance results of the BSRA series," *International Shipbuilding Progress*, vol. 18, no. 197, pp. 3–17, 1971.

[216] A. S. Sabit, "An analysis of the series 60 results: Part i, analysis of forms and resistance results," *International Shipbuilding Progress*, vol. 19, no. 211, pp. 81–97, 1972.

[217] A. S. Sabit, "The SSPA cargo liner series regression analysis of the resistance and propulsive coefficients," *International Shipbuilding Progress*, vol. 23, pp. 213–217, 1976.

[218] J. Holtrop and G. G. J. Mennen, "An approximate power prediction method," *International Shipbuilding Progress*, vol. 29, pp. 166–170, 1982.

[219] D. Radojcic, "An approximate method for calculation of resistance and trim of the planing hulls," *University of Southampton, Ship Science Report*, no. 23, 1985.

[220] V. Oortmerssen, "A power prediction method and its application to small ships.," *International Shipbuilding Progress*, vol. 18, no. 207, pp. 397–412, 1971.

[221] J. Robinson, "Performance prediction of chine and round bilge hull forms," in *International conference: Hydrodynamics of high speed craft*, (London), 1999.

[222] J. Holtrop, "A statistical re-analysis of resistance and propulsion data," *International Shipbuilding Progress*, pp. 272–276, 1984.

[223] H. Schneekluth and V. Bertram, *Ship Design for Efficiency and Economy.* Butterworth-Heinemann, 1998.

[224] V. Berlekom, "Wind forces on modern ship forms – effects on performance," *Transactions of the North East Institute of Engineers and Shipbuilders*, vol. 97, no. 4, 1981.

[225] F. P. Arribas, "Some methods to obtain the added resistance of a ship advancing in waves," *Ocean Engineering*, vol. 34, pp. 946–955, 2007.

[226] H. Maruo, "The excess resistance of a ship in rough seas," *International Shipbuilding Progress*, vol. 4, no. 35, 1957.

[227] H. Maruo, "The drift of a body floating on waves," *Journal of Ship Research*, vol. 4, no. 3, pp. 1–10, 1960.

[228] J. Gerritsma and W. Beukelman, "Analysis of the resistance increase in waves of a fast cargo ship," *International Shipbuilding Progress*, vol. 19, pp. 285–293, September 1972.

[229] N. Salvensen, E. Tuck, and O. Faltinsen, "Ship motions and sea loads," *Transactions of the Society of Naval Architects and Marine Engineers*, vol. 78, pp. 250–279, 1970.

[230] P. A. Wilson, "A review of the methods of calculation of added resistance for ships in a seaway," *Journal of Wind Engineering and Industrial Aerodynamics*, vol. 20, pp. 187–199, 1985.

[231] G. Aertssen, "Service performance and seakeeping trails on M.V. jordaens," *Transactions of the Royal Institution of Naval Architects*, vol. 108, no. 4, pp. 305–343, 1966.

[232] G. Aertssen, "Service performance and seakeeping trails on M.V. lukuga," *Transactions of the royal institution of naval architects*, pp. 293–335, 1963.

[233] R. L. Townsin and Y. J. Kwon, "Approximate formulae for the speed loss due to added resistance in wind and waves," *Transactions of the Royal Institution of Naval Architects*, vol. 125, pp. 199–207, 1983.

[234] W. Blendermann, "Parameter identification of wind loads on ships," *Journal of Wind Engineering and Industrial Aerodynamics*, vol. 51, no. 3, pp. 339–351, 1994.

[235] M. Haddara and C. G. Soares, "Wind loads on marine structures," *Marine Structures*, vol. 12, no. 3, pp. 199–209, 1999.

[236] ITTC, "Full scale measurements speed and power trials analysis of speed/power trial data," *ITTC Recommended Procedures and Guidelines, Procedure 7.5-04-01-01.2*, 2005.

[237] I. Simeonov, H. Kilifarev, and R. Ilarionov, "Embedded system for short-term weather forecasting," in *International Conference on Computer Systems and Technologies - CompSysTech06*, (Bulgaria), June 2006.

[238] "NOMADS." `http://nomads.ncep.noaa.gov/`. Accessed on: 21/10/2014.

[239] M. Bramer and M. Petridis, eds., *Research and Development in Intelligent Systems XXIX*. Springer, 2012.

[240] "Introduction to GRIB edition 1 and GRIB edition 2," tech. rep., World Meteorological Organization, June 2003.

[241] "zyGrib." `http://www.zygrib.org/`. Accessed on: 23/10/2014.

[242] C. M. Grinstead and J. L. Snell, *Introduction to Probability*. American Mathematical Society, second revised ed., 1998.

[243] D. W. Taylor, *The Speed and Power of Ships: a Manual of Marine Propulsion*. Washington, D.C.: Press of Ransdell, Incorporated, 1933.

[244] S. A. Harvald, "Wake of merchant ships.," *Danish Technical Press*, pp. 213–220, 1950.

[245] M. N. Parker, "The B.S.R.A. methodical series - an overall presentation," *Transactions of the Royal Institution of Naval Architects*, vol. 108, pp. 389–393, 1966.

[246] A. F. Molland, S. R. Turnock, and D. A. Hudson, *Ship Resistance and Propulsion : Practical Estimation of Propulsive Power*. Cambridge University Press, 2011.

[247] T. Górnicz and J. Kulczyk, "Application of CFD methods for the assessment of ship manoeuvrability in shallow water," *TransNav, the International Journal on Marine Navigation and Safety of Sea Transportation*, vol. 6, pp. 57–62, March 2012.

[248] A. Ogawa and H. Kasai, "On the mathematical model of manoeuvring motion of ships," *International Shipbuilding Progress*, vol. 25, no. 292, pp. 306–319, 1978.

[249] H. Kobayashi, J. Blok, R. Barr, Y. Kim, and J. Nowicki, "The specialist committee on esso osaka: Final report and recommendations to the 23rd ITTC," in *Proceedings of the 23rd International Towing Tank Conference*, pp. 581– 743, 2003.

[250] K. Kijima, "Some studies on the prediction for ship manoeuvrability," in *Proceeding of the International Conference of Ship Simulation and Ship Manoeuvrability*, (Japan), 2003.

[251] D.-I. F. Wirz, "Optimisation of the crash-stop manoeuvre of vessels employing slow-spped two-stroke engines and fixed pitch propellers," *Journal of Marine Engineering and Technology*, vol. 11, pp. 35–43, January 2012.

[252] M. Blanke, *Ship Propulsion Losses Related to Automatic Steering and Prime Mover Control*. PhD thesis, Technical University of Denmark, December 1981.

[253] N. Xiros, *Robust Control of Diesel Ship Propulsion - Advances in Industrial Control*. Springer-Verlag London Ltd., 2002.

[254] M. Horigome, M. Hara, T. Hotta, and K. Ohtsu, "Computer control of main diesel engine speed for merchant ships," in *Proceeding of ISME Kobe90*, vol. 2, (Kobe, Japan), 1990.

[255] J.-c. Park, "Modeling and simulation of selected distributed generation sources and their assessment," Master's thesis, West Virginia University, 1999.

[256] C. F. Taylor, *The Internal-combustion Engine in Theory and Practice: Thermodynamics, Fluid Flow, Performance*. MIT Press, second ed., 1985.

[257] G. Labreuche, A. Da Costa, Y. Chamaillard, A. Charlet, P. Higelin, and C. Perrier, "Total friction effective pressure and torque estimation," in *Proceedings of the 1st International Workshop on Modeling Emissions and Control in Automotive Engines, MECA'01*, (Italy), September 2001.

[258] C. Hui, W. Peili, and Z. Jundong, "Modeling and simulation of working process of marine diesel engine with a comprehensive method," *International Journal of Computer Information Systems and Industrial Management Applications*, vol. 5, pp. 480–487, 2013.

[259] D. Woodyard, ed., *Pounder's Marine Diesel Engines and Gas Turbines*. Elsevier Ltd., ninth ed., 2009.

[260] D. M. MacPherson, V. R. Puleo, and M. B. Packard, "Estimation of entrained water added mass properties for vibration analysis," *SNAME New England Section*, June 2007.

[261] K. E. Schoenherr, "Formulation of propeller blade strength," *Transactions of the Society of Naval Architects and Marine Engineers*, vol. 71, pp. 81–110, 1963.

[262] R. L. Harrington, ed., *Marine Engineering*. The Society of Naval Architects and Marine Engineers, 1992.

[263] *Vibration Control in Ships*. Veritec Marine Technology Consultants, 1985.

[264] G. Magazinović, "Screening of slow speed marine diesel propulsion shafting design space," *Strojarstvo*, vol. 51, no. 6, pp. 575–586, 2009.

[265] C. Wang, J. J. Corbett, and J. Firestone, "Modeling energy use and emissions from north american shipping: Application of the ship traffic, energy, and environment model," *Environmental Science and Technology*, vol. 41, pp. 3226–3232, 2007.

[266] A. Paxian, V. Eyring, W. Beer, R. Sausen, and C. Wright, "Present-day and future global bottom-up ship emission inventories including polar routes," *Environmental Science and Technology*, vol. 44, pp. 1333–1339, 2010.

[267] C. Wang, J. J. Corbett, and J. Firestone, "Improving spatial representation of global ship emissions inventories," *Environmental Science and Technology*, vol. 42, pp. 193–199, 2008.

[268] T. N. Veziroğlu, S. Şahi, *et al.*, "21st century′s energy: Hydrogen energy system," *Energy conversion and management*, vol. 49, no. 7, pp. 1820–1831, 2008.

[269] D. Cheddie and N. Munroe, "Review and comparison of approaches to proton exchange membrane fuel cell modeling," *Journal of Power Sources*, vol. 147, no. 1, pp. 72–84, 2005.

[270] S. Njoya, O. Tremblay, and L.-A. Dessaint, "A generic fuel cell model for the simulation of fuel cell vehicles," in *Vehicle Power and Propulsion Conference, 2009. VPPC'09. IEEE*, pp. 1722–1729, IEEE, 2009.

[271] S. M. C. Ang, E. S. Fraga, N. P. Brandon, N. J. Samsatli, and D. J. Brett, "Fuel cell systems optimisation–methods and strategies," *International Journal of Hydrogen Energy*, vol. 36, no. 22, pp. 14678–14703, 2011.

[272] I. Veldhuis, R. Richardson, and H. Stone, "Hydrogen fuel in a marine environment," *International Journal of Hydrogen Energy*, vol. 32, no. 13, pp. 2553–2566, 2007.

[273] L. Barelli, G. Bidini, and A. Ottaviano, "Optimization of a PEMFC/battery pack power system for a bus application," *Applied energy*, vol. 97, pp. 777–784, 2012.

[274] E. Ovrum and T. Bergh, "Modelling lithium-ion battery hybrid ship crane operation," *Applied Energy*, vol. 152, pp. 162–172, 2015.

[275] O. Tremblay and L.-A. Dessaint, "Experimental validation of a battery dynamic model for ev applications," *World Electric Vehicle Journal*, vol. 3, no. 1, pp. 1–10, 2009.

[276] R. Gupta, R. Lamba, and S. Padhee, "Thyristor based speed control techniques of dc motor: A comparative analysis," *International Journal of Scientific and Research Publications*, vol. 2, June 2012.

[277] M. Ouyang, L. Xu, J. Li, L. Lu, D. Gao, and Q. Xie, "Performance comparison of two fuel cell hybrid buses with different powertrain and energy management strategies," *Journal of Power Sources*, vol. 163, no. 1, pp. 467–479, 2006.

[278] L. Xu, M. Ouyang, J. Li, F. Yang, L. Lu, and J. Hua, "Application of pontryagin's minimal principle to the energy management strategy of plugin fuel cell electric vehicles," *International Journal of Hydrogen Energy*, vol. 38, no. 24, pp. 10104 – 10115, 2013.

[279] I. Valero, S. Bacha, and E. Rulliere, "Comparison of energy management controls for fuel cell applications," *Journal of power sources*, vol. 156, no. 1, pp. 50–56, 2006.

[280] A. Fadel and B. Zhou, "Power management methodologies for fuel cell-battery hybrid vehicles," tech. rep., SAE Technical Paper, 2010.

[281] L. Zhu, J. Han, D. Peng, T. Wang, T. Tang, and J.-F. Charpentier, "Fuzzy logic based energy management strategy for a fuel cell/battery/ultra-capacitor hybrid ship," in *Green Energy, 2014 International Conference on*, pp. 107–112, IEEE, 2014.

[282] N.-C. Shih, B.-J. Weng, J.-Y. Lee, and Y.-C. Hsiao, "Development of a 20 kw generic hybrid fuel cell power system for small ships and underwater vehicles," *International Journal of Hydrogen Energy*, vol. 39, no. 25, pp. 13894–13901, 2014.

[283] G. Paganelli, S. Delprat, T. Guerra, J. Rimaux, and J. Santin, "Equivalent consumption minimization strategy for parallel hybrid powertrains," in *Vehicular Technology Conference, 2002. VTC Spring 2002. IEEE 55th*, vol. 4, pp. 2076–2081, 2002.

[284] S. J. Moura, D. S. Callaway, H. K. Fathy, and J. L. Stein, "Tradeoffs between battery energy capacity and stochastic optimal power management in plug-in hybrid electric vehicles," *Journal of Power Sources*, vol. 195, no. 9, pp. 2979–2988, 2010.

[285] X. Zhang, C. C. Mi, A. Masrur, and D. Daniszewski, "Wavelet-transform-based power management of hybrid vehicles with multiple on-board energy sources including fuel cell, battery and ultracapacitor," *Journal of Power Sources*, vol. 185, no. 2, pp. 1533–1543, 2008.

[286] F. Segura and J. M. Andújar, "Power management based on sliding control applied to fuel cell systems: A further step towards the hybrid control concept," *Applied Energy*, vol. 99, pp. 213–225, 2012.

[287] M.-J. Kim and H. Peng, "Power management and design optimization of fuel cell/battery hybrid vehicles," *Journal of Power Sources*, vol. 165, no. 2, pp. 819 – 832, 2007.

[288] W.-S. Lin and C.-H. Zheng, "Energy management of a fuel cell/ultracapacitor hybrid power system using an adaptive optimal-control method," *Journal of Power Sources*, vol. 196, no. 6, pp. 3280 – 3289, 2011.

[289] S. F. Tie and C. W. Tan, "A review of energy sources and energy management system in electric vehicles," *Renewable and Sustainable Energy Reviews*, vol. 20, pp. 82 – 102, 2013.

[290] P. Garcia, L. M. Fernandez, C. A. Garcia, and F. Jurado, "Energy management system of fuel-cell-battery hybrid tramway," *Industrial Electronics, IEEE Transactions on*, vol. 57, no. 12, pp. 4013–4023, 2010.

[291] W. Choi, J. Howze, and P. Enjeti, "Development of an equivalent circuit model of a fuel cell to evaluate the effects of inverter ripple current," *Journal of Power Sources*, vol. 158, no. 2, pp. 1324 – 1332, 2006.

[292] "MATLAB control system toolbox." `http://uk.mathworks.com/products/control/`, 2016. Accessed: 2016-07-18.

[293] L. Xu, J. Li, J. Hua, X. Li, and M. Ouyang, "Optimal vehicle control strategy of a fuel cell/battery hybrid city bus," *International Journal of Hydrogen Energy*, vol. 34, no. 17, pp. 7323 – 7333, 2009.

[294] G. Paganelli, S. Delprat, T. M. Guerra, J. Rimaux, and J. J. Santin, "Equivalent consumption minimization strategy for parallel hybrid powertrains," in *Vehicular Technology Conference, 2002. VTC Spring 2002. IEEE 55th*, vol. 4, pp. 2076–2081 vol.4, 2002.

[295] L. Xu, J. Li, J. Hua, X. Li, and M. Ouyang, "Adaptive supervisory control strategy of a fuel cell/battery-powered city bus," *Journal of Power Sources*, vol. 194, no. 1, pp. 360–368, 2009.

[296] C. Thimm, "Zemships – the first fuel cell passenger ship in hamburg," in *ZERO REGIO Workshop*, (Italy), November 2007.

[297] C. Musardo, G. Rizzoni, Y. Guezennec, and B. Staccia, "A-ECMS: An adaptive algorithm for hybrid electric vehicle energy management," *European Journal of Control*, vol. 11, pp. 509–524, 2005.

[298] N. Xiros, "PID marine engine speed regulation under full load conditions for sensitivity h∞-norm specifications against propeller disturbance," *Journal of Marine Engineering and Technology*, vol. 3, no. 2, pp. 3–11, 2004.

[299] S. Wei and P. Zhou, "Development of a 3d dynamic programming method for weather routing," *TransNav: International Journal on Marine Navigation and Safety of Sea Transportation*, vol. 6, no. 1, pp. 79–85, 2012.

[300] Y.-J. Kwon, *The effect of weather, particularly short sea waves, on ship speed performance*. PhD thesis, University of Newcastle upon Tyne, 1981.

[301] "Capability of ship manoeuvring simulation models for approach channels and fairways in harbours," tech. rep., Permanent International Association of Navigation Congresses PIANC, 1992. Report of Working Group No 20 of Permanent Technical Committee II.

[302] A. Turk and J. Prpić-Oršić, "Estimation of extreme wind loads on marine objects," *Brodogradnja*, vol. 60, no. 2, pp. 147–156, 2009.

[303] C. Crane Jr, "Studies of ship maneuvering 'response to propeller and rudder actions'," tech. rep., DTIC Document, 1965.

[304] M. A. Roscher and D. U. Sauer, "Dynamic electric behavior and open-circuit-voltage modeling of lifepo 4-based lithium ion secondary batteries," *Journal of Power Sources*, vol. 196, no. 1, pp. 331–336, 2011.

[305] "AIS." `https://www.marinetraffic.com/hr/ais/home/`. Accessed on: 19/07/2014.

[306] "Simulink solvers." `http://uk.mathworks.com/help/simulink/ug/types-of-solvers.html`, 2016. Accessed on: 17/05/2016.

[307] E. Anderlini, H. Crossley, J. Hawkes, H. Le, J. Mozden, K. Neale, and B. Thornton, "The development of an autonomous self-propulsion vessel for powering and manoeuvring tests in an uncontrolled environment," tech. rep., Uinversity of Southampton, 2013.

[308] W. Blendermann, *Wind loading of ships: Collected data from wind tunnel tests in uniform flow*. Inst. für Schiffbau, 1996.

[309] "Winprop." `http://www.awe-communications.com/Products/`. Accessed on: 15/08/2014.

[310] S. Liu, A. Papanikolaou, and G. Zaraphonitis, "Prediction of added resistance of ships in waves," *Ocean Engineering*, vol. 38, pp. 641 – 650, 2011.

[311] `http://cogsys.imm.dtu.dk/propulsionmodelling/data.html`. Accessed on: 23/5/2015.

[312] B. S. Borowy and Z. M. Salameh, "Methodology for optimally sizing the combination of a battery bank and pv array in a wind/PV hybrid system," *Energy conversion, ieee transactions on*, vol. 11, no. 2, pp. 367–375, 1996.

[313] F. Segura, E. Durán, and J. Andújar, "Design, building and testing of a stand alone fuel cell hybrid system," *Journal of Power Sources*, vol. 193, no. 1, pp. 276–284, 2009.

[314] J. Bernard, S. Delprat, F. N. Büchi, and T. M. Guerra, "Fuel-cell hybrid powertrain: Toward minimization of hydrogen consumption," *Vehicular Technology, IEEE Transactions on*, vol. 58, no. 7, pp. 3168–3176, 2009.

[315] P. Melo, J. Ribau, and C. Silva, "Urban bus fleet conversion to hybrid fuel cell optimal powertrains," *Procedia-Social and Behavioral Sciences*, vol. 111, pp. 692–701, 2014.

[316] C. Zheng, G. Xu, J. Jeong, S. W. Cha, Y.-i. Park, and W. Lim, "Power source sizing of fuel cell hybrid vehicles considering vehicle performance and cost," *International journal of precision engineering and manufacturing*, vol. 15, no. 3, pp. 527–533, 2014.

[317] M. Kim, Y.-J. Sohn, W.-Y. Lee, and C.-S. Kim, "Fuzzy control based engine sizing optimization for a fuel cell/battery hybrid mini-bus," *Journal of Power Sources*, vol. 178, no. 2, pp. 706–710, 2008.

[318] C.-Y. Li and G.-P. Liu, "Optimal fuzzy power control and management of fuel cell/battery hybrid vehicles," *Journal of Power Sources*, vol. 192, no. 2, pp. 525 – 533, 2009.

[319] B. D. James, J. M. Moton, and W. G. Colella, "Mass production cost estimation of direct h2 pem fuel cell systems for transportation applications: 2014 update," *report by Strategic Analysis, Inc., under Award Number DEEE0005236 for the US Department of Energy*, December 2014.

[320] D. Steward, G. Saur, M. Penev, and T. Ramsden, "Lifecycle cost analysis of hydrogen versus other technologies for electrical energy storage," *US National Renewable Energy Laboratory (NREL)*, 2009.

[321] C. Spataru, Y. C. Kok, and M. Barrett, "Physical energy storage employed worldwide," *Energy Procedia*, vol. 62, pp. 452–461, 2014.

[322] S. Bashash, S. J. Moura, J. C. Forman, and H. K. Fathy, "Plug-in hybrid electric vehicle charge pattern optimization for energy cost and battery longevity," *Journal of power sources*, vol. 196, no. 1, pp. 541–549, 2011.

[323] Y. He, M. Chowdhury, P. Pisu, and Y. Ma, "An energy optimization strategy for power-split drivetrain plug-in hybrid electric vehicles," *Transportation Research Part C: Emerging Technologies*, vol. 22, pp. 29–41, 2012.

[324] L. Xu, F. Yang, J. Li, M. Ouyang, and J. Hua, "Real time optimal energy management strategy targeting at minimizing daily operation cost for a plug-in fuel cell city bus," *international journal of hydrogen energy*, vol. 37, no. 20, pp. 15380–15392, 2012.

[325] J. R. Bartels, M. B. Pate, and N. K. Olson, "An economic survey of hydrogen production from conventional and alternative energy sources," *International journal of hydrogen energy*, vol. 35, no. 16, pp. 8371–8384, 2010.

[326] P. Agnolucci, O. Akgul, W. McDowall, and L. G. Papageorgiou, "The importance of economies of scale, transport costs and demand patterns in optimising hydrogen fuelling infrastructure: An exploration with SHIPMod (spatial hydrogen infrastructure planning model)," *International Journal of Hydrogen Energy*, vol. 38, no. 26, pp. 11189 – 11201, 2013.

[327] F. Baldi, F. Ahlgren, T.-V. Nguyen, C. Gabrielii, and K. Andersson, "Energy and exergy analysis of a cruise ship," in *The 28th International Conference on Efficiency, Cost, Optimization, Simulation and Environmental Impact of Eeergy Systems, June 29-july 3, 2015, Pau, France*, Pau University, 2015.

[328] S. R. Massel, *Ocean waves breaking and marine aerosol fluxes*, vol. 38. Springer Science & Business Media, 2007.

[329] D. Tilman, C. L. Lehman, and C. E. Bristow, "Diversity-stability relationships: statistical inevitability or ecological consequence?," *The American Naturalist*, vol. 151, no. 3, pp. 277–282, 1998.

[330] C.-H. Chao and J.-J. Shieh, "A new control strategy for hybrid fuel cell-battery power systems with improved efficiency," *International Journal of Hydrogen Energy*, vol. 37, no. 17, pp. 13141 – 13146, 2012. 12th CHEC.

[331] J. Zhuo, C. Chakrabarti, K. Lee, N. Chang, and S. Vrudhula, "Maximizing the lifetime of embedded systems powered by fuel cell-battery hybrids," *IEEE Transactions on Very Large Scale Integration (VLSI) Systems*, vol. 17, no. 1, pp. 22–32, 2009.

[332] S. Lahmiri, "Wavelet low- and high-frequency components as features for predicting stock prices with backpropagation neural networks," *Journal of King Saud University - Computer and Information Sciences*, vol. 26, no. 2, pp. 218 – 227, 2014.

[333] A. Foley, B. Tyther, P. Calnan, and B. Gallachóir, "Impacts of electric vehicle charging under electricity market operations," *Applied Energy*, vol. 101, pp. 93 – 102, 2013. Sustainable Development of Energy, Water and Environment Systems.

[334] R. Winkel, U. Weddige, D. Johnsen, V. Hoen, and G. Papaefthymiou, "Potential for shore side electricity in europe," tech. rep., ECOFYS Consultancy, January 2015. Project number:TRANL14441.

[335] A. M. Bassam, A. B. Phillips, S. R. Turnock, and P. A. Wilson, "An improved energy management strategy for a hybrid fuel cell/battery passenger vessel," *International Journal of Hydrogen Energy*, 2016. `http://dx.doi.org/10.1016/j.ijhydene.2016.08.049`.

[336] A. M. Bassam, A. B. Phillips, S. R. Turnock, and P. A. Wilson, "Development of a multi-scheme energy management strategy for a hybrid fuel cell driven passenger ship," *International Journal of Hydrogen Energy*, 2016. `http://dx.doi.org/10.1016/j.ijhydene.2016.08.209`.

[337] A. M. Bassam, A. B. Phillips, S. R. Turnock, and P. A. Wilson, "Ship voyage energy efficiency assessment using ship simulators," in *VI International Conference on Computational Methods in Marine Engineering (MARINE 2015)*, (Rome, Italy), pp. 591–604, June 2015.

[338] E. Nyhus, "FCSHIP / New-H-Ship impact on RCS for fuel cells on ships." February 2005.

[339] "Coolcell." http://www.netinform.net/H2/H2Mobility/Detail.aspx?ID=368. Accessed on: 31/10/2014.

[340] "Advanced fuel cell technology," *FCT*, vol. 8, pp. 9–11, April 2004.

[341] K.-A. Adamson, "Opening doors to fuel cell commercialisation - fuel cells and marine applications," *Fuel Cell Today*, pp. 1–10, 2005.

[342] "H2yacht 675." http://h2yacht.com/Broschuere675.pdf. Accessed on: 31/10/2014.

[343] "H2yacht 540." http://www.h2yacht.com/html/technische_daten540.html. Accessed on: 31/10/2014.

[344] "Bavaria werft." http://www.netinform.net/H2/H2Mobility/Detail.aspx?ID=362. Accessed on: 31/10/2014.

[345] "Xperiance." http://www.netinform.net/H2/H2Mobility/Detail.aspx?ID=21. Accessed on: 31/10/2014.

[346] "Hydrogenics marine applications, electrolysers and fuel cell power modules & systems, Italy." May 2013.

[347] "Yacht with EFOY fuel cell comes second in transat race," *Fuel Cells Bulletin*, p. 4, January 2010.

[348] E. Raugel, V. Rigaud, and C. Lakeman, "Sea experiment of a survey AUV powered by a fuel cell system," in *2010 IEEE/OES Autonomous Underwater Vehicles*, pp. 1–3, Sept 2010.

[349] "Destination dunkerque." http://www.sfc.com/en/node/1264, 2010. Accessed on: 7/4/2016.

[350] "Cellkraft runs fuel cell boat on 160 km test," *Fuel Cells Bulletin*, p. 5, December 2010.

[351] "Acta unveils hydrogen powered yacht tender," *Fuel Cells Bulletin*, no. 7, p. 5, 2010.

[352] "Hydrogenics fuel cells to power UNIDO boat in turkey," *Fuel Cells Bulletin*, p. 4, March 2010.

[353] "Maike." http://www.baltic-sea-energy.de/?page_id=16&lang=en, 2010. Accessed on: 7/4/2016.

[354] "Taika." `http://www.fuelcellsystems.co.uk/2011/08/10/fuel-cell-systems-powers-azab-winner/`. Accessed on: 31/10/2014.

[355] C. Dre, "Existing and innovative technologies and operational measures reducing the environmental impact of regional research vessels," tech. rep., Eurofleets, 2011.

[356] M. Gurhan, M. Turhan, S. Kilicarslan, B. Gulseren, B. Akaydin, E. Ulgen, K. Atalay, S. Ozdemir, A. Askinci, B. Yildirim, C. Karabulut, E. Oner, and M. M. Sezer, "Marti (seagull): The first hydrogen powered boat of turkey," in *10thInternationalConferenceonCleanEnergy(ICCE-2010)*, (Famagusta,N.Cyprus), September 2010.

[357] T. Hyakudome, H. Yoshida, T. Nakatani, Y. Ohta, T. Tani, K. Sugihara, T. Moriga, T. Iwamoto, Y. Kawaharazaki, T. Oda, and Y. Fujita, "Development of fuel cell system for underwater power source," in *OCEANS - Bergen, 2013 MTS/IEEE*, pp. 1–6, June 2013.

[358] B. Tihanyi, "Use of fuel cells in small boats and yachts- a potential early application and market in hungary," (Budapest), May 2013.

[359] "Marex 320." `http://landauuk.com/news/28/76/Marex-Boats-and-Leonardo-Yachts-offer-EFOY-onboard`, 2013. Accessed on: 8/4/2016.

[360] "Star of hope." `http://www.digitimes.com/news/a20140523PR206.html?mod=0&chid=9`, 2014. Accessed on: 7/4/2016.

[361] "YC synergy powers electric yachts with fuel cell technology," *Fuel Cells Bulletin*, vol. 2014, no. 6, pp. 4 –, 2014.

[362] "Naruwa." `http://www.ycsynergy.com.tw/en/news.php`, 2014. Accessed on: 7/4/2016.

[363] K. Kijima, Y. Nakiri, S. Tanaka, and Y. Furukawa, "On a numerical simulation for predicting of ship manoeuvring perfromance," in *ITTC 90 Group Discussion 3*, pp. 559–568.

[364] J. Hooft and J. Pieffers, "Maneuverability of frigates in waves," *Marine technology*, vol. 25, no. 4, pp. 262–271, 1988.

[365] S. Khanfir, V. Nagarajan, K. Hasegawa, and S. K. Lee, "Estimation of mathematical model and its coefficients of ship manoeuvrability for a twin-propeller twin-rudder ship.," in *Proceedings of International Conference on Marine Simulation and Ship Manoeuvrability (MARSIM 2009)*, (Panama), 2009.

Fuel Cell Marine Application

Table 1: List of fuel cell existing projects and demonstration from year 2000

Year	Country	Specifications	Fuel Cell Type	Reference
2009-2014	The e4ships lighthouse project	Development and testing of fuel cells onboard cruise ships * *MS Forester* * *MS Mariella*	HTPEMFC & SOFC	[168]
2002-2004	FCSHIP Project	Comprehensive study on the technical feasibility, efficiency, cost benefit and environmental aspects related to application of fuel cell systems in ships.		[338]
2000	Germany	*Hydra*, Passenger boat, 20 passengers, 12m long and 3m wide, 6 kn, 6.9 kW	AFC	[148]
2000	Finland	Motorboat, Hydrogen fuelled, 30 kW	AFC	[148]
2000	Germany	*MS Weltfrieden*, 10 kW, project of Expo 2000, Hydrogen fuelled	PEMFC	[68]
2000	Japan	1500 DWT merchant ship, 500 kW	PEMFC	[68]
2000	Japan	499 GT Coastal vessel, 500 kW	PEMFC	[68]
2002	Japan	*Malt's Mermaid III*, 5.8m sail boat, APU, Methanol fuelled, 30 W	DMFC	[148]
2002	Switzerland	*Branec III*, 5.8m yacht, APU, 300 W	PEMFC	[148; 163]
2003	Japan	*CoolCell*, yacht, 12.26 m long, 3.76 m wide, 1.2 kW	PEMFC	[339]

2003	USA	*Duffy-Herreshoff 30*, Water Taxi, 18 passenger, 3 kW	PEMFC	[156]
2003	Germany	*NO. 1*, 12m yacht, APU, 4.8 kW	PEMFC	[148]
2003	Switzerland	*Hydroxy 3000*, catamaran, 3 kW	PEMFC	[148]
2004	Germany	*Mamelle*, 15m sailboat, 1.2 kW	DMFC	[148]
2005	USA	149 passenger ferry from San Francisco and Treasure Island, 24m long, 240 kW, Hydrogen fuelled	PEMFC	[340; 46]
2005	USA	*HaveBlue XV1*, sailboat, 10 kW, Hydrogen fuelled	PEMFC	[341]
2005	Germany	*H2Yacht 675*, 6.75m Yacht, 2.4 kW, 8 Person, Hydrogen Fuelled	PEMFC	[342]
2005	Germany	*H2Yacht 540*, 5.4m Yacht, 1.2 kW, 6 Person, Hydrogen Fuelled	PEMFC	[343]
2005	Germany	*Bavaria Werft*, electric motor boat, 4 passenger, 800 W, Hydrogen Fuelled		[344]
2006	Netherlands	*Xperiance*, yacht, 7 m long, 2.35 m wide, Hydrogen fuelled	PEMFC	[345]
2007	Germany	*Cobalt 233 ZET*, 24 kW, sports boat, top speed of 40 km/h	PEMFC	[346]
2007	UK	*Ross Barlow*, Waterway maintenance boat, student project, 18 m long, 5 kW	PEMFC	[148]
2007	UK	*Emerald Beneteau 411*, 12m yacht, reformed LPG fuelled, 5 kW	PEMFC	[148]
2007	USA	Trolling boat, 300 W, Hydrogen Fuelled	PEMFC	[148; 174]
2008	ZEMSHIP Project, Germany	*FCS Alsterwasser*, passenger ship, 100 passenger, 25.46 m long, 5.36 m wide		[148]
2008	Iceland	*Elding*, 125 tonne whale watching boat, APU, Hydrogen fuelled, 10 kW	PEMFC	[148; 171]
2008	Netherlands	Hydrogen Hybrid Harbour Tug (HHHT), 65 tonnes bollard pull tug, 200 kW, Hydrogen fuelled	PEMFC	[182]

2009	Netherlands	*Nemo H2*, passenger boat, 86 passengers, 22 m long, 4.25 m wide, 60-70 kW	PEMFC	[148; 166]
2009	FellowSHIP Program	Viking Lady, Offshore supply vessel, APU, 92.2 m long, 21 m wide, LNG fuelled, 320 kW	MCFC	[135; 148]
2009	USA	*New Clermont*, 7 m canal boat, student project, Hydrogen fuelled	PEMFC	[157]
2009	Germany	*Pogo2*, yacht	DMFC	[148; 347]
2009	Austria	*Riviera 600*, 16 m motor boat, Hydrogen fuelled, 4 kW	PEMFC	[148]
2009	Denmark	*Chaloupe*, 6.4 m boat, 500 W	DMFC	[148]
2009	France	*IDEFx*, AUV, 4.5 m long, 2850 m operational depth	PEMFC	[348]
2009	Greece	Testing *RFC-1000* unit on motorboat, reformed LPG fuelled, 1 kW	PEMFC	[148]
2009	Turkey	*Belbim*, 50 passengers sightseeing boat project, Hydrogen fuelled	PEMFC	[148; 346]
2009	UK	*Nightlife*, Yacht, 65 W to power the navigation, computer and communications equipment, Methanol fuelled	DMFC	[160]
2009	Italy	*Vaporetto*, passenger boat in Venice, Hydrogen fuelled	PEMFC	[346]
2010	MethAPU Project	*Undine*, Car carrier, APU, 228 m long, 33 m wide, Methanol fuelled, 20 kW	SOFC	[167]
2010	France	*Zero CO2*, 12m yacht, 35 kW, sail around the Mediterranean collecting scientific data on pollution	PEMFC	[148]
2010	Germany	*Destination Dunkerque*, Yacht, APU, 90 W	DMFC	[349]
2010	Sweeden	Small boat, 1 kW, reliability test with a length of 161 km, speed=4.6 kn, Methanol fuelled	PEMFC	[350]

2010	Italy	*HIDRO*, Hydrogen fuel cell tender serving sailing boats		[351]
2010	Turkey	*UNIDO boat*	PEMFC	[352]
2010		*Maike*, Sailing boat, 65 W, Methanol	DMFC	[353]
2011	USA	*Hornblower Hybrid*, 600 passenger ferry, 32 kW, combined with diesel, wind, solar and batteries	PEMFC	[346]
2011	UK	*Taika*, sailboat, 90 W, APU, Methanol fuelled, The boat won the 2011 Azores and Back (AZAB) 2,500-mile race	DMFC	[354]
2011	Canada	*Tsekoa II*, research vessel, Hydrogen fuelled, 33 m long	PEMFC	[355]
2012	UK	*Vento di Sardegna*, Sailboat, APU, Methanol fuelled	DMFC	[161]
2012	UK	*Hydrogenesis*, 12 passenger ferry, 12 kW, Bristol harbour, Hydrogen fuelled, 11 m long	PEMFC	[159]
2012	UK	*Hallin Marine 2*, Ocean rowing boat, 7.3 m long	DMFC	[162]
2012	Turkey	*MARTI (SEAGULL)*, 6 passenger boat, 8.5 kW, 7 kn speed, 8.13m length, 3.22m beam, Hydrogen fulled	PEMFC	[356]
2012	USA	*Duffy Voyager* Speedboat, 25 kW, 19 m long, Hydrogen fuelled	PEMFC	[156]
2013	Japan	*Jinbei*, AUV, 4m long, 3000 m working depth	PEMFC	[357]
2013	Hungary	6 passengers boat, 0.54 m long, 0.2 m wide, Hydrogen fuelled,	PEMFC	[358]
2013	Germany	*Marex 320*, Yacht, 9.9 m long, 3.3 m wide, Methanol fuelled	DMFC	[359]
2013	Germany	*Eagle 36*, Yacht, 35 ft long, 105 W, Methanol fuelled	DMFC	[359]
2013	Germany	*Eagle 44*, Yacht, 44 ft long, 105 W, Methanol fuelled	DMFC	[359]

2014	Taiwan	*Star of Hope*, Ferry, 90 passenger, 17 m long, 6 Kn speed	PEMFC	[360]
2014	Taiwan	*Mu Yang*, Yacht, 50 people	PEMFC	[361]
2014	Taiwan	*Naruwa*, Ferry	PEMFC	[362]
2014	Korea	20 m long tourist boat	PEMFC	[175]

Miscellaneous Calculations

Forces and moment acting on the hull is non-dimensionalised and expressed as follows [250]

$$\begin{aligned} X'_H &= X'_{\beta r} r' \sin\beta + X'_{uu} \cos^2\beta \\ Y'_H &= Y'_\beta \beta + Y'_r r' + Y'_{\beta\beta} \beta \left|\beta\right| + Y'_{rr} r' \left|r'\right| + (Y'_{\beta\beta r} \beta + Y'_{\beta rr} r')\beta r' \\ N'_H &= N'_\beta \beta + N'_r r' + N'_{\beta\beta} \beta \left|\beta\right| + N'_{rr} r' \left|r'\right| + (N'_{\beta\beta r} \beta + N'_{\beta rr} r')\beta r' \end{aligned} \tag{1}$$

where X,Y and N are non-dimensionalised as follows

$$\begin{aligned} X', Y' &= X, Y / \frac{1}{2}\rho L T U^2 \\ N' &= N / \frac{1}{2}\rho L^2 T U^2 \end{aligned} \tag{2}$$

The formulae of individual hydrodynamic derivatives for surge, sway and yaw motions can be approximated using the following equations [363]

$$
\begin{aligned}
X'_{\beta r} &= m'_y(1.5 - 1.66C_B) \\
X'_{uu} &= R_T/(0.5\rho LTU^2) \\
Y'_{\beta} &= 0.5\pi k + 1.4(C_B B/L) \\
Y'_{r} &= (m' + m'_x - 1.5(C_B B/L) \\
Y'_{\beta\beta} &= 0.5 + 2.5T(1 - C_B)/B \\
Y'_{rr} &= 0.343TC_B/B - 0.07 \\
Y'_{\beta\beta r} &= 1.5TC_B/B - 0.65 \\
Y'_{\beta rr} &= 5.95T(1 - C_B)/B \\
N'_{\beta} &= k \\
N'_{r} &= k^2 - 0.54K \\
N'_{\beta\beta} &= 0.066 - 0.96T(1 - C_B)/B \\
N'_{rr} &= 0.5C_B B/L - 0.09 \\
N'_{\beta rr} &= -(0.5TC_B/B - 0.05) \\
N'_{\beta\beta r} &= -(57.5(C_B B/L)^2 - 18.4C_B B/L + 1.6) \\
k &= 2T/L
\end{aligned}
\tag{3}
$$

Added mass on x and y directions can be approximated as follows [364]

$$
\begin{aligned}
m_x &= \frac{2.79\rho(C_B LBT)^{5/3}}{L^2} \\
m_y &= \frac{\pi}{2}(\rho LT^2)(1 + 0.16\frac{C_B B}{T} - \frac{5.1}{(L/B)^2})
\end{aligned}
\tag{4}
$$

Forces and moment induced by the propeller can be expressed as follows [249]

$$
\begin{aligned}
X_P &= (1-t)T_p = \rho D_P^4 n^2 (1-t) K_T \\
Y_P &= N_P = 0
\end{aligned}
\tag{5}
$$

For twin screw ships

$$
\begin{aligned}
X_P &= (1-t)(T_p^P + T_p^S) \\
Y_P &= N_P = 0
\end{aligned}
\tag{6}
$$

where superscript S and P refer to starboard and port sides of the ship. Hydrodynamic force and yaw moment induced by the rudder can be expressed as follows [249; 363]

$$
\begin{aligned}
X_R &= -(1-t_R)F_N \sin\alpha \\
Y_R &= -(1+a_H)F_N \cos\alpha \\
N_R &= -(x_R + a_H x_H)F_N \cos\alpha \\
F'_N &= \frac{A_R C N U_R^{2\prime}}{LT} \\
\alpha_R &= \delta - \gamma\beta'_R \\
\beta'_R &= \beta - 2x'_R r' \\
x'_R &= -0.5 \\
r' &= rL/U \\
\gamma &= -22.2(C_B B/L)^2 + 0.02(C_B B/L) + 0.68 \\
CN &= 6.13AR_R/(2.25 + AR_R) \\
U_R &= \sqrt{u_R^2 + v_R^2} \\
v_R &= -\delta_R \frac{u_R}{U_R} \\
\delta_R &= \alpha_R - \delta \\
u_R &= u(1-w_R)\sqrt{\eta(1+K(\sqrt{1+8K_T/\pi J^2}-1))^2 + (1-\eta)} \\
K &= K_x/\epsilon \\
\epsilon &= -156.2(C_B B/L)^2 + 41.6(C_B B/L) - 1.76 \\
\eta &= D_P/H \\
w_R &= \frac{w_{R0} w_P}{w_{P0}} \\
w_{R0} &= 1 - \epsilon(1 - w_{P0})
\end{aligned}
\tag{7}
$$

For twin screw ships [365]

$$
\begin{aligned}
X_R &= -(1-t_R)(F_N^P \sin\alpha^P + F_N^S \sin\alpha^S) \\
Y_R &= -(1+a_H)(F_N^P \cos\alpha^P + F_N^S \cos\alpha^S) \\
N_R &= -(x_R + a_H x_H)(F_N^P \cos\alpha^P + F_N^S \cos\alpha^S) - \frac{b}{2}(1-t_R)(F_N^P \sin\alpha^P + F_N^S \sin\alpha^S) \\
F_N^P &= \frac{\rho}{2} A_R (U_R^P)^2 f_a \sin\alpha_R^P \\
F_N^S &= \frac{\rho}{2} A_R (U_R^S)^2 f_a \sin\alpha_R^S \\
U_R^P &= \sqrt{u_R^2 + (v_R^P)^2} \\
U_R^S &= \sqrt{u_R^2 + (v_R^S)^2} \\
v_R^P &= -\delta^P \frac{u_R}{U_R} \\
v_R^S &= -\delta^S \frac{u_R}{U_R} \\
\alpha_R^P &= \delta^P - \gamma\beta_R' \\
\alpha_R^S &= \delta^S - \gamma\beta_R' \\
\delta_R^P &= \alpha_R^P - \delta^P \\
\delta_R^S &= \alpha_R^S - \delta^S
\end{aligned}
\tag{8}
$$

x_R: The distance of rudder from the ship centre of gravity,
x_H: The distance between the ship centre of gravity and centre of lateral force,
α : Rudder angle,
F_N: Rudder normal force,
t_R: Rudder deduction fraction,
a_H: Interaction coefficient between rudder and a ship hull,
A_R: Rudder area,
U_R: Inflow Velocity to the rudder,
AR_R: Rudder aspect ratio,
H: Rudder height,
D_P: Propeller diameter
b: The distance between the two rudders as shown in Figure 1.

t_R is a coefficient for additional drag and it can be approximated as follows:

$$1 - t_R = 0.28 C_B + 0.55 \tag{9}$$

a_H and x_H are taken from Figure 2

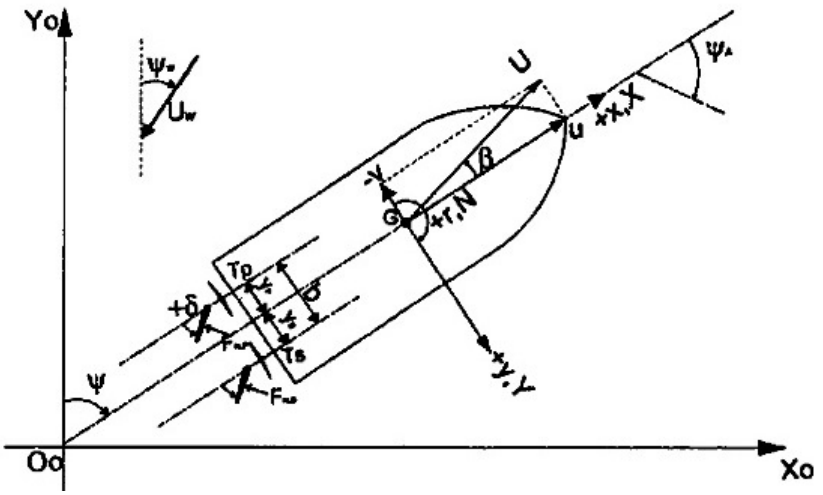

Figure 1: Coordinate system with body fixed axis at ship's center of gravity

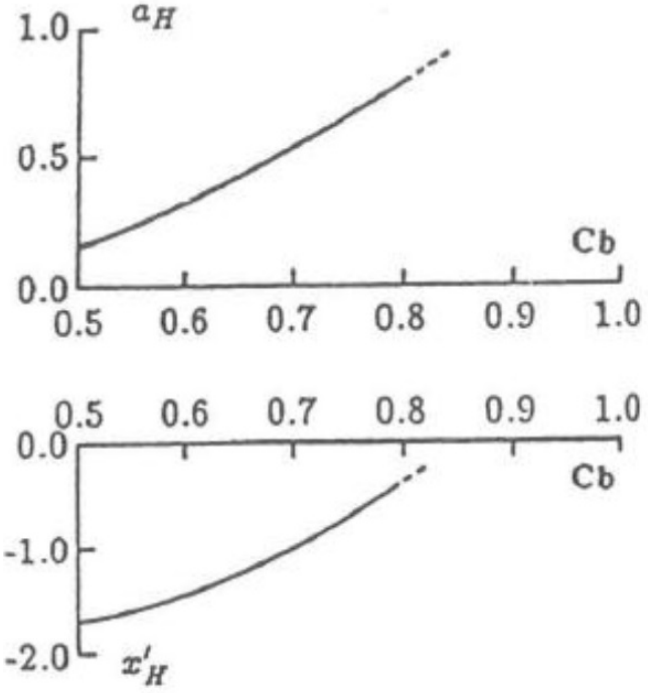

Figure 2: Rudder interaction coefficient